National Technical University of Athens
School of Civil Engineering
Geotechnical Department
MSc in Analysis and Design of Earthquake Resistant Structures
Postgraduate Diploma Thesis

Coupling of topographic and valley effects on seismic ground motion

Σύζευξη φαινομένων τοπογραφίας και κοιλάδας στην σεισμική εδαφική κίνηση

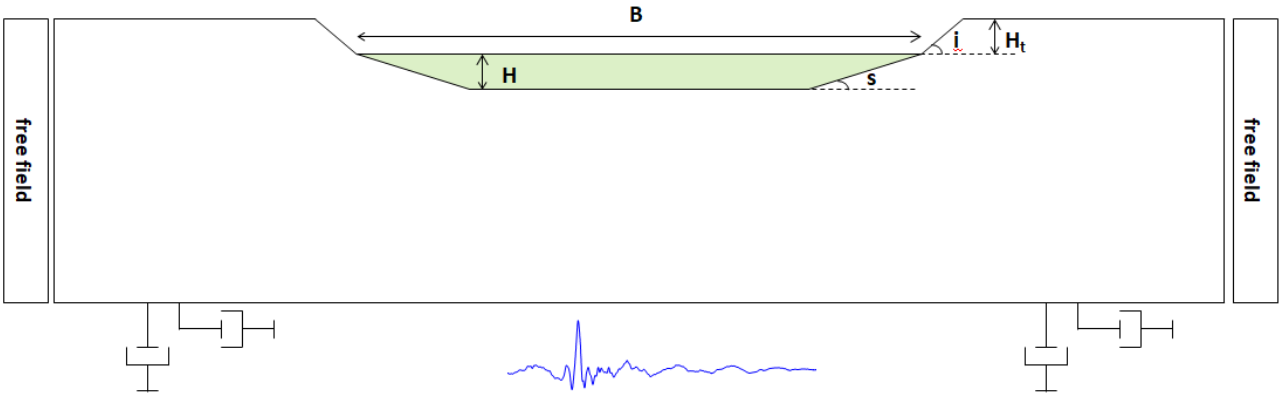

John Georgalas, Civil Engineer (NTUA)

Supervisor: **Achilleas Papadimitriou**, Associate Professor (NTUA)

Athens, June 2020

TABLE OF CONTENTS

ABSTRACT

This thesis concerns the parametric investigation of valley and topographic effects on seismic ground motion, with emphasis on the coupling between the two phenomena. For this purpose, 2D numerical seismic response analyses were performed for uniform, symmetrical, trapezoidal valleys with flat and non-flat outcrops on visco-elastic soil and bedrock with the finite difference method (FLAC, Itasca Inc 2005). All valleys had a width-over-thickness ratio B/H = 10, but different soil and bedrock mechanical properties. The excitations used were vertically incident SV waves with time-histories based on the earthquake recording of the Aigion (1995) earthquake, after appropriate scaling to attain the desired predominant period in the range (common for bedrock excitations) of 0.1 – 0.4sec.

Each 2D analysis was supplemented by two 1D ground response analyses under the same excitation: 1D_soil and 1D_rock. In the former, the response of a bedrock column having the soil layer of thickness H at its top was attained, while the latter studied the response of a uniform bedrock column. Care was taken for dense mesh discretization and proper boundary conditions, while Rayleigh damping was introduced, calibrated to provide the desired damping ratio ξ = 5% at the significant frequencies between the predominant frequency of the excitation and the fundamental period of the soil column. In order to determine the aggravation that is due purely to valley and topographic effects, the geomorphic aggravation factors AS_{ah} and AS_{av} were estimated for each ground surface location and for the horizontal and the parasitic vertical acceleration, respectively. Namely, for both directions the geomorphic aggravation factor for each structural period T is defined as the ratio of the spectral acceleration value from the 2D analysis over the corresponding spectral value from the appropriate 1D analysis: 1D_soil if the location sits on soil; 1D_rock if the location sits on outcropping rock.

At first, the effects of outcropping bedrock topography on seismic valley response were investigated. The parametric study covered 23 valley-bedrock outcrop-excitation combinations and investigated the effects of the predominant period of the excitation T_e, the inclination angles of the valley s and the outcropping bedrock i, the outcropping bedrock height H_t and the soil-to-bedrock impedance ratio a. The results from all the analyses for valleys with flat outcrops were compatible with the pertinent results in the literature. Namely, the geomorphic aggravation factors within the valley become more remarkable for structural periods T close to the predominant excitation period T_e and increase with increasing inclination angle of the valley s and decreasing impedance ratio a. For valleys with non-flat outcrops it was observed that the geomorphic aggravation spectra AS_{ah} and AS_{av} within the valley are affected by the outcropping bedrock height H_t, especially for low-frequency excitations, but remain practically unaffected by the inclination angle of the outcrops i.

Based on the above mentioned analyses, a quantification of the effects of a non-flat outcropping bedrock topography on seismic valley response for T=0s was introduced, i.e. correction factors CF_h and CF_v were defined at each location as the ratio of $AS_{ah}(T=0)$ and $AS_{av}(T=0)$ respectively for the case of the non-flat outcrop over the corresponding $AS_{ah}(T=0)$ and $AS_{av}(T=0)$ for the case of the flat outcrop. It was found that the CF_h within the valley varied between 0.7 and 1.06, on average, while the average CF_v varied between 0.9 and 1.4. Generally, the correction factors CF_h and CF_v become

more significant for higher and steeper outcrops (e.g. H_t=100m, i=45^o), especially for the parasitic vertical acceleration.

In the sequel, the opposite problem was examined, i.e. the valley effects on the seismic response of outcropping bedrock. For each case, a comparison was made between 2 models with the same outcropping bedrock geometry under the same excitation: one with an alluvial valley at the base of the topographic relief (valley model) and one with no such valley (no valley model). In the majority of the cases, the valley decreased AS_{ah} and increased AS_{av} at the outcropping bedrock, regardless of the outcropping bedrock height H_t and the inclination angles of the valley s and the outcrops i. It should be noted that for structural periods T > 1s, the valley effects become negligible.

Moreover, a quantification of the effects due to the existence of a valley at the base of the topographic relief for T=0s was introduced on the basis of the analyses for each pair of canyons. Namely, correction factors CF_h and CF_v were defined at each location as the ratio of AS_{ah}(T=0) and AS_{av}(T=0), respectively, for the valley model over the corresponding aggravation factor values for the no valley model of each pair. The results showed that valley effects on the topographic aggravation at the outcropping bedrock are almost negligible for the horizontal acceleration (CF_h varied between 0.85 and 1.05), but are potentially remarkable for the parasitic vertical acceleration ($0.8 \leq CF_v \leq 2.6$), especially for mild valleys and outcrops (e.g. s=i=22.5^o) under low-frequency excitations (e.g. T_e=0.4s). Additionally, the CF_v is generally smaller in front of the outcrop crest ($1.1 \leq CF_v \leq 1.4$, on average) and larger behind it ($1.2 \leq CF_v \leq 1.8$, on average).

ΠΕΡΙΛΗΨΗ

Η παρούσα εργασία αφορά στην παραμετρική διερεύνηση των επιδράσεων κοιλάδας και τοπογραφίας ανάγλυφου στη σεισμική κίνηση του εδάφους, με έμφαση στη σύζευξη μεταξύ των δύο φαινομένων. Για το σκοπό αυτό εκτελέστηκαν διδιάστατες αριθμητικές αναλύσεις σεισμικής εδαφικής απόκρισης για ομοιόμορφες, συμμετρικές, τραπεζοειδείς κοιλάδες με οριζόντιες και κεκλιμένες εξάρσεις βραχώδους υπόβαθρου επί ιξώδο-ελαστικού εδάφους με τη μέθοδο των πεπερασμένων διαφορών (FLAC, Itasca Inc 2005). Όλες οι κοιλάδες είχαν λόγο πλάτους προς πάχος B/H=10, αλλά σε κάθε περίπτωση είχαν διαφορετικές μηχανικές ιδιότητες για το έδαφος και τον βράχο. Οι διεγέρσεις που χρησιμοποιήθηκαν ήταν κατακορύφως προσπίπτοντα κύματα SV με χρονοϊστορίες που βασίστηκαν σε σεισμική καταγραφή του σεισμού του Αιγίου (1995). Η πραγματική χρονοϊστορία τροποποιήθηκε κατάλληλα έτσι ώστε να επιτευχθεί η επιθυμητή δεσπόζουσα περίοδος, η οποία κυμάνθηκε από 0,1 έως 0,4 δευτερόλεπτα (σύνηθες εύρος για διέγερση σε αναδυόμενο βράχο).

Η κάθε διδιάστατη ανάλυση συνοδεύτηκε από δύο μονοδιάστατες αναλύσεις σεισμικής απόκρισης υπό την ίδια διέγερση: την 1D_soil και την 1D_rock. Η πρώτη αφορά στην προσομοίωση της απόκρισης μιας εδαφικής στρώσης πάχους H επί βραχώδους υπόβαθρου, ενώ η δεύτερη μελέτησε την απόκριση μιας ομοιόμορφης στήλης βραχώδους υποβάθρου. Ιδιαίτερη προσοχή δόθηκε στην πυκνή διακριτοποίηση του κανάβου και στις κατάλληλες συνοριακές συνθήκες στο κάθε προσομοίωμα. Η υστερητική απόσβεση των γεωϋλικών προσομοιώθηκε μέσω της απόσβεσης τύπου Rayleigh, η οποία βαθμονομήθηκε κατάλληλα ώστε να παρέχει τον επιθυμητό λόγο απόσβεσης ξ = 5% στις σημαντικές συχνότητες του προβλήματος, δηλαδή μεταξύ της δεσπόζουσας συχνότητας διέγερσης και της θεμελιώδους ιδιοσυχνότητας της εδαφικής στήλης πάχους H. Προκειμένου να προσδιοριστεί η επίδραση που οφείλεται αποκλειστικά σε φαινόμενα κοιλάδας και τοπογραφίας ανάγλυφου, ορίσθηκαν οι λόγοι γεωμορφικής επιδείνωσης AS_{ah} και AS_{av} σε κάθε σημείο της επιφάνειας του εδάφους και για την οριζόντια και την παρασιτική κατακόρυφη επιτάχυνση, αντίστοιχα. Συγκεκριμένα, και για τις δύο κατευθύνσεις, ο λόγος γεωμορφικής επιδείνωσης για κάθε περίοδο κατασκευής T ορίζεται ως ο λόγος της φασματικής επιτάχυνσης που υπολογίστηκε από την διδιάστατη ανάλυση έναντι της αντίστοιχης φασματικής τιμής από την αρμόζουσα μονοδιάστατη ανάλυση: 1D_soil εάν το σημείο βρίσκεται στην επιφάνεια του εδάφους και 1D_rock εάν το σημείο βρίσκεται στην επιφάνεια του βράχου.

Αρχικά, διερευνήθηκαν οι επιδράσεις της τοπογραφίας του αναδυόμενου βραχώδους υπόβαθρου στην σεισμική απόκριση της κοιλάδας. Συνολικά μελετήθηκαν 23 συνδυασμοί κοιλάδας-τοπογραφίας βραχώδους υπόβαθρου- σεισμικής διέγερσης. Ταυτόχρονα, εξετάστηκαν οι επιδράσεις της δεσπόζουσας περιόδου της διέγερσης T_e, των γωνιών κλίσης της κοιλάδας s και των πρανών του αναδυόμενου βραχώδους υπόβαθρου i, του ύψους του αναδυόμενου υπόβαθρου H_t, και του λόγο εμπέδησης εδάφους-βράχου a. Τα αποτελέσματα από όλες τις αναλύσεις για κοιλάδες με οριζόντιες εξάρσεις βραχώδους υπόβαθρου ήταν συμβατά με τα σχετικά αποτελέσματα στην βιβλιογραφία. Αυτό σημαίνει ότι η γεωμορφική επιδείνωση εντός της κοιλάδας είναι πιο έντονη για περιόδους κατασκευής T κοντά στη δεσπόζουσα περίοδο της διέγερσης T_e και αυξάνονται με την αύξηση της γωνίας κλίσης της κοιλάδας s και τη μείωση του

λόγου εμπέδησης a. Για κοιλάδες με κεκλιμένες εξάρσεις βραχώδους υπόβαθρου παρατηρήθηκε ότι οι φασματικοί λόγοι γεωμορφικής επιδείνωσης AS_{ah} και AS_{av} εντός της κοιλάδας επηρεάζονται από το ύψος των πρανών H_t, ιδίως για διεγέρσεις χαμηλής συχνότητας, αλλά παραμένουν πρακτικά ανεπηρέαστοι από τη γωνία κλίσης των βραχώδων πρανών i.

Με βάση τις προαναφερθείσες αναλύσεις, εισήχθη ποσοτικός προσδιορισμός των επιδράσεων της κεκλιμένης τοπογραφίας αναδυόμενου βραχώδους υπόβαθρου στη σεισμική απόκριση της κοιλάδας για T = 0s. Πιο αναλυτικά, ορίστηκαν διορθωτικοί συντελεστές CF_h και CF_v σε κάθε σημείο της επιφάνειας της κοιλάδας ως ο λόγος των φασματικών τιμών $AS_{ah}(T=0)$ και $AS_{av}(T=0)$, αντίστοιχα, για τις περιπτώσεις κεκλιμένου αναδυόμενου βραχώδους υπόβαθρου προς τις αντίστοιχες τιμές $AS_{ah}(T=0)$ και $AS_{av}(T=0)$ που αφορούν στις περιπτώσεις οριζόντιου υποβάθρου. Διαπιστώθηκε ότι οι τιμές του CF_h εντός της κοιλάδας κυμαίνονται μεταξύ 0,7 και 1,06, κατά μέση τιμή, ενώ οι μέσες τιμές του CF_v κυμάνθηκαν μεταξύ 0,9 και 1,4. Γενικά, οι διορθωτικοί συντελεστές CF_h και CF_v καθίστανται πιο σημαντικοί για υψηλότερες και απότομες εξάρσεις βραχώδους υπόβαθρου (π.χ. H_t = 100m, i = 45^o), ιδιαίτερα για την παρασιτική κατακόρυφη επιτάχυνση.

Στη συνέχεια, εξετάστηκε το αντίστροφο πρόβλημα, δηλαδή η επίδραση της κοιλάδας στη σεισμική απόκριση του αναδυόμενου βραχώδους υπόβαθρου. Για κάθε περίπτωση, πραγματοποιήθηκε σύγκριση της απόκρισης μεταξύ 2 γεωμορφολογικών δομών με την ίδια γεωμετρία βραχώδους υπόβαθρου κάτω από την ίδια διέγερση: ενός με αλλουβιακή κοιλάδα στη βάση του βραχώδους υπόβαθρου (valley model) και ενός χωρίς τέτοια κοιλάδα (no valley model). Στην πλειονότητα των περιπτώσεων, η κοιλάδα μείωσε τις φασματικές τιμές AS_{ah} και αύξησε τις φασματικές τιμές AS_{av} στο αναδυόμενο υπόβαθρο, ανεξάρτητα από το ύψος των πρανών H_t και τις γωνίες κλίσης της κοιλάδας s και των πρανών i. Αξίζει να σημειωθεί ότι για περιόδους κατασκευής T > 1s, οι επιδράσεις της κοιλάδας είναι αμελητέες.

Επιπλέον, πραγματοποιήθηκε ποσοτικός προσδιορισμός των επιπτώσεων της ύπαρξης κοιλάδας στη βάση του αναδυόμενου βραχώδους υπόβαθρου για T=0s, με βάση τις αποκρίσεις των 2 συγκρινόμενων γεωμορφολογικών δομών κάθε περίπτωσης. Πιο συγκεκριμένα, ορίστηκαν και πάλι συντελεστές διόρθωσης CF_h και CF_v σε κάθε σημείο ως ο λόγος των τιμών γεωμορφικής επιδείνωσης $AS_{ah}(T=0)$ και $AS_{av}(T=0)$, αντίστοιχα, για τη δομή με κοιλάδα στον πόδα έναντι των αντίστοιχων τιμών γεωμορφικής επιδείνωσης για τη δομή χωρίς κοιλάδα. Τα αποτελέσματα έδειξαν ότι οι επιδράσεις της κοιλάδας στην τοπογραφική επιδείνωση του αναδυόμενου υπόβαθρου είναι σχεδόν αμελητέες για την οριζόντια επιτάχυνση (οι τιμές του CF_h κυμαίνονταν μεταξύ 0,85 και 1,05), αλλά είναι δυνητικά σημαντικές για την παρασιτική κατακόρυφη επιτάχυνση (0,8 ≤ CFv ≤ 2,6), ιδιαίτερα για κοιλάδες και βραχώδη πρανή με ήπιες κλίσεις (π.χ. s = i = 22,5^o) κάτω από διεγέρσεις χαμηλής συχνότητας (π.χ. T_e = 0,4s). Επιπροσθέτως, οι τιμές του CF_v είναι γενικά μικρότερες μπροστά από τη στέψη του βραχώδους πρανούς (1,1 ≤ CFv ≤ 1,4, κατά μέση τιμή) και μεγαλύτερες πίσω από αυτή (1,2 ≤ CFv ≤ 1,8, κατά μέση τιμή).

CHAPTER 1

INTRODUCTION

1.1 Objective

It is well known that the local geological and geotechnical conditions affect considerably the intensity of ground shaking. There are many case histories in the literature where the soil stiffness and thickness, as well as the local topography, have been depicted as the reasons for the observed spatial variability of seismic motion at the ground surface. The extent of their influence depends on the geometry and material properties of the subsurface materials, on site topography, and on the characteristics of the input motion.

This thesis focuses on the investigation of valley and topographic effects on seismic ground motion. Both topographic and valley effects have been studied extensively over the last few decades. It has been shown that under certain conditions, these effects can be significant. The majority of the pertinent papers in the literature have studied the seismic response at the ground surface either for alluvial valleys with flat outcrops, or for homogeneous canyons, slopes and ridges without alluvial deposits at their base. In reality, though, the outcropping bedrock topographies at the edges of an alluvial valley are rarely flat. In such cases, the ground motion at the surface is expected to be affected not only by the valley itself, but also by the outcropping bedrock topography. Hence, it is uncertain whether the results from the pertinent studies from the literature may also be applied in such non-flat geometries. In the same train of thought, it is uncertain whether the literature results for topographic aggravation of homogeneous canyons, slopes and ridges may also be applied in the quite common cases where there are alluvial deposits at the base of these topographic relieves.

Hence, the main objective of this thesis is to investigate the coupling of topographic and valley effects on seismic ground motion. In other words, it examines how the valley response is affected by the outcropping bedrock topography and the opposite, i.e. how the outcropping bedrock response is affected by the existence of a valley at its base. For this reason, 2D numerical seismic response analyses were performed for uniform, symmetrical, trapezoidal valleys with flat and non-flat outcrops on visco-elastic soil and bedrock with the finite difference method (FLAC, Itasca Inc 2005). The results along the ground surface were presented in terms of geomorphic aggravation factors AS_{ah} and AS_{av} for the horizontal and the parasitic vertical acceleration, respectively, which properly exclude the aggravation due to 1D soil effects. The study focuses primarily on the aggravation for the peak ground acceleration (T=0s) and secondarily on what happens for other structural periods T. In this effort, the effects of the main characteristics of the valley, the

outcropping bedrock and the seismic excitation on the values of AS_{ah} and AS_{av} were determined, as a means to quantify when and where this coupling of topographic and valley effects is important and not.

1.2 Thesis outline

The present thesis consists of 6 Chapters. This first one is introductory and explains the main purpose and the organization of the study. **Chapter 2** provides a literature review about valley and topographic effects over the last few decades. At first, historical examples of valley and topographic effects on seismic ground motion are presented. In the sequel, the most significant results from the literature are presented for valleys of all shapes with flat outcrops, as well as for homogeneous topographic irregularities, such as canyons, slopes and ridges. Based on recent publications, the coupling of valley and topographic effects is explained, as an introduction to the main objective of this study.

The numerical methodology used in this thesis is presented in **Chapter 3**. More specifically, the analysis models for all examined cases are defined, along with their parameters, the boundary conditions and the mesh discretization limitations. Then, the soil and the outcropping bedrock properties are presented, as well as the excitation parameters and the assumed damping formulation. In addition, the quantitative indices of seismic aggravation used in this thesis are defined in this Chapter, which ends with a summary of all hereby examined cases.

Chapter 4 investigates the effects of outcropping bedrock topography on valley response, in terms of the spatial variability of geomorphic aggravation along the valley for different structural periods T and for the whole elastic response spectrum for different locations along the valley. A quantification of the effects of a non-flat outcropping bedrock topography is introduced on the basis of all performed analyses.

In the sequel, **Chapter 5** studies the valley effects on the seismic response of outcropping bedrock. For each case, a comparison is made between 2 models with the same outcropping bedrock geometry under the same excitation; one with an alluvial valley at the base of the topographic relief (valley model) and one with no such valley (no valley model). The aggravation results are presented in the same format with Chapter 4. Similarly, a quantification of the effects due to the existence of a valley at the base of the topographic relief is introduced on the basis of all performed analyses.

Finally, **Chapter 6** presents the most important conclusions retrieved from Chapters 4 and 5, referring to topographic and valley effects, as well as their coupling. It must be stated here that this thesis is a first attempt to determine the coupling of topographic and valley effects on seismic ground motion. Hence, proposals for future research are also included in this Chapter, in order to generalize or even correct, if necessary, the derived conclusions.

CHAPTER 2

LITERATURE REVIEW

2.1 Prominent examples of topography and valley effects on seismic ground motion

The term "local site effects" has been used for many years to describe exclusively the influence of soil stratigraphy on the seismic ground motion. Such effects are usually taken into account by the well - known one dimensional (1-D) ground response analysis, assuming parallel soil layers of infinite extent excited by vertically incident waves. Most of the seismic provisions of building codes worldwide account for soil effects through single amplification factors applied to the acceleration design spectra, factors that have been derived by statistical recordings by assuming 1-D conditions.

However, during numerous strong earthquakes in recent years (Spitak 1988, Loma Prieta 1989, Northridge 1994, Kobe 1995, Athens 1999) the reported variability of ground shaking or the non-uniform distribution of damage could not be sufficiently explained by simple 1-D analysis. The aforementioned discrepancy may be attributed to the existence of subsurface irregularities or surface topography.

Since many cities are located on or near alluvial valleys, the effects of basin geometry on ground motion is of great interest in geotechnical earthquake engineering. The curvature of a basin in which softer alluvial soils have been deposited can trap body waves and cause some incident body waves to propagate through the alluvium as surface waves (Helmberger and Vidale, 1988). These waves can produce stronger shaking and longer durations than would be predicted by one-dimensional analyses that consider only vertically propagating S-waves.

A typical example of valley effects is the damage distribution observed during the 1988 Armenia earthquake. Yegian et al. (1994), trying to correlate the observed damage with the ground shaking in the city of Kirovakan, located about 10 to 15 km from the surface outbreak of the fault, pointed out that 1-D analyses substantially underestimated the ground surface motion in a region of Kirovakan in which the soil profile constitutes a small triangular-shaped alluvial valley (**Figure 2.1**). The observed damage was adequately explained by Bielak et al. (1999) who provided a satisfactory explanation performing two-dimensional (2-D) ground response analyses for the same valley.

Perhaps the best well known example of apparent topographic effects was produced by an acceleration time history recording on the abutment of Pacoima dam in southern California (**Figure 2.2**). The Pacoima dam accelerograph at S16 recorded peak horizontal accelerations of about 1.25g in each of two perpendicular directions in the 1971 San Fernando (M_L = 6.4) earthquake, values that were considerably larger than expected for an earthquake of this magnitude. The accelerograph,

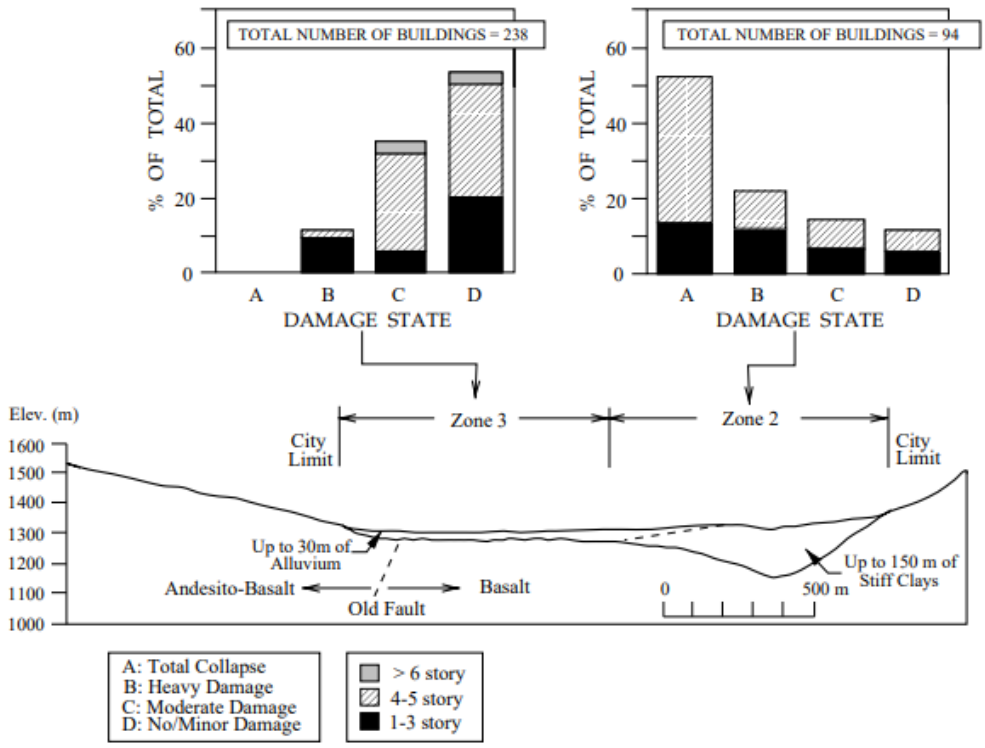

Figure 2.1: A geotechnical profile in Kirovakan and the corresponding damage statistics during 1988 Armenia earthquake (after Yegian et al., 1994c).

however, was located at the crest of a narrow, rocky ridge adjacent to the dam (Trifunac and Hudson, 1971). Subsequent investigations have attributed a good part of the unusually high peak accelerations to dynamic response of the ridge itself - a topographic effect. The accelerogram at S16E component is shown at **Figure 2.3**.

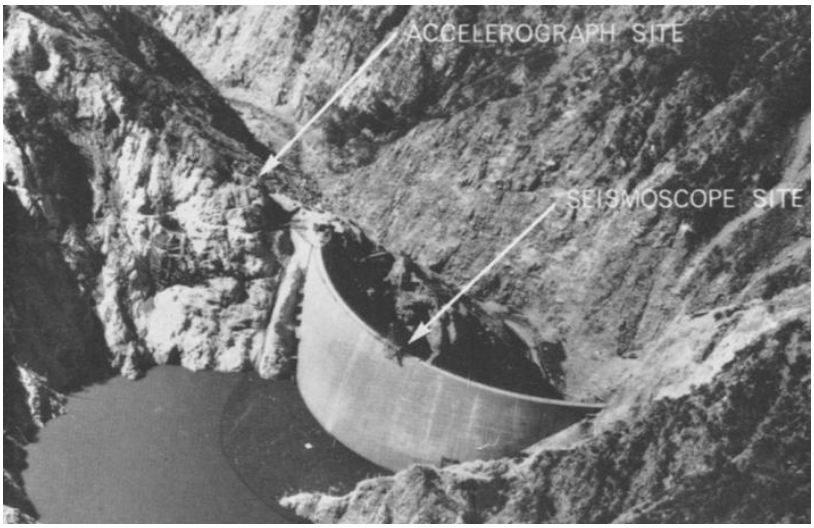

Figure 2.2: Close view to the Pacoima dam (Trifunac and Hudson, 1971).

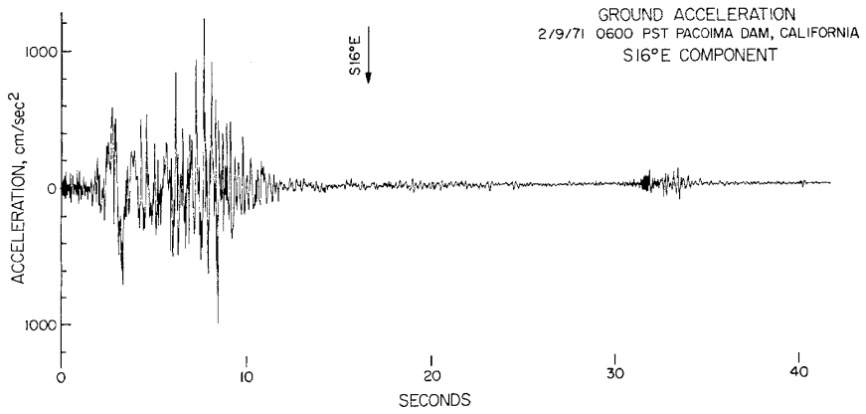

Figure 2.3: Time history of acceleration at S16E component of Pacoima dam during 1971 San Fernando earthquake (Trifunac and Hudson, 1971).

A clear example of the influence of site effects is found in data from a dense array used to monitor topographic amplification of a ridge in France (Pedersen et al., 1994a). An array of seven seismometers were placed across a 300 m high linear ridge in France to monitor motions from regional earthquakes, as shown in **Figure 2.4**. Two of the stations (S2 and S3) were founded on hard limestone, whereas the remaining three stations were founded on unconsolidated sediments. Clear amplification can be seen from the raw data presented in **Figure 2.5** when comparing the crest station (S2) to the other rock station down the slope (S3). It can also be seen that much greater site amplification occurs at the three stations founded on soil. This is a clear example of the potential for misleading interpretation when considering the amplification from the base to the crest of the ridge as the effect of topography, since this disregards site effects. In fact, Pedersen et al. (1994a) calculated the spectral ratios between the two rock stations S2 and S3 for their analysis of the effect of topography and found peak amplifications of the order of 4.5. They concluded that one of the difficulties in studying the effect of topography is the lack of a reference station for most sets of field data, as well as the lack of information on incident angle. These data were in good agreement with the predicted response using the indirect boundary-element method.

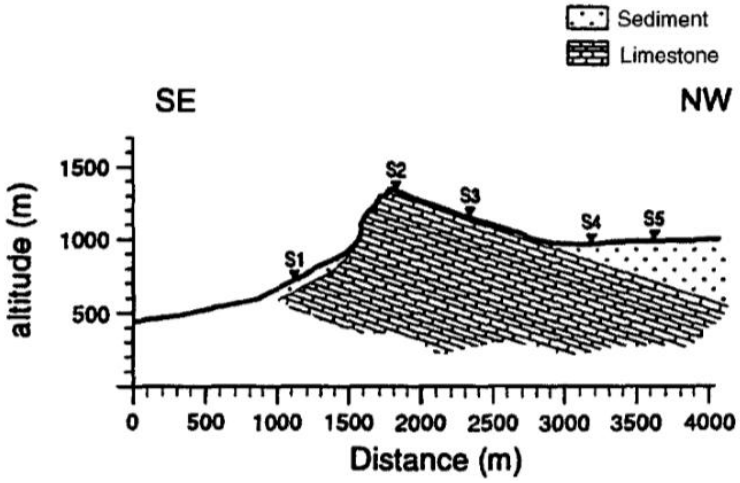

Figure 2.4: Geological cross section of Mt. St. Eynard with seismograph stations shown as triangles (from Pedersen et al., 1994a).

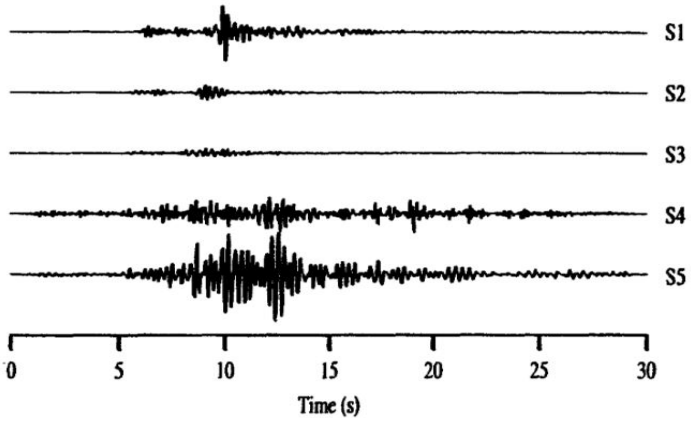

Figure 2.5: Example of topographic and site effects in velocity data obtained from Mt. St. Eynard array. Vertical component for Mb = 1.4 event at a distance of 45 km (from Pedersen et al., 1994a).

In addition to the theoretical predictions, the amplification of surface motion in ridge-or steep slope-type topography has also been verified from measurements during earthquake events. The diagram of **Figure 2.6** depicts the variation of normalized peak recorded horizontal accelerations from five earthquakes in Japan as a function of elevation across a ridge. The normalization in this diagram is referred to the crest motion and in addition to the mean values, the standard error bars are also included in the graph. The measurements indicate an amplification at the crest (relatively to the base) varying from 1.8 to 5.5 with a mean value of 2.5.

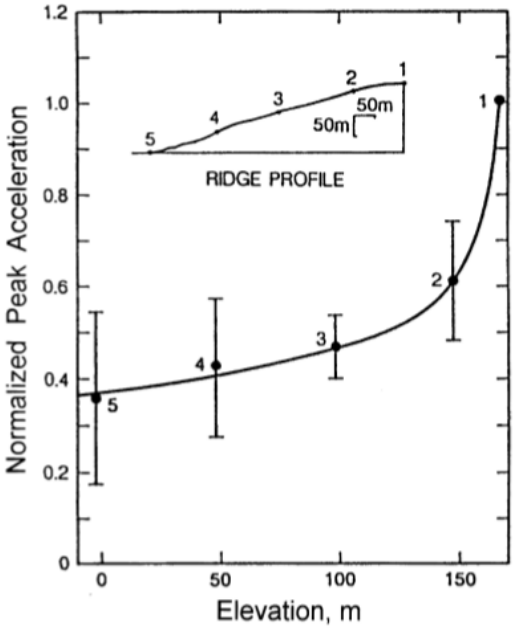

Figure 2.6: Relative distribution of peak horizontal accelerations along a ridge from Matsuzaki area in Japan (Jibson, 1987).

In terms of damage patterns, increasing damages have been reported along the slope and the top of hills after the Chile 1985 earthquake. A characteristic example of increased earthquake damages

close to the crest of a step-like topography has been reported by Castellani et al. for the case of the Irpinia 1980 earthquake and is illustrated in **Figure 2.7**. In this case the damages of an Italian village sitting at the top of a hill, were concentrated close to the crest of a steep slope whereas they were insignificant in the direction away from the crest.

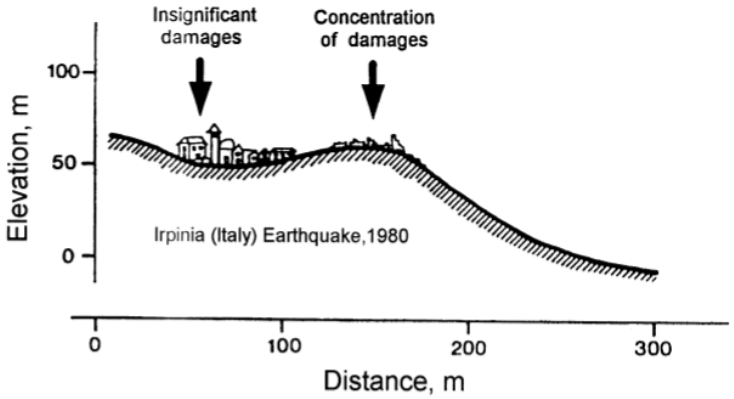

Figure 2.7: Effect of surface topography on damage distribution in the Irpinia (Italy) 1980 earthquake (Castellani et al., 1982).

These and many other examples from previous earthquakes prove that topography and valley effects may play an important role in seismic ground response. Many researchers have measured and simulated such 2D or 3D effects worldwide. A brief presentation of such studies is given in the following sections of this chapter.

2.2 Overview of valley effects on seismic ground motion

Since the 1980's, seismic site amplification phenomena within soft soil filled valleys with basin irregular shapes have been identified and studied. Such phenomena, which are called hereafter "valley effects" can be summarized as those generated at, across the valley edges, by the body waves that are transformed into surface waves travelling horizontally within the soft soil layer.

Some of the first attempts to study the effect of topography on seismic waves have been concerned with the scattering of incident waves and conversion of body to surface-wave energy (Gilbert and Knopoff, 1960; Hudson, 1967; Hudson and Knopoff, 1967; Mclvor, 1969). The theories used in these studies are not valid for motions in the vicinity of the scatterer, when the slopes are steep, or when the topography and seismic disturbances are of comparable wavelength. In such cases a numerical treatment of the problem is required.

Aki and Larner (1970) developed a method to study the surface motion of a layered medium having an irregular interface due to incident plane SH waves. Bard and Bouchon (1980) used the Aki and Larner method to investigate the seismic response of sediment-filled valleys to incident SH waves. The study revealed the important role played by the non-planar interface, which, when the incident wavelengths are comparable to the depth of the valley, results in the generation of Love

waves which may have much larger amplitude than the disturbance associated with the direct incident signal. In the presence of a high-velocity contrast between the sediments and the underlying bedrock, these local surface waves can be reflected several times at the edges of the valley, resulting in a long duration of the ground shaking in the basin. In the case of a lower impedance contrast, these waves may produce disturbances on the outer sides of the valley.

King and Tucker (1984) measured ground motions along transverse longitudinal profiles across the Chusal valley near the Afghanistan border of the former Soviet Union. Interpretation of the response in a series of small ($M_L \leq 4$) earthquakes suggested that one-dimensional ground response analyses could predict the average response of sediments near the center of the valley but not at the edges. Significant differences between the amplification functions at the center and edges of the valley were observed, explaining why the motions at those locations were considerably different. Similar effects have been observed for other valleys (e.g., Caracas in 1967, San Fernando in 1971, and Leninakan, Armenia in 1988) in different earthquakes.

Bard and Bouchon (1985) proposed an empirical formula, plotted in **Figure 2.8**, that can be applied to sine-shaped valleys in order to recognize the possible presence of such 2D valley effects:

$$\frac{h}{l} = \frac{0.65}{\sqrt{C_v - 1}}$$

where C_v is the soil-bedrock velocity contrast, l is the half width of the valley and h is the thickness of the soil deposit. Such a curve can be interpreted as an empirical boundary between truly 2D valley effects, in the upper part of the plot, and side effects that are focused at the valley edges which are coupled to 1D behavior, in the lower part of the plot. However, it is worth noticing that this curve has been derived from numerical simulations of propagation of P and S waves under simplified hypotheses on soil behavior and valley geometry. The curve of Figure 2.8 has been obtained with sine-shaped valleys only, but may be shown (Bard, 1983) to be valid also for any valley shape, provided that the real shape ratio h/l be replaced by an "equivalent" shape ratio h/2w where 2w is the total width over which the sediment thickness is more than half its maximum value.

Moreover, Bard and Bouchon (1985) predicted the 2D resonance frequency of a soft rectangular inclusion. **Figure 2.9** shows the dependence of the dimensionless frequency f_o/f_h on the shape ratio for incoming SH, SV, and P waves (f_h is the 1D frequency and f_o the fundamental 2D resonance frequency), provided that the equivalent width 2w is chosen equal to the valley half-width I. This relation can be extended to any valley shape, taking as equivalent width 2w the length over which the local sediment thickness is greater than half the maximum thickness (Bard, 1983). It can be concluded that for deep and narrow valleys the 2D resonance frequency can be quite larger than the 1D fundamental frequency, especially for SH and SV waves.

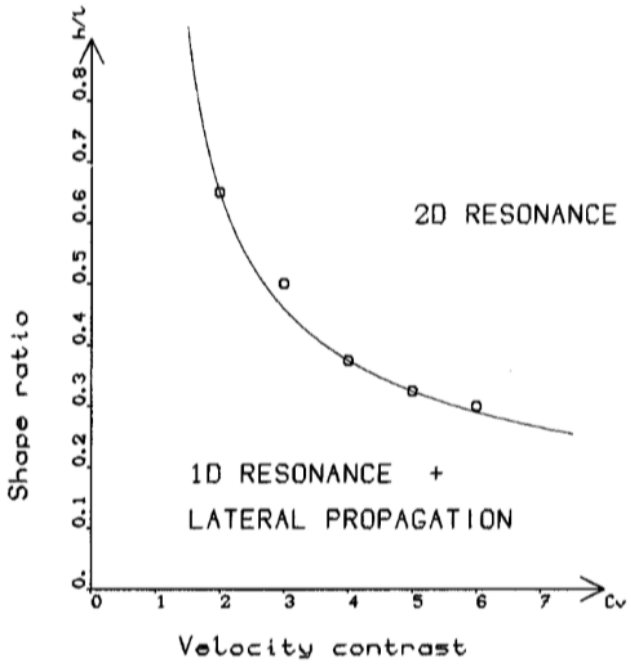

Figure 2.8: Velocity contrast vs shape ratio diagram for detecting conditions for the 2D valley effects (Bard and Bouchon, 1985).

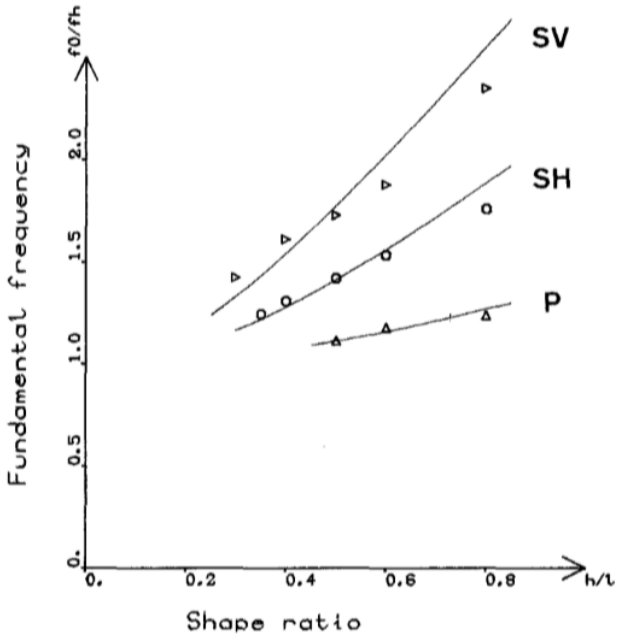

Figure 2.9: Dependence of the dimensionless frequency f_o/f_h on the shape ratio for the SH, SV, and P fundamental modes (Bard and Bouchon, 1985).

Bard and Gariel (1986) used an analytical approach to study the two-dimensional response of shallow and deep alluvial valleys. By comparing computed amplification functions for the two-dimensional case with those based on the assumption of one-dimensional wave propagation, the accuracy of the one-dimensional assumption could be demonstrated. As shown in **Figure 2.10a**, the 1-D and 2-D amplification functions at the center of a shallow, flat valley (Station 8) were quite

similar, which indicates that 1-D analyses would be appropriate in this area. Closer to the edge of the valley (Station 4), however, the amplification functions were considerably different. For the deep valley shown in **Figure 2.10b**, agreement between the 1-D and 2-D amplification functions was much better at the center of the valley than near the edges, but was not as good as for the shallow valley. For alluvial valleys with irregular shape, such combined concave/convex regions, theoretical studies (e.g., Rial et al., 1992) indicate that very complex, even chaotic, motions can result.

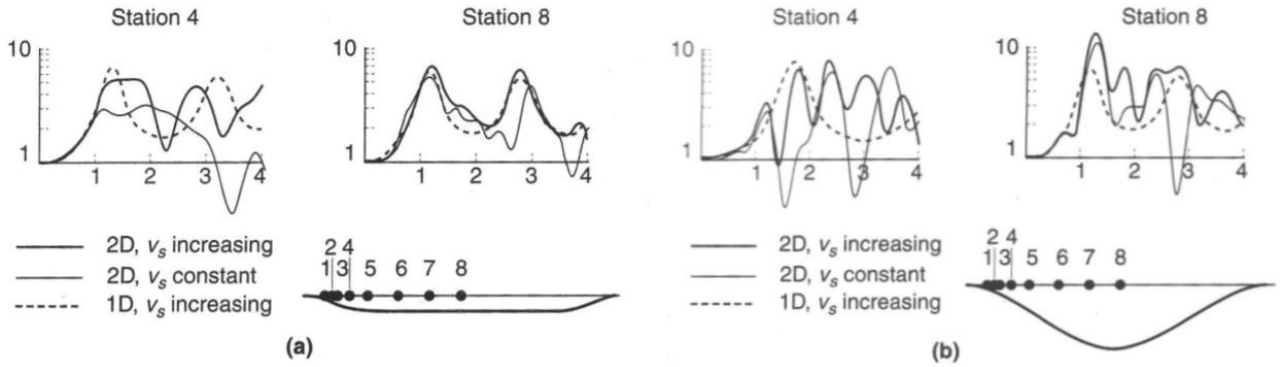

Figure 2.10: Comparison of amplification functions for 1-D and 2-D analyses of (a) shallow, flat basin, and (b) deep basin (Bard and Gariel, 1986).

Later on, Silva (1988) summarized the effects of topographic and subsurface irregularities with comments on their quantitative predictability, as presented in **Table 2.1**. He suggested to define as 'shallow' valleys those with a shape ratio less than 0.25 and as 'deep' valleys those with SR values greater than 0.25, where SR is defined as the ratio between the thickness of the soil at the centre of the valley and the half width of the basin.

Table 2.1: Effects of topographic and subsurface irregularities (after Silva 1988, modified).

Structure	Conditions	Effects	Most suitable quantitative predictions
Shallow and wide soil filled valley (depth/ half width: H/ L<0.25)	Effects most pronounced near edges; largely vertically propagating shear waves away from edges	Broadband amplification near edges due to generation of surface waves	One-dimensional model may under-predict at higher frequencies by about 2 near edges
Deep and narrow soil filled valley (H/ L>0.25)	Effects throughout valley width	Broadband amplification across the valley due to whole valley modes	One-dimensional model may under-predict for a wide bandwidth by about 2 to 4; resonant frequencies shifted from one dimension

Graves (1993) modeled successfully the characteristics in the Marina District of San Francisco during the 1989 Loma Prieta earthquake that the usual one-dimensional analysis was unable to model the motions. He showed that the wave that enters the layer may resonate in the layer, but cannot become trapped for the case of one-dimensional wave propagation as shown in **Figure 2.11**.

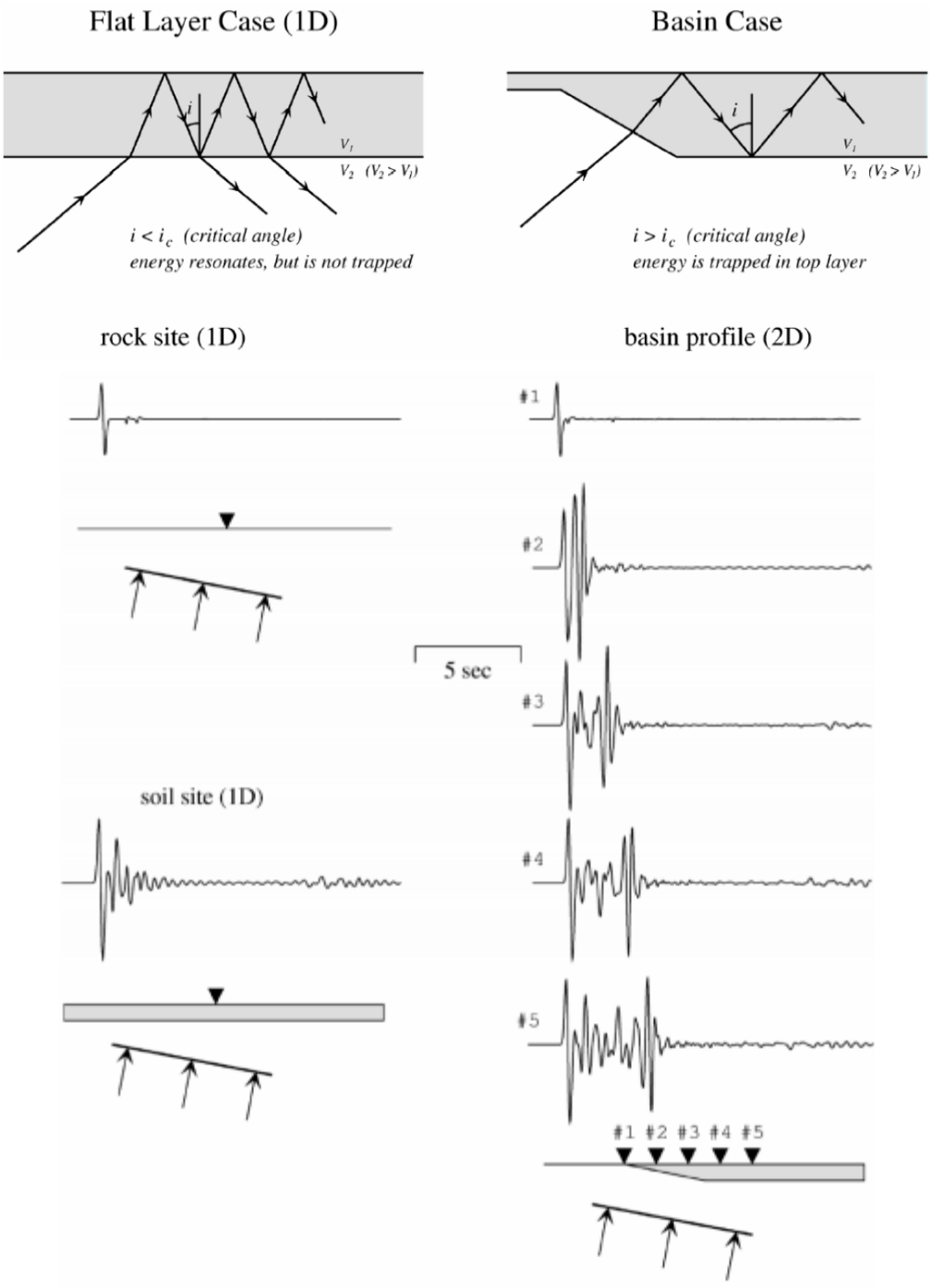

Figure 2.11: Reflection of seismic waves (Graves, 1993).

In the two-dimensional case, Graves (1993) found that if the wave is propagating in the direction in which the basin is thickening and enters the basin through its edge, it can become trapped within the basin if post-critical incidence angles develop. The resulting total internal reflection at the base of the layer is illustrated at the top right of **Figure 2.11**. In the lower part of **Figure 2.11**, simple calculations of the basin response are compared with those for the simple horizontal layered

model. In each case, a plane wave is incident at an inclined angle from below. The left side of the figure shows the amplification due to impedance contrast effects that occurs on a flat soil layer overlying rock (bottom) relative to the rock response (top). A similar amplification effect is shown for the basin case on the right side of **Figure 2.11**. However, in addition to this amplification, the body wave entering the edge of the basin becomes trapped, thus generating a surface wave that propagates across the basin.

More recent weak motion studies by Hartzell et al. (2000) have shown that in some cases, one-dimensional modeling is capable of accounting for observed amplification at intermediate to low frequencies (f < 2 Hz). However, in other cases two-dimensional and three-dimensional models are necessary to explain observed amplification levels, particularly when the measure of amplification is sensitive to duration. Hartzell et al. (2000) suggested that use of the two-dimensional and three-dimensional models is necessary for locations near a steeply sloping basin edge.

Results obtained by Field et al. (2000) for sites in the Los Angeles basin stated that amplification increase significantly with basin depth, with representative results for peak ground acceleration (PGA) and 1.0 sec period spectral acceleration (1.0-sec SA) shown in **Figure 2.12**. The amplification factors are defined relative to the prediction appropriate to each site class (i.e., not relative to a particular geologic formation).

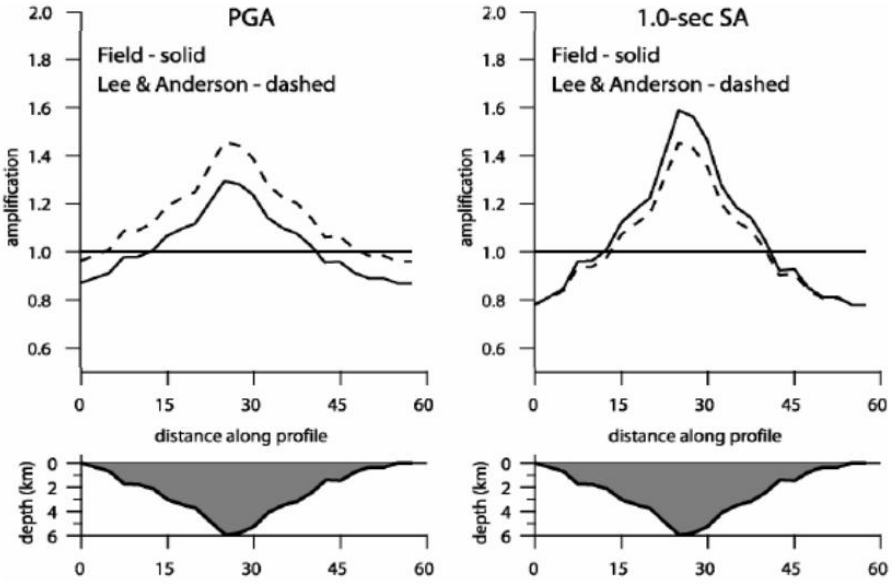

Figure 2.12: Basin depth amplification factors implied by the attenuation relationships by Lee and Anderson (2000) and Field (2000) for sites along cross section through Los Angeles basin (Field et al., 2000).

Faccioli et al. (2002) examined valley effects using weak motion data recorded in three Alpine valleys in Northern Italy. After the analyses, two aspects of the ground response were highlighted. The first one was that the dominant frequencies of motions, corresponding to the peaks of amplification functions, seem mostly controlled by the one-dimensional response of the local

sedimentary soil column. Hence, in the case of weak or moderate ground motions, the frequencies in question can be estimated with sufficient accuracy by simple tools if deep geotechnical borings and/or reliable geophysical surveys (e.g. seismic reflection profiles) are available for depicting the layer structure and estimating the S wave propagation velocities. The second aspect, however, was that 1D wave propagation models cannot account for the magnitude of the amplification and the width of the relevant frequency band observed in weak motion records. In some cases the 2D models can provide a satisfactory explanation of the observed behavior, while in other ones they also are inadequate. Possibly, only by bringing into the picture the full 3D geometry can one expect to improve the accuracy of the numerical simulations.

The influence of bi-dimensionality on the response of the alluvial valleys was also studied by Gatmiri et al.(2008). For this purpose, acceleration responses of filled valleys were compared with the responses of 1-D column of soil. The height of the 1-D reference column was chosen equal to the thickness of the sedimentary layer under the observation point considered on the surface of the filled valley. Their main results can be summarized in the following:

1. The intensity of the ground shaking may be amplified at certain locations more than what 1-D wave theory predicts. Such aggravation may be observed not only on the amplitude of the ground shaking (in terms of peak ground acceleration or velocity), but on its spectral content as well.
2. The spatial variability of the ground surface motion may be substantial, even for closely-spaced locations characterized by the same soil profile. The ensuing differential motions are usually of great interest on the seismic response of long structures such as bridges and pipelines.
3. The maximal amplification is reached at the central point of the valleys.
4. In the central zone of valleys, results provided by 1-D analysis can be used to estimate the spectral acceleration response of a filled valley.

Gelagoti et al. (2010) examined the sensitivity of 2D wave effects to crucial problem parameters, such as the frequency content of the base motion, its details and soil nonlinearity, utilizing a soft shallow alluvial valley as a test case. **Figure 2.13** depicts the spatial distribution of the aggravation factor $AG=A_{2D}/A_{1D}$ (defined as the ratio of peak ground accelerations from the 2D and 1D analyses) along the valley surface for three Ricker wavelets and three different damping ratios (ξ=2%, 5% and 10%). They proved that in the case of high-frequency seismic excitation, 1D soil amplification is prevailing at the central part of the valley (AG≈1), while strongly 2D phenomena are restricted at the corners, where trapping of obliquely incident body waves amplifies the motion, resulting in aggravation of AG≈1.3. On the other hand, for low-frequency seismic excitations, the wavelength becomes too large to be affected by the topographic anomaly (i.e., the slope of the supporting bedrock), and focusing effects are overshadowed by the horizontally propagating surface waves, leading to a shift of the location of the maximum AG toward the center of the valley. The increase of damping ξ mainly influences surface wave propagation, reducing AG toward the center of the valley. Yet it does not appear to have any effect on AG at valley edges.

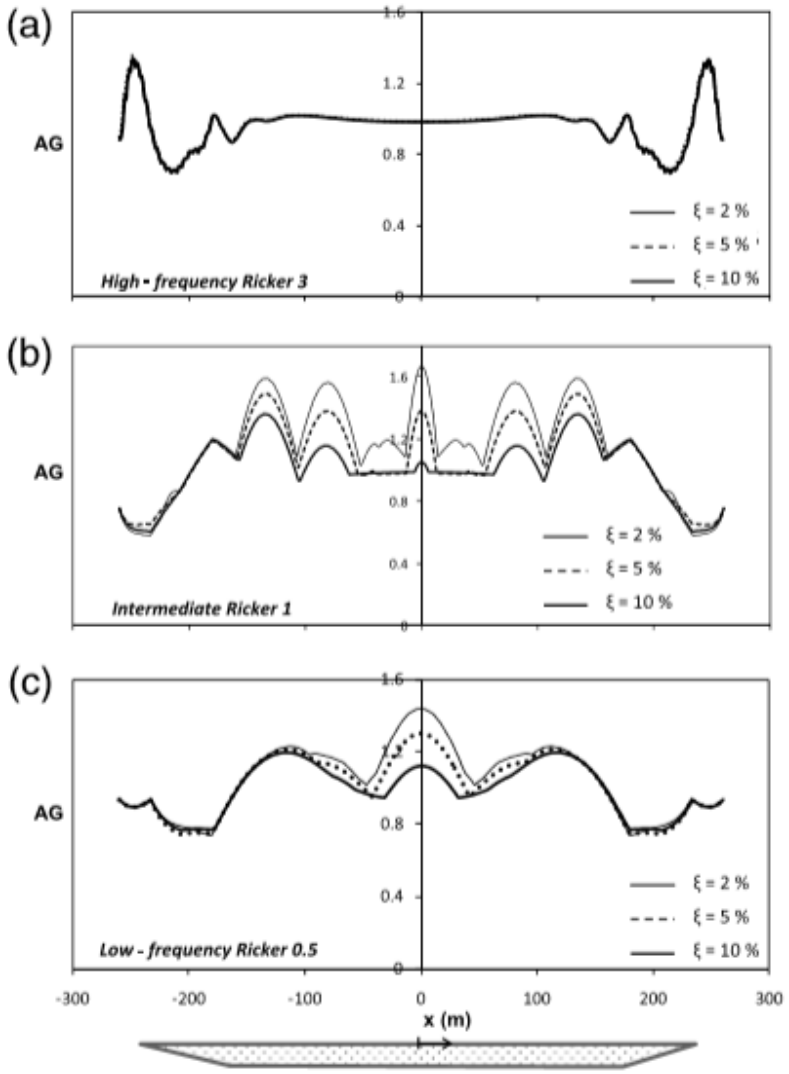

Figure 2.13: The effect of damping ratio–elastic analysis. Distribution of the aggravation factor AG along the valley surface for ξ=2%, 5%, and 10% for: (a) the high-frequency Ricker 3 wavelet, (b) the intermediate Ricker 1, and (c) the low-frequency Ricker 0.5 (Gelagoti et al., 2010).

Papadimitriou et al. (2011) also performed parametric numerical analyses in an attempt to start quantifying basin effects. The analyses performed in 2D symmetric trapezoidal valleys with uniform soil and rock conditions under vertically incident SV waves. The horizontal and vertical geomorphic aggravation factors Ah and Av respectively are defined at each location of the ground surface, as the ratio of the PHA over the value of PHA from the appropriate 1D analysis (PHAs if the location sits on soil or PHA_r if it sits on outcropping rock). They found out that the important problem parameters are the normalized valley width B/λ and thickness λ/H, as well as the impedance ratio $a=(\rho_s V_s)/(\rho_b V_b)$, where ρ and V are the density and shear wave velocity of the soil (s) and outcropping bedrock (b). Other parameters, of lesser importance, are the slope inclination i at the valley boundaries and damping ξ. The effects of λ/H, B/λ and a on Ah and Av along the ground surface of trapezoidal valleys, with the horizontal distance x normalized over B are presented in

Figures 2.14-2.16. It can be concluded that geomorphic aggravation generally decreases with increasing values of B/λ, λ/H and a. In other words, geomorphic aggravation is significant for narrow and thick valleys, especially when the soil is relatively much softer than the bedrock. In general, in narrow and thick valleys the peak horizontal aggravations are observed in the center of the valley. As the valley becomes wider and/or thinner, the location of peak horizontal aggravation shifts gradually towards the vicinity of its boundaries. Also, the location of peak vertical aggravation does not coincide with that of the peak horizontal.

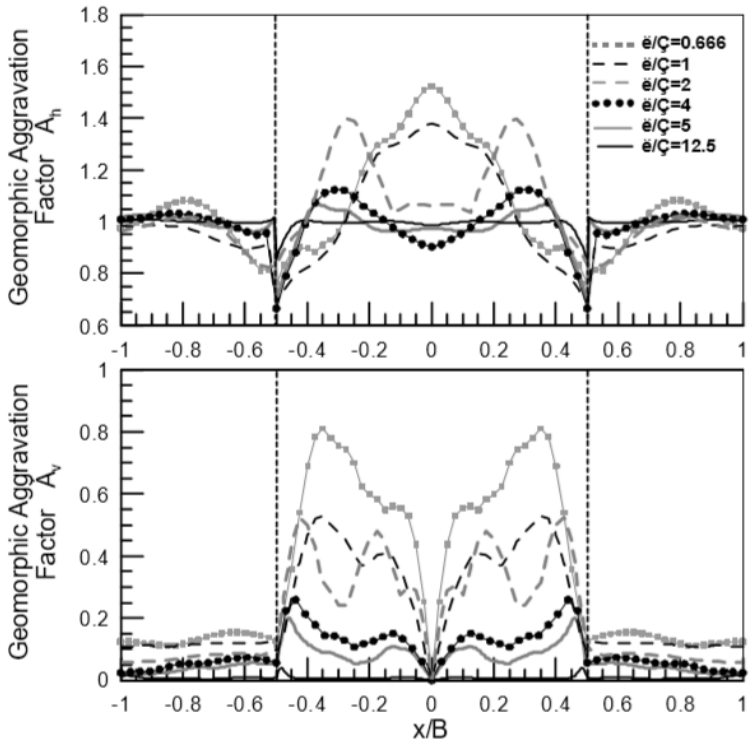

Figure 2.14: Effect of normalized ratio λ/H on the spatial variability of Geomorphic Aggravation Factors Ah and Av along the ground surface of trapezoidal valleys, with the horizontal distance x normalized over B (common B/λ=4, i=45^o, a=0.5, ξ=5%) (Papadimitriou et al., 2011).

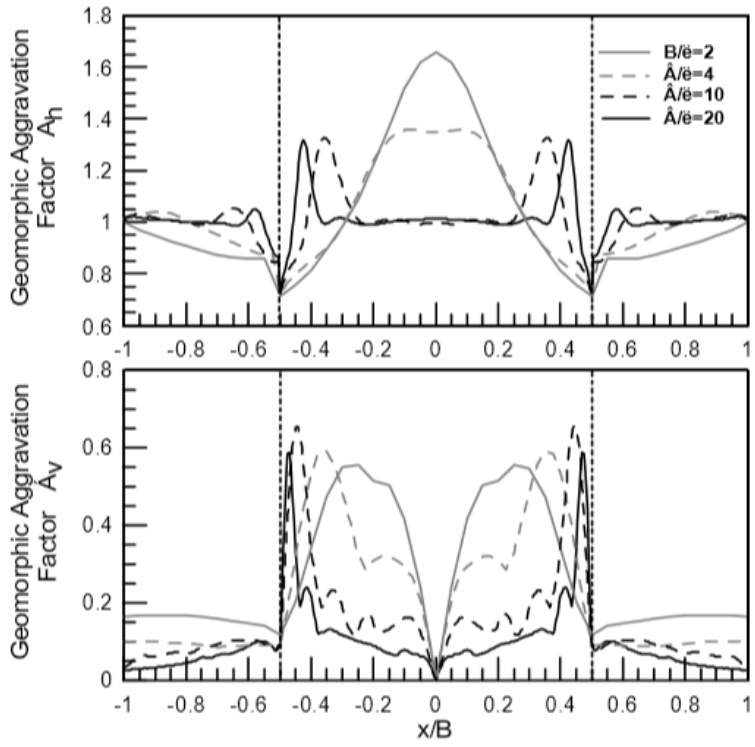

Figure 2.15: Effect of normalized width B/λ on the spatial variability of Geomorphic Aggravation Factors Ah and Av along the ground surface of trapezoidal valleys, with the horizontal distance x normalized over B (common λ/H=1, i=45^o, a=0.5, ξ=5%) (Papadimitriou et al., 2011).

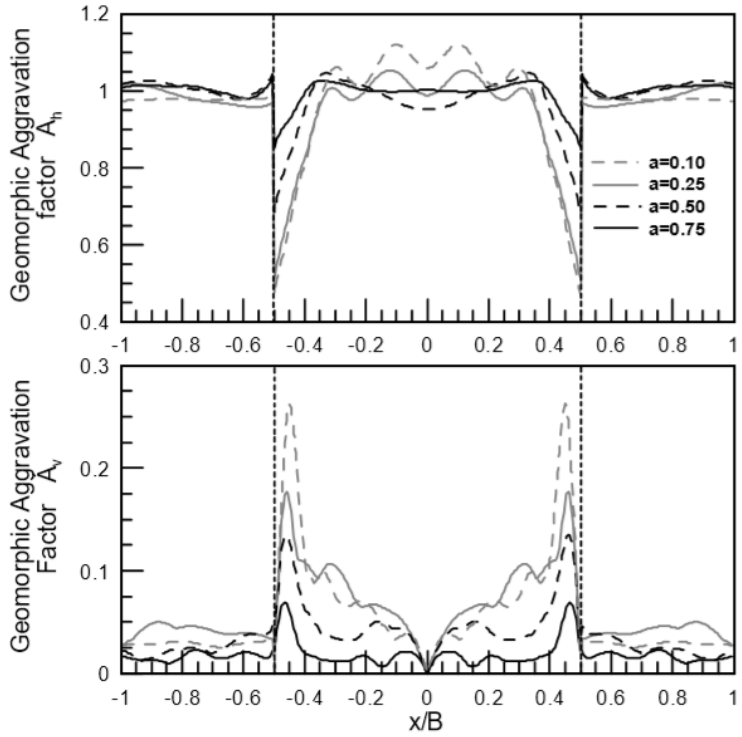

Figure 2.16: Effect of impedance ratio a on the spatial variability of Geomorphic Aggravation Factors Ah and Av along the ground surface of trapezoidal valleys, with the horizontal distance x normalized over B (common B/λ=4, λ/H=5, i=45°, ξ=5%) (Papadimitriou et al., 2011).

2.3 Overview of topography effects on seismic ground motion

It is often reported after destructive earthquakes in hilly areas that buildings at the top of massive crests suffer more intensive damage than those located at the base. Stewart (2001) categorized the two-dimensional surface geometries as ridges, canyons and slopes as shown in **Figure 2.17**. Numerous studies have investigated topographic effects for an isolated, two-dimensional, homogeneous ridge, canyon and slope on the surface of a homogeneous half space.

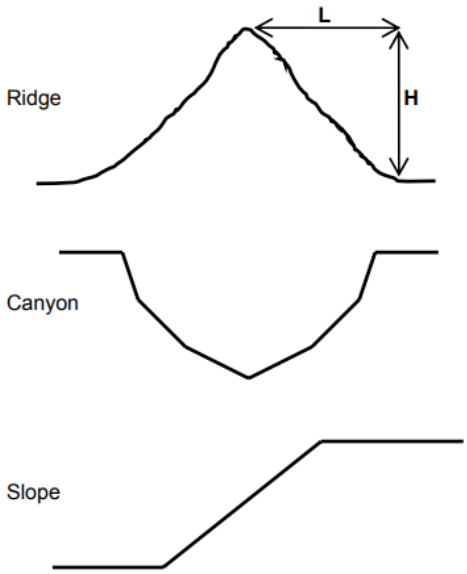

Figure 2.17: Generalized 2D geometries of irregular surface topography (Stewart, 2001).

Pioneering work on the subject was accomplished by Aki and Larner (1970) who introduced a numerical method based on a discrete superposition of plane waves. This method was later extended by other investigators such as Boore (1972), Bouchon (1973), Bard (1982) and Geli et. al. (1988). Useful results were also reported by Wong and Trifunac (1974), Wong (1982) and Sanchez-Sesma et al. (1985). It is worth mentioning that when comparing observed and theoretically predicted amplifications of surface motions due to surface topography, it is usually found that the observed values are much greater than the predicted ones. Thus, the observed amplifications range from 2 to 20 in the spectral domain and from 2 to 5 in the time domain. The difference between predicted and observed values is attributed to the influence of 3-D effects which are beyond the scope of this study.

Boore (1972) used the finite difference method to simulate the propagation of a transient SH-disturbance incident on a non-planar free surface. Spectral ratio results for one of the tested model topographies are presented in **Figure 2.18**. Each shows an amplification at the crest of the ridge and an oscillating amplification to de-amplification pattern on the ridge flanks. Furthermore, the amplification results tend to unity as the frequency decreases. Although in all tested models an amplification was always observed at the ridge crest, the complicated pattern on the ridge flanks cautions against making general conclusions about amplifications at ridge crests. The important

result was that topography can cause significant amplifications (approaching 100 %) and can influence motion of surprisingly long wavelength (25 % amplification when λ/l = 6, where λ = wavelength and l = scale length, chosen as the half-width of the mountain in this case).

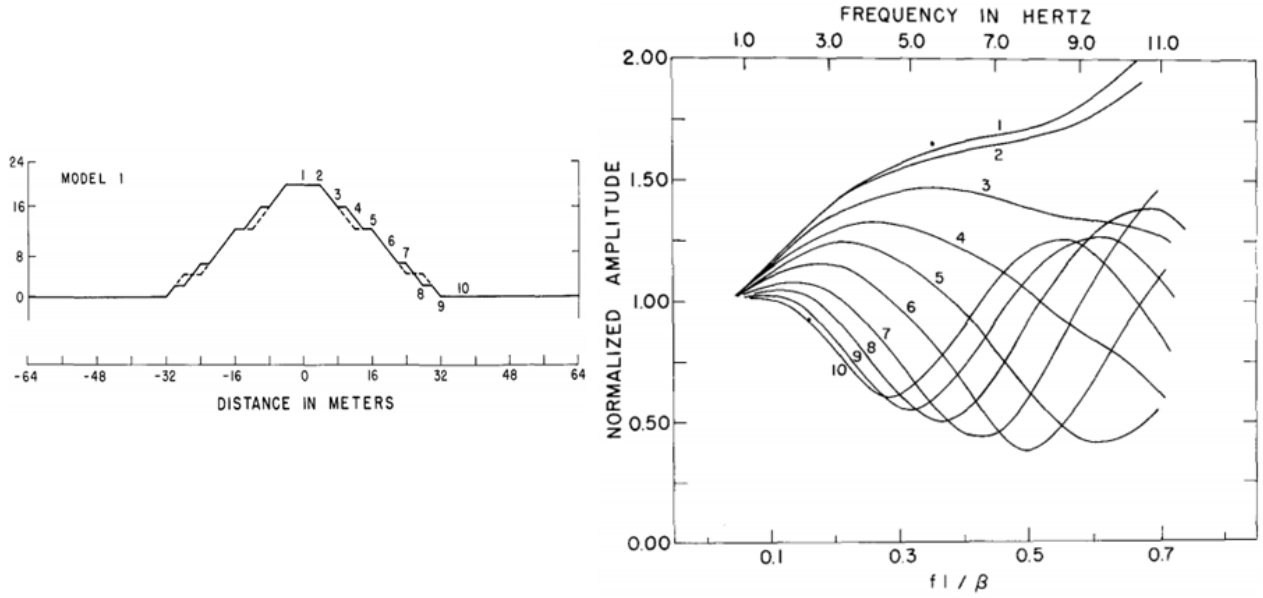

Figure 2.18: Spectral ratio results for one of the tested geometries at various localities along the surface. Upper frequency scales represent assumed shear velocity of 500 m/sec (Boore, 1972, modified).

Bouchon (1973) studied the effect of topography on surface motion in the cases of incident SH, P and SV waves by using the Aki and Larner (1970) method. Several types of topography ranging from a ridge to a valley were used. Different incidence angles were considered for a wavelength interval extending from 2h to 20h, where h is the vertical dimension of the topographic anomaly. Bouchon (1973) found that, the surface displacement appears to be very much influenced by surface irregularities. He also stated that, in the case of a ridge, a zone of amplification took place near the top, whereas, a zone of attenuation occurred near the bottom.

After the 1971 San Fernando earthquake, Trifunac (1973) and Wong and Trifunac (1974) studied the effect of canyon geometry on ground motion assuming linear-elastic medium and simple canyon geometry such as a semi-cylinder or a semi-ellipse. A general overview of ground motion variations across a simplified canyon geometry was provided by Trifunac (1973) as shown in **Figure 2.19**. Trifunac (1973) indicated the ground motion amplitude at various locations across a canyon as a function of normalized frequency η = 2a / λ for vertically incident SH waves (where λ is the wavelength and a is the radius of the semi-cylinder canyon). He found that amplification is strongly frequency dependent and becomes significant when wavelengths are similar to or smaller than the canyon dimension. Maximum amplification was found equal to 1.4 and occurred near the canyon edge and remained approximately constant for η > 0.5, while the maximum base de-amplification was reported as 0.5. He also found that if the same canyon geometry is subjected to an inclined SH wave arriving from the left, wave trapping on the left side of the canyon wall would cause higher

amplification levels than on the right side, with amplification levels as high as being possible for horizontally propagating waves. Similar studies for P and SV waves were performed by Wong (1982) and Lee and Cao (1989) and indicated amplification levels generally smaller than those for SH waves.

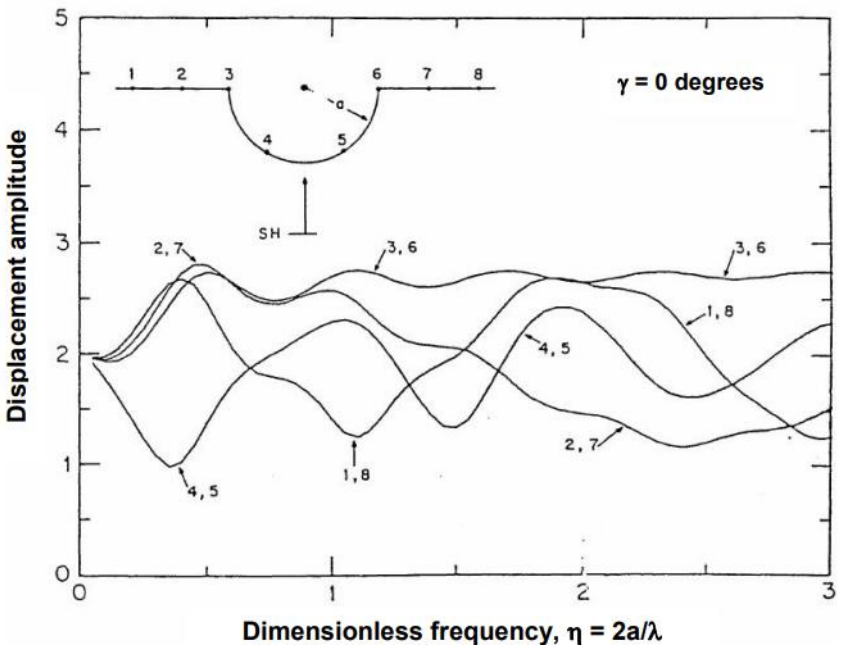

Figure 2.19: Amplification at various locations across a canyon as a function of normalized frequency subjected to vertically incident SH waves (Trifunac, 1973).

Boore et al. (1981) studied the effect of a cliff slope to the dispersion of the incident waves. For incident S-waves, there is higher dispersion at the crest when compared to the dispersion at the toe, both for vertical slopes as well as for 45^{o} slope angles. For incident P-waves, the dispersion is higher for vertical slopes than for 45^{o} slope angles, whilst higher dispersion is observed at the toe of the cliff. Finally, for both slope angles (45^{o} and 90^{o}), it is observed that dispersion of S-waves results to Rayleigh waves with broader bandwidth than Rayleigh waves from P-wave dispersion. They also predict dispersive Rayleigh waves with amplitudes approximately 40% of the amplitude of the corresponding incident wave (P or SV) at the free-field surface, for wavelengths λ somewhat larger than the height H of the vertical slope.

Aki (1988) used a simple structure of a wedge-shaped medium to illustrate the effects of topography, **Figure 2.20a**. An exact solution exists for SH waves propagating normal to the ridge and polarized parallel to the ridge axis, which predicts a displacement amplification at the vertex equal to 2/v, where the ridge angle is vπ (0 < v < 2). Faccioli (1991) used this triangular wedge structure to model approximately ridge-valley topography, as shown in **Figure 2.20b**. This simple model predicts an amplification at the crest relative to the base and may be used for rough numerical estimates of amplifications at the crest of ridges or de-amplifications at the bottom of valleys or canyons.

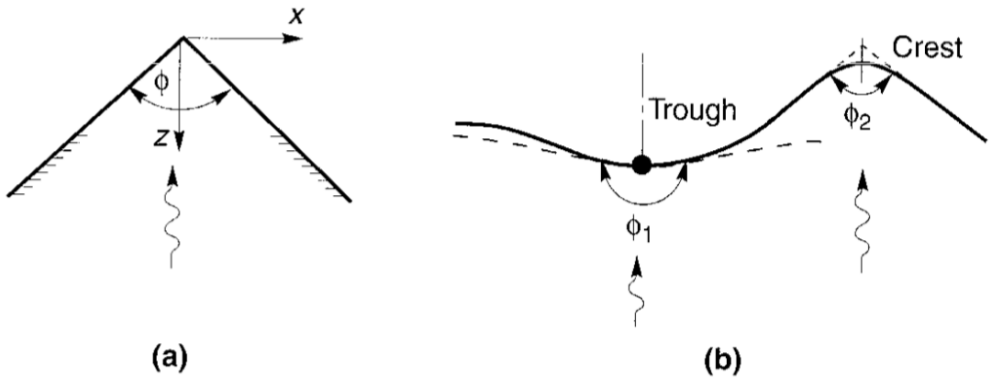

Figure 2.20: Characterization of simple topographic irregularities: (a) notation for a triangular wedge; (b) approximation of actual ground surface (solid line) at trough and crest by wedges (After Faccioli, 1991).

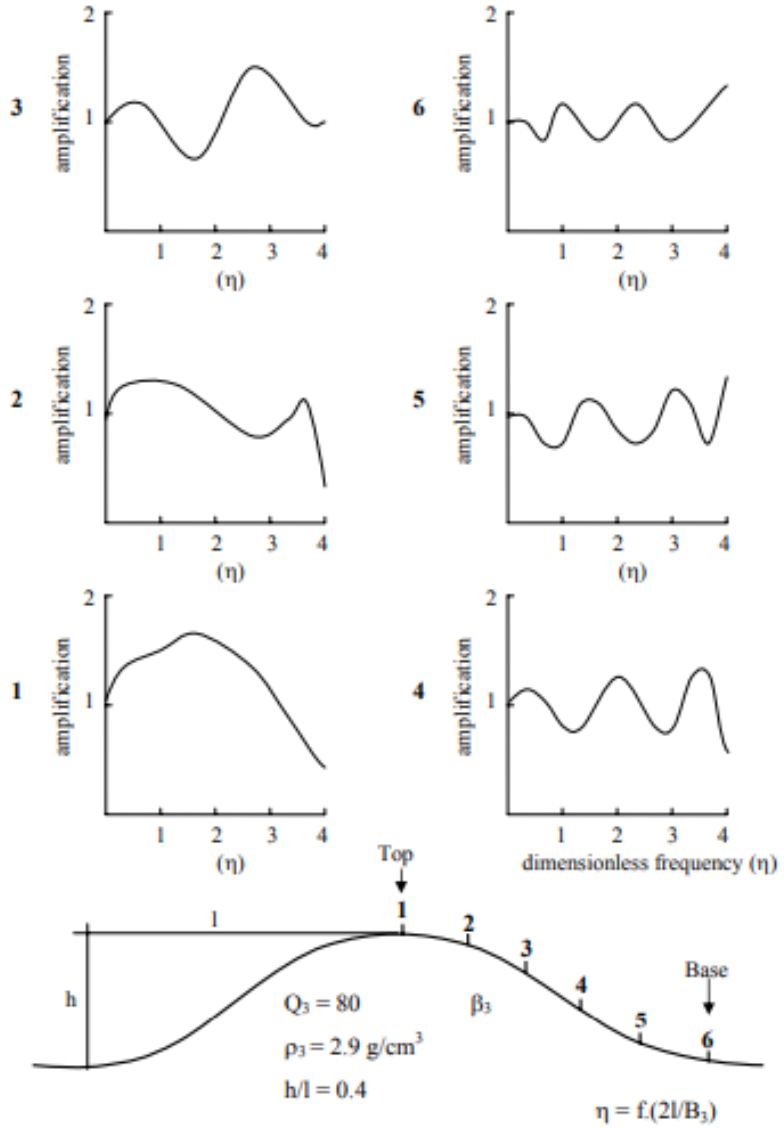

Figure 2.21: Amplification as a function of normalized frequency across ridge subjected to vertically incident SH wave (Geli et. al., 1988).

Geli et al. (1988) and Bard (1995) from 11 analytical studies found that, levels of crest-to-base time-domain amplification (i.e. ratios of peak motions) vary between 1 and 2 (average ≈ 1.5) for shape ratios h/l ≈ 0.4 subjected to vertically incident SH waves as illustrated in **Figure 2.21**. Broadband crest amplification is maximized at dimensionless frequency η = 2L/λ = 2, which corresponds to a wavelength (λ) equal to the ridge half-width. The maximum spectral acceleration is about 1.6 for this case. Geli et al. (1988) found that amplification is generally lower for incident P waves than S waves, while the amplification is slightly greater for horizontal in-plane motions as compared to out-of-plane motions. According to Pedersen et al. (1994) although simple and repeatable trends in the results could not be identified, amplification is also sensitive to the angle of incident wave field with respect to the vertical direction.

Ashford and Sitar (1997) examined the effect of inclined shear waves on the seismic response of a steep bluff using generalized consistent transmitting boundaries. The response of the stepped half-space to inclined SH waves is presented in **Figure 2.22**. In each case, the response due to the wave traveling into the slope is greater than for the wave angle traveling away from the slope. For all angles considered, waves traveling into the slope result in greater amplification than for vertically propagating waves, and this effect increases with increasing frequency. The first peak of amplification occurs at H/λ = 0.2 and increases from 25% for the vertically propagating wave to nearly 70% for a wave inclined at 30°. The opposite is true for waves traveling away from the slope. The motion is attenuated with increasing incident angle, and the attenuation increases with frequency. At H/λ = 0.2, the response is the same as that for the free field for inclinations of 20° and 30°. Though greater amplification and attenuation was observed at higher frequencies for waves traveling into and away from the slope, respectively, these motions tend to get damped out at higher levels of damping (Ashford and Sitar, 1994).

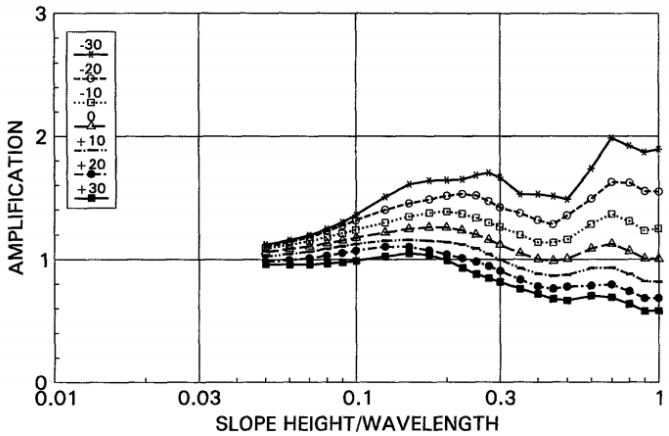

Figure 2.22: Amplification at the crest of a vertical slope subjected to inclined SH waves incident from - 30 ° to + 30 °. Amplification expressed as the ratio between the transfer function at crest to transfer function in the free field behind the crest (Ashford and Sitar, 1997).

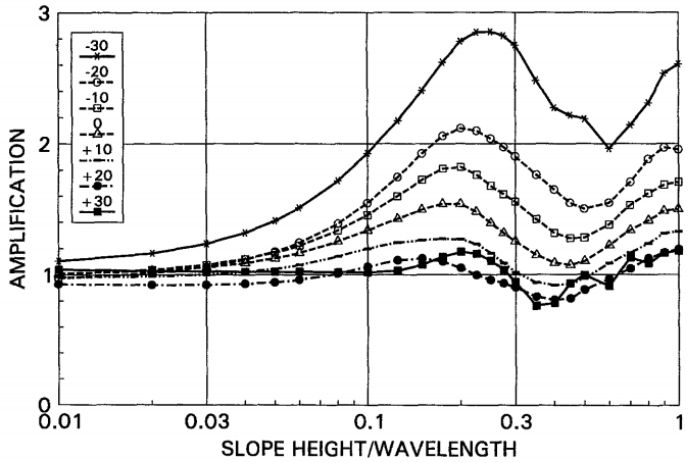

Figure 2.23: Horizontal amplification at the crest of a vertical slope for inclined SV wave incident from - 30 ° to + 30 ° (Ashford and Sitar, 1997).

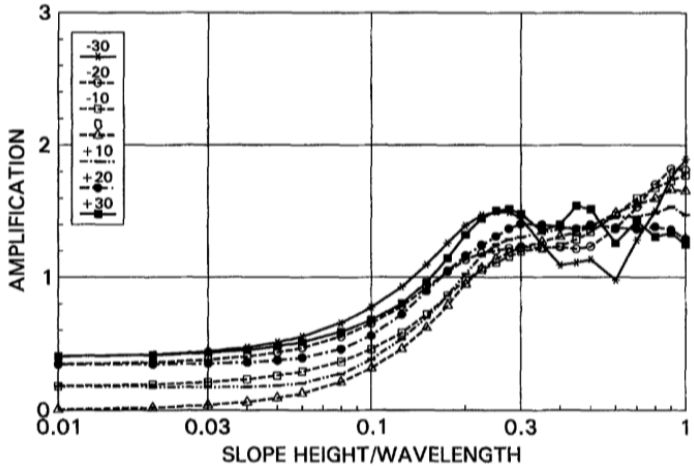

Figure 2.24: Vertical amplification at the crest of a vertical slope for inclined SV wave incident from - 30 ° to + 30 °(Ashford and Sitar, 1997) .

The horizontal response of the stepped half-space subjected to inclined SV waves is presented in **Figure 2.23**, while the vertical response is presented in **Figure 2.24**. Results similar to those for SH waves are obtained for the horizontal component of the SV wave, except that the amplification is much greater for waves traveling into the slope, in excess of 100%, and there is less attenuation for waves traveling away from the slope. In contrast to the horizontal response, the direction of wave propagation appears to make little difference in the vertical response due to SV waves. This dependency on direction of propagation for horizontal, but not vertical, response is in general agreement with results of Pedersen et al. (1994b). There is a notable increase in the vertical response due to SV waves at low frequencies, which increases with incident angle independent of the direction of propagation, due to wave splitting on the free surface.

Stewart and Sholtis (1999) evaluated topographic effects across a slope face from strong motion data, with appropriate corrections for ground response variability. In their study the data obtained from the 1983 Coalinga main shock and two aftershocks (M=6.4) was used. The investigated site had recordings above and below a 21 m high cut slope. Crest amplification of 5% damped

acceleration response spectra identified from the three recordings are presented in **Figure 2.25**. The maximum crest amplification is about 1.2, which is reasonably consistent with the results obtained by Ashford and Sitar (1997) and Ashford et al. (1997).

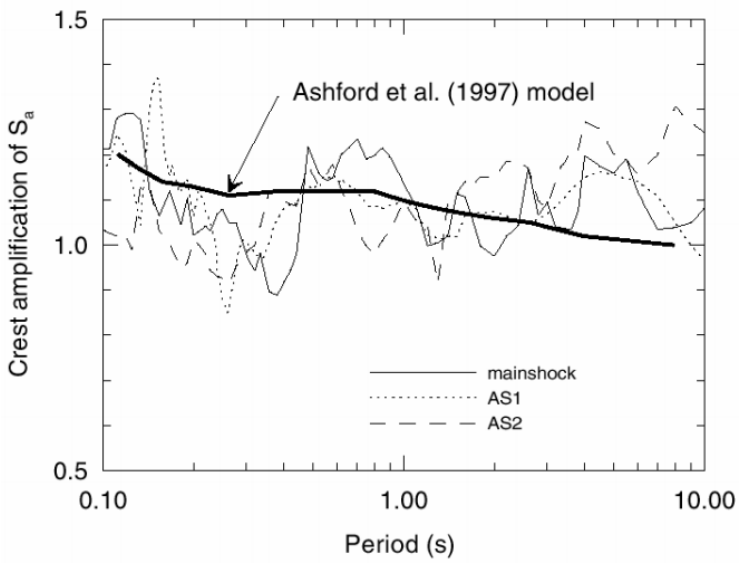

Figure 2.26: Amplification at crest of a 21m tall, 3H:1V cut slope for vertically incident waves (Stewart and Sholtis, 1999).

Bouckovalas and Papadimitriou (2005) performed numerical analyses with the Finite Difference method for linear visco-elastic soil in order to evaluate the slope topography effects on seismic ground motion. A schematic illustration of the 2D analyzed mesh and the boundary conditions is provided in **Figure 2.26**. The results of the numerical analyses were normalized against the representative free-field response of the ground, which is free from any topographic effects. For this reason, each 2D analysis was supplemented by two 1D analyses: one for the free field in front of the toe of the slope and the other for the free field behind its crest.

Typical results are presented in **Figure 2.27**, for the specific case of uniform soil, slope inclination $i=30^o$, normalized height $H/\lambda=2.0$, critical damping ratio $\xi=5\%$ and six significant cycles of base excitation (N=6). This figure shows the variation of the topography aggravation factors $A_h = a_h/a_{h,ff}$ and $A_v = a_v/a_{h,ff}$ with distance from the crest x, where a_h and a_v denote the peak horizontal and peak vertical accelerations at each point of the ground surface and $a_{h,ff}$ is the free-field value for the peak horizontal acceleration. It was shown that even a purely horizontal excitation (vertically propagating SV wave) results in considerable (parasitic) vertical motion at the ground surface near the slope. Moreover, the topography aggravation of the horizontal ground motion $A_h = a_h/a_{h,ff}$ fluctuates intensively with distance away from the crest of the slope, alternating between amplification and de-amplification within very short horizontal lengths. It was also noticed that the horizontal ground motion is de-amplified at the toe of the slope and amplified near the crest.

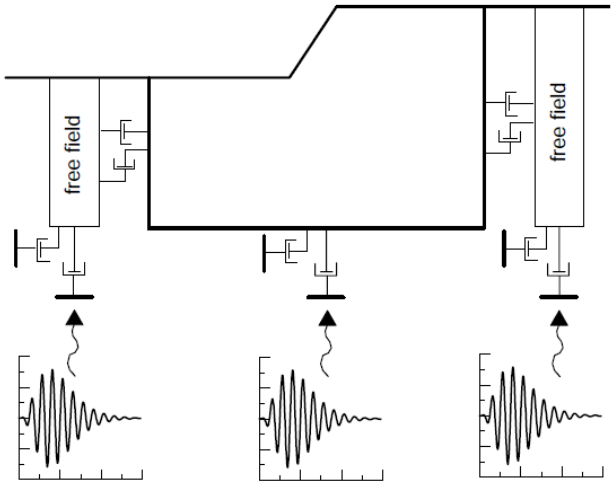

Figure 2.26: Schematic illustration of finite difference model for the numerical analyses of step-like slope topography effects (Bouckovalas and Papadimitriou, 2005).

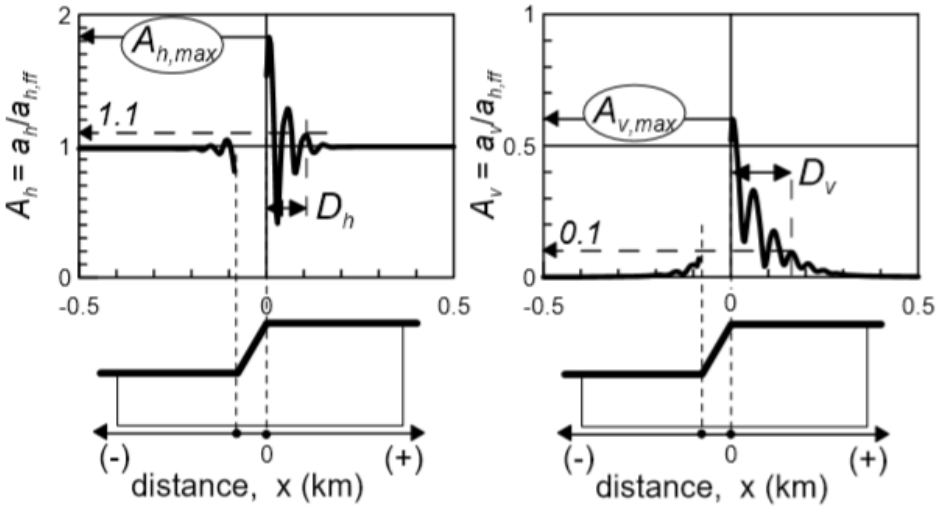

Figure 2.27: Typical results for the topographic aggravation of the peak horizontal A_h and the peak parasitic vertical A_v acceleration, as a function of horizontal distance x from the crest for H/λ=2, i=30^o, N=6, ξ=5% (Bouckovalas and Papadimitriou, 2005).

They also examined the effects of slope angle i, normalized height H/λ, number of significant excitation cycles N and soil damping ξ. It was observed that the increase of the slope angle i and the normalized height of the slope H/λ cause more intense aggravation of the horizontal and vertical ground motions (factors A_h and A_v) and increase the distance to the free field in front and behind the slope (**Figures 2.28 and 2.29**). On the contrary, the hysteretic damping ratio of the soil ξ has a significant effect only on the distance to the free field, while the number of significant excitation cycles N has a relatively minor overall effect. The results in terms of A_h and A_v from analyses for small soil damping ($\xi \leq 5\%$) agree in both qualitative and quantitative terms with the works of Ashford and Sitar (1997) and Ashford et al (1997), as shown in **Figure 2.30**.

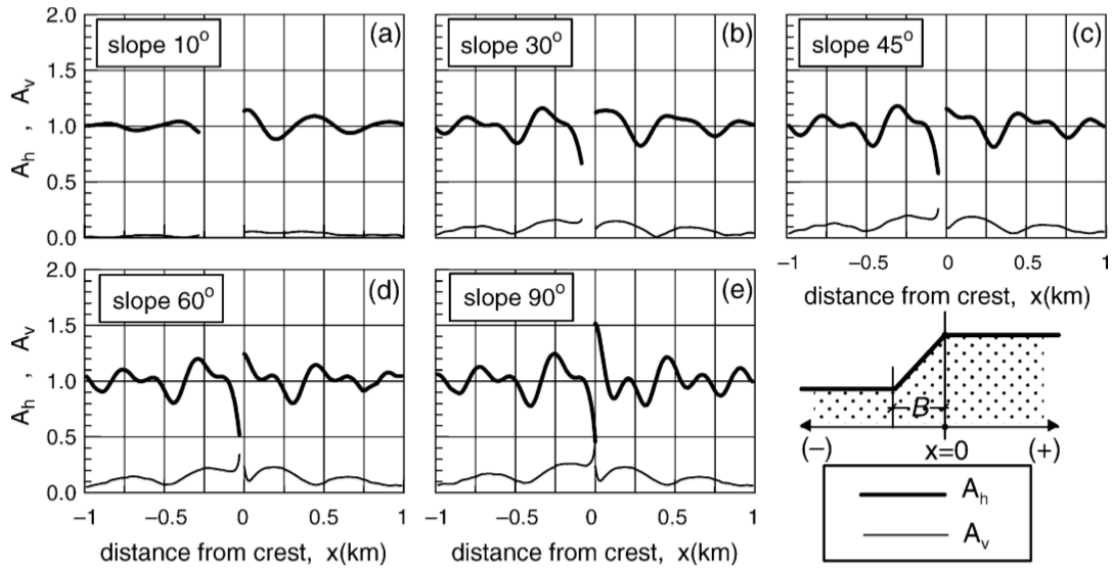

Figure 2.28: Effect of slope inclination i on the amplification of peak horizontal Ah and apparition of parasitic vertical Av acceleration, as a function of horizontal distance x from the crest of a step-like slope (H/λ=0.2, harmonic motion, ξ=5%) (Bouckovalas and Papadimitriou, 2005).

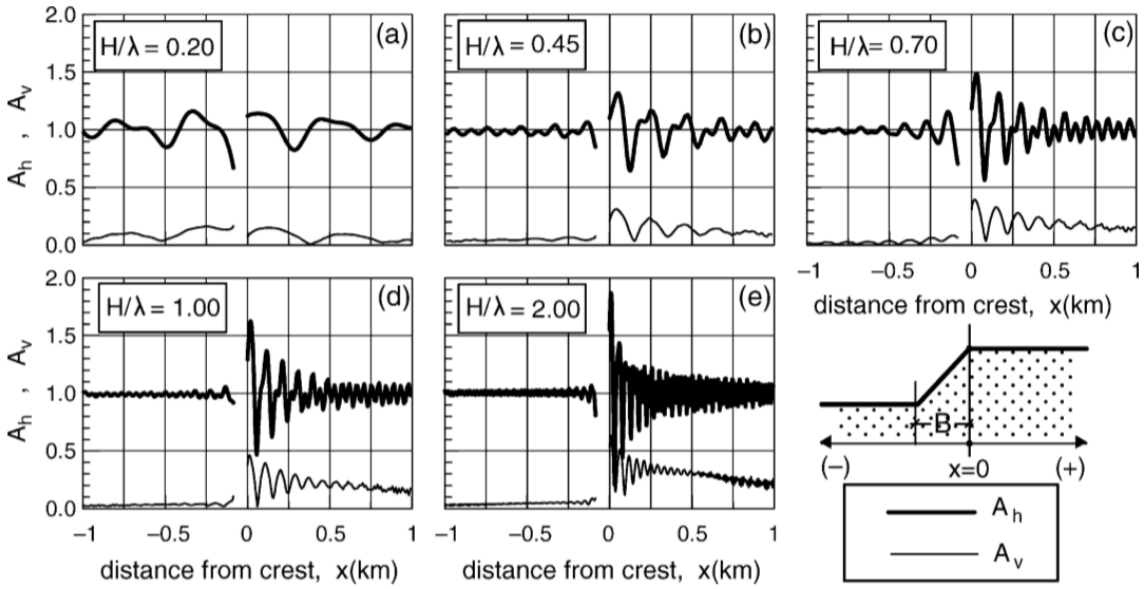

Figure 2.29: Effect of normalized height H/l on the amplification of peak horizontal Ah and apparition of parasitic vertical Av acceleration, as a function of horizontal distance x from the crest of a step-like slope (i=30°, harmonic motion, ξ=5%) (Bouckovalas and Papadimitriou, 2005).

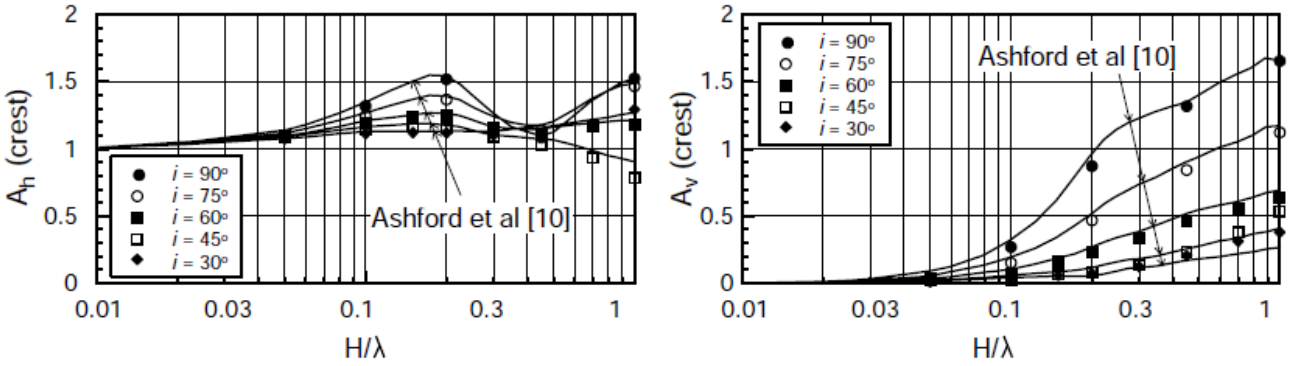

Figure 2.30: Comparison of results from parametric analyses with published predictions for the crest of step-like uniform slopes (ξ=5%, harmonic base excitation) (Bouckovalas and Papadimitriou, 2005).

Based on their previous results, Bouckovalas and Papadimitriou (2006) proposed the following modifications to code provisions of EC-8, for the cases of slopes:

1. Topography aggravation may be neglected, if the average slope inclination i < 17° and the height of the slope H < max[13m, 0.16λ], where λ is the predominant wavelength of the shear waves in the slope.
2. In general, two topography aggravation factors are defined, one for the horizontal and one for the vertical direction, that are denoted as S_{hT} and S_{vT}, respectively.
3. For slopes that are both higher and steeper than the above lower bounds, the topographic amplification factors vary with location. If x is the horizontal distance from the crest of the slope (where x > 0 behind the crest), the amplification factors per location x are given by:

$$S_{hT} = \left\{ \begin{array}{lll} 1.1 + \dfrac{A_{h,max} - 1.1}{B}(x + B) & , & x \le 0 \\ A_{h,max} & , & 0 \le x \le 0.2D \\ A_{h,max} - \dfrac{A_{h,max} - 1.1}{0.8D}(x - 0.2D) & , & 0.2D \le x \end{array} \right\} \ge 1.0$$

$$S_{vT} = \left\{ \begin{array}{lll} 0.1 + \dfrac{A_{v,max} - 0.1}{0.2D}(x + B + 0.2D) & , & x \le -B \\ A_{v,max} & , & -B \le x \le 0.2D \\ A_{v,max} - \dfrac{A_{v,max} - 0.1}{0.5D}(x - 0.2D) & , & 0.2D \le x \end{array} \right\} \ge 0.0$$

where B = H/tani, the horizontal projection of the slope, $A_{h,max}$ and $A_{v,max}$ the coefficients of maximum topographic aggravation for the horizontal and parasitic vertical motions and D is the distances to the free field behind the crest, that are given in simplified form by:

$$A_{h,max} = 0.2(H/\lambda)^{0.4}\left(\frac{I^2 + 2I^6}{I^3 + 0.02}\right)$$

$$A_{v,max} = 0.7(H/\lambda)^{0.8}\left(I^{0.5} + 1.5I^5\right)$$

$$D/H = 2\left[\frac{(H/\lambda)}{(\mathrm{H}/\lambda)^2 + 0.2}\right]\left(\frac{\mathrm{I}^{1.5} + 3.3\mathrm{I}^8}{\mathrm{I}^4 + 0.07}\right)$$

where I = i/90°.

Gatmiri et al. (2008) studied topographic irregularities and considered various examples that cover different 2-D geometries. They examined slopes, canyons and ridges and observed the influence of the ratio of the characteristic dimension of the relief over the wavelength (dimensionless frequency), as well as the slope angle of irregularities. In general, the seismic ground motion was amplified at the crest of ridges, at the upper corner of slopes and at the edges of canyons; it was systematically attenuated at the base of these relieves. The effects of topography were also affected by the slope angle of the relief. Generally, the steeper the slope of the relief was, the more the effects of topography due to this relief were accentuated. As expected, although the input signal was a planar SV wave with vertical incidence, the vertical component of the surface motion was non-zero. The amplitude of this so called parasitic vertical component was comparable to that of the horizontal component. At a distance depending on the exciting frequency and on the dimensions of the topography, the response of the site approached that of the half-space.

For completeness, it is noted here that according to EC-8, for important structures (importance factor > 1.0) topographic amplification effects should be taken into account. Some simplified amplification factors for the seismic action should be used in the stability verification of ground slopes. Such factors, denoted by S_T, are in first approximation considered independent of the fundamental period of vibration and, hence, should multiply as a constant scaling factor the ordinates of the elastic design response spectrum given in EN1998-1. These amplification factors should in preference be applied when the slopes belongs to two dimensional topographic irregularities, such as long ridges and cliffs with height greater than about 30 m (EN1998-1 Annex A). The topography effects may be neglected for average slope angles less than about 15°, while a specific study is recommended in the case of strongly irregular local topography. For angles greater than 15° and topographic reliefs taller than 30 m the following are recommended:

1. Isolated cliffs and slopes: $S_T > 1.2$ should be used for sites near the top edge.
2. Ridges with crest width significantly less than the base width: $S_T > 1.4$ should be used near the top of the slopes for average slope angles > 30° and $S_T > 1.2$ for smaller slope angles.
3. Presence of a looser surface layer: In the presence of a looser surface layer, the smallest S_T value given in (a) and (b) should be increased by at least 20%.
4. Spatial variation of amplification factor: The value of S_T may be assumed to decrease as a linear function of height above the base of the cliff or ridge, and to become unity at the base. There is no reference to what happens behind the crest of the topographic relieves.

2.4 Coupling of topography and valley effects on seismic ground response

Topographic and valley effects have so far been studied separately in the literature and has helped us understand the main mechanisms of the problem. For example, most analytical and numerical studies for valley effects (e.g Bard and Bouchon, 1985) assumed valleys with flat horizontal surface. Nevertheless, in real cases the slopes at the edges of a valley usually extend higher than the surface of the valley. Thus, a topography-valley interaction can be observed, leading to different ground response than what a flat horizontal ground surface yields. This more realistic approach has been the subject of some recent publications outlined below.

Gatmiri and Foroutan (2012) performed a numerical analysis on the seismic site effects due to local topographical and geotechnical characteristics using a hybrid code, combining finite elements in the near field and boundary elements in the far field. The shapes of the studied valleys were triangular, trapezoidal and rectangular. As can be seen in **Figure 2.31**, valleys are characterized by their half width at the surface, L, at the base, L_1, and their depth H. The sediment depth is characterized by H_1.

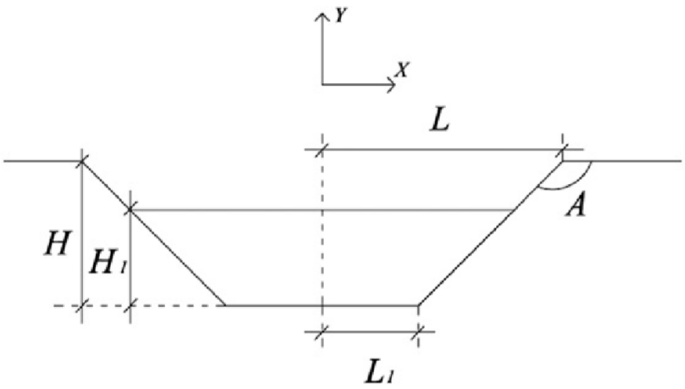

Figure 2.31: Geometry of the studied valleys (Gatmiri and Foroutan, 2012).

The reference site is at a distance of 5L from the center of the valley at the rock outcrop. The maximum value of the ratio of acceleration response spectra at observation point to the reference site is defined as the spectral ratio (SR). In addition, S is the surface of the configuration, S_1 is the sediment surface and A the angle between the slope and horizontal line at the crest of the rock outcrop.

The results shown in **Figure 2.32** are for rectangular valleys, where maximum amplification was observed. In empty valleys an attenuation of the spectral ratio can be seen at the center of valleys, X/L = 0, and the strongest amplification is observed at the upper corner of valleys X/L = 1. By increasing filling ratio H_1/H, the critical point of amplification transfers from the edge to the center. In other words, existence of sediments can de-amplify the valley's response at the edge and amplify it at the center.

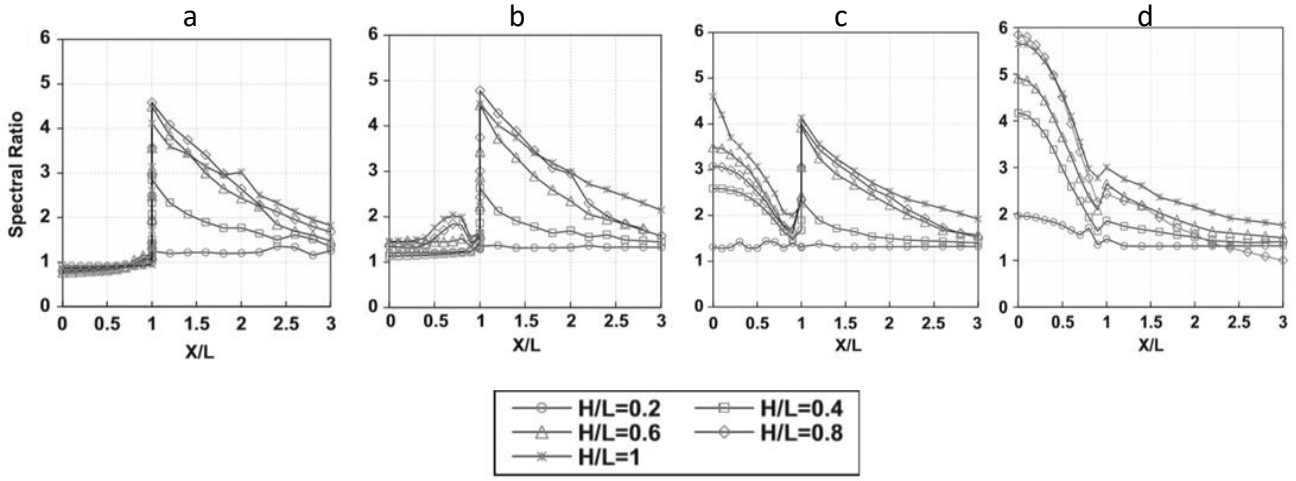

Figure 2.32: Spectral ratio as a function of a dimensional offset variable X/L for rectangle valleys, (a) empty, (b) $H_1/H = 1/3$, (c) $H_1/H = 2/3$, (d) full valley (Gatmiri and Foroutan, 2012, modified).

In configurations with specified filling ratio H_1/H and at a constant depth ratio H/L by shifting from rectangular to triangular shape, the seismic response of the valley at the center decreases. On the other hand, by increasing the depth ratio H/L an increasing trend of the seismic response can be seen for rectangular valleys. The rate of the increase of the spectral ratio (SR) decreases by increasing the depth ratio H/L. In trapezoidal and triangular valleys, by increasing the depth ratio H/L, the spectral ratio increases to some extent and then declines. As expected, the spectral ratio has an inverse relation to the impedance ratio.

Gatmiri and Amini (2014) also studied the spectral response of sediment-filled valleys with elliptic and sinusoidal shape as illustrated in **Figure 2.33**. In both cases, when the valleys are empty, moving from X/L = 0 to 1 causes the spectral ratio to increase. At low filling ratios H_1/H (less or equal to 1/3) the spectral ratios value in the center of the valley does not significantly change. For intermediate filling ratios ($1/3<H_1/H<1$) the seismic response spectra at the center increases. In this case depth of sediments is considerable and the topographical effects may not be dominant. In all valleys there is a local maximum at the edge of the valley, a local maximum at the center of the valley (which can be attributed to topographical and soil effects respectively) and a minimum at the contact point between sediments and bedrock. In most valleys, especially for valleys with large depth ratios (e.g H/L>2/3), the center of the valley is more critical than its edge. In sediment filled valleys, seismic amplification completely levels off at the edge of valleys in a way that the spectral ratio curves are smoother than those of empty or semi-filled valleys at this point while no local maximum exists.

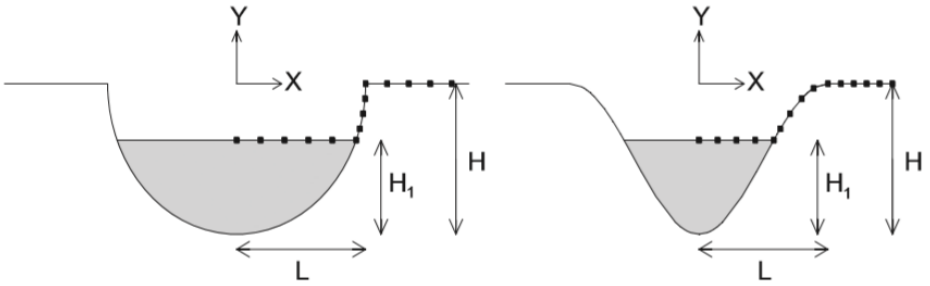

Figure 2.33: Geometrical characteristics and observation points for the studied valleys (Gatmiri and Amini, 2014).

The aforementioned two papers assumed canyons with different valley heights, or different filling ratios. However, the opposite has not been studied, i.e. for the same valley what are the effects of different canyon geometries. And this is the path followed in this study.

CHAPTER 3

METHODOLOGY OUTLINE

3.1 Assumptions and parameters

The objective of this study is to investigate the coupling of surface and subsurface topography effects on the seismic ground response at the ground surface. For this purpose, 2D (plane strain) numerical seismic ground response analyses were performed for uniform trapezoidal valleys with FLAC (Itasca Inc 2005). This code is widely used, mainly for solving 2D geotechnical (dynamic and static) problems with the finite difference method. Each 2D analysis was supplemented by two 1D ground response analyses; 1D_soil and 1D_rock. The reason these two different 1D analyses were used is explained in section 3.2 of this Chapter.

For the representation of the actual behavior of a soil filled valley on outcropping bedrock (2D analysis), symmetrical trapezoidal valleys were used, with **B**, **H** and **s** being the width at the free surface, the (maximum) thickness and the inclination angle at the edges, respectively (**Figure 3.1**). The height of the outcropping bedrock measured from the free surface of the valley is depicted by $\mathbf{H_t}$, while **i** is the inclination angle of the outcropping bedrock in the step-like topographic feature. For all the analyses B = 500 m and H = 50 m (corresponding to B/H = 10). An example of a typical model with FLAC for an analysis with B/H=10, i=s=45^o and H_t=50m is depicted in **Figure 3.2**.

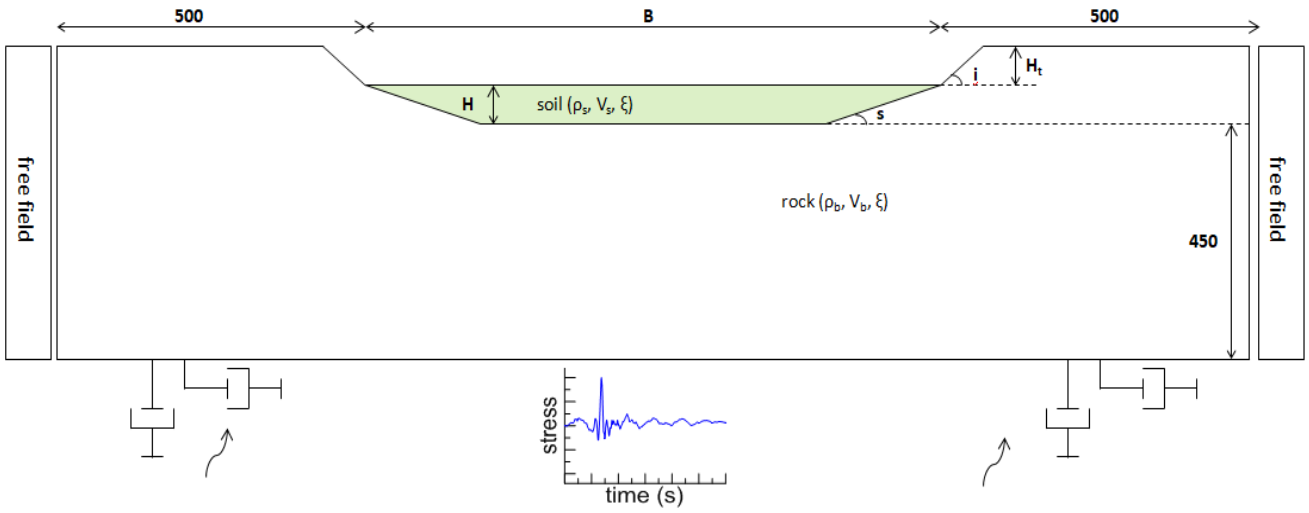

Figure 3.1: Illustration of the basic elements of the 2D ground response analysis for the valley.

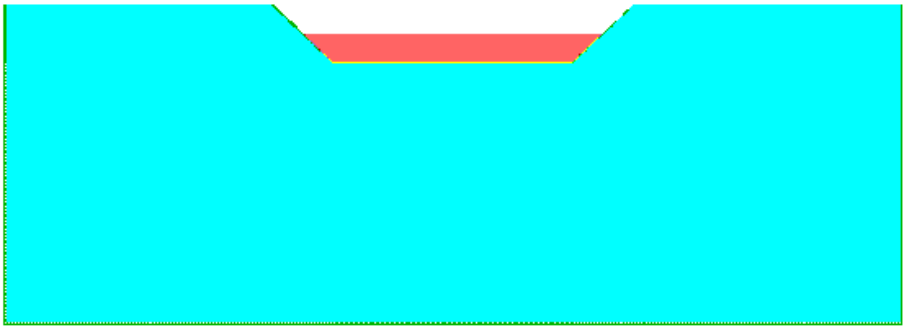

Figure 3.2: Example for 2D analysis with B/H=10, i=s=45^{o} and H_t=50m.

The basic elements of the 1D_soil seismic response analysis are presented in **Figure 3.3**. In this case, the soil deposit has the same thickness H with the valley, but extends horizontally until the edges of the model. The length of the soil layer is 1500 m. The respective model in FLAC is presented in **Figure 3.4**. For 1D_rock analyses, the model includes only rock and the height of the mesh is the same with the 2D analysis, as implied by **Figure 3.5**. An example for B/H=10 and H_t=50 m is shown in **Figure 3.6**. Moreover, a fine discretization of each model into zones is necessary. More specifically, 33000 to 54000 quadrilateral zones were used to simulate the uniform soil mass and rock, with a maximum height equal to 1/10 – 1/40 of the predominant wavelength of the seismic excitation in order to avoid the numerical distortion of its frequency content. To disallow artificial reflections at the boundaries, the finite difference mesh extended 500 m horizontally at both sides of the valley and 450 m vertically from the valley. For the same purpose, free-field boundaries were applied at the lateral sides of the models to represent the infinite horizontal extension of the half-space and quiet (horizontal and vertical) boundaries were assigned at the bottom of the mesh.

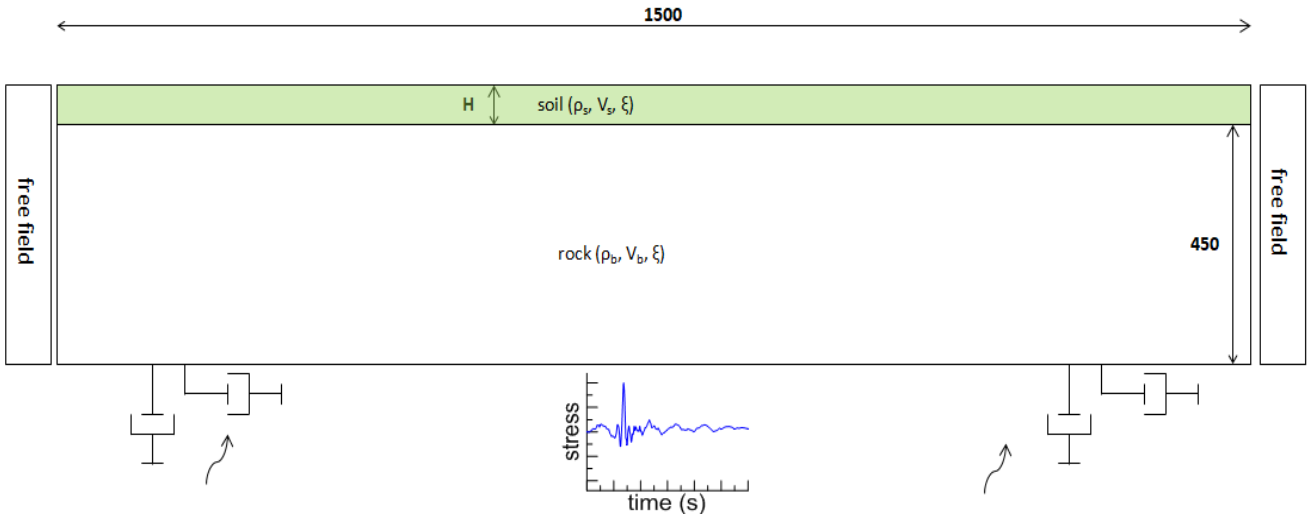

Figure 3.3: Illustration of the basic elements of 1D_soil seismic response analysis.

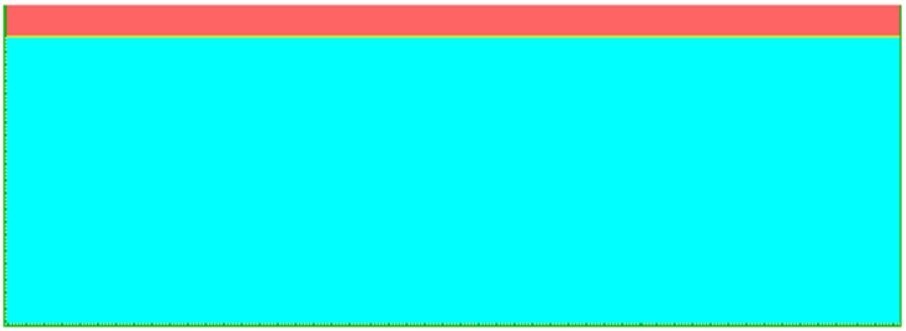

Figure 3.4: Example for 1D_soil analysis, that complements the 2D analysis in Figure 3.2 .

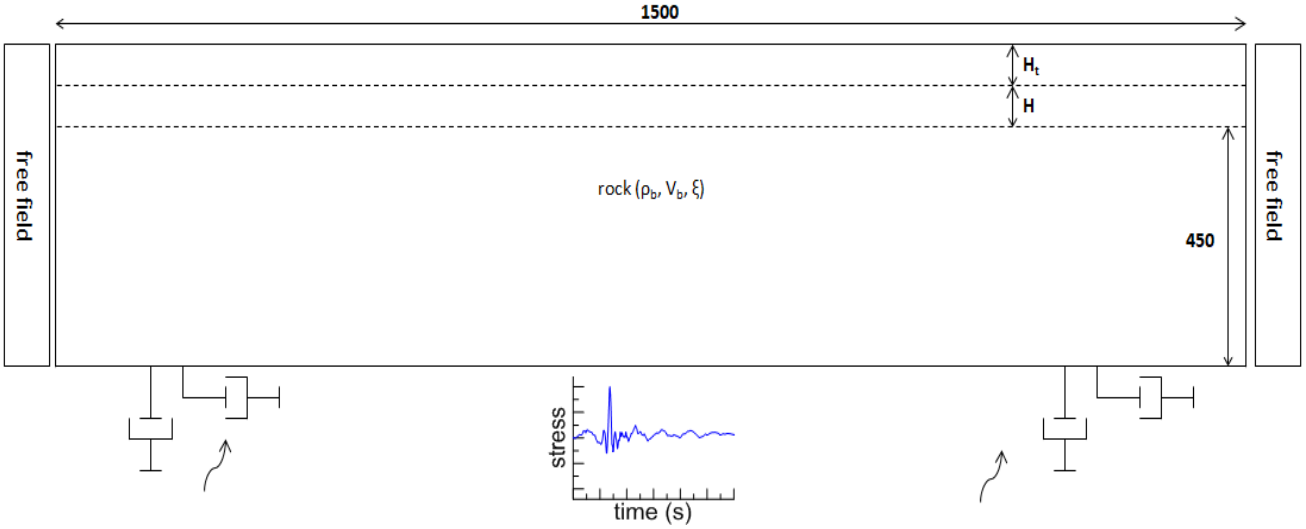

Figure 3.5: Illustration of the basic elements of the 1D_rock seismic response analysis.

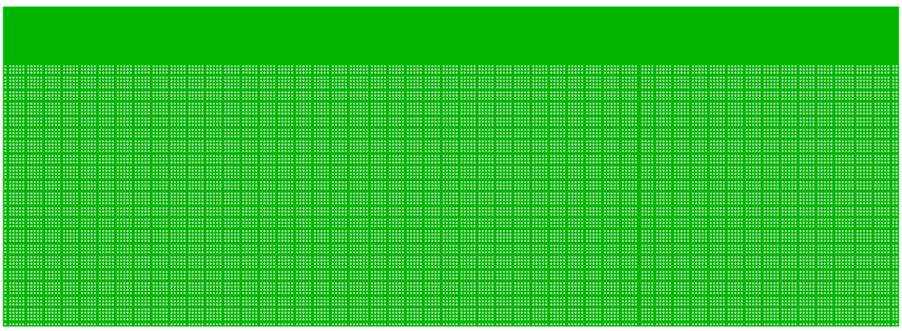

Figure 3.6: Example of mesh generated with FLAC for 1D_rock analysis (H_t=0 m).

The soil and the outcropping bedrock are uniform and visco-elastic. This assumption is not only based on the fact that the calculations are simpler (and faster) than using a non-linear response model It is also based on the fact that this work focuses on amplification factors for an a priori fixed level of damping (5%), something that cannot be achieved with the use of a non-linear model. The chosen level corresponds to low to medium intensity motions, which are expected to show the highest valley and topography effects on seismic ground motion. In other words, the hereby presented results in terms of amplification factors are considered conservative for medium and especially high intensity motions. Both the soil and rock materials have density $\rho_b = \rho_s = 2$ Mg/m^3 and Poisson ratio $\nu = 0.35$. The shear wave velocity of the bedrock is $V_b = 1000$ m/s, whereas for the soil is $V_s = 500$ m/s and $V_s = 250$ m/s depending on the examined case. The impedance ratio **a** is given by:

$$a = \frac{\rho_s V_s}{\rho_b V_b}$$

The seismic excitation used in all analyses was based on the earthquake recording of the Aigion (1995) earthquake in Greece. It is characterized by 1 significant cycle and a bell-shaped elastic response spectrum. Nevertheless, it was not used as recorded, but it was appropriately scaled to attain the desired shear wave length λ in the soil layer. In more detail, the scaling was applied to the time-step of the time-history aiming to the desired predominant period T_e, and hence to the desired $\lambda = V_s T_e$. The analyses were performed for $T_e = 0.1$ s, 0.25 s and 0.4 s in order to include predominant periods of common earthquakes at outcropping bedrock in Europe (see spectrum for M > 5.5 and Ground Type A in EC8). In all cases the excitation was applied as a time-history of shear stress at the bottom horizontal boundary of the mesh, thus applying vertically incident SV waves to the soil bedrock system. Selecting to apply the excitation as a time-history of stress, rather than displacement (velocity or acceleration) allows in concept free vibration of the bottom boundary, thus disallowing (fixed ends) artificial reflections. In addition, the quiet boundaries thereby assigned aid in absorbing the energy of the waves that are, in reality, refracted in the bedrock. The acceleration time histories of the base excitations used in the analyses and their elastic acceleration response spectra are presented in **Figures 3.7** and **3.8** respectively.

In the visco-elastic, the actual, frequency-independent, hysteretic damping of a geomaterial is simulated with the use of Rayleigh damping which is frequency-dependent (**Figure 3.9**). As in all commercial codes, combined (mass and stiffness) Rayleigh damping assigns a minimum value of damping ξ_{min} to a desired target frequency f_{min} and larger values of damping to frequencies larger and smaller than f_{min}. This means that the desired value of critical damping ratio ξ was set equal to ξ_{min}, but still f_{min} had to be calibrated within the frequency range of interest in each analysis. For the purpose of this study, the frequency range of interest lies between the predominant frequency of the (bedrock) excitation $f_e = 1/T_e$ and fundamental frequency of the soil layer $f_s = 1/T_s = V_s/4H$. This because the f_e of the seismic motion at the soil surface is expected to be shifted from that of the bedrock excitation towards that of the soil layer, for reasons of (1D) soil amplification. Hence:

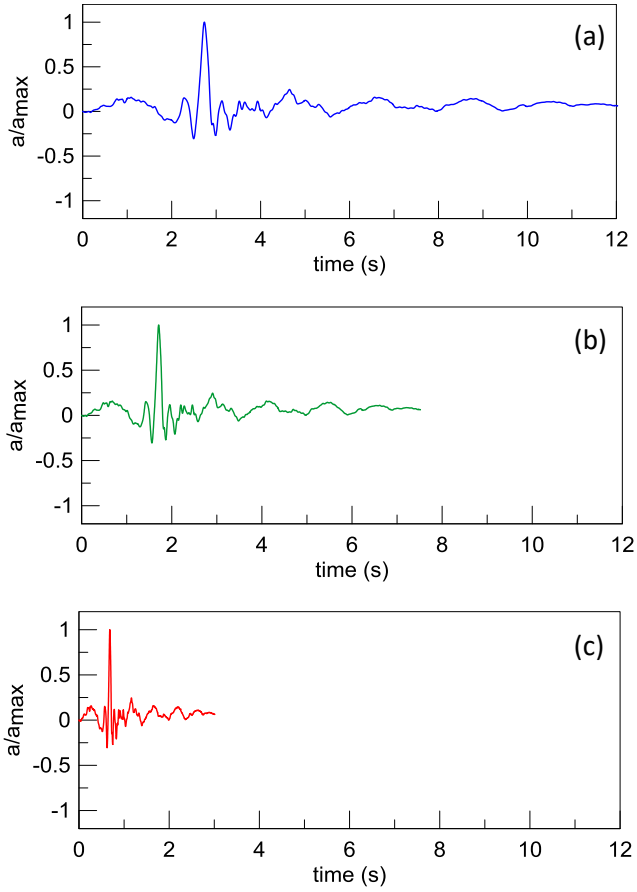

Figure 3.7: Normalized acceleration time histories from Aigion earthquake (1995) with modified predominant period (a) T_e=0.4 s, (b) T_e=0.25 s, (c) T_e=0.1 s.

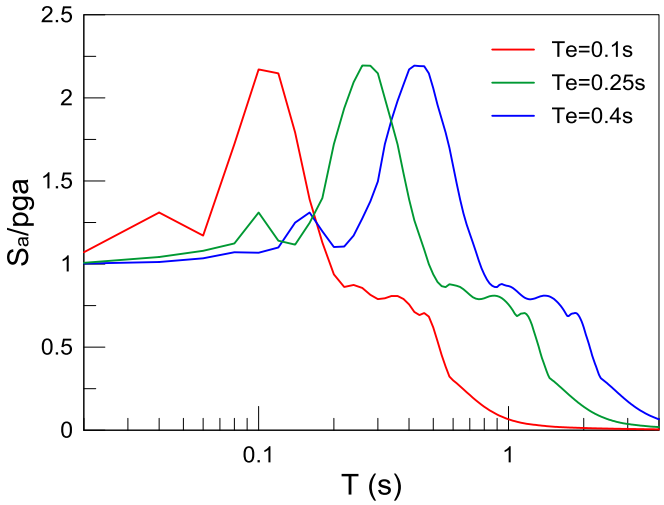

Figure 3.8: Normalized elastic acceleration response spectra for Aigion excitation with T_e=0.1, 0.25 and 0.4 s.

$$f_{min} = \frac{f_e + f_s}{2}$$

The aforementioned fixed damping of the visco-elastic analyses of 5% is set as the value of ξ_{min}. This value is analysis-specific and so is the f_{min}, hence they both apply to all geomaterials within the mesh and all 3 ground response analyses for each case (2D, 1D_soil, 1D_rock).

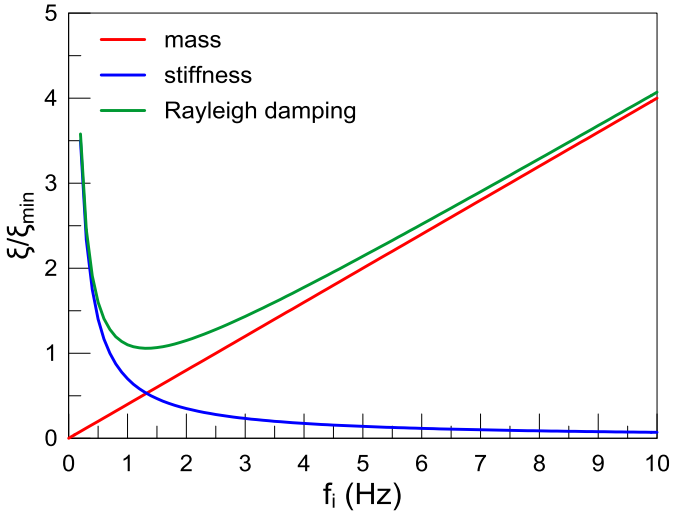

Figure 3.9: (Combined mass and stiffness) Rayleigh damping as a function of frequency.

3.2 The definition of geomorphic aggravation

Performing 2D basin analyses provides a full picture of the variability of seismic motion at the ground surface of the soil and the outcropping rock. Nevertheless, of importance here is the depiction of valley and topography effects, i.e. of the geomorphic aggravation of the peak ground acceleration at each location of the ground surface for each exemplary case. This cannot be accurately depicted by a single analysis, because it is unclear whether the observed variability is an effect of the valley and the topography, or of the soil or rock conditions at each location. Hence, for each 2D basin analysis, a couple of 1D analyses were also performed with FLAC for the same excitation and damping configuration, one where the soil layer is of infinite width (depicting free-field soil response under 1D conditions; denoted as 1D_soil) and one where the whole profile is rock (depicting the free field rock response under 1D conditions; denoted as 1D_rock).

As a first step, from the 2D analysis the horizontal and parasitic vertical acceleration time histories at each location of the ground surface were retrieved. Note that the term “parasitic” is introduced for the vertical acceleration, since the incident motion is purely horizontal vibration (vertically incident SV waves) and therefore any vertical vibration at the ground surface is purely a result of wave refractions at the inclined boundaries of the basin and horizontally travelling Rayleigh waves. The same procedure was followed for 1D_soil and 1D_rock analyses, but only for the horizontal acceleration, since they correspond to purely 1D conditions. Given the foregoing values, the

acceleration spectra S_{ah}, S_{av} were determined from the 2D analysis and S_{as}, S_{ar} from the 1D_soil and the 1D_rock analyses, respectively. The horizontal geomorphic aggravation factor AS_{ah} for each period is defined at each location of the ground surface, as the ratio of S_{ah} over the corresponding spectral value from the appropriate 1D analysis (i.e. S_{as} or S_{ar}). In particular, if the location at the ground surface sits on soil (within the alluvial section of the valley), then the horizontal geomorphic aggravation factor is $AS_{ah} = S_{ah}/S_{as}$, while if the location at the ground surface sits on outcropping rock, then $AS_{ah} = S_{ah}/S_{ar}$. Similarly, the parasitic vertical geomorphic aggravation factor AS_{av} is defined at each location of the ground surface, as the ratio of the S_{av} over the corresponding spectral value from the appropriate 1D analysis (i.e. S_{as} or S_{ar}), as for AS_{ah}. Moreover, this selection for the denominator of AS_{av} provides a measure of the relative importance of the parasitic vertical motion, as compared to its horizontal counterpart.

It is of importance to this study to clearly distinguish between geomorphic aggravation that is due purely to the existence of a non-horizontal soil-bedrock interface (valley and topography effects) and the aggravation due to the soil layer alone (soil effects). For this purpose, **Figure 3.10** provides an example comparison of the total aggravation of peak horizontal acceleration (due to soil and valley/topography effects) along a valley with B/H=10 to the geomorphic aggravation (valley/topography effects) defined in terms of AS_{ah}, all for T=0s (i.e. for the peak ground acceleration). Note that for total aggravation the AS_{ah} is defined by considering S_{ar} as the denominator for all locations, and hence total and geomorphic aggravations differ only along the valley. In this figure, the horizontal distance X of any location from the valley axis of symmetry is presented normalized by the width B of the valley. Hence, the valley is depicted between X/B=-0.5 and X/B=0.5, while the outcropping bedrock at |X/B| > 0.5.

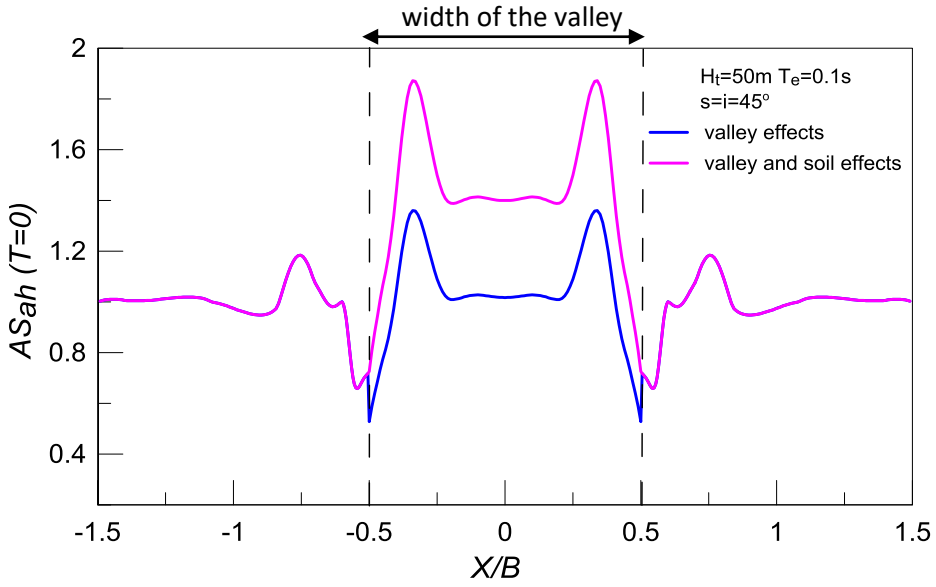

Figure 3.10: Spatial variability of total and geomorphic aggravation of peak horizontal acceleration along the ground surface of the valley; Results for B/H = 10, H_t = 50m, s = i = 45°, a = 0.5 and T_e = 0.1s.

Observe in this figure that the aggravation patterns are geometrically symmetric, as a combined effect of the symmetry of the valley and the vertical incidence of SV waves in this study. Furthermore, the curve for total aggravation (purple line) is translated as compared to that for AS_{ah} (blue line) all along the soil surface, but the two curves coincide at locations along the outcropping rock. This means that soil effects are zero along rock (by definition), but non-zero along the soil surface.

Note that there is a conceptual problem in the definition of AS_{ah} (and AS_{av}, not shown in **Figure 3.10**) at locations over the inclined boundaries of the valley. This has to do with the fact that the denominator S_{as} in their definition corresponds to 1D conditions of a soil layer having thickness equal H, something that is true for all locations along the central part of the valley, but not the locations over the inclined boundaries. This problem is significant in nearly triangular valleys, but not so important in wide valleys, as the one depicted in **Figure 3.10**, where the locations over the inclined boundaries are of small width compared to the total width B. Yet, there is no easy way of taking into account this gradual change in the thickness of the soil layer along these locations. Moreover, the easy alternative of using S_{ar} as denominator for the definition of AS_{ah} all along the valley would create the problem depicted in **Figure 3.10**, i.e. an erroneous consideration of both basin and soil effects as geomorphic aggravation all along the valley.

3.3 Parametric study

In order to study the valley response for different outcropping bedrock topographies, numerical analyses were performed for a valley with constant aspect ratio B/H=10. The analyses considered changes in the predominant period of the excitation T_e, the inclination angles of the valley s and the outcropping bedrock i, the outcropping bedrock height H_t and the soil-rock impedance ratio a. For this study, 23 different cases were examined, for period T_e=0.1 s, 0.25 s and 0.4 s, angle s=45^o and 22.5^o, angle i=45^o and 22.5^o, height H_t=0 m, 50 m and 100 m and ratio a=0.5 and 0.25. The results for these cases are presented in Chapter 4. Then, in Chapter 5, the effect of having or not a soft alluvial basin at the base of a topographic relief is studied by analyzing an additional set of 8 more cases, which correspond to the same aspect ratio B/H=10, height H_t=50 and 100 m, period T_e=0.1 s, 0.25 s and 0.4 s, angle s=45^o and 22.5^o and angle i=45^o and 22.5^o, by setting the impedance ratio a=1.0. In other words, the cases considered in Chapter 5 are canyon topographies of exactly the same geometry as those in Chapter 4, with the only difference being the value of impedance ratio a. It is reminded here that reference is made to cases and not analyses, since each case requires the execution of 1D seismic response analyses for accurate estimation of amplification factors. In total, 31 cases where examined, with their parameters presented in **Table 3.1**.

Table 3.1: Parameters of the examined cases.

# case	B/H	T_e (s)	s (°)	i (°)	H_t (m)	a
1	10	0.10	45	-	0	0.50
2	10	0.10	45	45	50	0.50
3	10	0.10	45	45	100	0.50
4	10	0.25	45	-	0	0.50
5	10	0.25	45	45	50	0.50
6	10	0.25	45	45	100	0.50
7	10	0.40	45	-	0	0.50
8	10	0.40	45	45	50	0.50
9	10	0.40	45	45	100	0.50
10	10	0.10	22.5	-	0	0.50
11	10	0.10	22.5	22.5	50	0.50
12	10	0.40	22.5	-	0	0.50
13	10	0.40	22.5	22.5	50	0.50
14	10	0.10	22.5	45	50	0.50
15	10	0.10	45	22.5	50	0.50
16	10	0.40	22.5	45	50	0.50
17	10	0.40	45	22.5	50	0.50
18	10	0.10	45	-	0	0.25
19	10	0.10	45	45	50	0.25
20	10	0.10	45	45	100	0.25
21	10	0.40	45	-	0	0.25
22	10	0.40	45	45	50	0.25
23	10	0.40	45	45	100	0.25
24	10	0.10	45	45	50	1.00
25	10	0.25	45	45	50	1.00
26	10	0.40	45	45	50	1.00
27	10	0.10	45	45	100	1.00
28	10	0.25	45	45	100	1.00
29	10	0.40	45	45	100	1.00
30	10	0.10	22.5	22.5	50	1.00
31	10	0.40	22.5	22.5	50	1.00

CHAPTER 4

EFFECTS OF OUTCROPPING BEDROCK TOPOGRAPHY ON SEISMIC VALLEY RESPONSE

4.1 Introduction

This Chapter investigates how is the seismic response of a valley affected due to different outcropping bedrock topographies at its edges. As outlined in Chapter 3, for this purpose, 23 cases were studied for a valley with a constant aspect ratio B/H=10 (where width B = 500m, thickness H = 50m) using the finite difference code FLAC (Itasca Inc. 2005). Based on the definitions in Chapter 3, the studied problem is characterized by a number of parameters dealing with valley and outcropping bedrock geometry (height H_t, angle s, angle i), soil conditions (densities ρ_s and ρ_b, shear wave velocities V_s and V_b, damping ξ_{min}) and excitation characteristics (intensity, predominant period $T_e=1/f_e$, type of waveform, angle of incidence). The analyses are visco-elastic. Hence, the intensity of the excitation does not affect the results in terms of aggravation factors, since geomaterial stiffness and damping remain constant. The selected value of ξ_{min} = 5% corresponds to low to medium intensity motions, so if one would be interested in results for higher intensities, the analyses should be repeated for higher damping values. Based on Chapter 3, a single type of waveform was hereby used (one with a single significant cycle and a bell-shaped elastic response spectrum) and the angle of incidence was considered vertical in all cases. Only the period T_e was varied here, within the range of 0.1 – 0.4s. Nevertheless, it is considered that the performed parametric analysis covers a wide range of cases in practice and establishes what governs the coupling of valley and topography effects on seismic ground response. This is especially true given that in wave propagation problems in elastic (or visco-elastic) media, dimensional analysis introduces normalized problem parameters, which generalize the presented results for many cases in practice.

In the following analyses, the results are presented in 3 different types of figures. The first one shows the spatial variability of geomorphic aggravation factors AS_{ah} and AS_{av} for T=0s with normalized distance from the center of the valley X/B. The second one presents the geomorphic aggravation spectra AS_{ah} and AS_{av} at the locations of peak aggravation for T=0s along the valley, wherever these appear for the horizontal and the parasitic vertical acceleration. Finally, the third type of figure depicts the spatial variability of geomorphic aggravation factors AS_{ah} and AS_{av} for specific structural periods T with normalized distance from the center of the valley X/B. These

periods T = 0, 0.2, 0.4 and 1.0 sec, corresponding to the ground response and the response of usual low-rise (T = 0.2s), medium rise (T = 0.4s) and high-rise buildings (T = 1.0s).

Since the purpose of this Chapter is mainly the study of the valley's response, the focus of the investigation is on locations within the valley, rather than on locations in the outcropping bedrock. The parametric study investigated the effects of the predominant period of the excitation T_e, the inclination angles of the valley s and the outcropping bedrock i, the outcropping bedrock height H_t and the impedance ratio a.

4.2 Effects for steep valleys s = 45^o with steep outcrops i = 45^o and high impedance ratio a = 0.5

In this paragraph, the valleys have buried and outcropping bedrock inclination angles (s and i, respectively) equal to 45^o, i.e. they correspond to steep valleys with steep outcrops. The shear wave velocity for the outcropping bedrock is V_b = 1000 m/s and for the soil is V_s = 500 m/s (stiff soil), leading to a high impedance ratio a = 0.50. What varies in these analyses are: a) the outcropping bedrock height H_t = 0, 50 and 100m; b) the predominant excitation period T_e = 0.1s (high-frequency), 0.25s (intermediate-frequency) and 0.4s (low-frequency).

The effects of outcropping bedrock height H_t under a high-frequency excitation T_e = 0.1s are demonstrated in **Figures 4.1 - 4.5**. As shown in **Figure 4.1**, the maximum aggravation of AS_{ah} (T = 0) is observed near the edges of the valley, as expected for wide valleys under high frequency excitations, while the same stands for the parasitic vertical component AS_{av} (T = 0). The maximum aggravations are not negligible ($maxAS_{ah}(T=0) \approx 1.35$, $maxAS_{av}(T=0) \approx 0.6$), while the height of the outcropping bedrock H_t seems insignificant for the response within the valley, at least for T_e = 0.1s. On the contrary, the response at the outcropping bedrock is affected by the height H_t. Specifically, the peak aggravation increases with H_t and is observed in the vicinity of the crest, that appears at an increasing horizontal distance X/B from the edge of the valley. The effect of H_t is more pronounced in the parasitic vertical accelerations. Focusing on the locations where the $maxAS_{ah}(T=0)$ and $maxAS_{av}(T=0)$ are observed, **Figure 4.2** compares their aggravation spectra for different values of height H_t. It is observed that these spectra are quite similar in shape, regardless of H_t value. For example, they show the highest aggravation values for small periods (e.g. roughly up to T = T_e = 0.1s), while for large periods the aggravation values are insignificant.

Then, **Figures 4.3 to 4.5**, present the spatial variability of aggravation factors for different structural periods (including the T=0s of **Figure 4.1**). For clarity, each of these figures presents the results for a specific outcropping bedrock height H_t. As expected from the previous figures, the variability of geomorphic aggravation for different periods T is similar, for any outcropping bedrock height H_t. For example, observe how for large T values, the peak AS_{ah} becomes lower and appears near the center of the valley. Other than the expected variability for different T values, the effect of outcropping bedrock height H_t is unimportant for all period T values, at least for the high-frequency motion with T_e=0.1s studied in these figures.

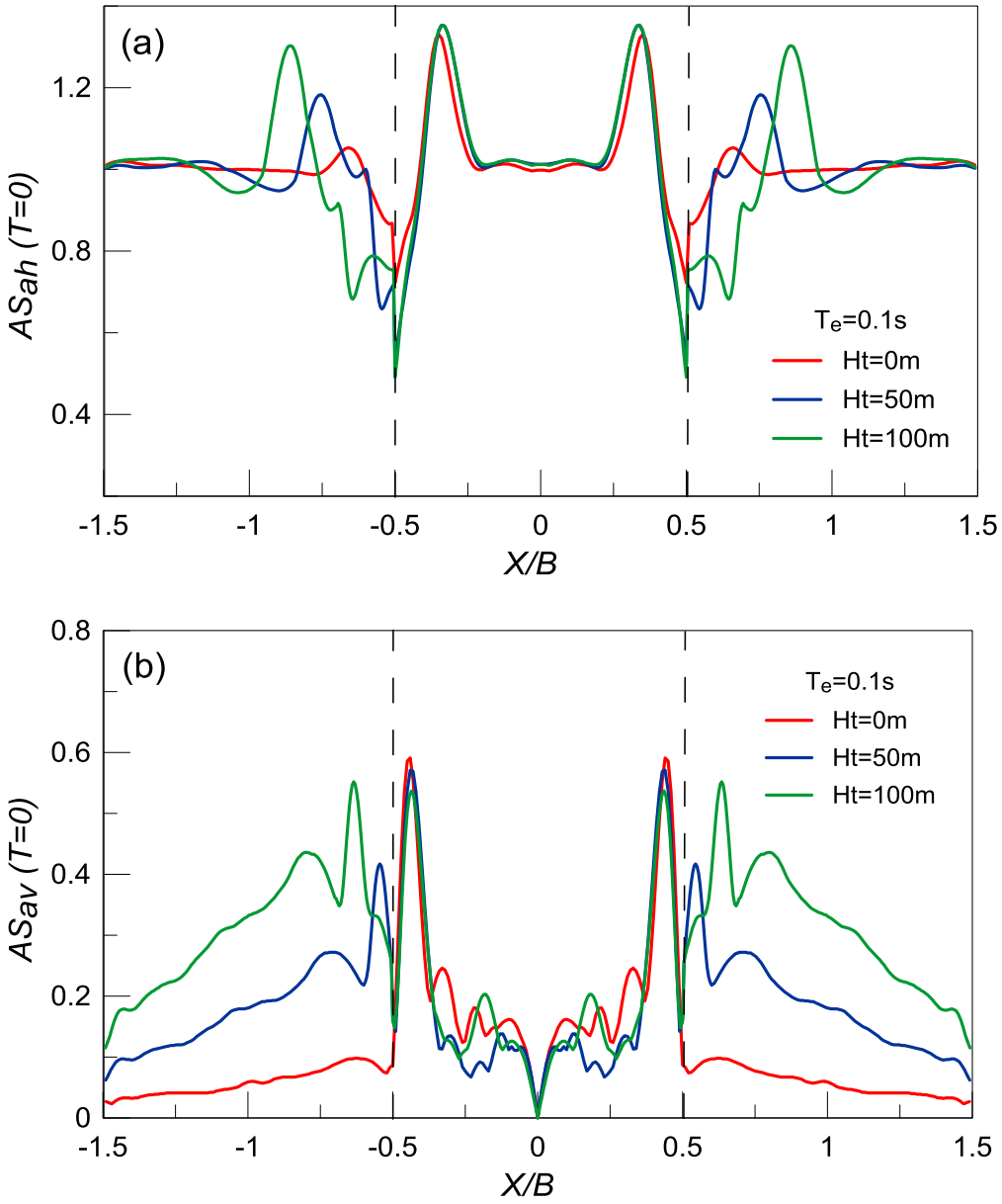

Figure 4.1: Effect of height H_t of steep (i=45^o) outcropping bedrock on the spatial variability of geomorphic aggravation factors AS_{ah} and AS_{av} for T=0s with normalized distance X/B from the center of the steep valley (s=45^o) with high impedance ratio a = 0.5; Results for high frequency excitation with T_e = 0.1s.

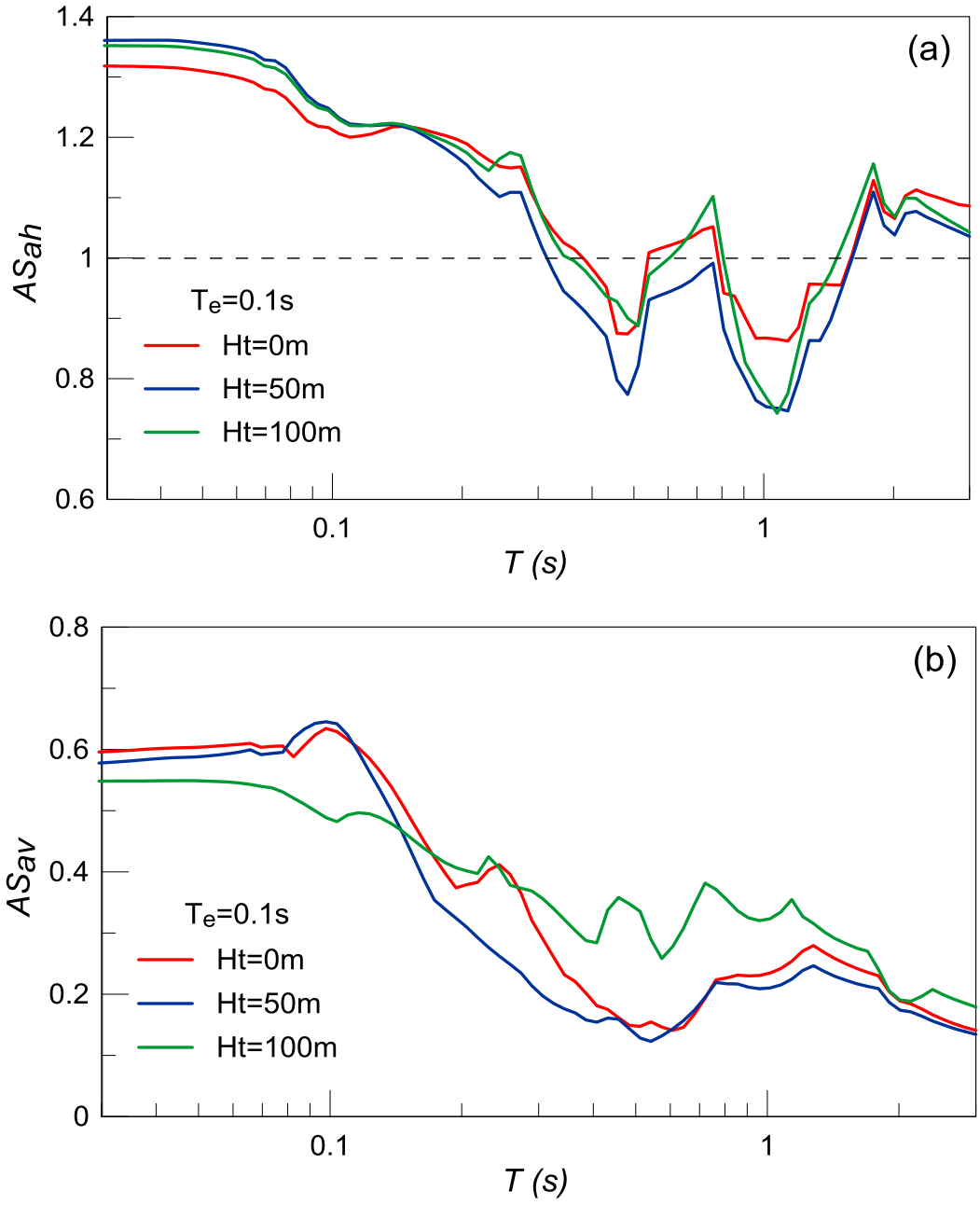

Figure 4.2: Effect of height H_t of steep (i=45^o) outcropping bedrock on geomorphic aggravation spectra AS_{ah} and AS_{av} at the location of peak aggravation for T=0s along the steep (s=45^o) valley with high impedance ratio a=0.5; Results for high-frequency excitation with T_e = 0.1s.

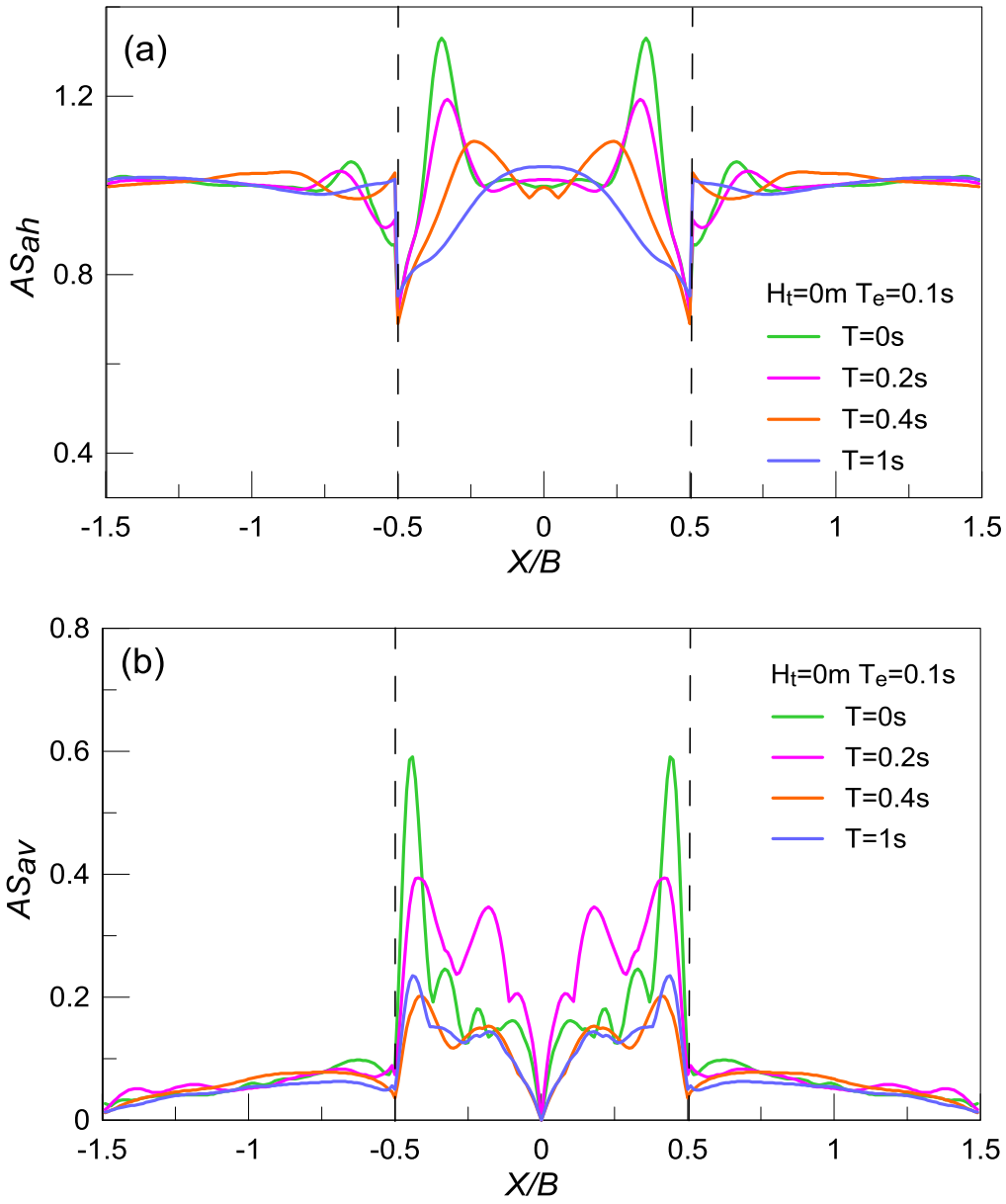

Figure 4.3: Spatial variability of geomorphic aggravation factors AS_{ah} and AS_{av} for specific structural periods T with normalized distance X/B from the center of the steep (s=45^{o}) valley with high impedance ratio a=0.5; Results for outcropping bedrock height H_t = 0m and a high-frequency excitation with T_e = 0.1s.

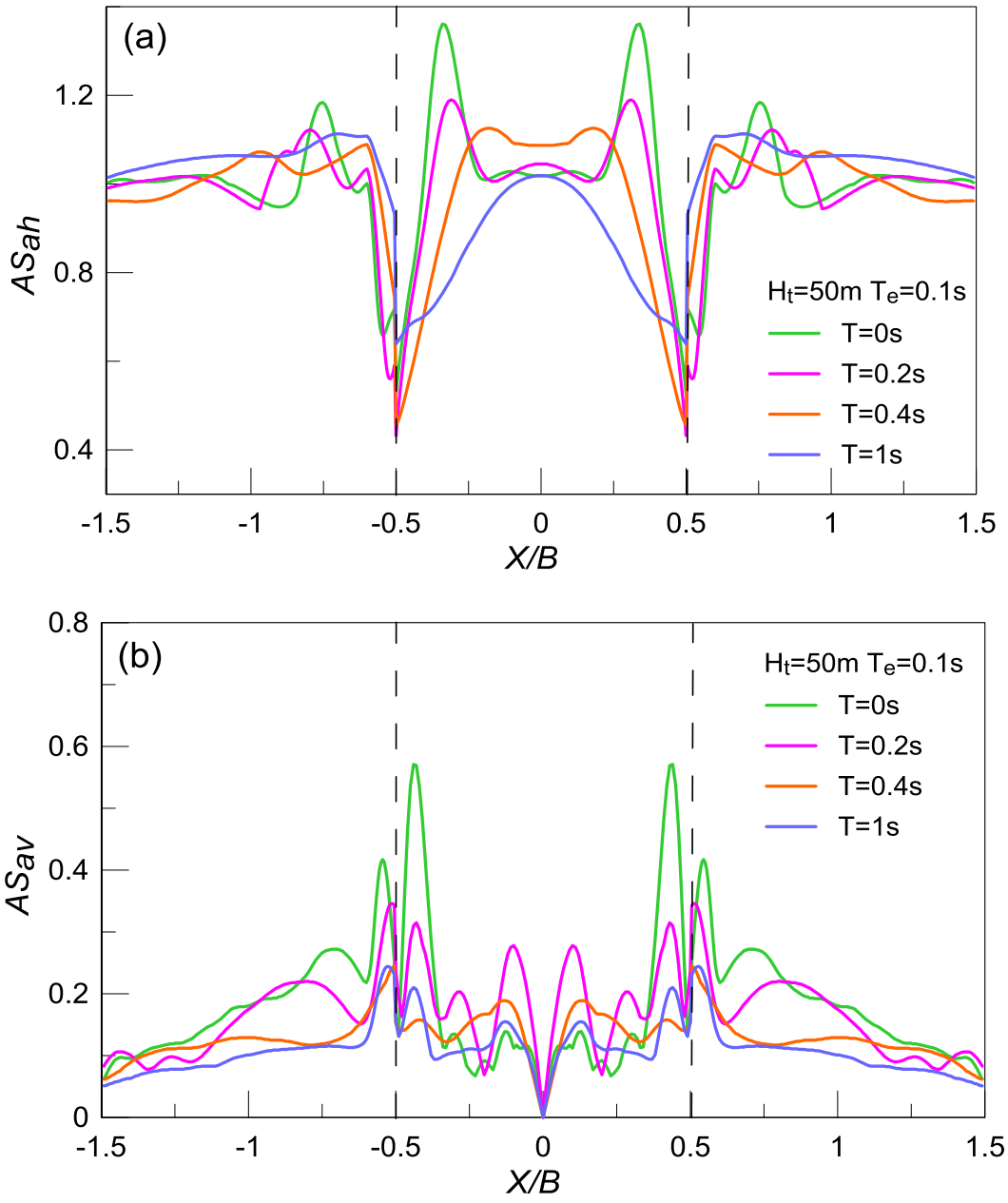

Figure 4.4: Spatial variability of geomorphic aggravation factors AS_{ah} and AS_{av} for specific structural periods T with normalized distance X/B from the center of the steep (s=45^{o}) valley with high impedance ratio a=0.5; Results for height H_t = 50m of steep (i=45^{o}) outcropping bedrock and a high-frequency excitation with T_e = 0.1s.

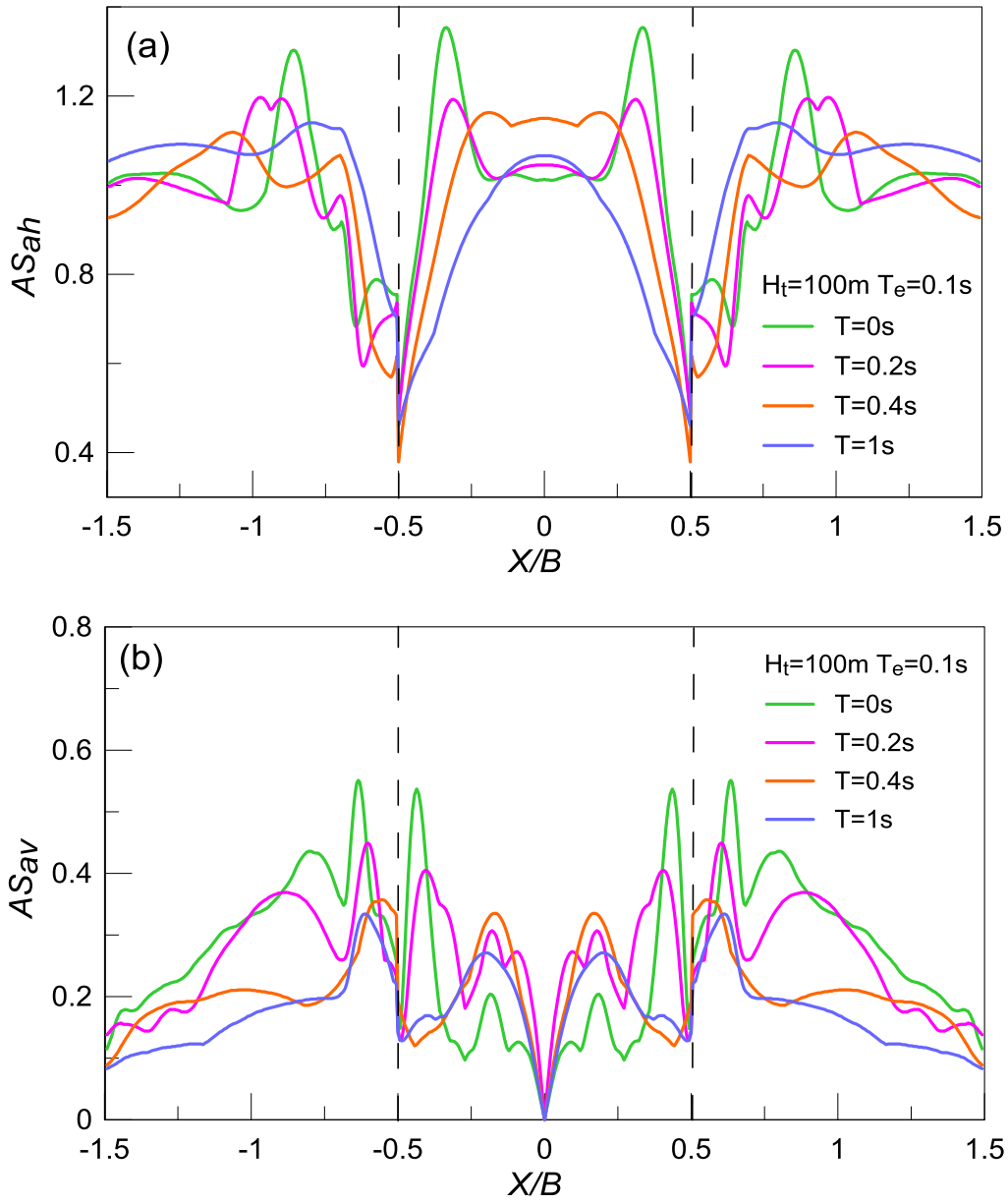

Figure 4.5: Spatial variability of geomorphic aggravation factors AS_{ah} and AS_{av} for specific structural periods T with normalized distance X/B from the center of the steep (s=45^{o}) valley with high impedance ratio a=0.5; Results for height H_t = 100m of steep (i=45^{o}) outcropping bedrock and a high-frequency excitation with T_e = 0.1s.

In the sequel, **Figures 4.6 to 4.10** present the aggravation results for the same valley-outcropping bedrock combinations of **Figures 4.1 to 4.5**, in the same format, but for a low-frequency excitation with T_e = 0.4s. Specifically, observe in **Figure 4.6**, that for such an excitation, the same valley appears like being narrower, since the peak (horizontal) aggravations appear at its center. In addition, observe how the $maxAS_{ah}(T=0)$ = 1.02 – 1.15 and $maxAS_{av}(T=0)$ = 0.16 – 0.29, i.e. they are significantly lower than for the high-frequency motion with T_e = 0.1s. More importantly, based on **Figure 4.6**, there is a clear increasing effect of outcropping bedrock height H_t on both $AS_{ah}(T=0)$ and $AS_{av}(T=0)$ when T_e = 0.4s, contrary to the negligible effect for T_e=0.1s shown in **Figure 4.1**. At the outcropping bedrock locations, the effect of H_t is not as significant as it appears for T_e = 0.1s, since it shows a clear increasing effect only for the parasitic vertical acceleration $AS_{av}(T=0)$. Then, in **Figure 4.7**, the aggravation spectra are compared for different outcrop heights H_t at the locations where the $maxAS_{ah}(T=0)$ and $maxAS_{av}(T=0)$ appear. This figure shows that the maximum aggravation values appear for low periods up to T = T_e = 0.4s and reduce thereafter, as expected. It also shows that the shape of the aggravation spectrum is not affected by the height H_t. Hence, the effect of H_t appears mostly as a uniform scaling of the spectrum.

Figures 4.8 to 4.10 present the spatial variability of aggravation factors for different structural periods (including the T=0s of **Figure 4.6**), but each one of them presents the results for a specific H_t value. As expected from the previous figures, the variability of geomorphic aggravation for different periods T is similar, but not identical for different H_t values. Specifically, within the valley the horizontal aggravation becomes maximum at its center for all periods T, while the values of this aggravation for any value of T more or less increase with H_t. Similarly, an increase of H_t leads to a slight increase of parasitic vertical aggravation values for any value of T. In more detail, significant values of AS_{ah} and AS_{av} are observed for periods T smaller or equal to T_e (= 0.4s, here) and reducing thereafter. As for specific structural periods, for H_t = 0m (**Figure 4.8**), the peak values of AS_{ah} are almost the same for all periods, while for H_t = 50m and 100m (**Figures 4.9 and 4.10**), the AS_{ah} is maximized for structural period T = T_e (= 0.4s).

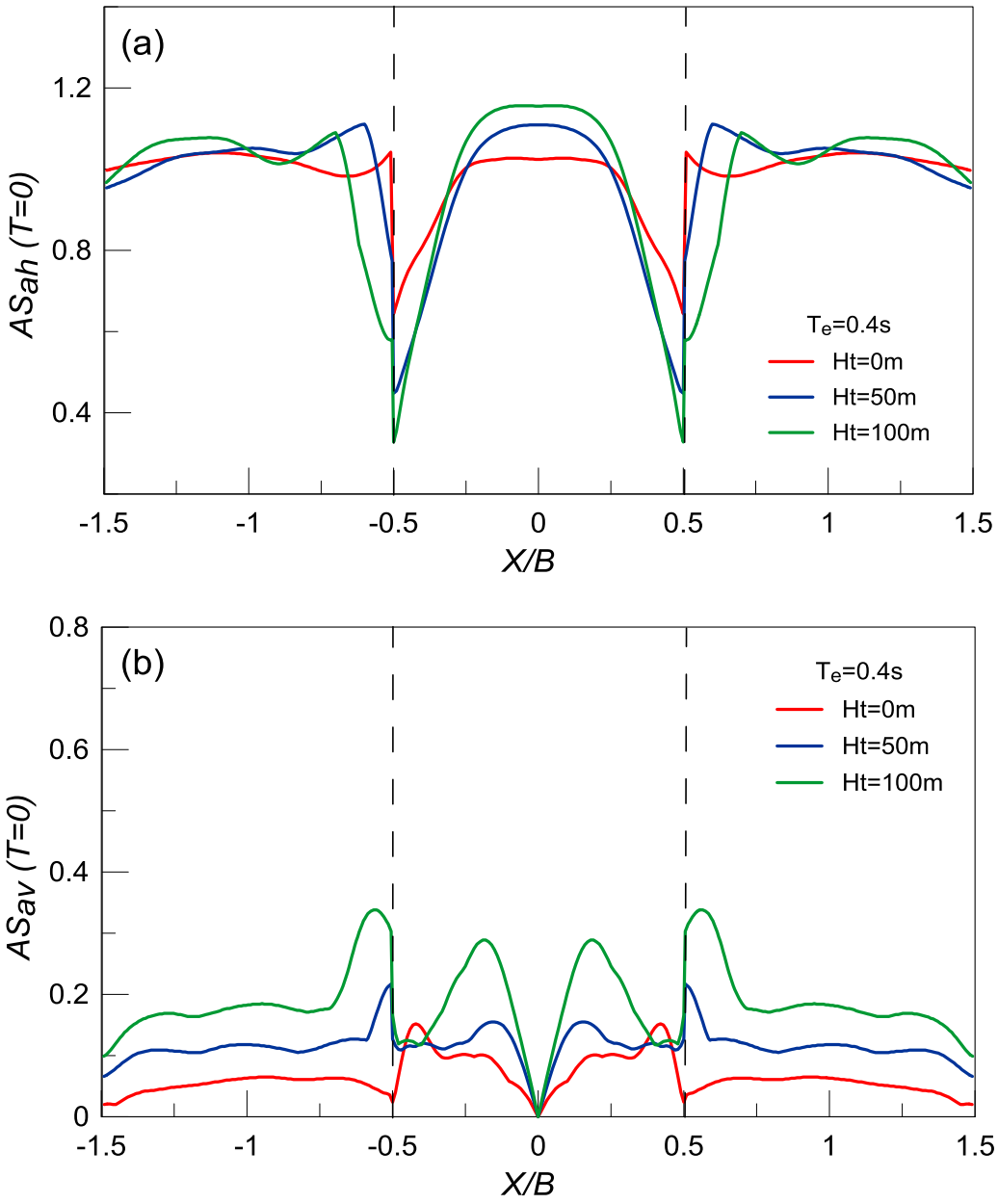

Figure 4.6: Effect of height H_t of steep (i=45^o) outcropping bedrock on the spatial variability of geomorphic aggravation factors AS_{ah} and AS_{av} for T=0s with normalized distance X/B from the center of the steep (s=45^o) valley with high impedance ratio a=0.5; Results for low frequency excitation with T_e = 0.4s.

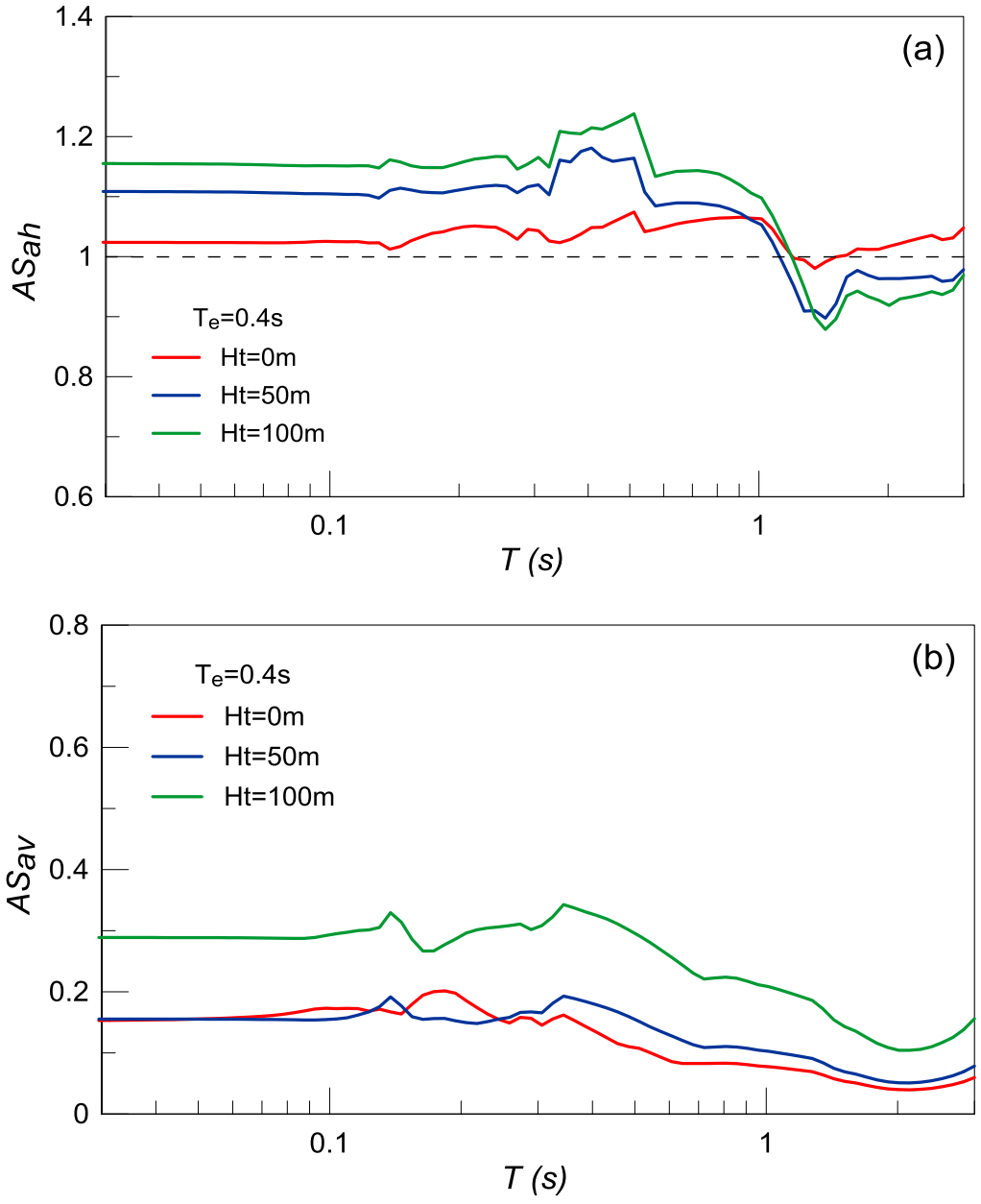

Figure 4.7: Effect of height H_t of steep (i=45^o) outcropping bedrock on geomorphic aggravation spectra AS_{ah} and AS_{av} at the location of peak aggravation for T=0s along the steep (s=45^o) valley with high impedance ratio a=0.5; Results for low-frequency excitation with T_e = 0.4s.

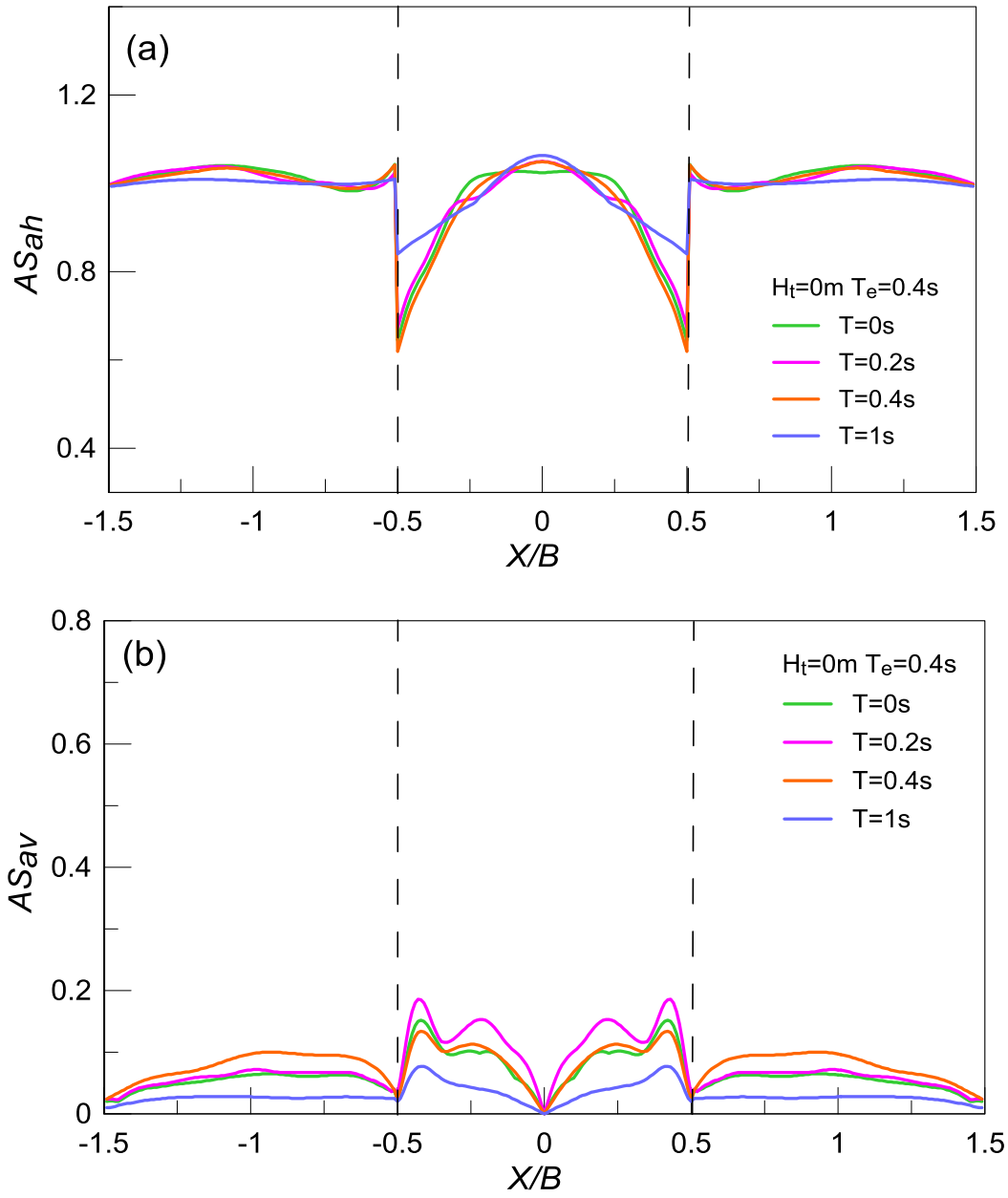

Figure 4.8: Spatial variability of geomorphic aggravation factors AS_{ah} and AS_{av} for specific structural periods T with normalized distance X/B from the center of the steep (s=45^{o}) valley with high impedance ratio a=0.5; Results for outcropping bedrock height H_t = 0m and a low-frequency excitation with T_e = 0.4s.

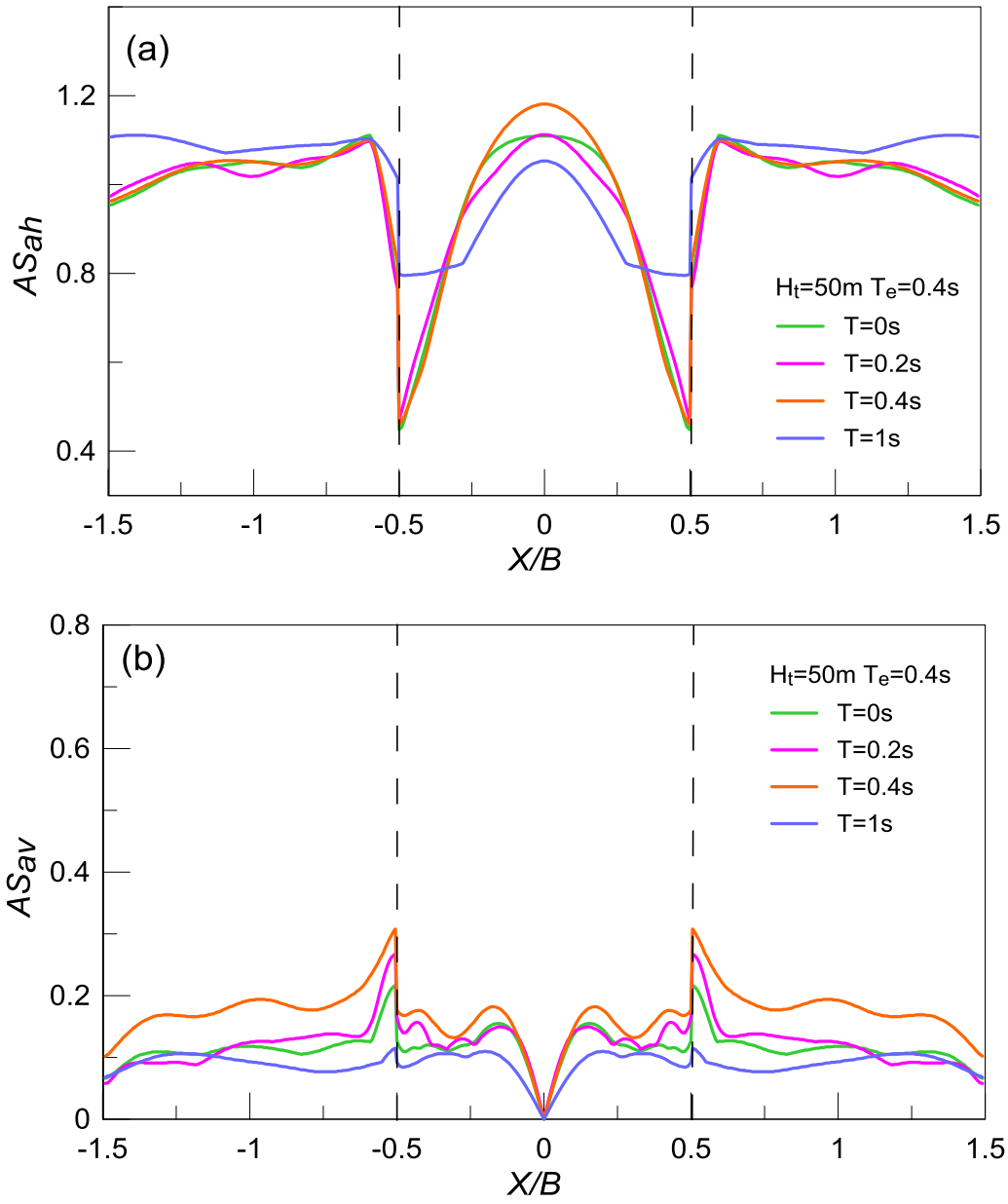

Figure 4.9: Spatial variability of geomorphic aggravation factors AS_{ah} and AS_{av} for specific structural periods T with normalized distance X/B from the center of the steep (s=45^{o}) valley with high impedance ratio a=0.5; Results for height H_t = 50m of steep (i=45^{o}) outcropping bedrock and a low-frequency excitation with T_e = 0.4s.

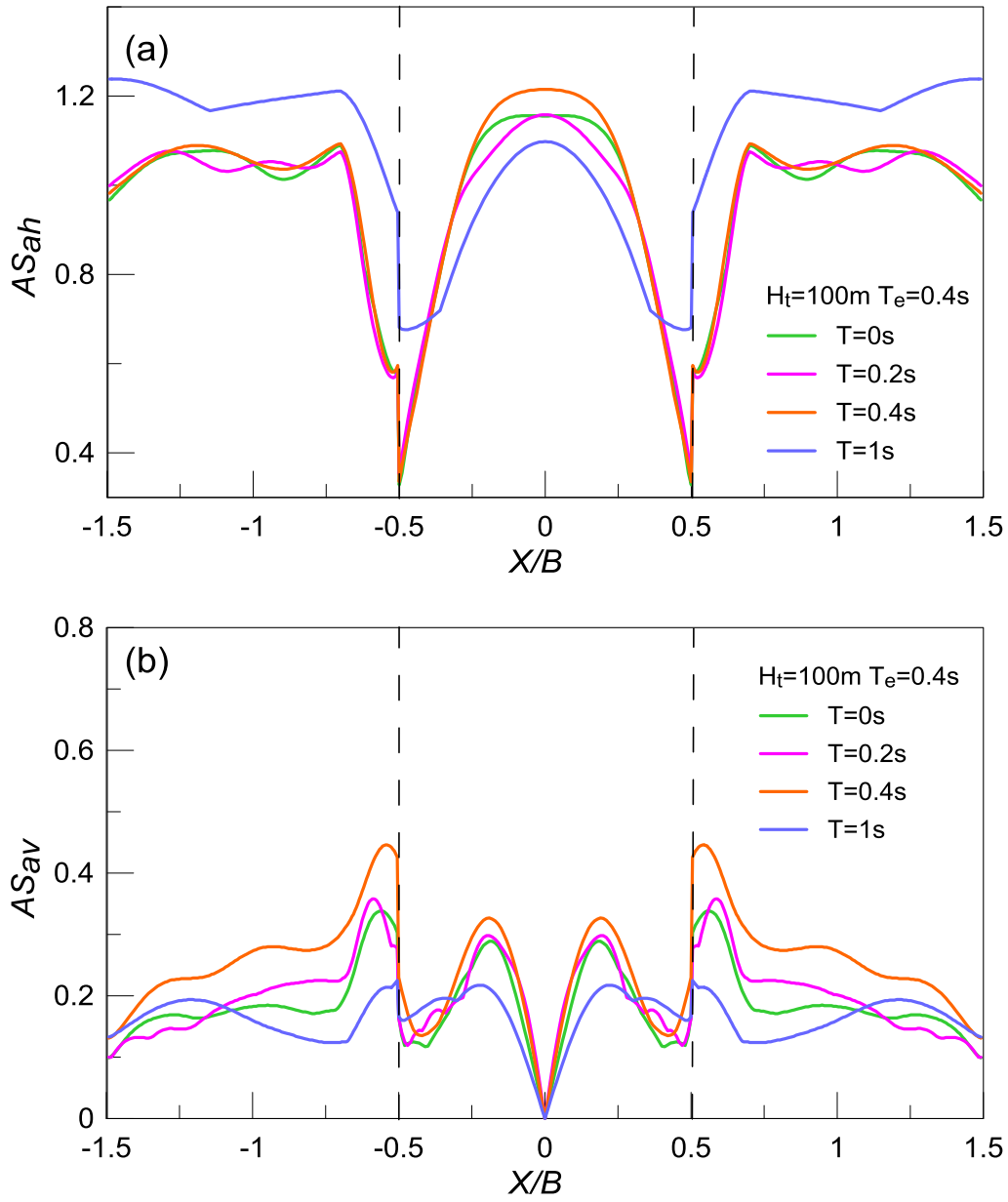

Figure 4.10: Spatial variability of geomorphic aggravation factors AS_{ah} and AS_{av} for specific structural periods T with normalized distance X/B from the center of the steep (s=45^o) valley with high impedance ratio a=0.5; Results for height H_t = 100m of steep (i=45^o) outcropping bedrock and a low-frequency excitation with T_e = 0.4s.

In the previous figures, it is established that the height of the outcropping bedrock H_t increases the horizontal and parasitic vertical aggravations only for the low-frequency excitation with T_e = 0.4s, while for the high-frequency excitation with T_e = 0.1s the results showed negligible effects on the aggravation within the valley. Hence, it is interesting to investigate the effect of height H_t for an intermediate-frequency motion with T_e = 0.25s. This is performed in **Figures 4.11 to 4.15**, that present the aggravation results for the same valley-outcropping bedrock combinations of the previous figures (keeping the **s**ame format), but for an intermediate-frequency motion with T_e = 0.25s. Specifically, observe in **Figure 4.11**, that for such an excitation, the response of the same valley seems like being narrower than for T_e = 0.1s (**Figure 4.1**) and wider than for T_e = 0.4s (**Figure 4.6**). This is deduced by the fact that for the horizontal aggravation, unlike the response for T_e = 0.4s where there is a single peak at the valley center, for T_e = 0.25s there are 2 peaks but closer to the center of the valley than for T_e = 0.1s. In addition, the $maxAS_{ah}(T=0)$ = 1.28 – 1.32 and $maxAS_{av}(T=0)$ = 0.28 – 0.41, i.e. they are slightly lower than for the high-frequency motion with T_e = 0.1s, but definitely higher than the values for T_e = 0.4s. More importantly, based on **Figure 4.11**, an increasing effect of outcropping bedrock height H_t exists on both $AS_{ah}(T=0)$ and $AS_{av}(T=0)$ within the valley, but it is less intense than for T_e = 0.4s (**Figure 4.6**) and definitely not negligible as for T_e=0.1s (**Figure 4.1**). At the outcropping bedrock locations, the increasing effect of H_t is again intermediate between what appears for T_e = 0.1s and 0.4s. In any case, it is very clear for the parasitic vertical acceleration $AS_{av}(T=0)$, while for the $AS_{ah}(T=0)$ is clear than for T_e = 0.4s, but less intense than for T_e = 0.1s. Then, in **Figure 4.12**, the aggravation spectra are compared for different outcrop heights H_t at the locations where the $maxAS_{ah}(T=0)$ and $maxAS_{av}(T=0)$ appear. Similarly, to what appeared for T_e = 0.1s and 0.4s, this figure shows that the maximum aggravation values appear for low periods up to T = T_e (=0.25s here) and reduce thereafter. It also shows that the shape of the aggravation spectrum is not affected by the height H_t, so the effect of H_t appears mostly as a uniform scaling of the spectrum, which is a function of T_e (and H_t).

Figures 4.13 to 4.15 present the spatial variability of aggravation factors for different structural periods (including the T=0s of **Figure 4.11**), but each one of them presents the results for a specific height H_t. Based on previous figures, the variability of geomorphic aggravation for different periods T is similar, but not identical for different H_t values. Specifically, within the valley the horizontal aggravation has 2 peaks for low periods (up to T = 0.4s) and only one (at the center) for large periods (T = 1.0s), i.e. it retains, more or less, qualitatively the spectral response for H_t = 0m and for higher outcropping bedrock heights. Moreover, an increase of H_t leads to a slight increase of parasitic vertical aggravation values for any value of T, and this is more intense at the outcropping bedrock locations.

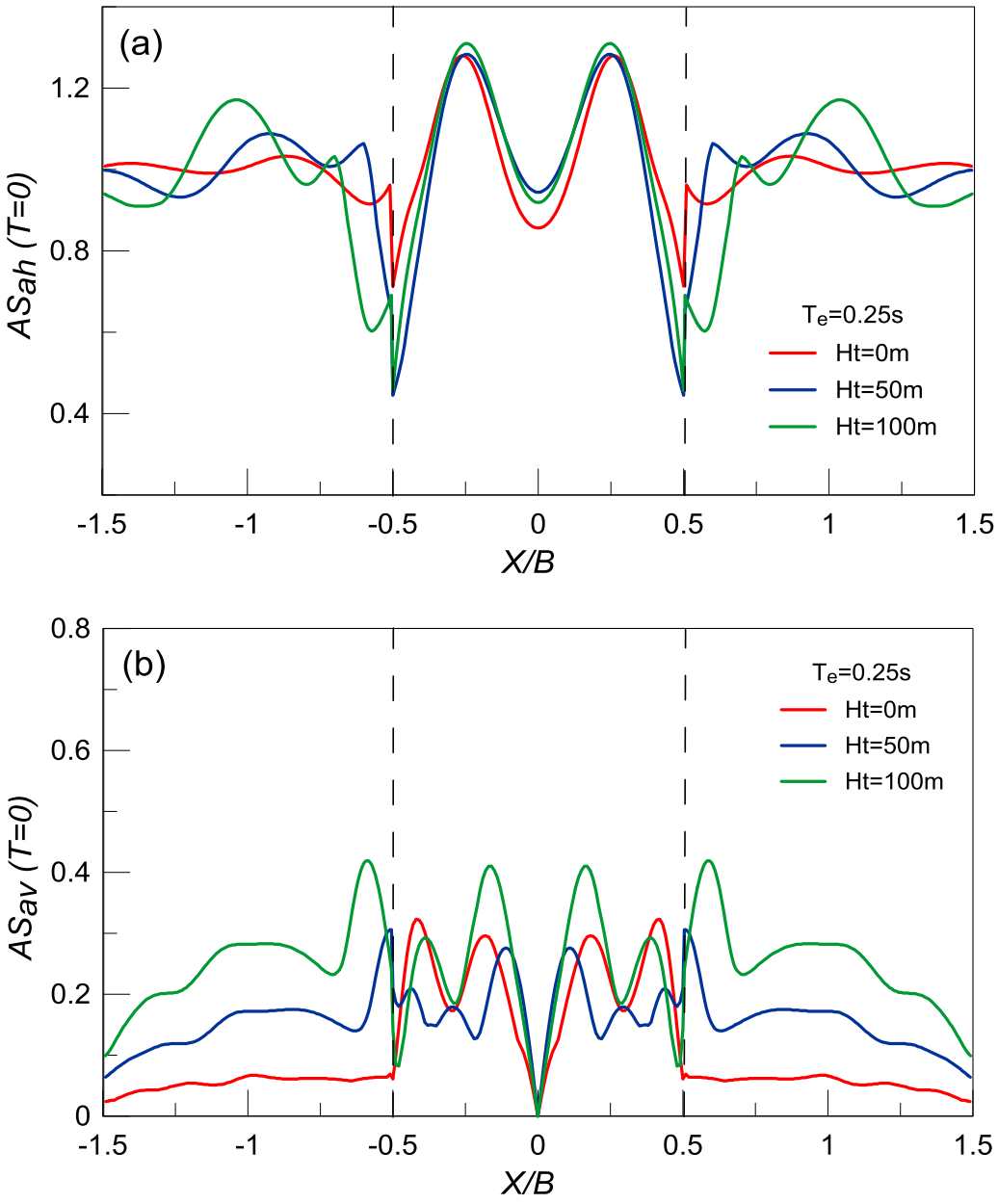

Figure 4.11: Effect of height H_t of steep (i=45^o) outcropping bedrock on the spatial variability of geomorphic aggravation factors AS_{ah} and AS_{av} for T=0s with normalized distance X/B from the center of the steep (s=45^o) valley with high impedance ratio a=0.5; Results for an intermediate frequency excitation with T_e = 0.25s.

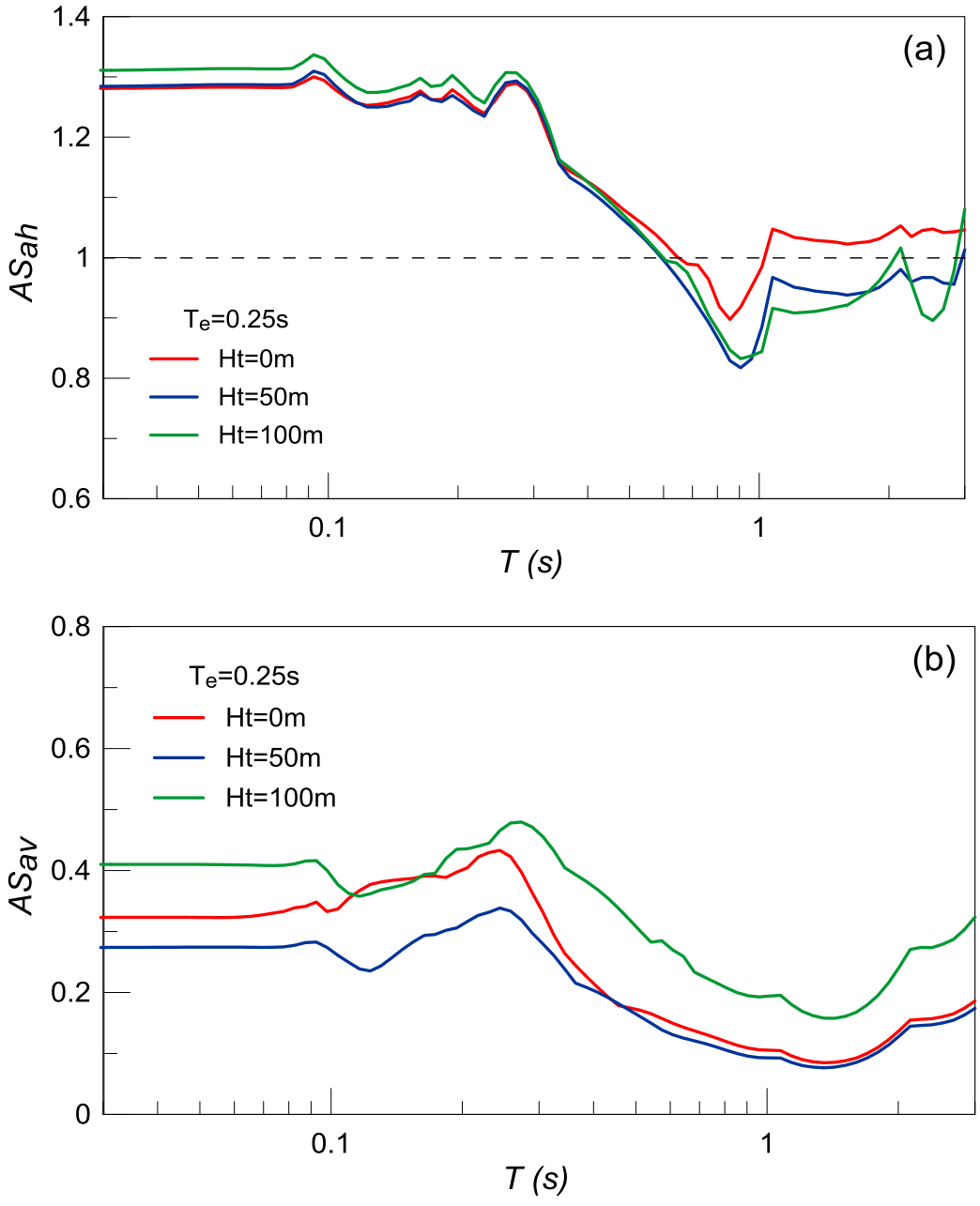

Figure 4.12: Effect of height H_t of steep (i=45^o) outcropping bedrock on geomorphic aggravation spectra AS_{ah} and AS_{av} at the location of peak aggravation for T=0s along the steep (s=45^o) valley with high impedance ratio a=0.5; Results for an intermediate-frequency excitation with T_e = 0.25s.

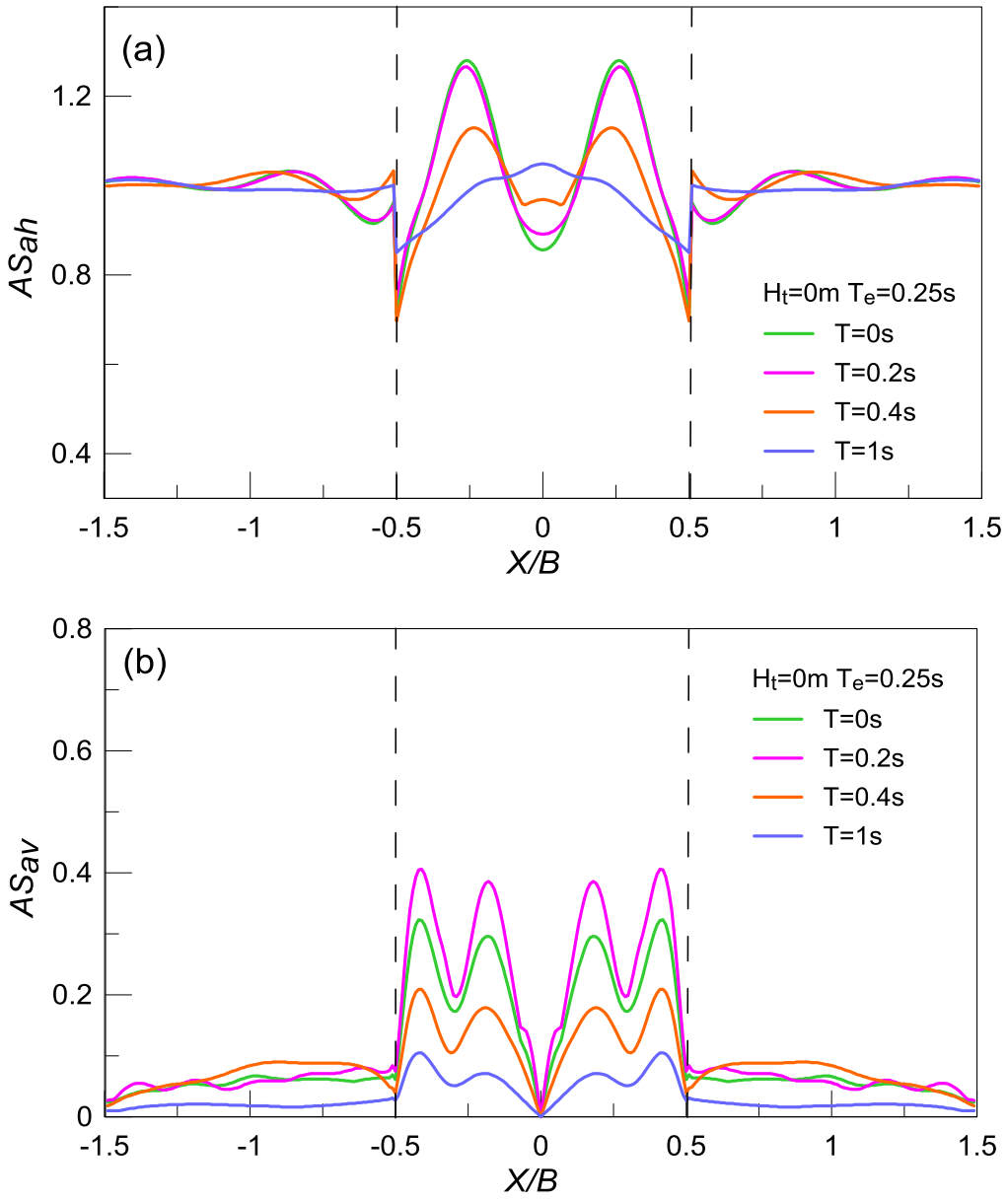

Figure 4.13: Spatial variability of geomorphic aggravation factors AS_{ah} and AS_{av} for specific structural periods T with normalized distance X/B from the center of the steep (s=45^{o}) valley with high impedance ratio a=0.5; Results for outcropping bedrock height H_t = 0m and an intermediate-frequency excitation with T_e = 0.25s.

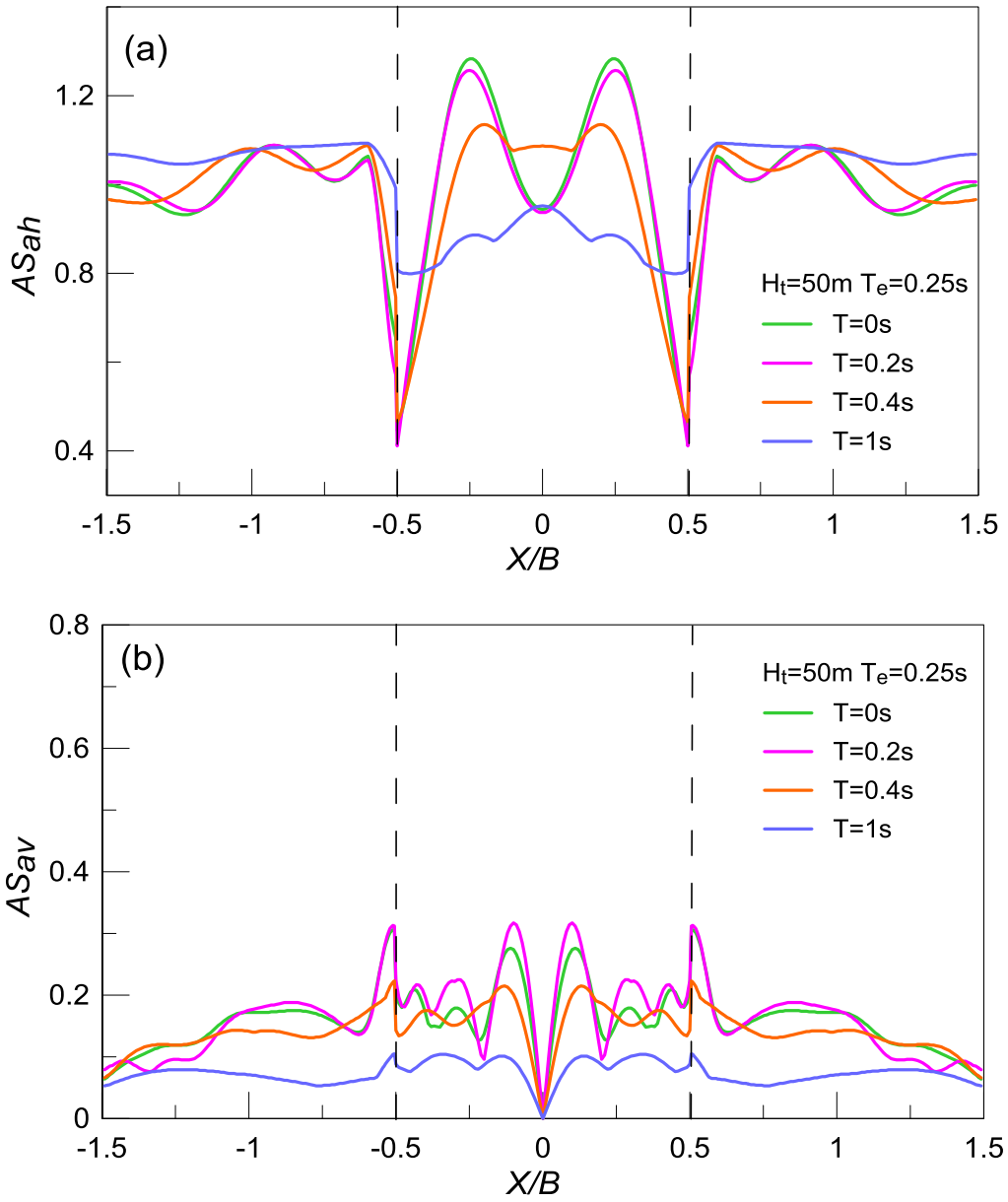

Figure 4.14: Spatial variability of geomorphic aggravation factors AS_{ah} and AS_{av} for specific structural periods T with normalized distance X/B from the center of the steep (s=45^{o}) valley with high impedance ratio a=0.5; Results for height H_t = 50m of steep (i=45^{o}) outcropping bedrock and an intermediate-frequency excitation with T_e = 0.25s.

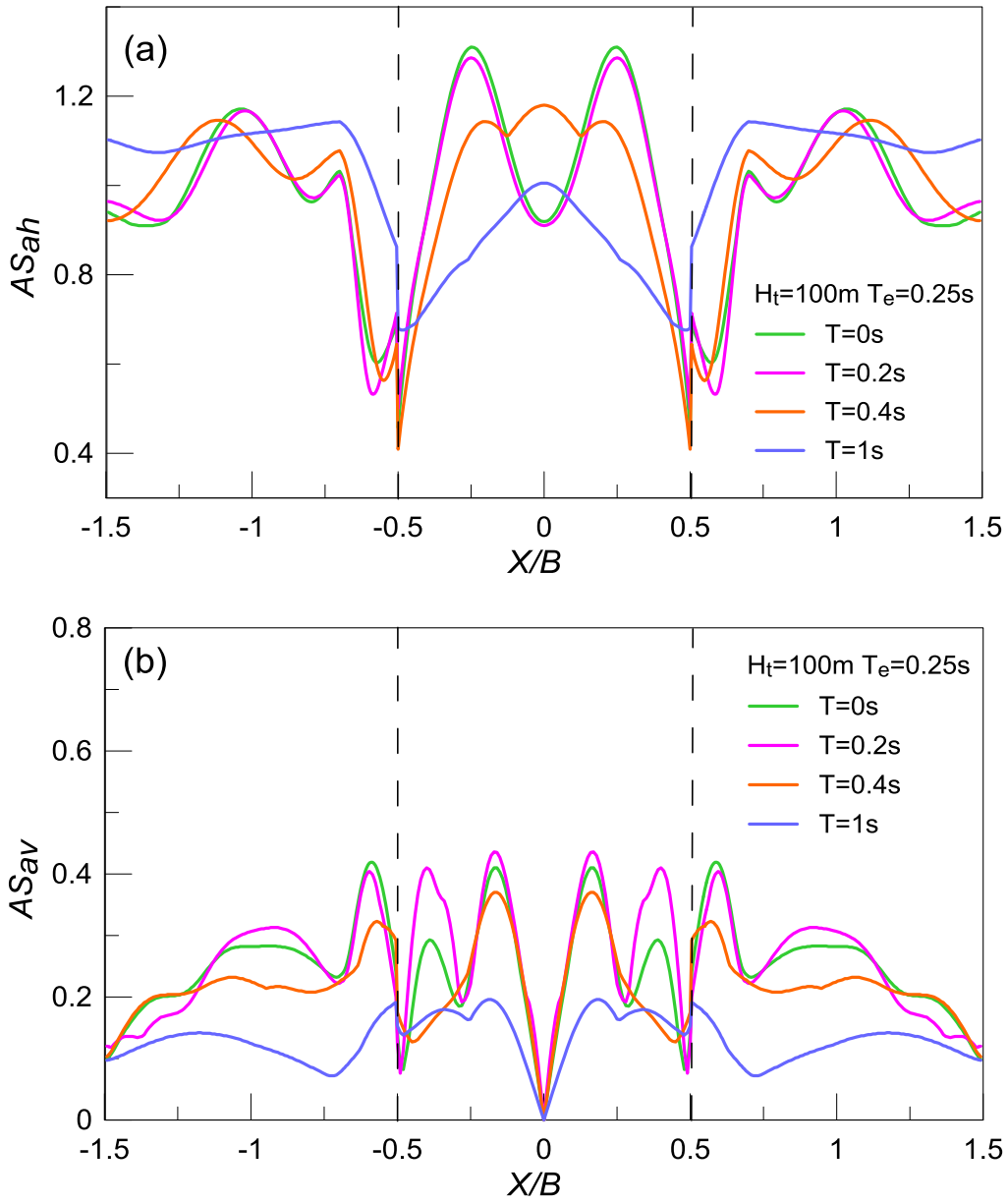

Figure 4.15: Spatial variability of geomorphic aggravation factors AS_{ah} and AS_{av} for specific structural periods T with normalized distance X/B from the center of the steep (s=45^{o}) valley with high impedance ratio a=0.5; Results for height H_t = 100m of steep (i=45^{o}) outcropping bedrock and an intermediate-frequency excitation with T_e = 0.25s.

4.3 Effects for mild valleys s = 22.5^o with mild outcrops i = 22.5^o and high impedance ratio a = 0.5

In this paragraph, the valleys have buried and outcropping bedrock inclination angles (s and i, respectively) equal to 22.5^o, i.e. half of 45^o that which was the inclination angle in paragraph 4.2. Hence, the results in the current paragraph correspond to mildly-inclined valleys with mildly-inclined outcrops, or mild valleys with mild outcrops for brevity. The shear wave velocity for the outcropping bedrock is again V_b = 1000 m/s and for the soil is V_s = 500 m/s (stiff soil), leading to a high impedance ratio a = 0.50. What varies in these analyses are: a) the outcropping bedrock height H_t = 0 and 100m; b) the predominant excitation period T_e = 0.1s (high-frequency) and 0.4s (low-frequency).

The effects of outcropping bedrock height H_t under a high-frequency excitation T_e = 0.1s are demonstrated in **Figures 4.16 - 4.19**. As shown in **Figure 4.16,** for both outcropping bedrock heights H_t=0m and H_t=50m the locations of peak horizontal and vertical aggravation for T = 0s are close to one another, regardless of H_t value, similarly to what appeared for the steep valley with steep outcrops (**Figure 4.1**). Nevertheless, the peak horizontal and vertical aggravation values for T = 0s are clearly smaller than what appeared for the steep valley with steep outcrops. More specifically, for s = i = 45^o and H_t=50m, maxAS_{ah}(T=0)=1.3 and maxAS_{av}(T=0)=0.55, while for s = i = 22.5^o and H_t=50m, maxAS_{ah}(T=0)=1.1 and maxAS_{av}(T=0)=0.35, within the valley. Hence, the geomorphic aggravation within the valley appears to be less significant with milder inclination angles s and i, in accordance to similar findings from the literature. Additionally, an increase of outcropping bedrock height H_t increases slightly the geomorphic aggravation within the valley, but more importantly the values of aggravation at the outcropping bedrock itself. As illustrated in **Figure 4.16**, for flat outcropping bedrock (H_t=0m) AS_{ah}(T=0) takes values close to 1 at the outcropping bedrock, while for H_t=50m maxAS_{ah}(T=0)=1.35 behind the crest. The same holds for the AS_{av}(T=0) at the outcropping bedrock with AS_{av}(T=0) being close to zero for H_t=0m and maxAS_{av}(T=0)=0.2 for H_t=50m. Observe that for steep valley with steep outcrops (**Figure 4.1**) the corresponding values at the outcropping bedrock are maxAS_{ah}(T=0)=1.15 and maxAS_{av}(T=0)=0.4. The geomorphic aggravation spectra AS_{ah} and AS_{av} at the location of peak aggravation for T=0s along the valley, presented in **Figure 4.17**, show the highest aggravation values for small periods (e.g. roughly up to T = T_e = 0.1s and decreasing thereafter). Also, the effect of H_t is slightly increasing for both AS_{ah} and AS_{av}. In comparison to the case with s = i = 45^o (**Figure 4.2**), the shape of the aggravation spectra is similar, but the values are decreased. Thus, the general conclusion about smaller aggravation values for milder inclination angles is also true for every structural period. **Figures 4.18 and 4.19** present the spatial variability of aggravation factors for different structural periods T for H_t=0m and H_t=50m, respectively. They show that for both H_t = 0 and 50m, the AS_{ah} decreases at the edges of the valley as the structural period T increases, while for T=0.4s the AS_{ah} reaches a local maximum at the center of the valley. This period value coincides with the fundamental period of the soil within the valley, since T_s = 4∗50/500 = 0.4s. On the other hand, the AS_{av} takes the maximum value for T = 0.2s and decreased thereafter. Note also that for H_t=50m the geomorphic aggravation is once again more intense than for H_t=0m.

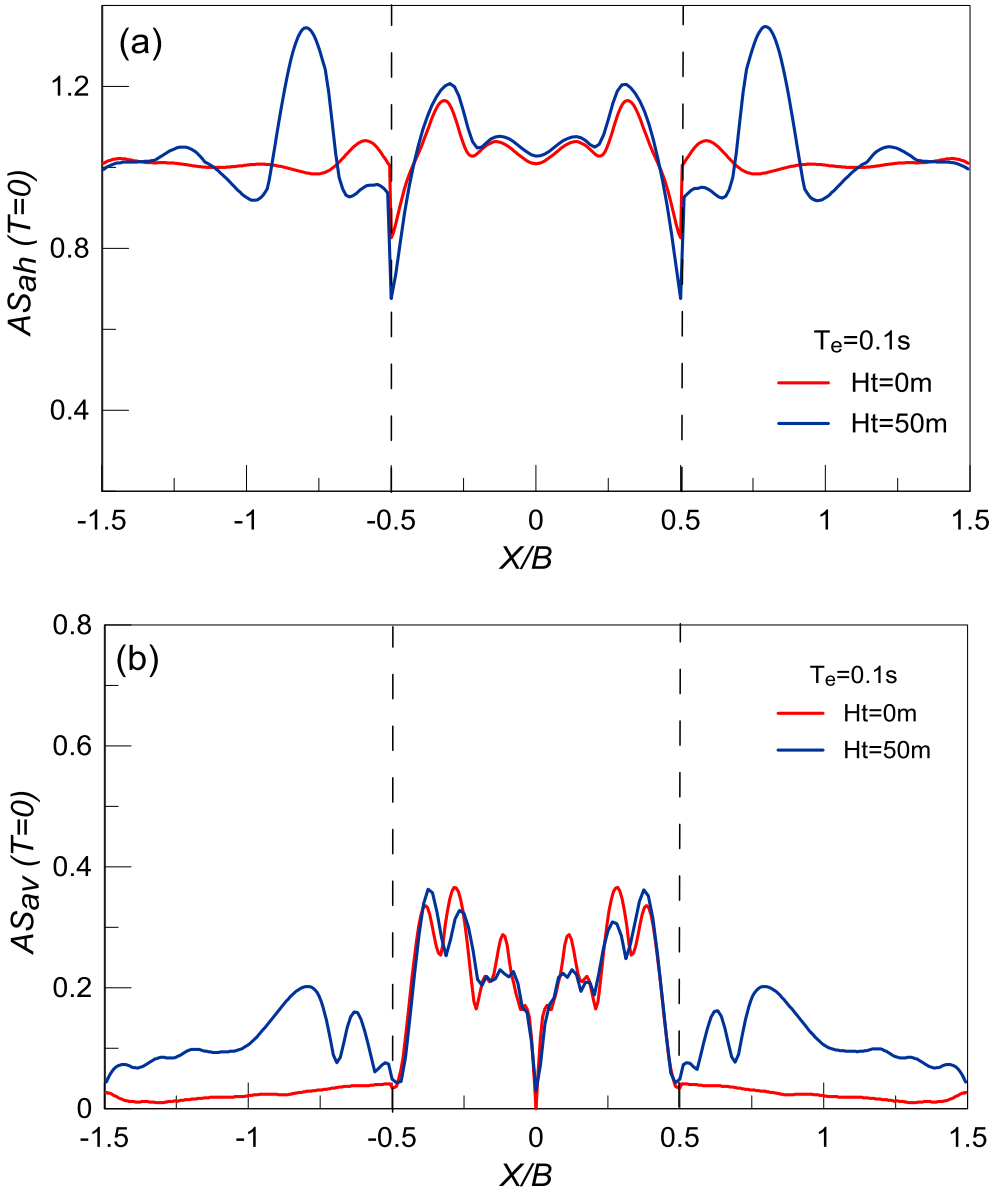

Figure 4.16: Effect of height H_t of mild (i=22.5^o) outcropping bedrock on the spatial variability of geomorphic aggravation factors AS_{ah} and AS_{av} for T=0s with normalized distance X/B from the center of the mild valley (s=22.5^o) with high impedance ratio a=0.5; Results for high frequency excitation with T_e = 0.1s.

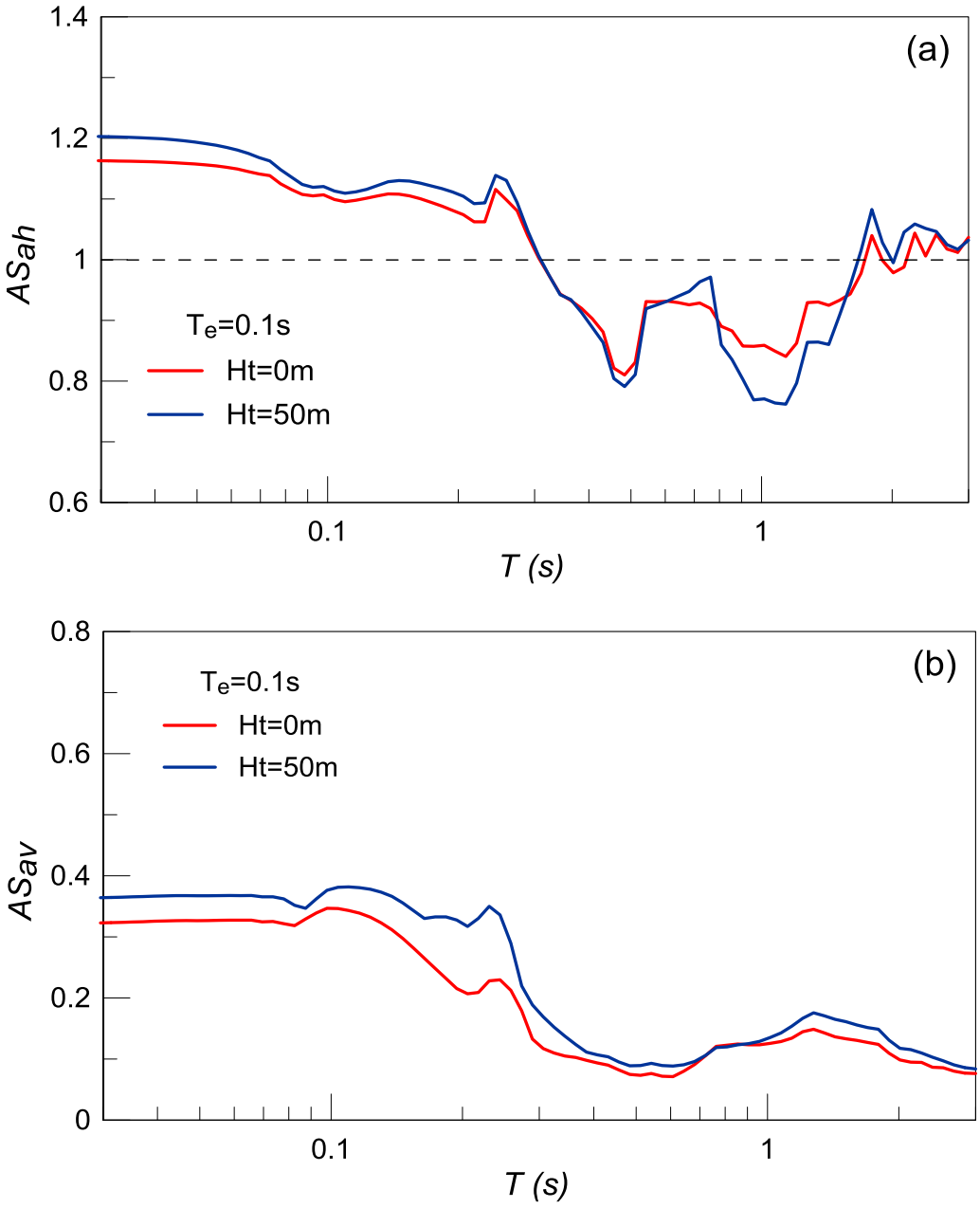

Figure 4.17: Effect of height H_t of mild (i=22.5^o) outcropping bedrock on geomorphic aggravation spectra AS_{ah} and AS_{av} at the location of peak aggravation for T=0s along the mild (s=22.5^o) valley with high impedance ratio a=0.5; Results for high-frequency excitation with T_e = 0.1s.

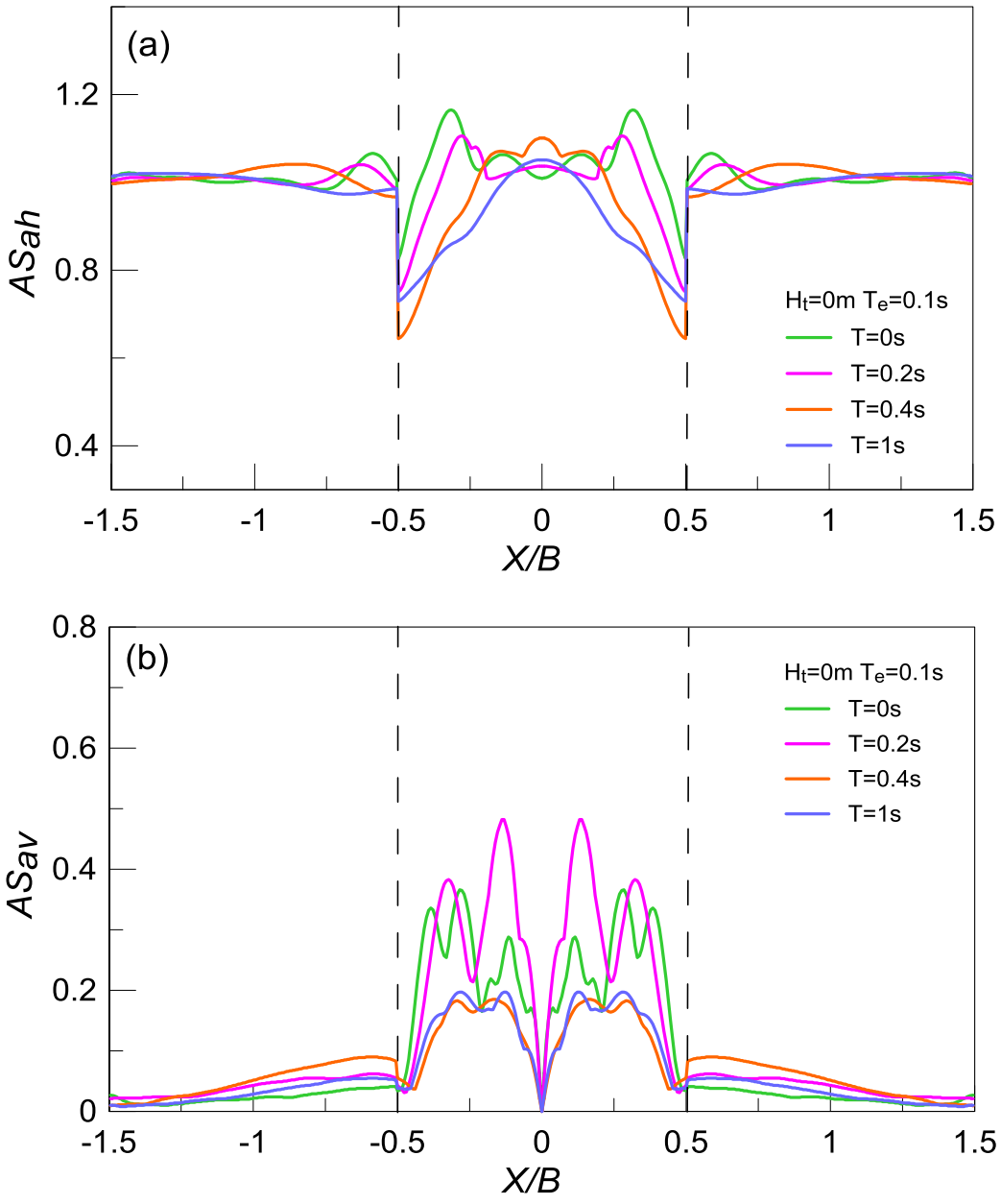

Figure 4.18: Spatial variability of geomorphic aggravation factors AS_{ah} and AS_{av} for specific structural periods T with normalized distance X/B from the center of the mild (s=22.5^{o}) valley with high impedance ratio a=0.5; Results for outcropping bedrock height H_t = 0m and a high-frequency excitation with T_e = 0.1s.

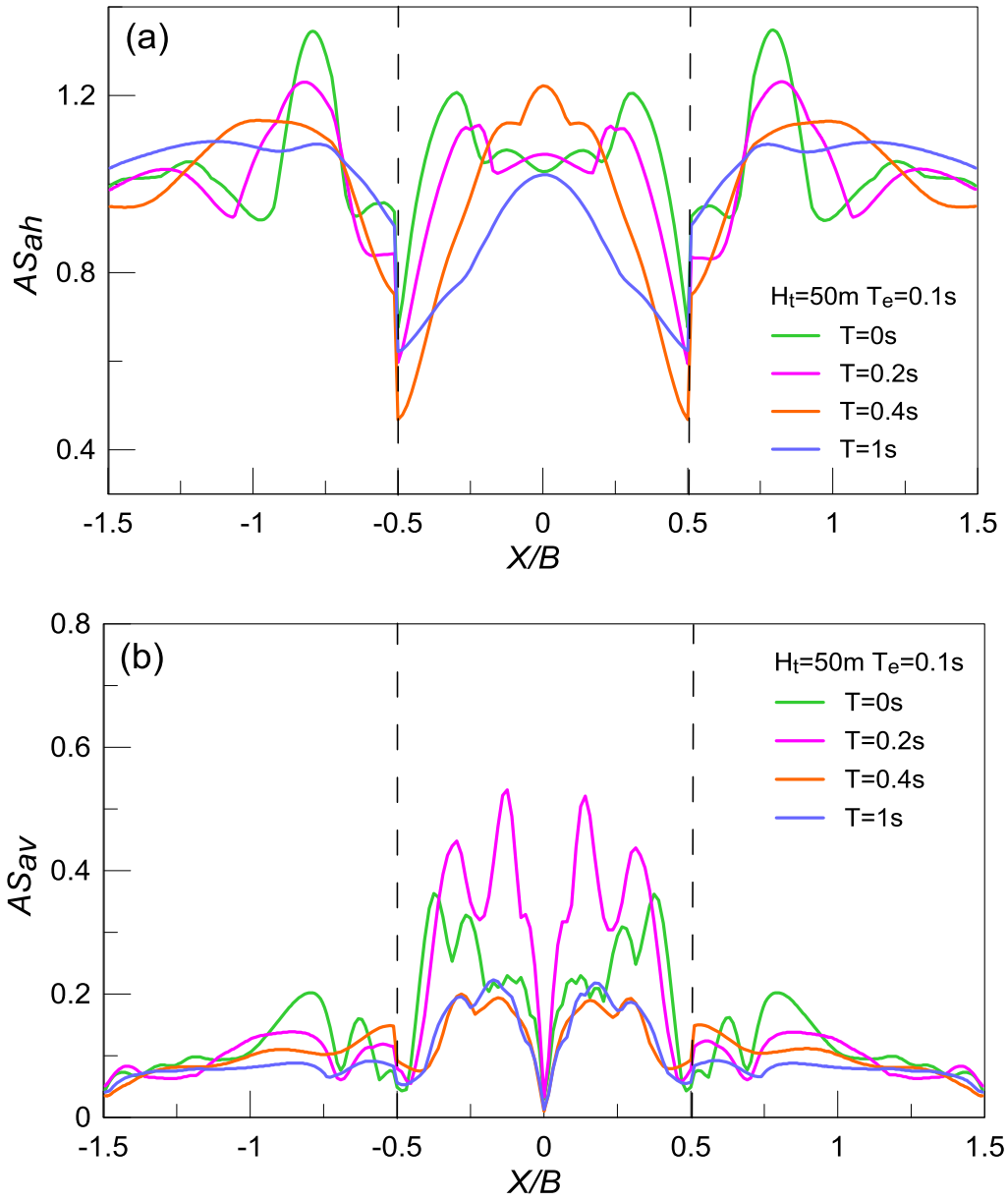

Figure 4.19: Spatial variability of geomorphic aggravation factors AS_{ah} and AS_{av} for specific structural periods T with normalized distance X/B from the center of the mild (s=22.5°) valley with high impedance ratio a=0.5; Results for height H_t = 50m of mild (i=22.5°) outcropping bedrock and a high-frequency excitation with T_e = 0.1s.

In the following, **Figures 4.20 to 4.23** present the aggravation results for the same valley but for a low-frequency excitation with T_e = 0.4s. As demonstrated in **Figure 4.20**, the $AS_{ah}(T=0)$ becomes maximum at the center of the valley, while the height H_t increases both the horizontal and vertical aggravation. Observe that in **Figure 4.6**, showing the same results for s = i = 45^o, the peak horizontal aggravations for T=0s appear at the center of the valley as well, but the values are slightly smaller. The geomorphic aggravation spectra at the center of the valley, presented in **Figure 4.21**, show the peak spectral aggravation values $maxAS_{ah}$ and $maxAS_{av}$ at periods T around the excitation period T_e = 0.4s. The effect of outcropping bedrock height H_t is more intense for the horizontal direction at periods smaller or equal to T=0.4s. For the (parasitic) vertical component this effect is noticeable only for periods T from 0.2s to 0.4s. For periods larger than T=1s, the effect of H_t is decreasing, but this area of the aggravation spectra is generally not essential for engineering practice. In comparison with the corresponding results for s = i = 45^o (**Figure 4.7**), the shape of the aggravation spectra is practically the same.

Figures 4.22 and 4.23 present the spatial variability of aggravation factors for different structural periods (including the T=0s of **Figure 4.20**), but each one of them presents the results for a specific H_t value. As expected from the previous figures, the peak horizontal aggravation happens for T=0.4s, which coincides with the predominant excitation period T_e. On the other hand, the AS_{av} reaches its maximum value for T=0.2s. As the outcropping bedrock height H_t increases from 0 to 50m, the aggravation is more significant and the differences in the results for the periods of interest become larger.

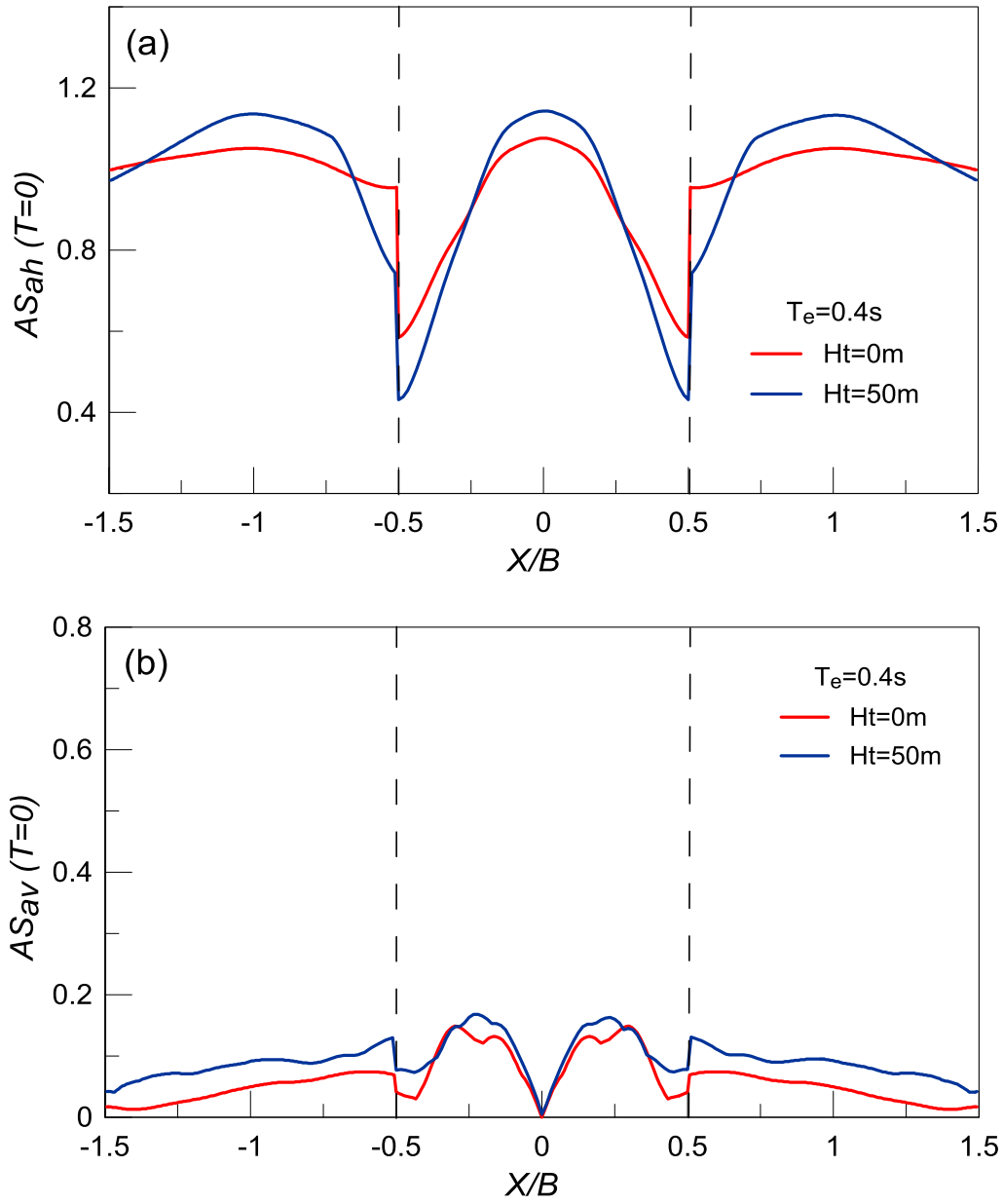

Figure 4.20: Effect of height H_t of mild (i=22.5^o) outcropping bedrock on the spatial variability of geomorphic aggravation factors AS_{ah} and AS_{av} for T=0s with normalized distance X/B from the center of the mild valley (s=22.5^o) with high impedance ratio a=0.5; Results for low frequency excitation with T_e = 0.4s.

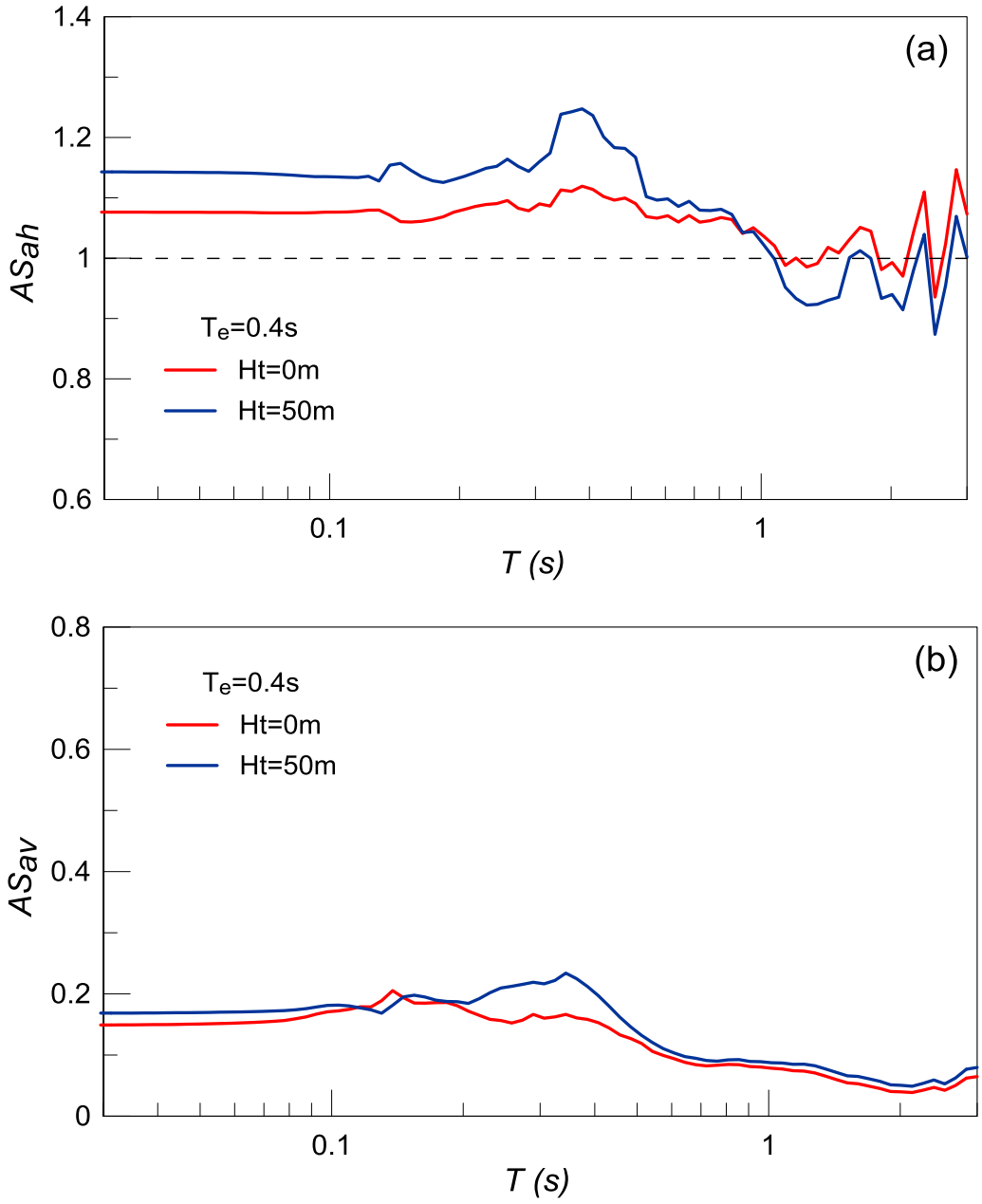

Figure 4.21: Effect of height H_t of mild (i=22.5^o) outcropping bedrock on geomorphic aggravation spectra AS_{ah} and AS_{av} at the location of peak aggravation for T=0s along the mild (s=22.5^o) valley with high impedance ratio a=0.5; Results for low-frequency excitation with T_e = 0.4s.

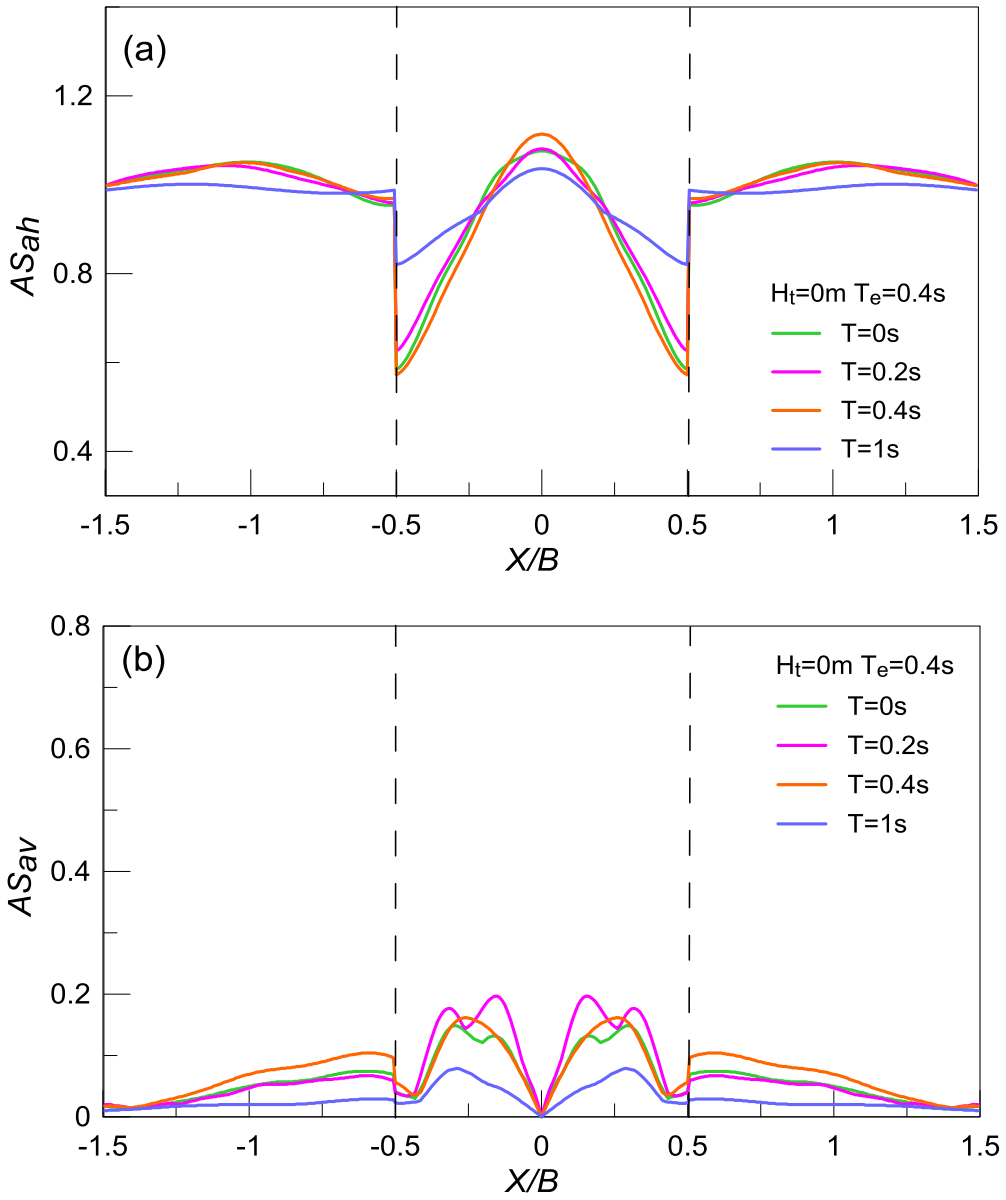

Figure 4.22: Spatial variability of geomorphic aggravation factors AS_{ah} and AS_{av} for specific structural periods T with normalized distance X/B from the center of the mild (s=22.5^o) valley with high impedance ratio a=0.5; Results for outcropping bedrock height H_t = 0m and a low frequency excitation with T_e = 0.4s.

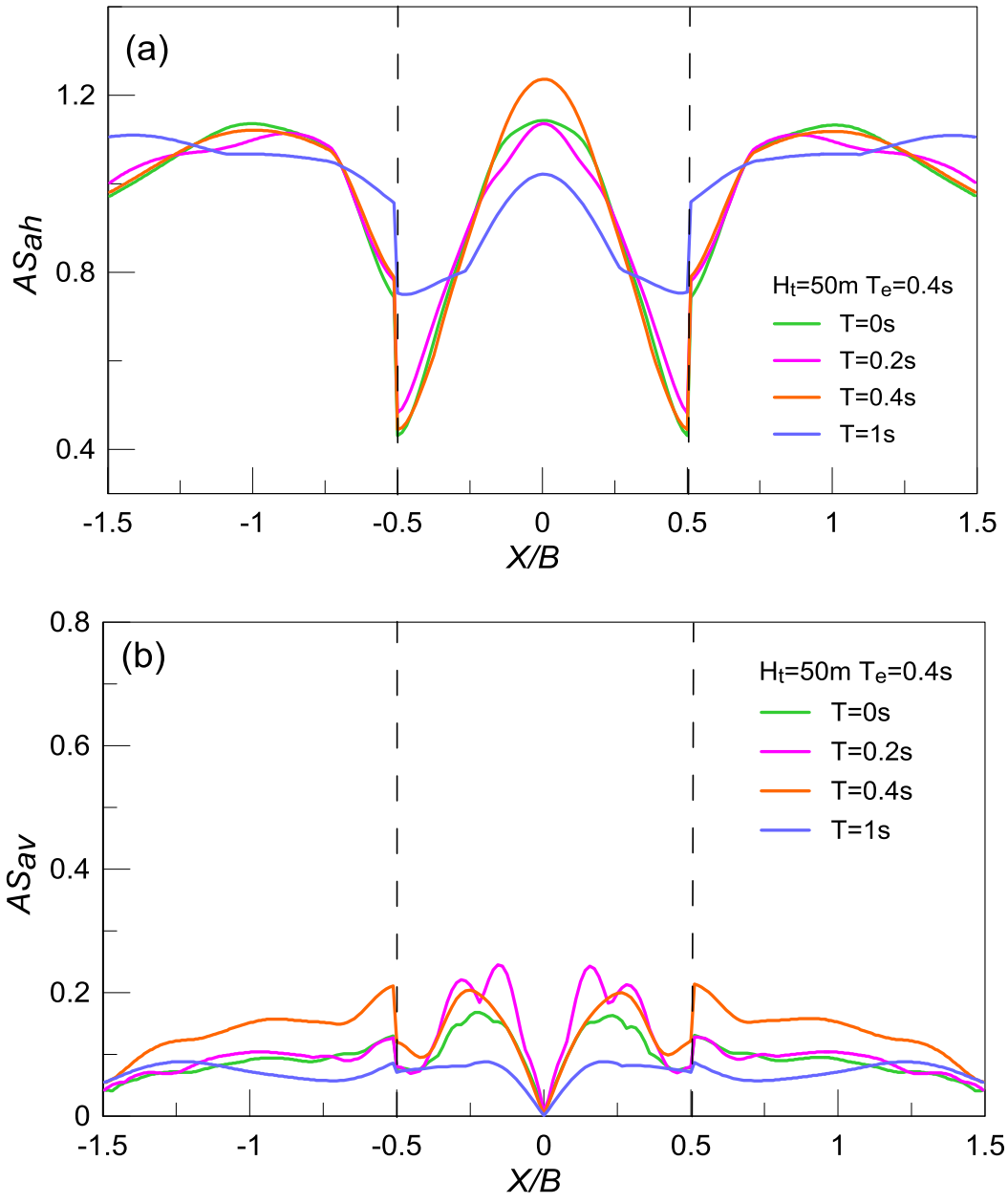

Figure 4.23: Spatial variability of geomorphic aggravation factors AS_{ah} and AS_{av} for specific structural periods T with normalized distance X/B from the center of the mild (s=22.5^o) valley with high impedance ratio a=0.5; Results for height H_t = 50m of mild (i=22.5^o) outcropping bedrock and a low frequency excitation with T_e = 0.4s.

4.4 Effects for differently inclined valleys and outcrops with a high impedance ratio a = 0.5

In this paragraph, the inclination angles of the valley edges (s) and the bedrock outcrops (i) are not the same, as in the analyses in the previous paragraphs. The purpose of these additional analyses is to ascertain whether this difference in inclination angles plays an important role in the seismic response of the valley. The first set of analyses is performed for a mild valley (s=22.5^o) with steep outcrops (i=45^o) and outcropping bedrock height H_t=50m. In order to determine the effect of differently inclined valleys and outcrops, the corresponding results for a mild valley with mild outcrops (s = i = 22.5^o) and H_t=50m are also included, for comparison purposes, along with the results for a mild valley with flat outcrops (H_t=0m, with black dashed line). The same procedure is followed for a steep valley (s=45^o) with mild outcrops (i=22.5^o) and H_t=50m. In that case, the comparison is made between a steep valley with steep outcrops (s=i=45^o) and H_t=50m, and a steep valley with flat outcrops (H_t=0m). The shear wave velocity for the outcropping bedrock is V_b = 1000 m/s and for the soil is V_s = 500 m/s (stiff soil), leading to a high impedance ratio a = 0.50. The predominant excitation period varies from T_e = 0.1s (high-frequency) to T_e = 0.4s (low-frequency).

The results for a valley with mild inclination angle s=22.5^o and steep outcrops (i=45^o) are presented in **Figures 4.24 to 4.29**. As shown in **Figure 4.24**, for a high-frequency excitation with T_e=0.1s, the horizontal and vertical aggravation for T=0s within the valley is practically the same for both the steep (i=45^o) and the mild (i=22.5^o) outcrops. On the contrary, at the outcropping bedrock the steep outcrops (i=45^o) de-amplify AS_{ah}(T=0) and amplify AS_{av}(T=0) in comparison to what is observed when the outcrops have a mild inclination (i=22.5^o). The geomorphic aggravation spectra at the location of peak aggravation for T=0s along the valley are compared in **Figure 4.25**. This figure shows higher values of AS_{ah} for the steep outcrops, especially for periods smaller than T=0.3s. This observation stands for AS_{av} only for periods smaller than T=0.1s. The picture is not clear for larger periods, but the overall differences are not significant. **Figure 4.26** presents the spatial variability of aggravation factors for different structural periods T (including the T=0s of **Figure 4.24**) for the mild valley (s=22.5^o) with steep outcrops (i=45^o) with height H_t=50m. As expected from the previous figures, the results for each period T within the valley are identical with those of a mild valley with mild outcrops (s=i=22.5^o). The decrease of AS_{ah} and the increase of AS_{av} at the outcrops observed for T=0s is also verified for the other structural periods T.

The same comparison procedure is followed for the same valley combinations under a low-frequency excitation with T_e=0.4s. As shown in **Figure 4.27**, the aggravation in both directions within the mild valley is identical for mild and steep outcrops. At the outcropping bedrock, for steep outcrops, the peak value of AS_{ah} is closer to the hill crest, while AS_{av} is slightly increased with respect to the mild outcrops case. The geomorphic aggravation spectra at the location of peak aggravation for T=0s along the valley are compared in **Figure 4.28**. This comparison proves that the inclination angle of the outcrops for the mild valley has no effect on both AS_{ah} and AS_{av} regardless of the structural period T. **Figure 4.29** shows the spatial variability of aggravation factors for different structural periods T for the mild valley with steep outcrops. Observe that again the results within the valley are the same. Therefore, the effect of inclination angle i of the outcrops is practically insignificant for a mild valley, regardless of the applied excitation period T_e.

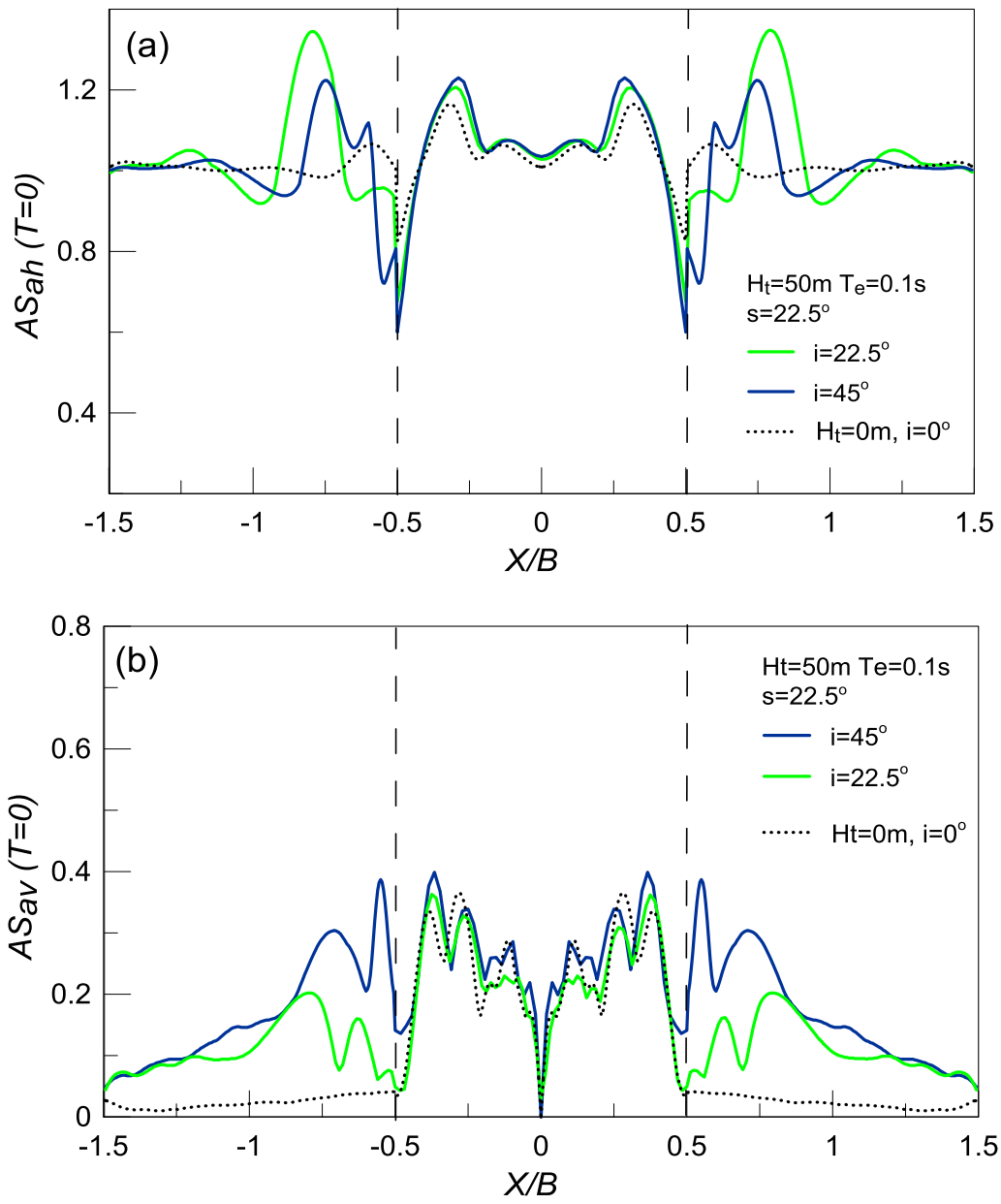

Figure 4.24: Effect of inclination angle i of outcropping bedrock on the spatial variability of geomorphic aggravation factors AS_{ah} and AS_{av} for T=0s with normalized distance X/B from the center of the mild (s=22.5°) valley with high impedance ratio a=0.5; Results for high frequency excitation with T_e = 0.1s, H_t = 50m and s = 22.5° and comparison for valley with H_t = 0m and s = 22.5°.

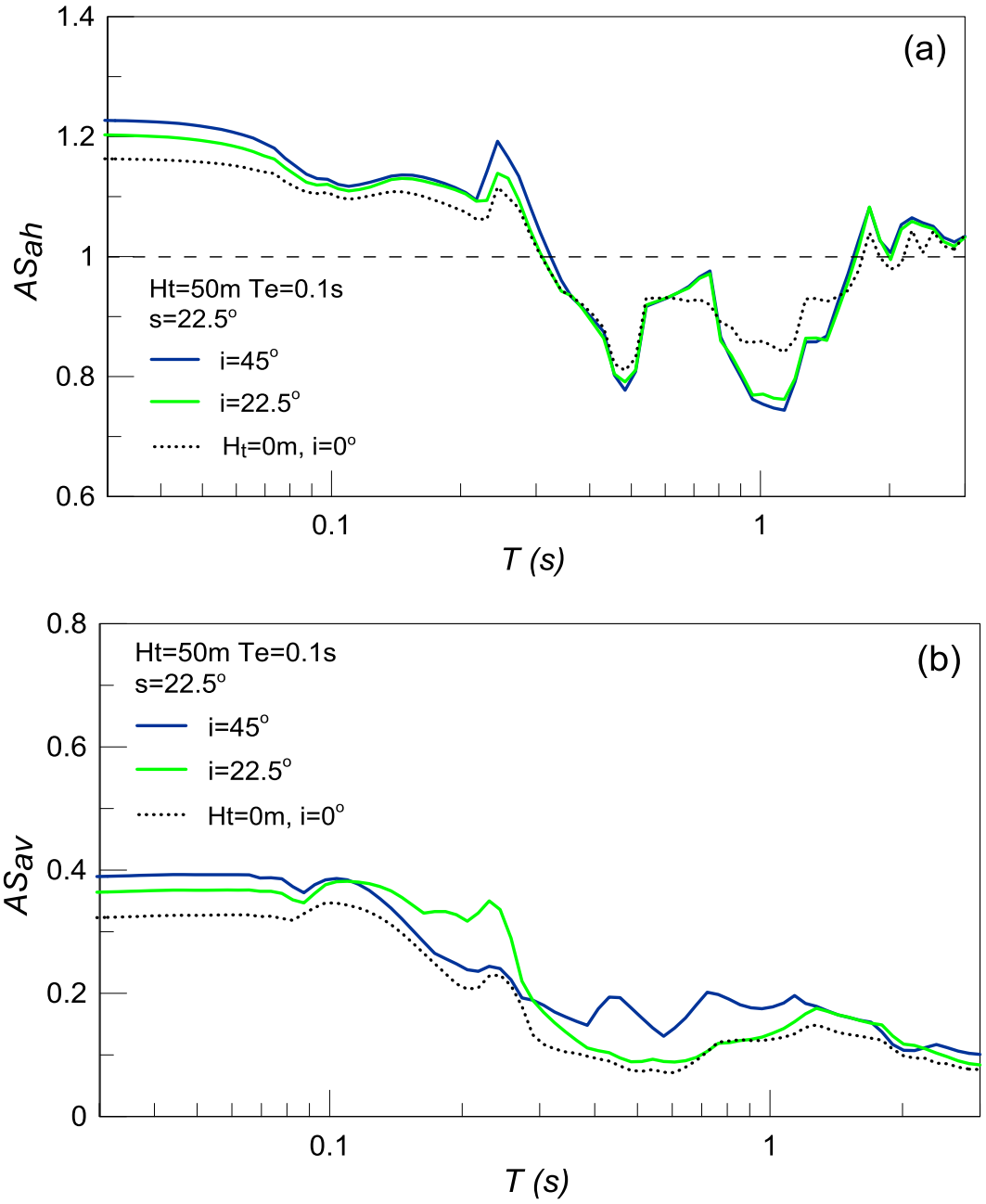

Figure 4.25: Effect of inclination angle i of outcropping bedrock on geomorphic aggravation spectra AS_{ah} and AS_{av} at the location of peak aggravation for T=0s along the mild (s=22.5°) valley with high impedance ratio a=0.5; Results for high-frequency excitation with T_e = 0.1s, Ht = 50m and comparison for valley with H_t = 0m and s = 22.5°.

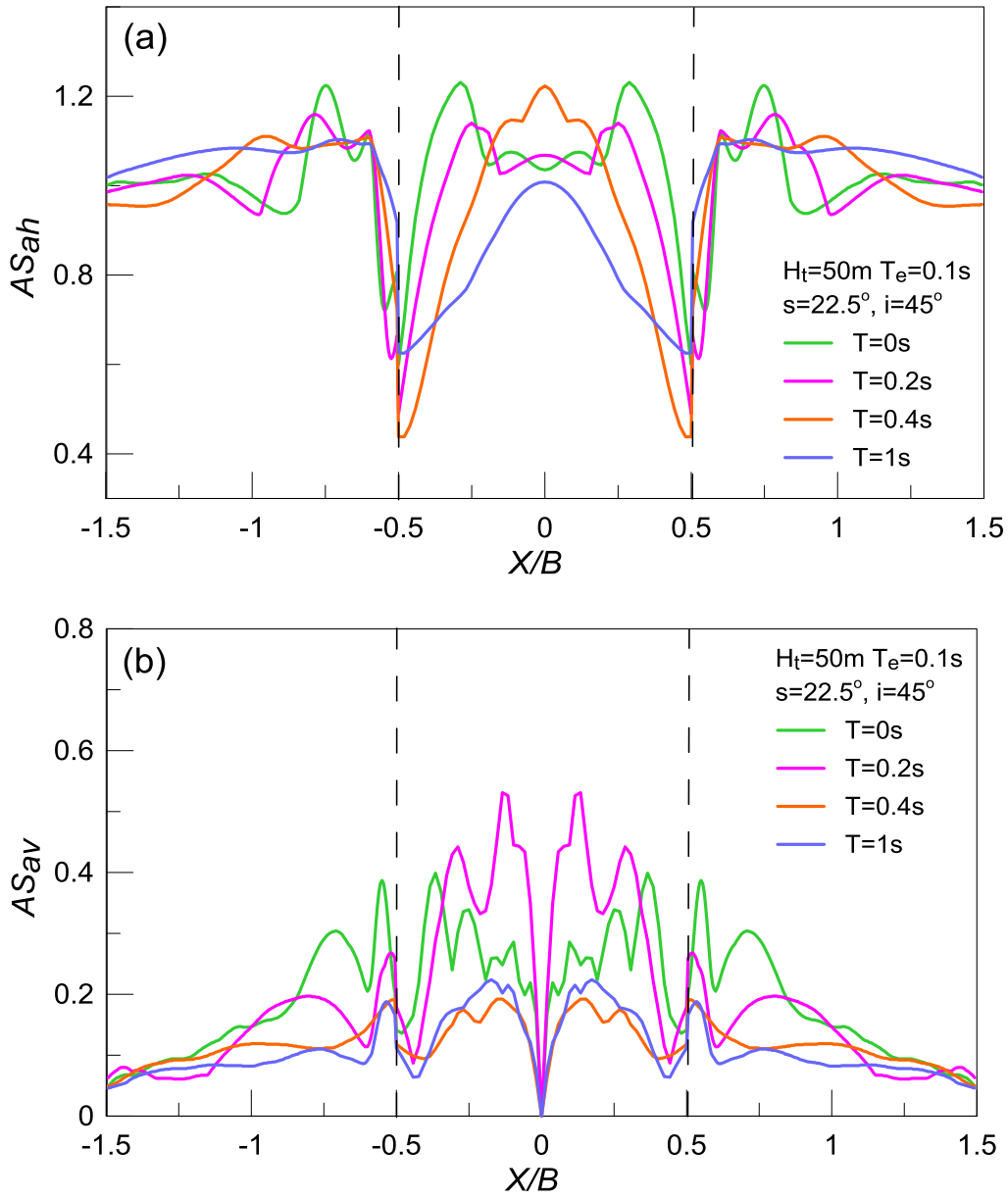

Figure 4.26: Spatial variability of geomorphic aggravation factors AS_{ah} and AS_{av} for specific structural periods T with normalized distance X/B from the center of the mild (s=22.5°) valley with high impedance ratio a=0.5; Results for outcropping bedrock height H_t = 50m, i=45° and a high-frequency excitation with T_e = 0.1s.

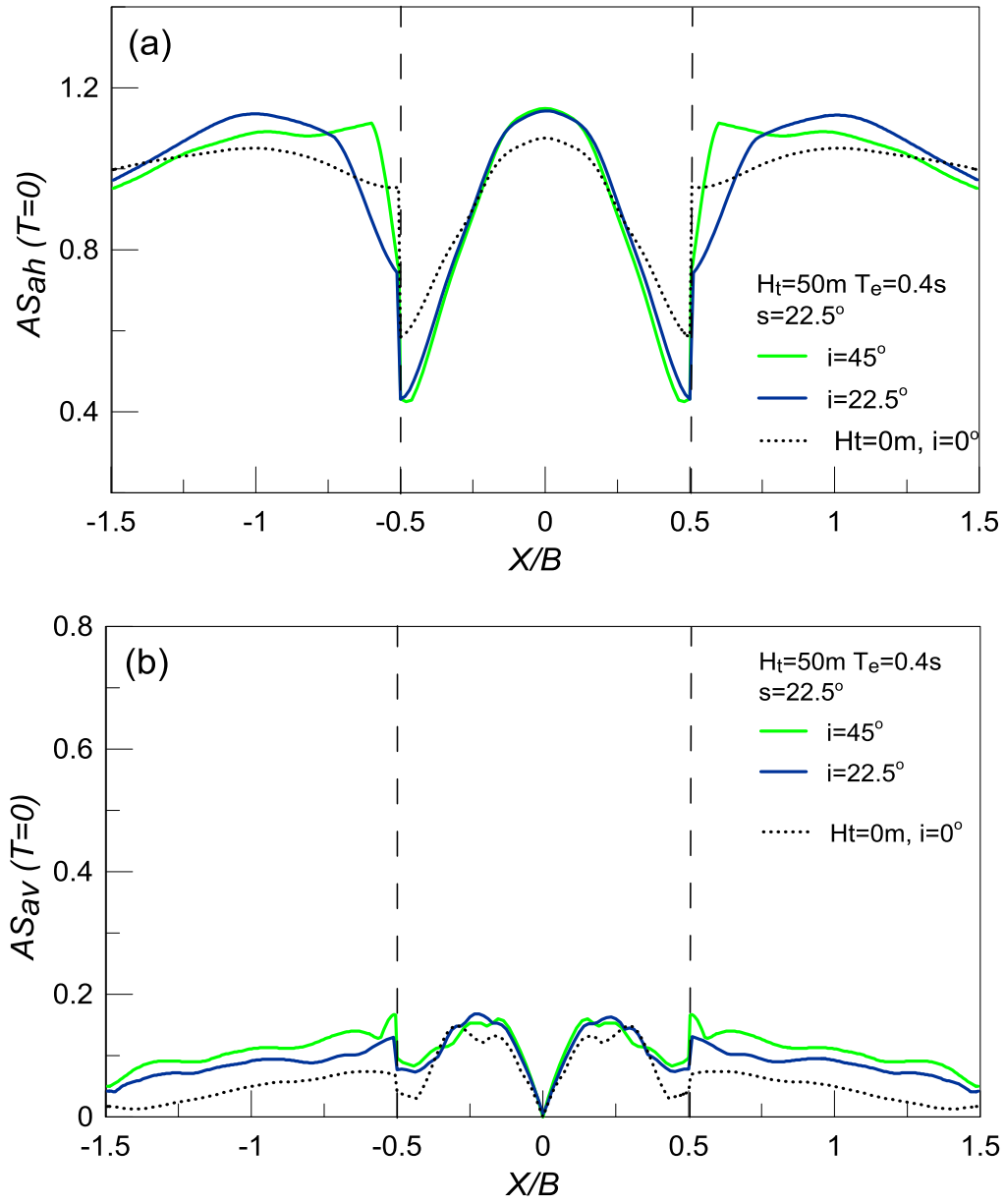

Figure 4.27: Effect of inclination angle i of outcropping bedrock on the spatial variability of geomorphic aggravation factors AS_{ah} and AS_{av} for T=0s with normalized distance X/B from the center of the mild (s=22.5°) valley with high impedance ratio a=0.5; Results for low frequency excitation with T_e = 0.4s, H_t = 50m and comparison for valley with H_t = 0m and s = 22.5°.

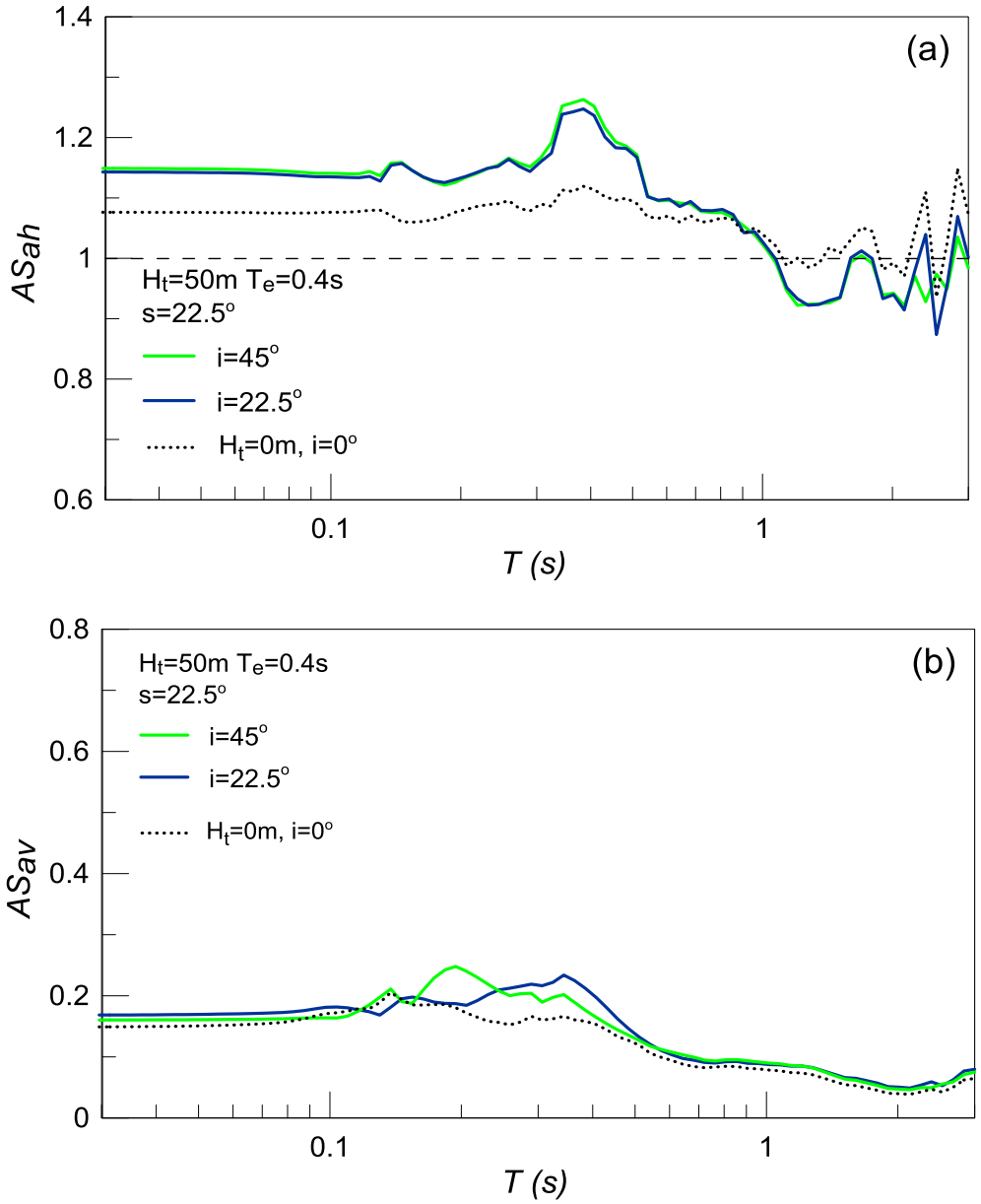

Figure 4.28: Effect of inclination angle i of outcropping bedrock on geomorphic aggravation spectra AS_{ah} and AS_{av} at the location of peak aggravation for T=0s along the mild (s=22.5°) valley with high impedance ratio a=0.5; Results for low-frequency excitation with T_e = 0.4s, Ht = 50m and comparison for valley with H_t = 0m and s = 22.5°.

.

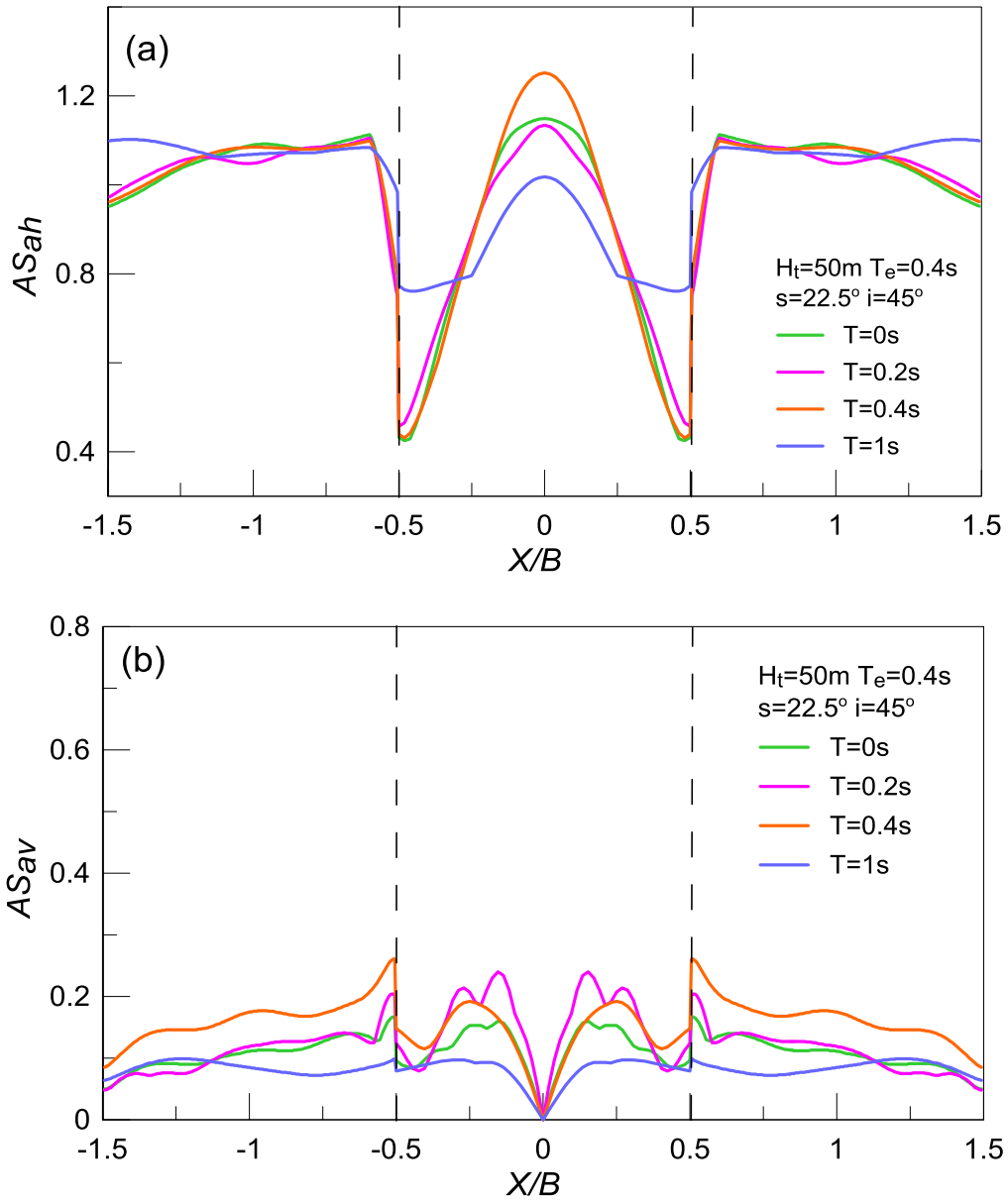

Figure 4.29: Spatial variability of geomorphic aggravation factors AS_{ah} and AS_{av} for specific structural periods T with normalized distance X/B from the center of the mild (s=22.5°) valley with high impedance ratio a=0.5; Results for outcropping bedrock height H_t = 50m, i=45° and a low-frequency excitation with T_e = 0.4s.

In the sequel, **Figures 4.30 to 4.35** present the aggravation results for the steep valley (s=45^o) with mild outcrops (i=22.5^o), i.e. the opposite combination of inclinations that was presented in **Figures 4.24 to 4.29**. Specifically, as shown in **Figure 4.30**, for the high-frequency excitation (T_e=0.1s), the seismic response of the steep valley is not affected by the inclination angle i of the outcrops. At the same time, the effect of outcropping bedrock height H_t is negligible, as has been proven for all the valley cases under a high-frequency excitation. Nevertheless, the mild outcrops increase AS_{ah}(T=0) and decrease AS_{av}(T=0) outside of the valley. Specifically, for i=22.5^o maxAS_{ah}(T=0)=1.3 and maxAS_{av}(T=0)=0.15 are observed, while for i=45^o maxAS_{ah}(T=0)=1.15 and maxAS_{av}(T=0)=0.4, respectively. Notice that a similar effect was also depicted for the mild valley under an excitation with T_e=0.1s (see **Figure 4.24**). Hence, it can be concluded that milder outcrops for high-frequency excitations increase AS_{ah}(T=0) and decrease AS_{av}(T=0) outside the boundaries of valleys, regardless of their inclination angle, and this holds true at least for a high impedance ratio (a=0.5) that characterizes all analyses presented so far. In the sequel, **Figure 4.31** presents the geomorphic aggravation spectra at the location of peak aggravation for T=0s along the steep valley. The mild outcrops cause a minor decrease on AS_{ah} and AS_{av} for periods smaller or equal to T=0.1s. The same holds in **Figure 4.25** for the mild valley case. **Figure 4.32** shows the spatial variability of aggravation factors for different structural periods T for the steep valley with mild outcrops. The aggravation within the valley is identical with **Figure 4.4** for the steep outcrops and the only differences are observed at the outcropping bedrock. The conclusion for T=0s, underlined in **Figure 4.24,** is extrapolated here for all values of the structural period.

The corresponding results for a low-frequency excitation with T_e=0.4s are demonstrated in **Figures 4.33 to 4.35**. As illustrated in **Figure 4.33**, the effect of height H_t is significant for AS_{ah}(T=0) and AS_{av}(T=0), but the inclination angle of the outcrops plays no role in the response of the valley. It is worth mentioning here that these results are similar to those of **Figure 4.27**, which refers to the mild valley. **Figure 4.34** presents the geomorphic aggravation spectra at the location of peak aggravation for T=0s along the steep valley. The horizontal aggravation spectra AS_{ah} for mild and steep outcrops coincide for the period range shown, while for the parasitic vertical aggravation spectra AS_{av} the values are slightly lower for milder outcrops. **Figure 4.35** shows the spatial variability of aggravation factors for different structural periods for the steep valley with mild outcrops. As expected, the results within the valley are the same as for the same valley with steep outcrops (**Figure 4.9**), with AS_{ah} and AS_{av} taking their maximum values for T=0.4s.

From all the analyses in this paragraph it can be concluded that for high impedance ratio (a=0.5) the inclination angle of the outcrops has negligible effects on AS_{ah} and AS_{av} within the valley, for all the examined periods and valley inclinations. The only significant effects were observed at the outcropping bedrock. Specifically, for a high-frequency excitation (T_e=0.1s), mild outcrops increase AS_{ah} and decrease AS_{av} for periods smaller or equal to T=0.1s, while for a low-frequency excitation (T_e=0.4s), mild outcrops shift the local maximum of AS_{ah}(T=0) behind the bedrock outcrop crest and slightly decrease AS_{av}.

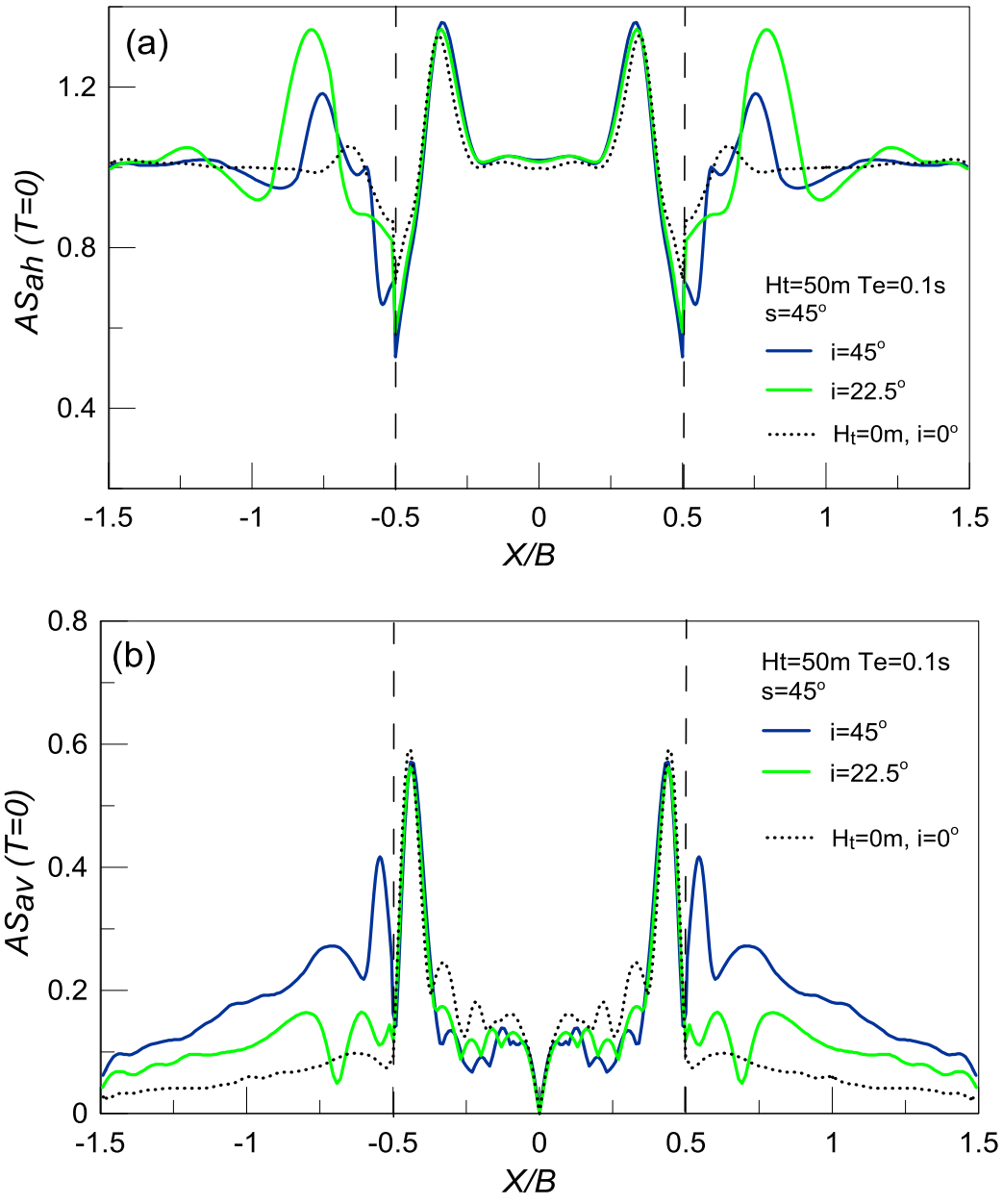

Figure 4.30: Effect of inclination angle i of outcropping bedrock on the spatial variability of geomorphic aggravation factors AS_{ah} and AS_{av} for T=0s with normalized distance X/B from the center of the steep (s=45°) valley with high impedance ratio a=0.5; Results for high frequency excitation with T_e = 0.1s, H_t = 50m and comparison for valley with H_t = 0m and s = 45°.

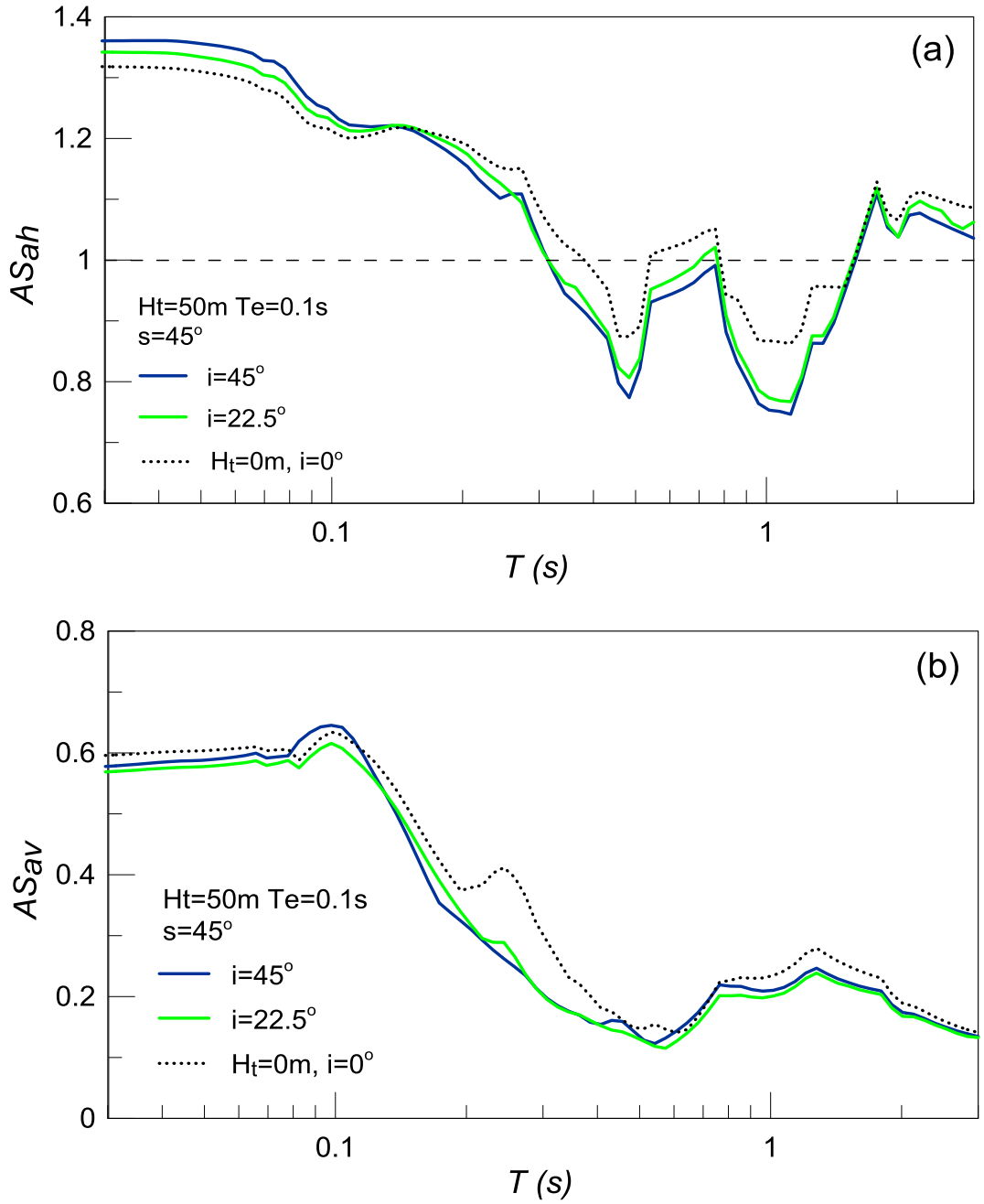

Figure 4.31: Effect of inclination angle i of outcropping bedrock on geomorphic aggravation spectra AS_{ah} and AS_{av} at the location of peak aggravation for T=0s along the steep (s=45°) valley with high impedance ratio a=0.5; Results for high-frequency excitation with T_e = 0.1s, H_t = 50m and comparison for valley with H_t = 0m and s = 45°.

.

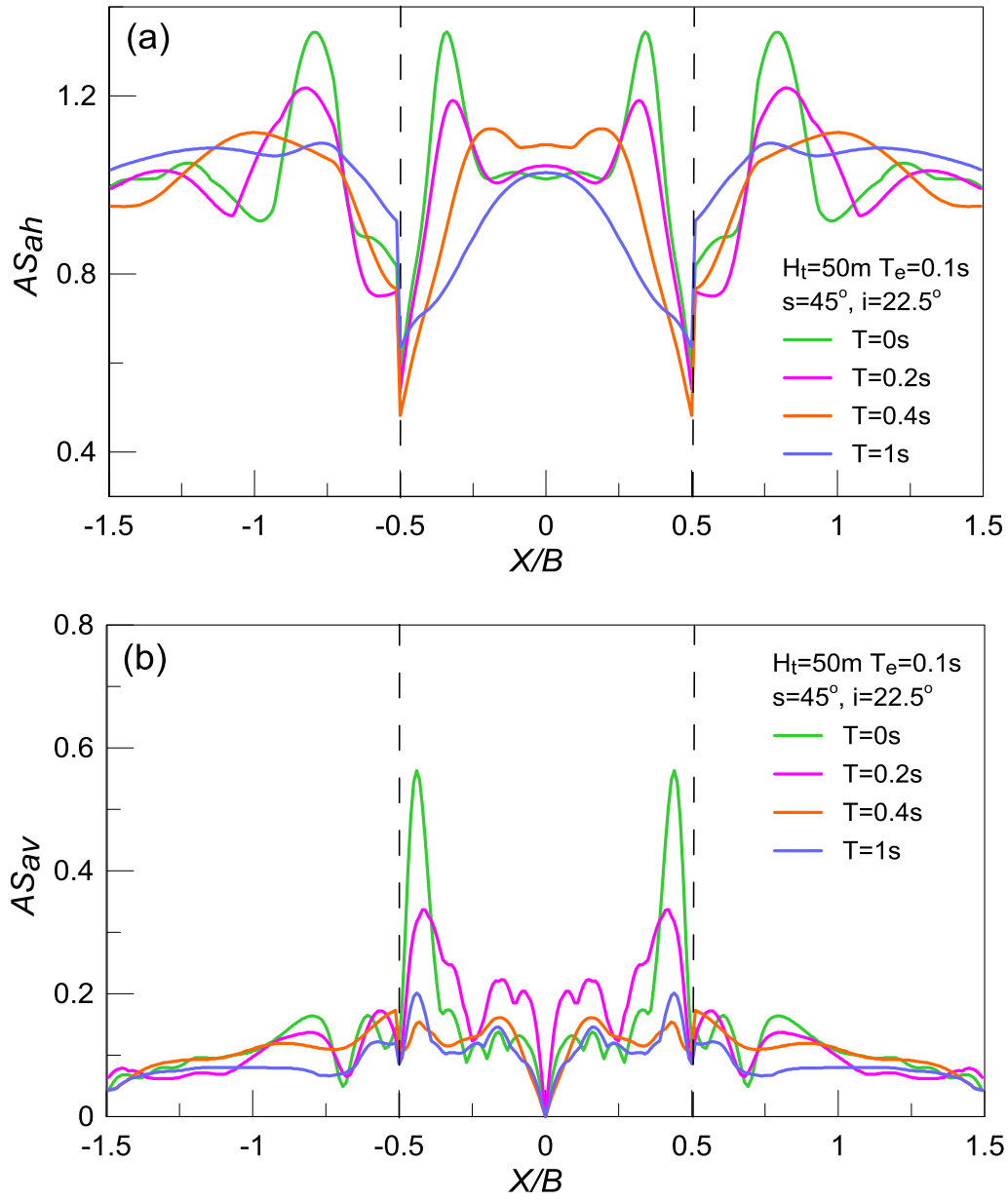

Figure 4.32: Spatial variability of geomorphic aggravation factors AS_{ah} and AS_{av} for specific structural periods T with normalized distance X/B from the center of the steep (s=45°) valley with high impedance ratio a=0.5; Results for outcropping bedrock height H_t = 50m, i=22.5° and a high-frequency excitation with T_e = 0.1s.

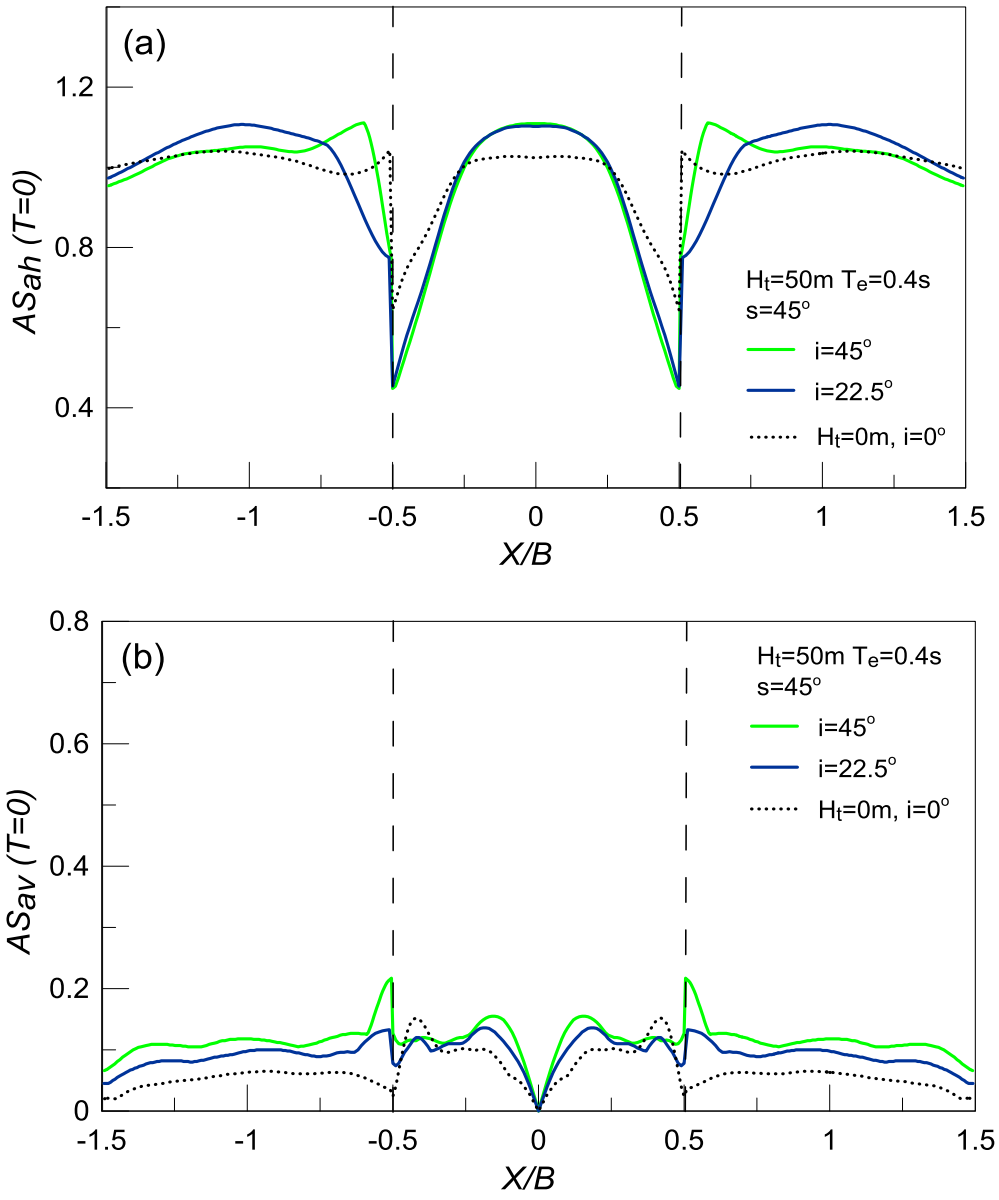

Figure 4.33: Effect of inclination angle i of outcropping bedrock on the spatial variability of geomorphic aggravation factors AS_{ah} and AS_{av} for T=0s with normalized distance X/B from the center of the steep (s=45^o) valley with high impedance ratio a=0.5; Results for low frequency excitation with T_e = 0.4s, H_t = 50m and comparison for valley with H_t = 0m and s = 45^o.

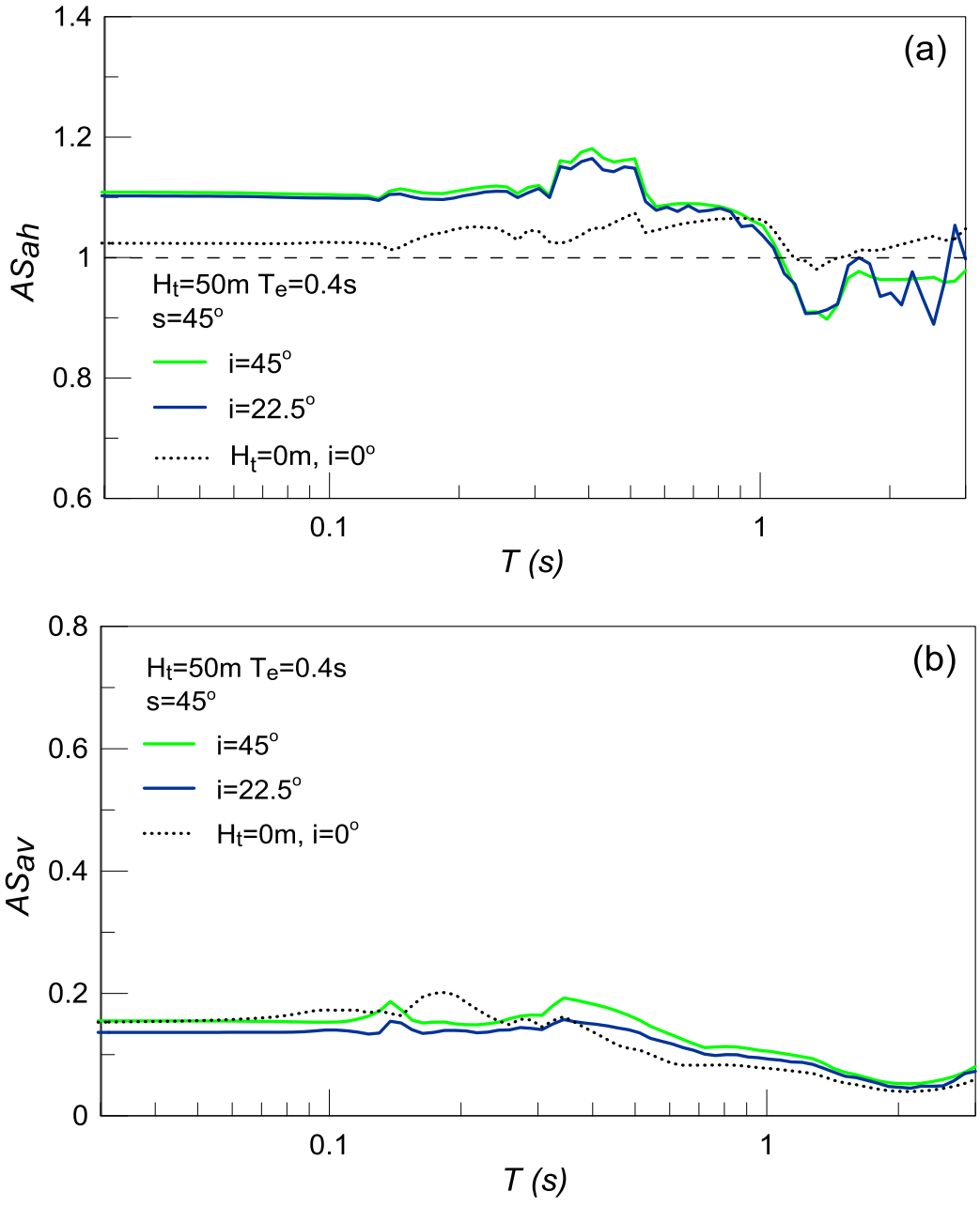

Figure 4.34: Effect of inclination angle i of outcropping bedrock on geomorphic aggravation spectra AS_{ah} and AS_{av} at the location of peak aggravation for T=0s along the steep (s=45°) valley with high impedance ratio a=0.5; Results for low-frequency excitation with T_e = 0.4s, H_t = 50m and comparison for valley with H_t = 0m and s = 45°.

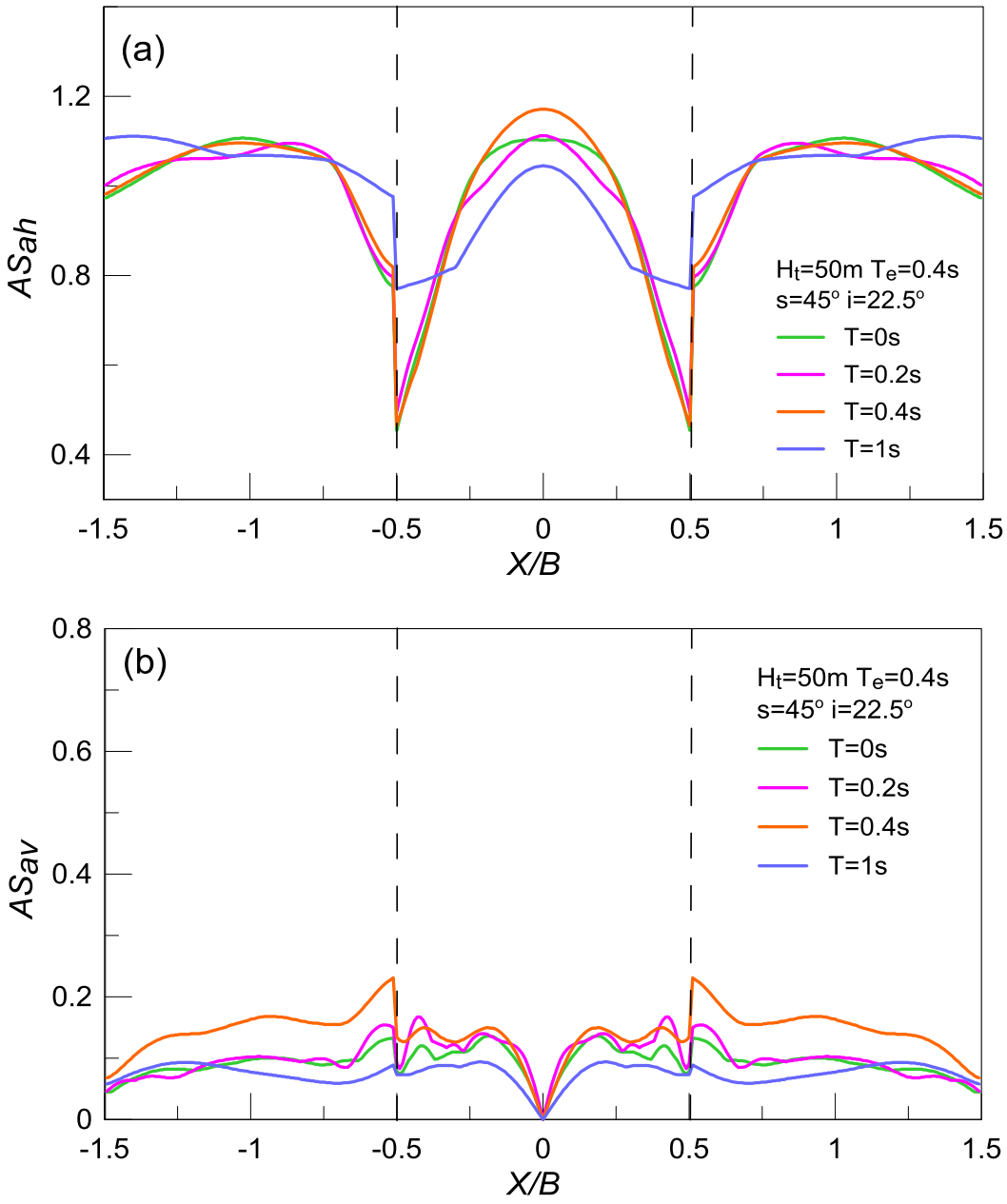

Figure 4.35: Spatial variability of geomorphic aggravation factors AS_{ah} and AS_{av} for specific structural periods T with normalized distance X/B from the center of the steep (s=45°) valley with high impedance ratio a=0.5; Results for outcropping bedrock height H_t = 50m, i=22.5° and a high-frequency excitation with T_e = 0.4s.

4.5 Effects for steep valleys s = 45^o with steep outcrops i = 45^o and low impedance ratio a = 0.25

In all analyses presented so far in this Chapter the shear wave velocity for the outcropping bedrock was V_b = 1000 m/s and for the soil was V_s = 500 m/s (stiff soil), leading to a high impedance ratio a = 0.50. However, alluvial valleys quite commonly have lower impedance ratios, where soft soil overlies rock. From previous valley response studies (e.g. Papadimitriou et al., 2011) it has been established that, quantitatively, the peak aggravation values increase with reducing value of the impedance ratio a. For this purpose, this paragraph investigates the effect of low impedance ratio to the geomorphic horizontal and vertical aggravation for steep valleys (s=45^o) with steep outcrops (i=45^o). The shear wave velocity for the outcropping bedrock remains V_b = 1000 m/s, but this time a soft soil with V_s = 250 m/s is considered, leading to a low impedance ratio a = 0.25. What varies in the analyses presented here are: a) the outcropping bedrock height H_t = 0, 50 and 100m; b) the predominant excitation period T_e = 0.1s (high-frequency) and 0.4s (low-frequency).

The effects of outcropping bedrock height H_t for impedance ratio a=0.25 under a high-frequency excitation T_e = 0.1s are demonstrated in **Figures 4.36 - 4.40**. From **Figure 4.36** it is obvious that the peak aggravation values are increased, with respect to the results for a=0.50 (**Figure 4.1**). In detail, the peak horizontal aggravation is increased from maxAS_{ah}(T=0)=1.3 for a=0.50 to maxAS_{ah}(T=0) = 1.45-1.6 for a=0.25. In the vertical direction the effect is stronger, with maxAS_{av}(T=0)=0.5-0.6 for a=0.50 and maxAS_{av}(T=0)=1.2-1.5 for a=0.25. The locations of peak aggravation for both AS_{ah} and AS_{av} are near the boundaries of the valley, as for a=0.50. Also, observe that at the outcropping bedrock the results remain practically unaffected by the impedance ratio a. The effect of height H_t is decreasing for low impedance ratio, while it was slightly increasing for a=0.50. Focusing on the locations where the maxAS_{ah}(T=0) and maxAS_{av}(T=0) are observed, **Figure 4.37** compares their aggravation spectra for different values of height H_t. The decreasing effect of H_t is observed for the whole of the aggravation spectrum. Note that larger spectral values appear for periods smaller or equal to T=0.1s and reduce thereafter. **Figures 4.38 to 4.40**, present the spatial variability of aggravation factors for different structural periods (including the values for T=0s of **Figure 4.36**). For clarity, each of these figures presents the results for a specific outcropping bedrock height H_t. As expected, the aggravation within the valley is smaller for the larger structural periods T. An unexpected result is the increase of AS_{ah}(T=0.4) with height H_t close to the boundaries of the valley.

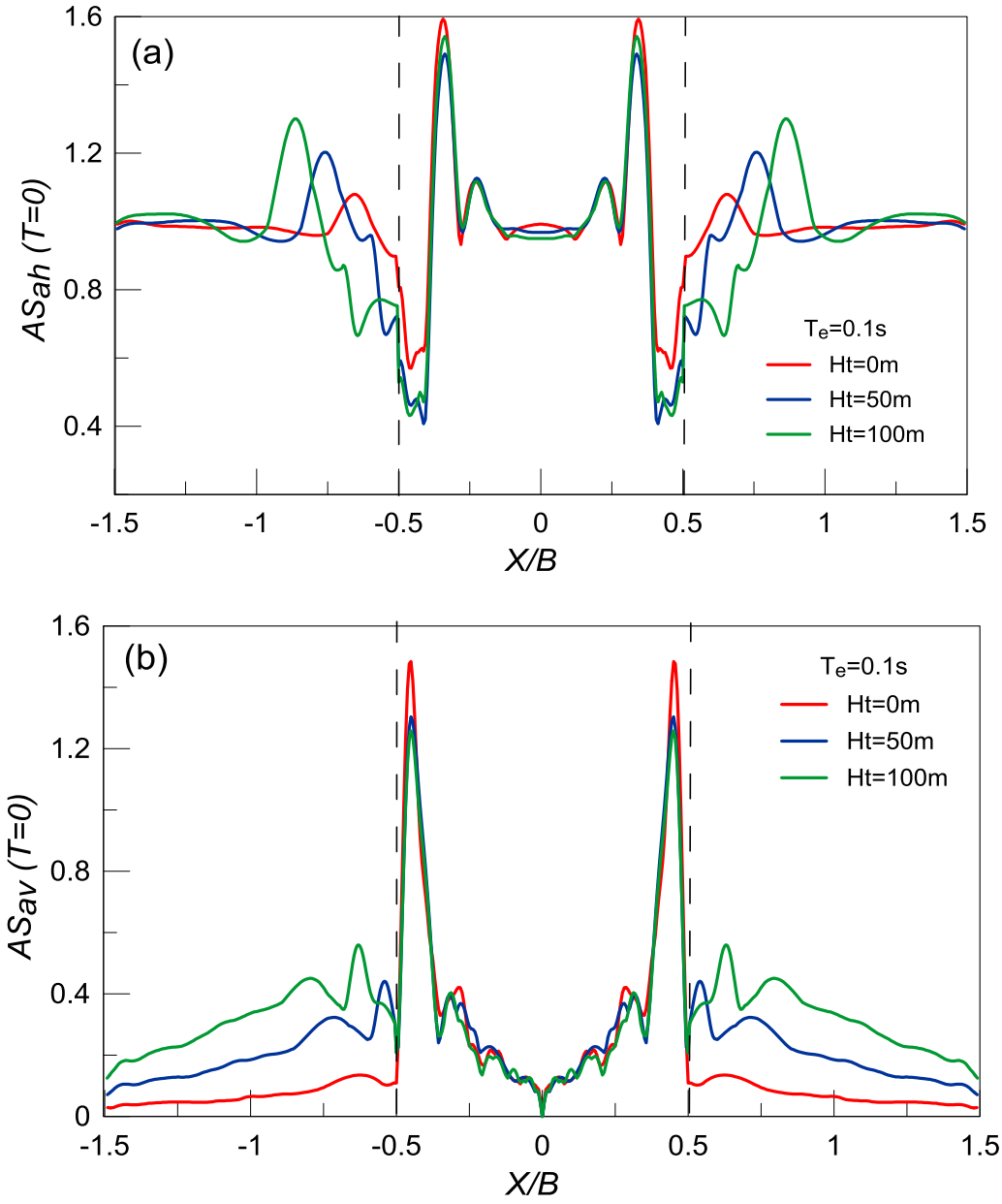

Figure 4.36: Effect of height H_t of steep (i=45^o) outcropping bedrock on the spatial variability of geomorphic aggravation factors AS_{ah} and AS_{av} for T=0s with normalized distance X/B from the center of the steep (s=45^o) valley with low impedance ratio a = 0.25; Results for high frequency excitation with T_e = 0.1s.

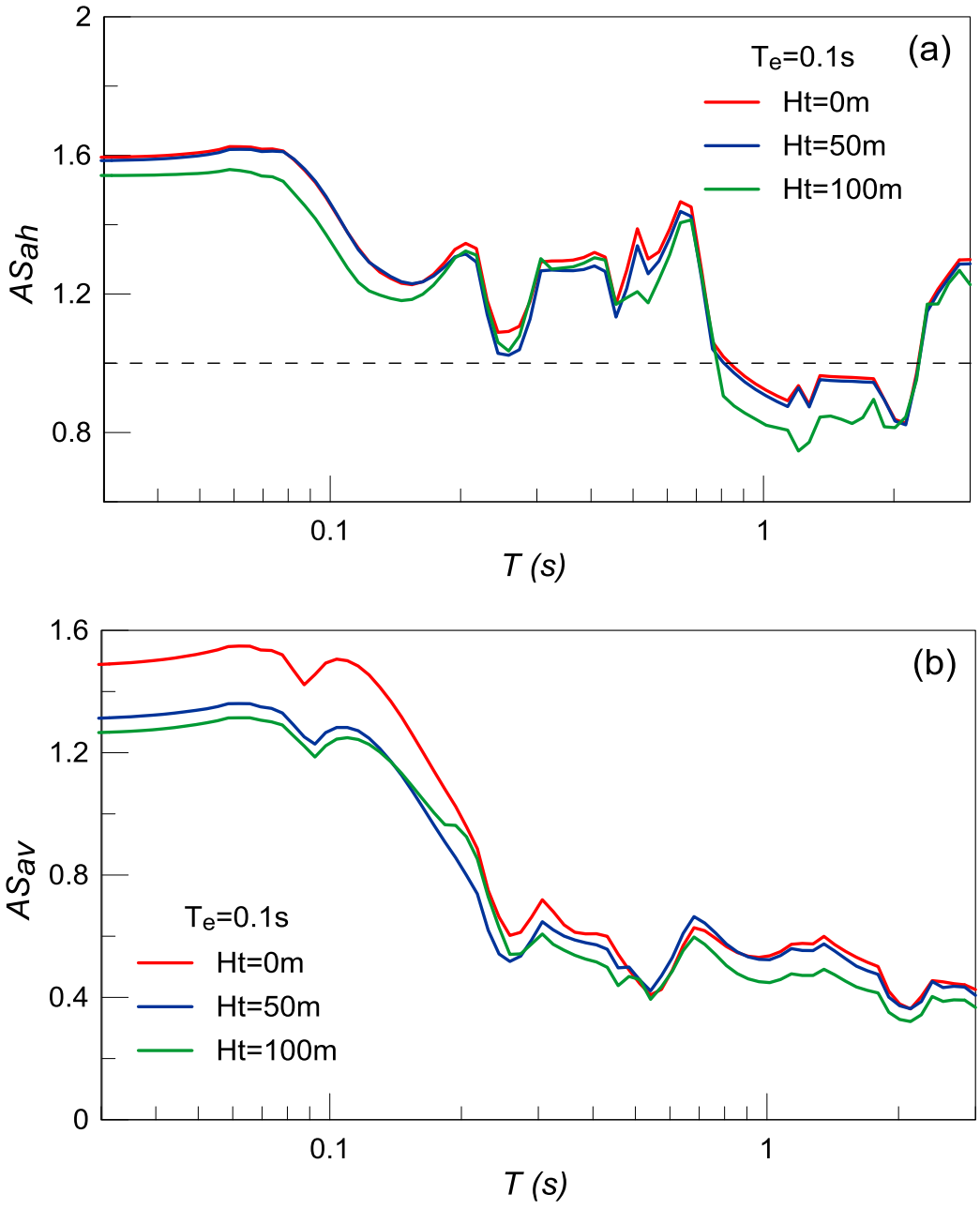

Figure 4.37: Effect of height H_t of steep (i=45^o) outcropping bedrock on geomorphic aggravation spectra AS_{ah} and AS_{av} at the locations of peak aggravation for T=0s along the steep (s=45^o) valley with low impedance ratio a = 0.25; Results for high-frequency excitation with T_e = 0.1s.

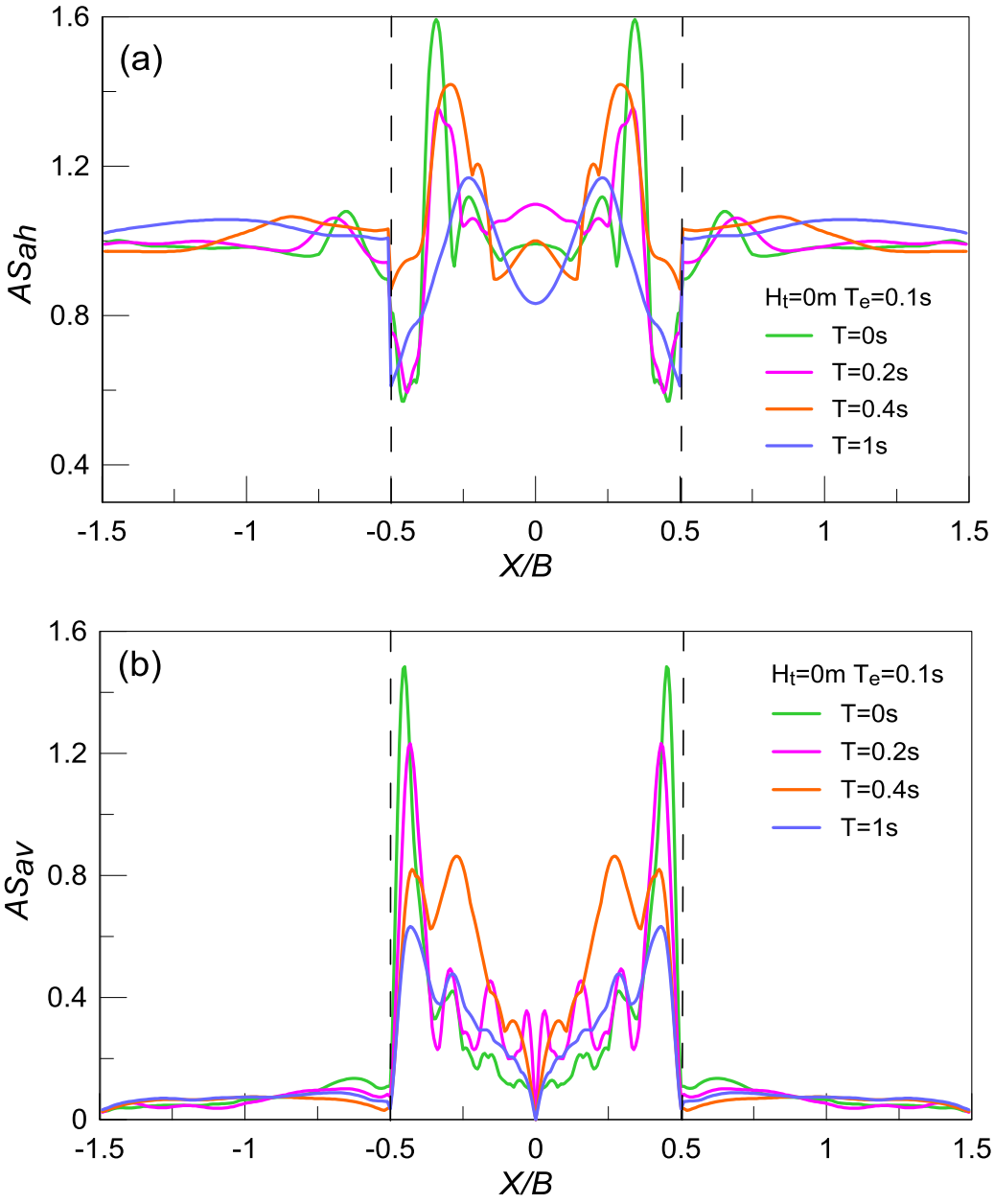

Figure 4.38: Spatial variability of geomorphic aggravation factors AS_{ah} and AS_{av} for specific structural periods T with normalized distance X/B from the center of the steep (s=45^{o}) valley with low impedance ratio a = 0.25; Results for outcropping bedrock height H_t = 0m and a high-frequency excitation with T_e = 0.1s.

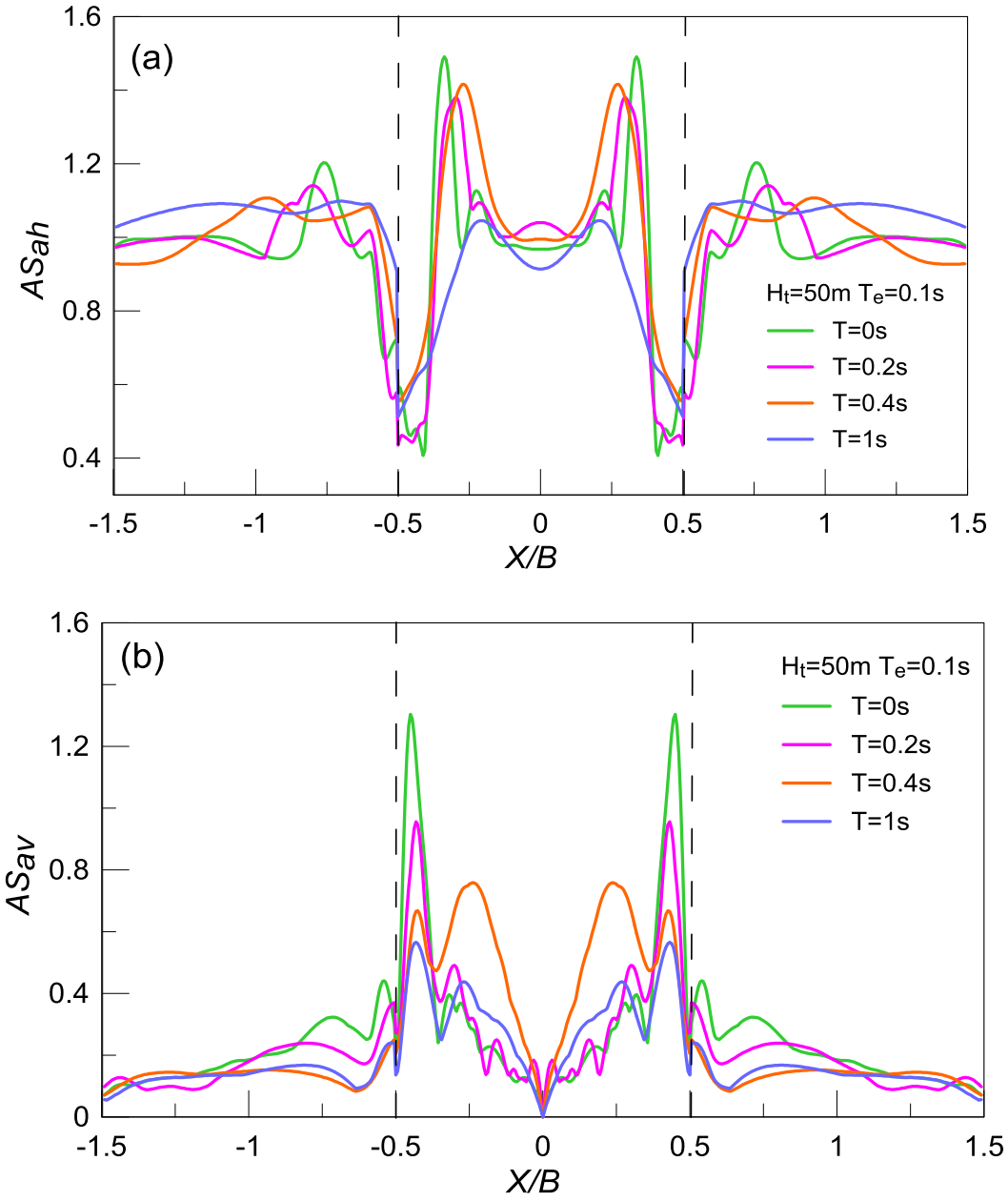

Figure 4.39: Spatial variability of geomorphic aggravation factors AS_{ah} and AS_{av} for specific structural periods T with normalized distance X/B from the center of the steep (s=45°) valley with low impedance ratio a = 0.25; Results for height H_t = 50m of steep (i=45°) outcropping bedrock and a high-frequency excitation with T_e = 0.1s.

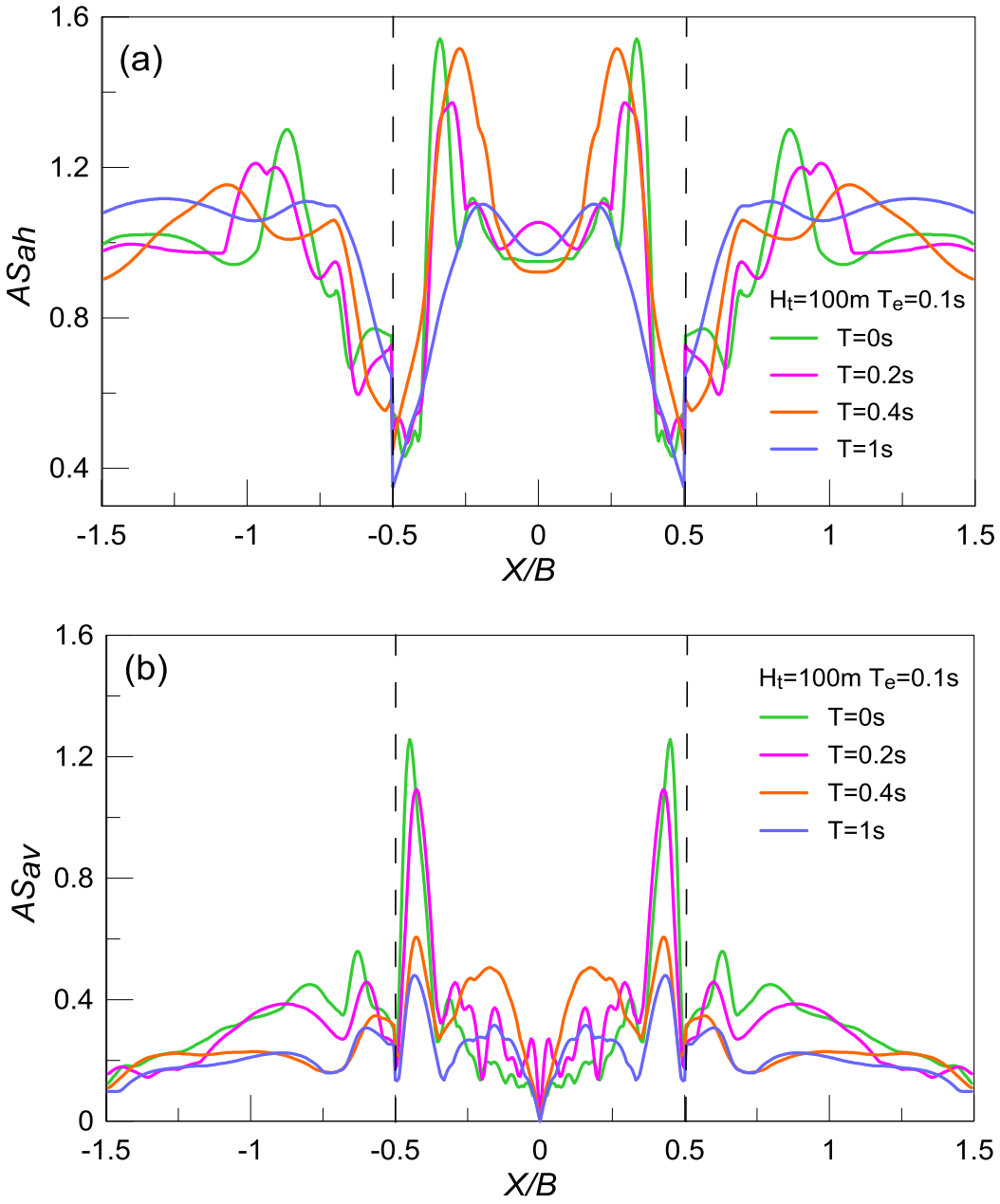

Figure 4.40: Spatial variability of geomorphic aggravation factors AS_{ah} and AS_{av} for specific structural periods T with normalized distance X/B from the center of the steep (s=45°) valley with low impedance ratio a = 0.25; Results for height H_t = 100m of steep (i=45°) outcropping bedrock and a high-frequency excitation with T_e = 0.1s.

In the sequel, the effects of outcropping bedrock height H_t for impedance ratio a=0.25 under a low-frequency excitation T_e = 0.4s are presented in **Figures 4.41 - 4.45**. As shown in **Figure 4.41**, the aggravation for T=0s within the valley increases for low impedance ratio, as happens for the high-frequency excitation as well. Nevertheless, the maxAS_{ah}(T=0) is not observed at the center of the valley, as was the case for high impedance ratio a=0.50 (**Figure 4.6**). It is observed that for AS_{ah}(T=0) relatively large values of geomorphic aggravation appear in more than one location along the valley. Specifically, for flat outcrops (H_t=0m) the AS_{ah}(T=0) has three peaks along the valley, while for H_t=50m and H_t=100m two peaks appear close to the boundaries of the valley. In addition, the effect of height H_t is not clear for the horizontal aggravation, since the lowest values of AS_{ah}(T=0) correspond to H_t=50m and the highest to H_t=100m. However, in the vertical direction the effect of H_t is clearly decreasing. At the same time, in **Figure 4.6** for high impedance ratio a=0.50, the effect of H_t was clearly increasing for both AS_{ah}(T=0) and AS_{av}(T=0). Note that comparing the results at the outcropping bedrock in **Figure 4.41** with the results in **Figure 4.6** reveals zero effect of the impedance ratio a. In **Figure 4.42**, the aggravation spectra are compared for different outcrop heights H_t at the locations where the maxAS_{ah}(T=0) and maxAS_{av}(T=0) appear. Observe that the effect of H_t remains the same for the whole of the aggravation spectrum. In addition, significant spectral values appear for periods smaller or equal to T=0.5s and reduce thereafter. **Figures 4.43 to 4.45** present the spatial variability of aggravation factors for different structural periods (including the T=0s of **Figure 4.41**), but each one of them presents the results for a specific H_t value. As expected from the aggravation spectra in **Figure 4.42**, regardless of height H_t, the maximum horizontal aggravation happens for T=0s and the maximum vertical aggravation for T=0.4s. Note that in all cases, the aggravation values at the outcropping bedrock are not significant.

From the abovementioned analyses, it can be concluded that as the impedance ratio a decreases, the geomorphic aggravation values AS_{ah} and AS_{av} increase throughout the valley. The locations of peak aggravation are not shifted for a high-frequency excitation (T_e=0.1s), but they are totally different for a low-frequency excitation (T_e=0.4s). In most cases, the effect of outcropping bedrock height H_t is decreasing for low impedance ratio (a=0.25), while it was clearly increasing for high impedance ratio (a=0.50). Yet, the behavior of the outcropping bedrock is practically unaffected by the impedance ratio a.

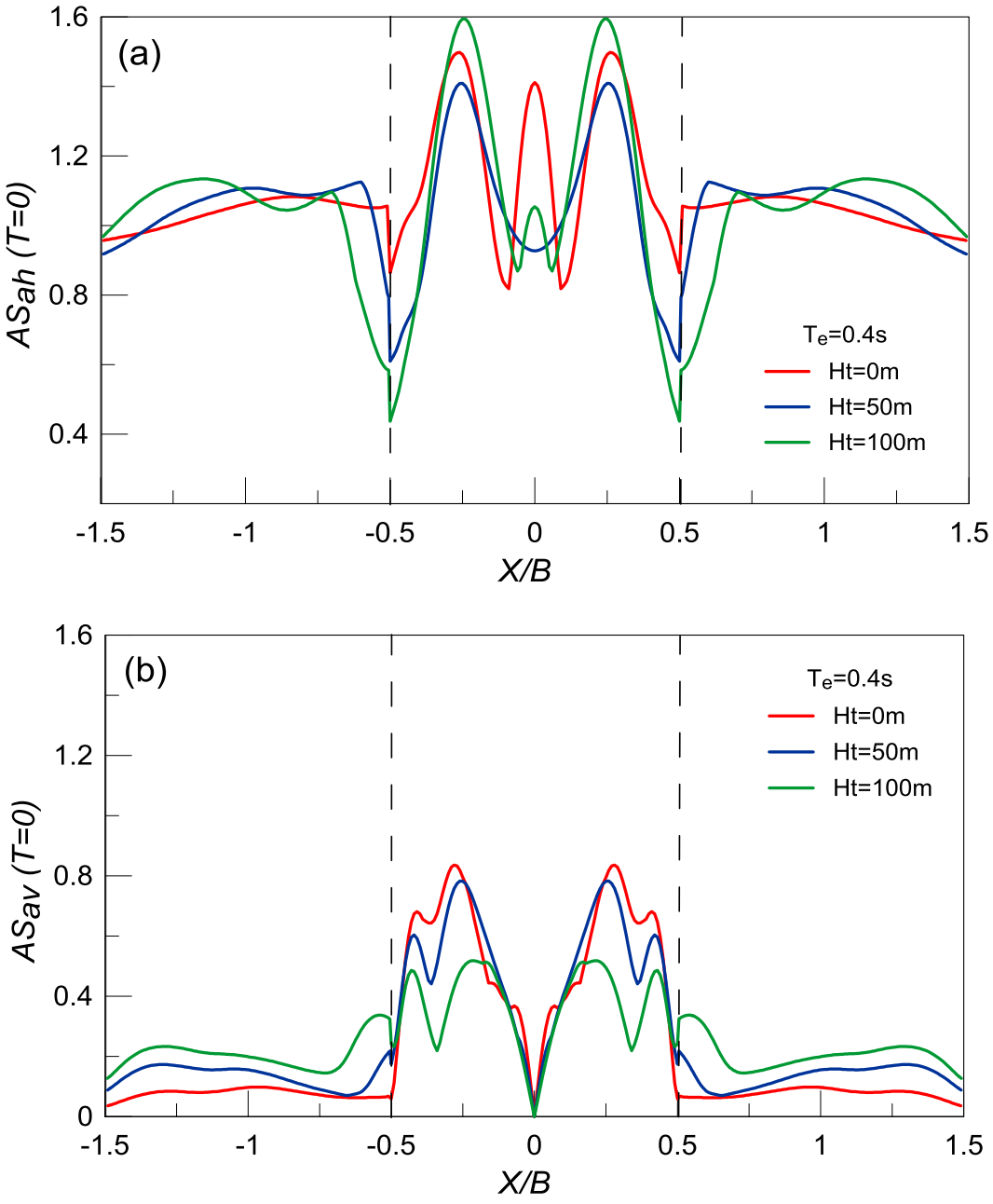

Figure 4.41: Effect of height H_t of steep (i=45^o) outcropping bedrock on the spatial variability of geomorphic aggravation factors AS_{ah} and AS_{av} for T=0s with normalized distance X/B from the center of the steep (s=45^o) valley with low impedance ratio a = 0.25; Results for low frequency excitation with T_e = 0.4s.

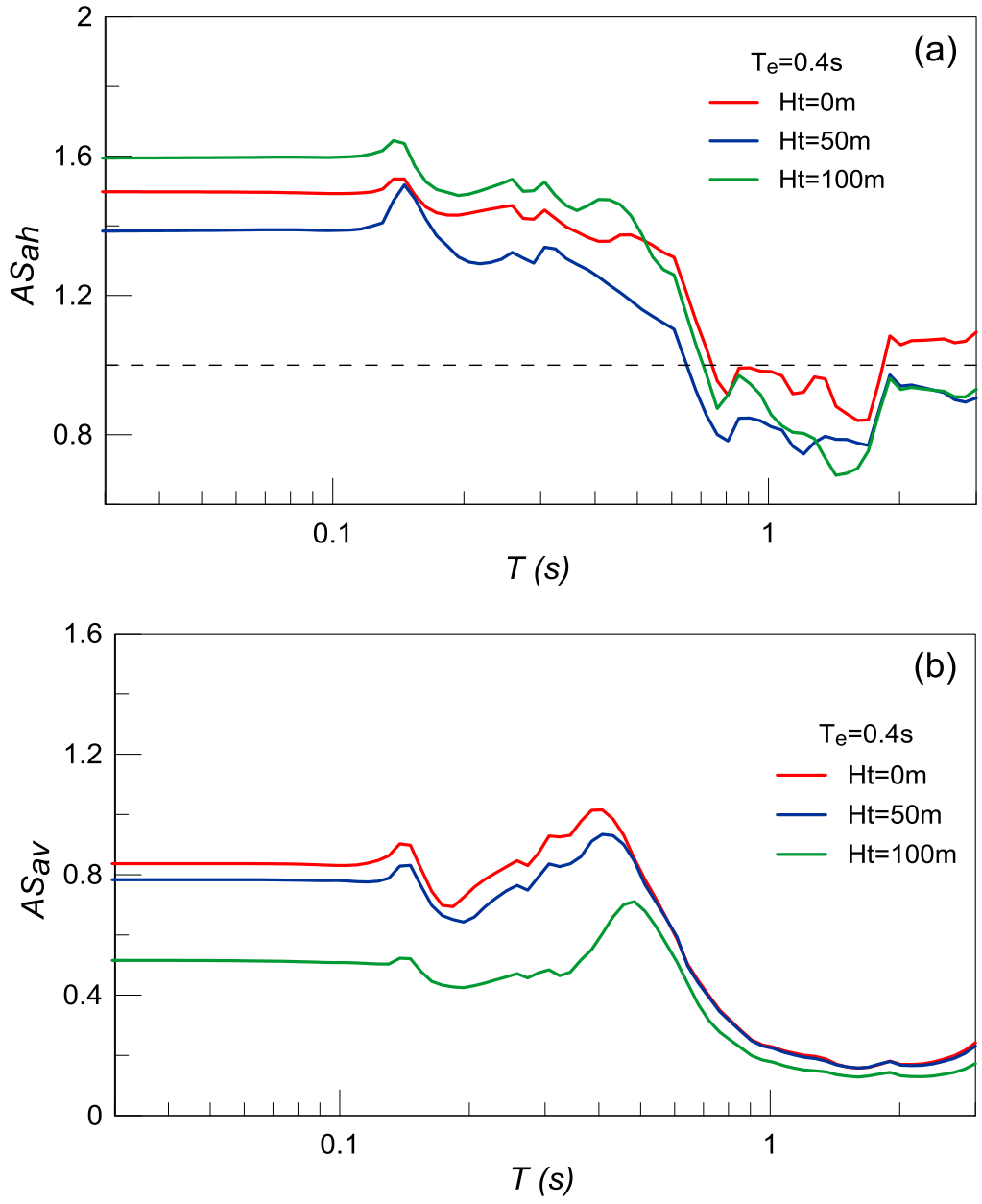

Figure 4.42: Effect of height H_t of steep (i=45°) outcropping bedrock on geomorphic aggravation spectra AS_{ah} and AS_{av} at the location of peak aggravation for T=0s along the steep (s=45°) valley with low impedance ratio a = 0.25; Results for low-frequency excitation with T_e = 0.4s.

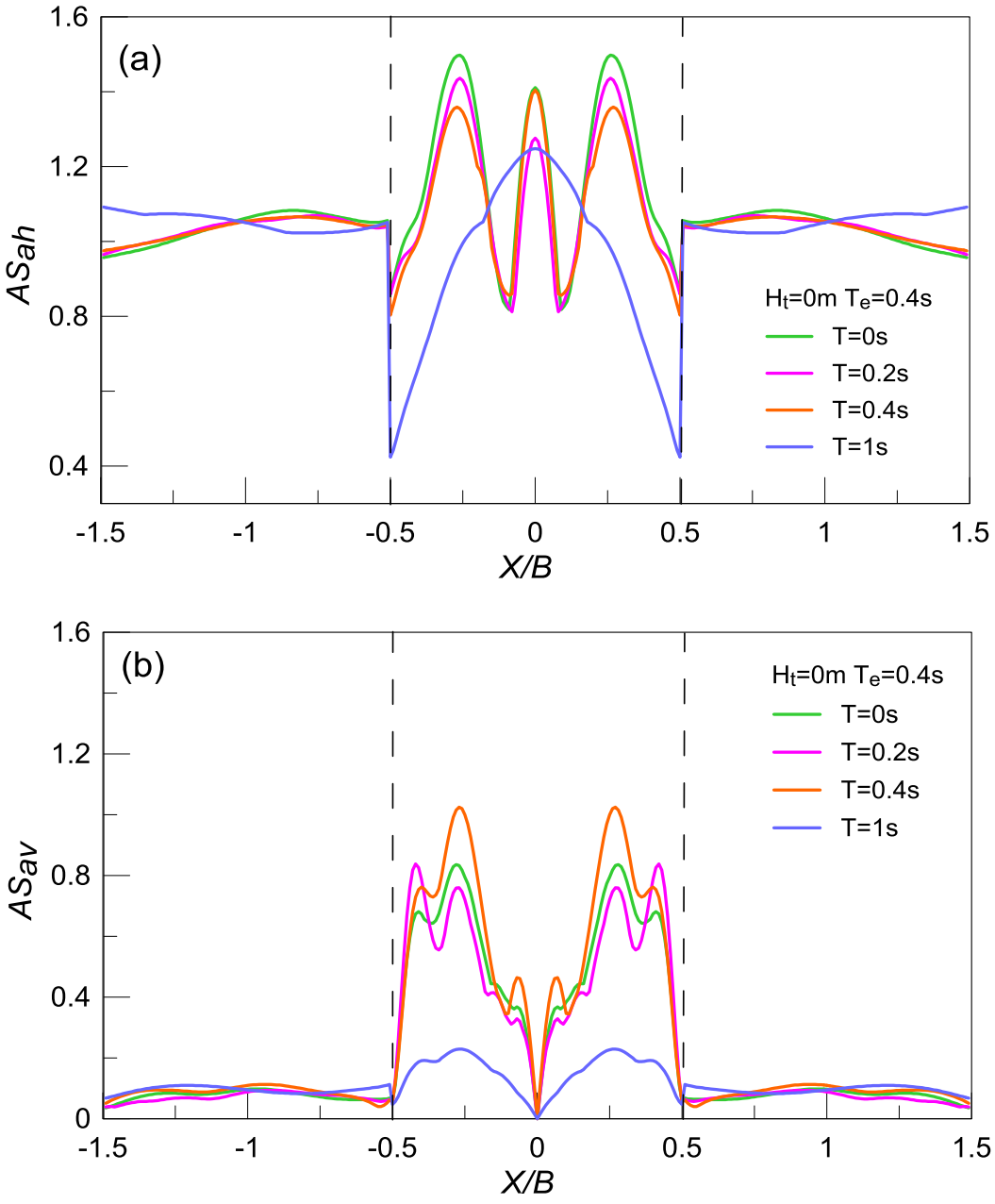

Figure 4.43: Spatial variability of geomorphic aggravation factors AS_{ah} and AS_{av} for specific structural periods T with normalized distance X/B from the center of the steep (s=45^{o}) valley with low impedance ratio a = 0.25; Results for outcropping bedrock height H_t = 0m and a low-frequency excitation with T_e = 0.4s.

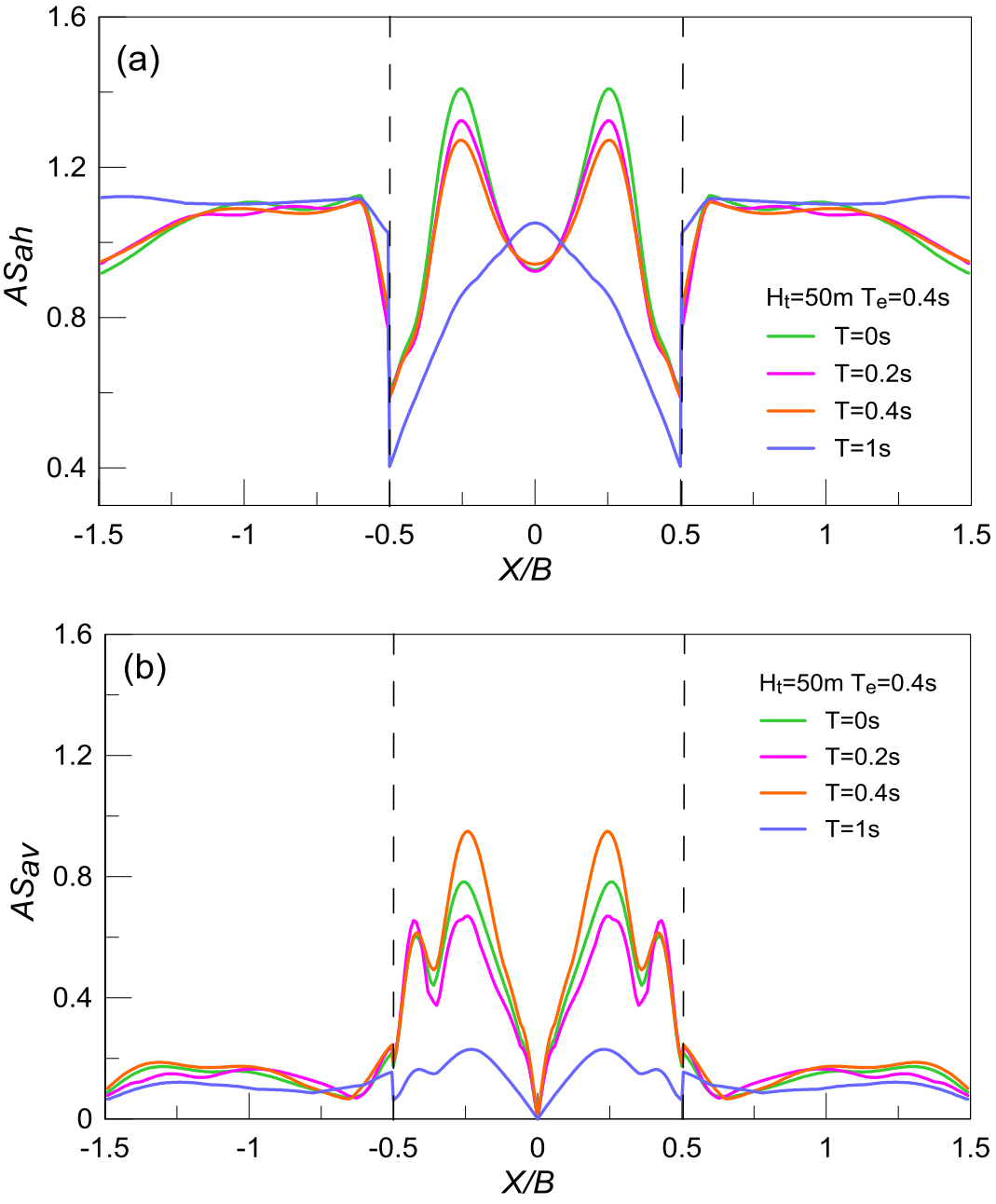

Figure 4.44: Spatial variability of geomorphic aggravation factors AS_{ah} and AS_{av} for specific structural periods T with normalized distance X/B from the center of the steep (s=45^{o}) valley with low impedance ratio a = 0.25; Results for height H_t = 50m of steep (i=45^{o}) outcropping bedrock and a low-frequency excitation with T_e = 0.4s.

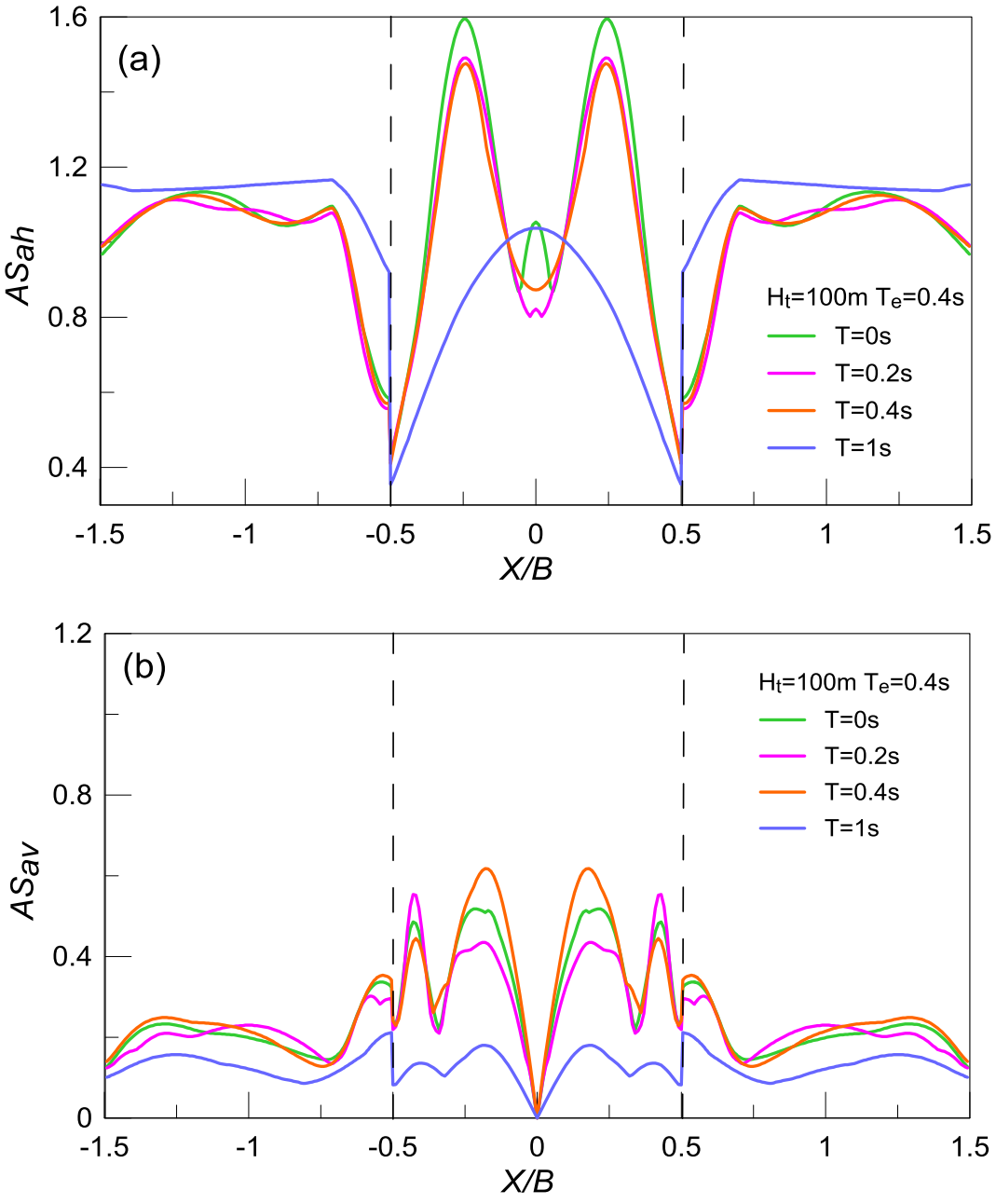

Figure 4.45: Spatial variability of geomorphic aggravation factors AS_{ah} and AS_{av} for specific structural periods T with normalized distance X/B from the center of the steep (s=45^{o}) valley with low impedance ratio a = 0.25; Results for height H_t = 100m of steep (i=45^{o}) outcropping bedrock and a low-frequency excitation with T_e = 0.4s.

4.6 Quantification of effects of outcropping bedrock topography on valley response

The abovementioned analyses indicate that the effects of outcropping bedrock topography on the seismic valley response can be remarkable, under certain circumstances. It has already been observed that these effects are more severe under a low frequency excitation (T_e=0.4s) and a low impedance ratio (a=0.25). Nevertheless, of importance in this study is the effect of outcropping bedrock height H_t, since this parameter separates the valleys with flat and non-flat bedrock outcrops.

As pointed out in Chapter 2, the majority of the papers in the literature present results for valleys with flat outcrops, i.e. with H_t=0m. Hence, in order to exploit the significant pertinent literature and generalize it even for cases that do not have flat outcrops, a correction factor CF would prove useful. This factor could be potentially used to "correct" the seismic response of a valley with flat outcrops in order to yield the response of the same valley under the same excitation with non-flat outcrops. In general, this CF is expected to be a function of the structural period T, and governed by a number of problem parameters. As a starting point, this thesis focuses on the value of CF for the peak ground acceleration, namely for T=0s, for both the horizontal component (CF_h) and the parasitic vertical component (CF_v). Hence, the horizontal correction factor $CF_h(T=0)$ is defined at each location of the valley, as the ratio of the horizontal geomorphic aggravation factor for T=0s $AS_{ah}(T=0)$ which corresponds to non-flat outcrops ($H_t \neq 0$m) over the horizontal geomorphic aggravation factor for T=0s $AS_{ah}(T=0)$ which corresponds to flat outcrops ($H_t = 0$m). Similarly, the vertical correction factor $CF_v(T=0)$ is defined at each location of the valley, as the ratio of $AS_{av}(T=0)$ for $H_t \neq 0$m over $AS_{av}(T=0)$ for $H_t = 0$m. Evidently, if the correction factors take values above 1.0, the aggravation is higher for the valley with non-flat outcrops, while the opposite occurs for values below 1.0.

The results are presented only in terms of normalized distance from the center of the valley X/B. According to the previously examined cases, the locations of $maxAS_{ah}(T=0)$ and $maxAS_{av}(T=0)$ are different along the same valley, under the same excitation, for $H_t \neq 0$m and $H_t = 0$m. Hence, the correction factors at the location of maximum aggravation for T=0s along the valley cannot be defined robustly. Since this Chapter investigates the effects of outcropping bedrock on valley response, the correction factors are defined exclusively within the valley boundaries, i.e. for $0.5 \leq X/B \leq 0.5$. Furthermore, in paragraph 3.3 of Chapter 3, it was pointed out that the normalized results in terms of AS_{ah} and AS_{av} are not entirely accurate at locations over the inclined boundaries of the valley, where the soil thickness is not smaller than H. For this reason, the main focus of our analysis is at the locations of the so-called inner valley, i.e. at the central part of the valley where the thickness of the soil is equal to H and the definitions of AS_{ah} and AS_{av} are fully accurate. In the figures that follow the extent of the inner valley is denoted for each valley geometry with vertical dashed lines and a double pointing arrow. Finally, it must be noted here that there is a conceptual problem in the definition of $CF_v(T=0)$ at the center of the valley. The reason is that at this location the vertical aggravation factor $AS_{av}(T) = 0$ always, since our analyses correspond to symmetric valleys with vertically incident SV waves. In this respect, the denominator of $CF_v(T=0)$ is equal to zero making the definition problematic. However, since we know that $AS_{av}(T=0) = 0$ for both flat

and non-flat outcrops, we assign that $CF_v(T=0) = 1$ at the center of the valley for all cases studied herein.

Figures 4.46 to 4.48 present the spatial variability of correction factors $CF_h(T=0)$ and $CF_v(T=0)$ for steep valleys ($s=45^o$) with steep outcrops ($i=45^o$) and a high impedance ratio a=0.5. As shown in **Figure 4.46**, for a high-frequency excitation with T_e=0.1s, $CF_h(T=0)$ remains unaffected by the outcropping bedrock height H_t in the inner valley. In detail, for both H_t=50 and 100m, $maxCF_h(T=0)$=1.1 at X/B=0.3, while at the central area of the valley $CF_h(T=0)$ is practically equal to 1. With respect to the vertical correction factor $CF_v(T=0)$, the range of the values is more significant, varying between 0.5 and 1.5. In addition, the results are not identical for the two heights H_t, with $CF_v(T=0)$ for H_t=100m being significantly larger than for H_t=50m at X/B=0.18. In the same line of thought, the correction factors for a low-frequency excitation with T_e=0.4s are demonstrated in **Figure 4.47**. In this case, the peak horizontal values appear at the central area of the valley and the values are slightly larger for H_t=100m. Observe that $CF_v(T=0)$ is also maximized at the central area of the valley, but the range within the valley is remarkable, compared to the previous cases. Specifically, for H_t=50m, $CF_v(T=0)$ takes values between 1 and 2.25, while for H_t=100m the range varies between 1 and 3.5. Following the same pattern of presentation as in paragraph 4.2, the spatial variability of correction factors is also determined for an intermediate-frequency excitation with T_e=0.25s. **Figure 4.48** shows that $maxCF_h(T=0)$=1.1 and appears at the center of the valley, similarly with what happened for T_e=0.4s. Nevertheless, unlike **Figure 4.47** for the low-frequency excitation, the differences between H_t=50 and 100m are negligible for T_e = 0.25s. As for the vertical component, $CF_v(T=0)$ is generally larger for H_t=100m, except the peak values close to the center of the valley, which are slightly larger for H_t=50m.

Based on the above, the CF values take generally larger values for the parasitic vertical acceleration and for low-period excitations. The effect of height H_t of the outcrop seems to play a clearly increasing role only for the above cases. In addition, the CF_h and CF_v become lower and higher than 1.0 near the valley boundaries, i.e. outside the inner valleys. However, these results pertain to steep valleys with steep outcrops. Of interest is also to study how much are these CF values affected by the inclination angles of the valley (s) and the outcrops (i). Hence, in order to investigate their effects on $CF_h(T=0)$ and $CF_v(T=0)$, **Figures 4.49 and 4.50** compare the spatial variability of correction factors for mild inclination angles ($s=i=22.5^o$) and steep angles ($s=i=45^o$) for H_t=50m and a high impedance ratio a=0.5. Note that the inner valley is not the same for different inclination angles, thus the inner valley boundaries for each case are denoted with differently colored dashed lines. The results for a high-frequency excitation with T_e=0.1s are demonstrated in **Figure 4.49**. Observe that $CF_h(T=0)$ is practically equal to 1 close to the center of the valley, but at the vicinity of the valley boundaries the values are slightly increased for the steeper inclination angles. On the other hand, $CF_v(T=0)$ takes values close to 1 for mild inclination angles, but for steep angles the values remain mostly lower than 1, implying $AS_{av}(T=0)$ is larger for flat outcropping bedrock. The corresponding results for a low-frequency excitation with T_e=0.4s are illustrated in **Figure 4.50**. It is obvious that $CF_h(T=0)$ remains practically unaffected by the inclination angles s and i. Conversely, $CF_v(T=0)$ is strongly depending on the inclination angles, with larger values observed for $s=i=45^o$, but only for the low-period excitation. For example, for steep angles ($s=i=45^o$)

maxCF_v(T=0)=2.25, while for mild angles (s=i=22.5°) maxCF_v(T=0)=1.25 within the inner valleys of the two cases with T_e = 0.4s.

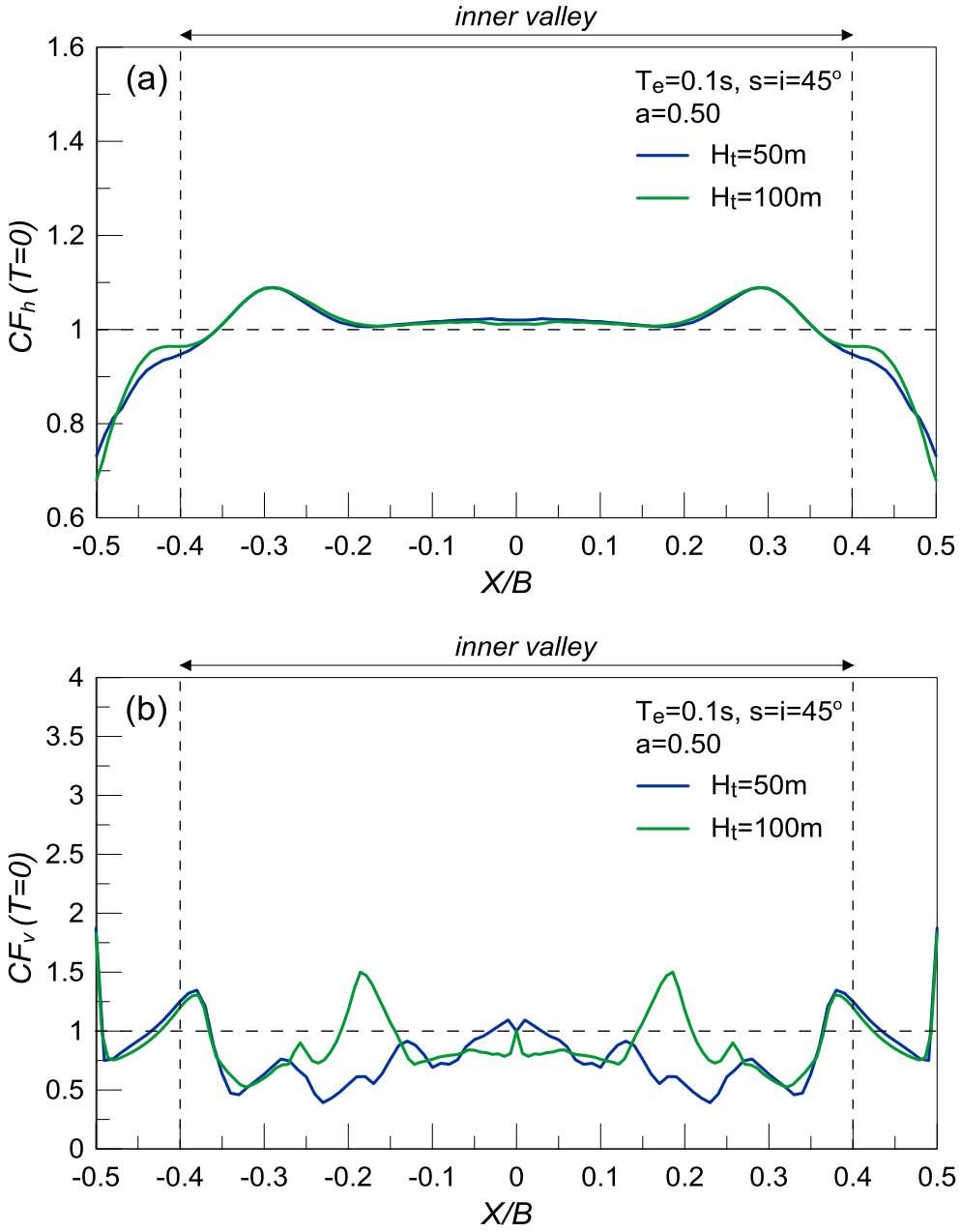

Figure 4.46: Effect of height H_t of steep (i=45°) outcropping bedrock on the spatial variability of correction factors CF_h and CF_v for T=0s with normalized distance X/B from the center of the steep valley (s=45°) with high impedance ratio a = 0.5; Results for high frequency excitation with T_e = 0.1s.

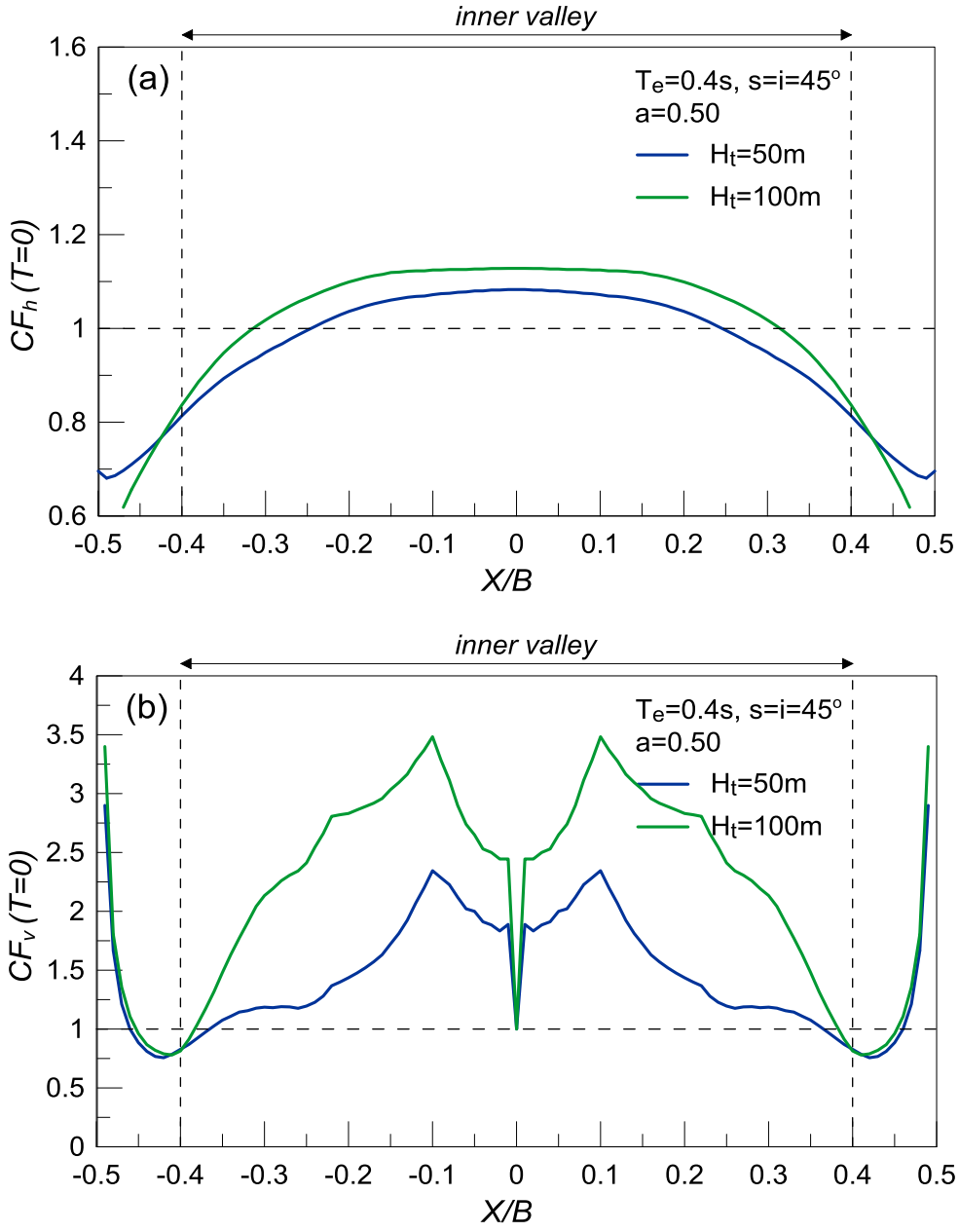

Figure 4.47: Effect of height H_t of steep (i=45°) outcropping bedrock on the spatial variability of correction factors CF_h and CF_v for T=0s with normalized distance X/B from the center of the steep valley (s=45°) with high impedance ratio a = 0.5; Results for low frequency excitation with T_e = 0.4s.

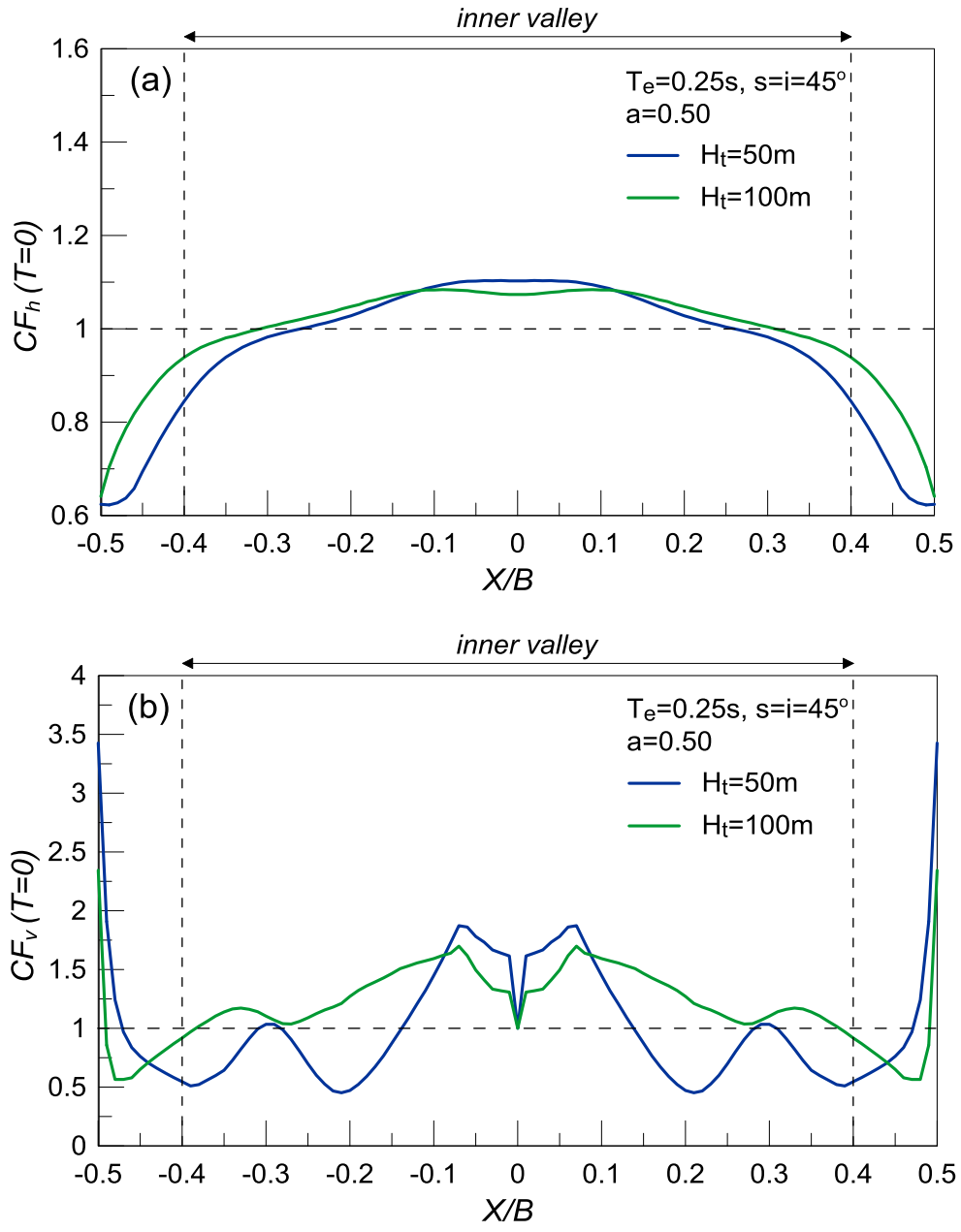

Figure 4.48: Effect of height H_t of steep (i=45°) outcropping bedrock on the spatial variability of correction factors CF_h and CF_v for T=0s with normalized distance X/B from the center of the steep valley (s=45°) with high impedance ratio a = 0.5; Results for intermediate frequency excitation with T_e = 0.25s.

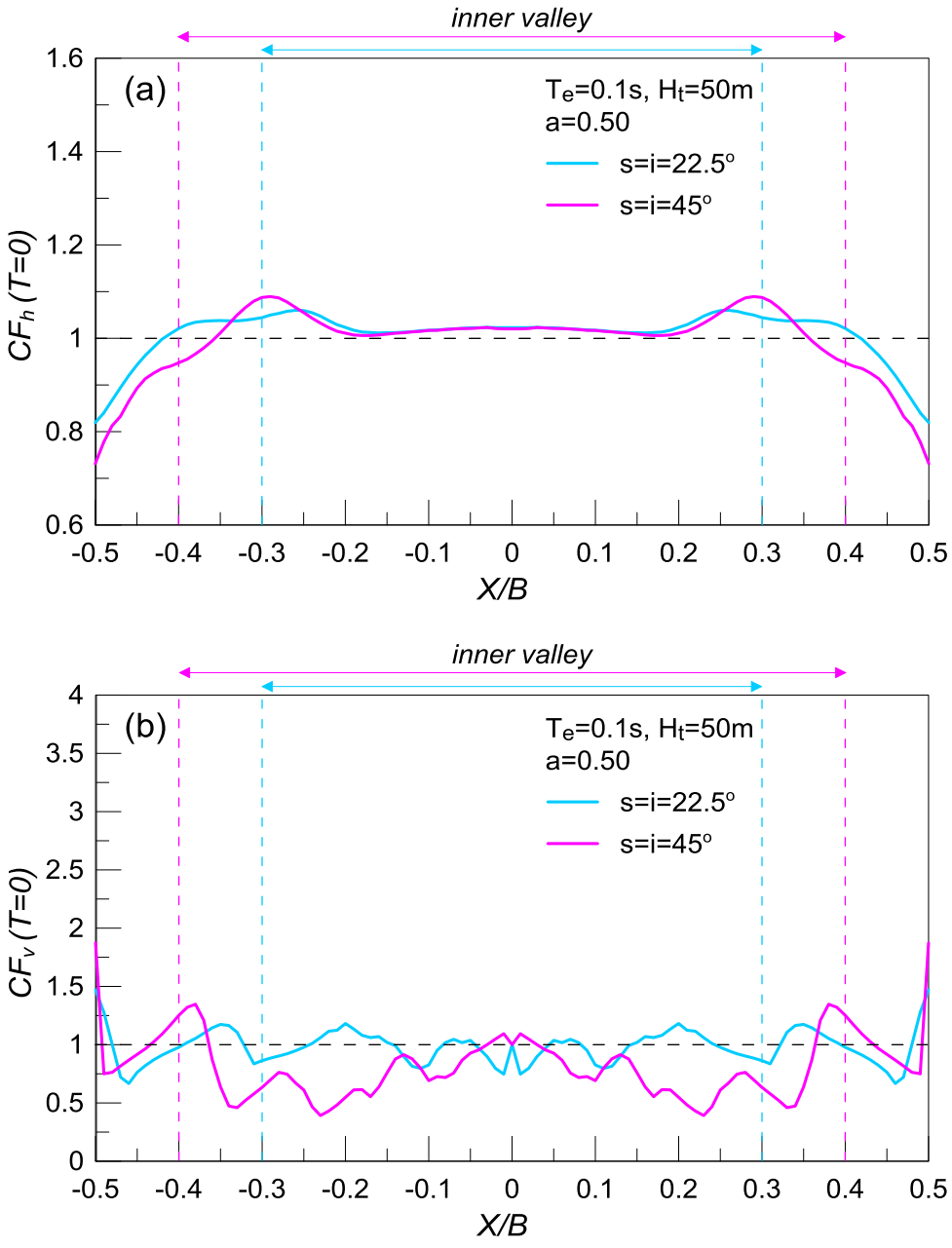

Figure 4.49: Effect of inclination angles s and i on the spatial variability of correction factors CF_h and CF_v for T=0s with normalized distance X/B from the center of the valley with high impedance ratio a = 0.5; Results for outcropping bedrock height H_t=50m and a high frequency excitation with T_e = 0.1s.

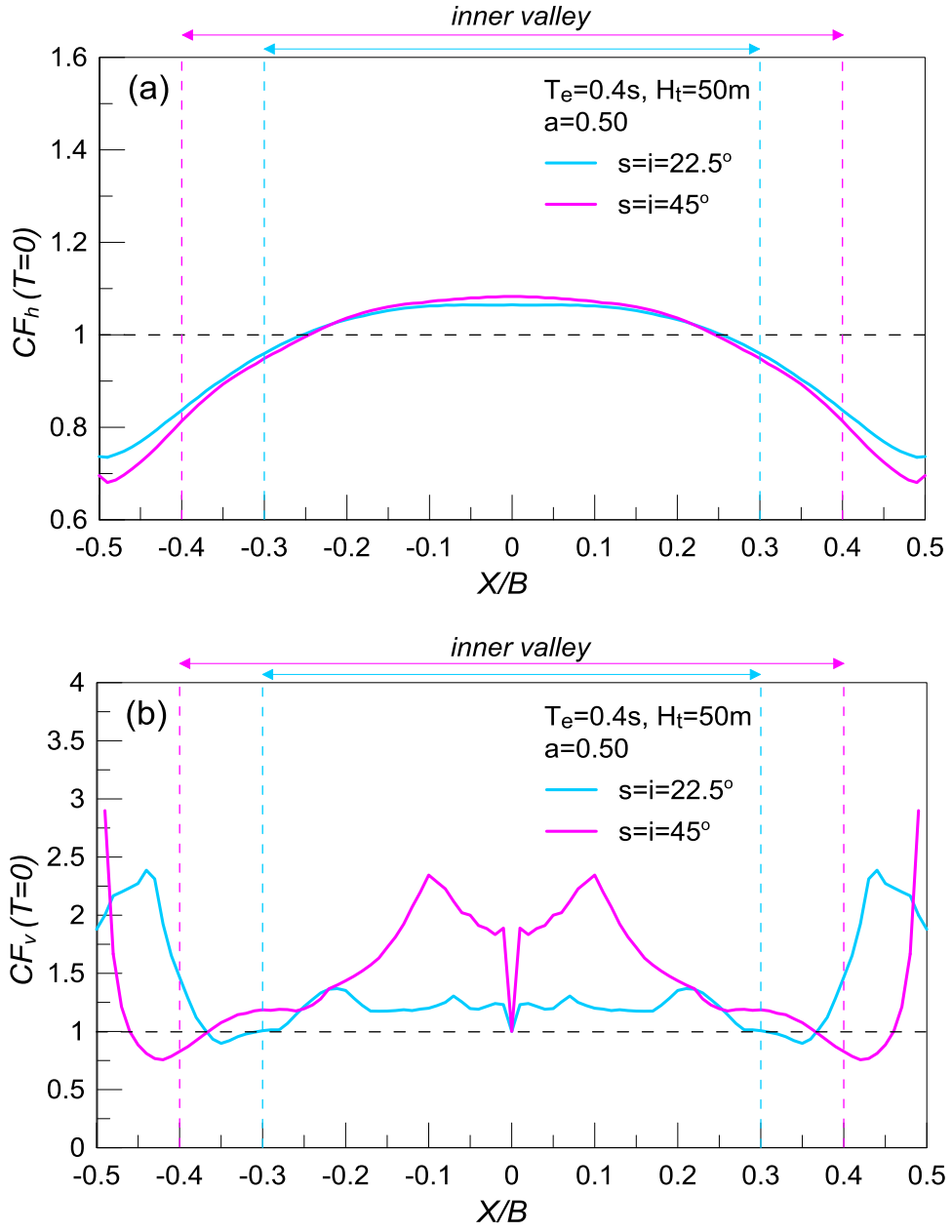

Figure 4.50: Effect of inclination angles s and i on the spatial variability of correction factors CF_h and CF_v for T=0s with normalized distance X/B from the center of the valley with high impedance ratio a = 0.5; Results for outcropping bedrock height H_t=50m and a low frequency excitation with T_e = 0.4s.

The effect of differently inclined valleys and bedrock outcrops on the correction factors $CF_h(T=0)$ and $CF_v(T=0)$ is investigated in **Figures 4.51 to 4.54**. As shown in **Figure 4.51**, for mild valleys ($s=22.5^o$) subjected to a high-frequency excitation ($T_e=0.1s$), a slight increase of $CF_h(T=0)$ and $CF_v(T=0)$ is observed for steep outcrops ($i=45^o$). However, for a low-frequency excitation ($T_e=0.4s$) the differences between steep and mild outcrops are negligible, as implied by **Figure 4.52**. The same procedure is followed for steep valleys ($s=45^o$) with differently inclined outcrops. **Figure 4.53** shows that for steep outcrops and a high-frequency excitation ($T_e=0.1s$) there is a slight increase of $CF_h(T=0)$ close to the edges of the valley. Nevertheless, $CF_v(T=0)$ values are lower for steep outcrops, while for both $i=22.5^o$ and $i=45^o$ remain mostly below 1. At the same time, **Figure 4.54** depicts that for a low-frequency excitation with $T_e=0.4s$, $CF_h(T=0)$ remains unaffected by the inclination angle of the outcrops, as was also the case in **Figure 4.52** for the mild valley. Yet, this is not the case for $CF_v(T=0)$, as this clearly increases for steep outcrops. In detail, for $i=22.5^o$ $maxCF_v(T=0)=1.75$, while for $i=45^o$ $maxCF_v(T=0)=2.25$. In general, the effect of inclination angle i of the bedrock outcrop seems to become important for the low frequency excitation only, and mostly for the CF_v values, regardless of whether the valley itself is steep ($s=45^o$) or not ($s=22.5^o$).

Finally, in **Figures 4.55 and 4.56** the correction factors CF_h and CF_v for T=0s are presented for steep valleys with steep outcrops and a low impedance ratio a=0.25. As illustrated in **Figure 4.55**, for a high-frequency excitation with $T_e=0.1s$, the $CF_h(T=0)$ is similar for the two outcropping bedrock heights H_t, with the values varying around 1.0. Note that close to the edges of the valley, the $CF_h(T=0)$ is slightly increased for $H_t=100m$. For $CF_v(T=0)$ the values are also gathered close to 1.0, but they seem slightly larger for $H_t=50m$. However, the variation of the correction factors is more significant for a low-frequency excitation with $T_e=0.4s$, as shown in **Figure 4.56**. More specifically, for $H_t=50m$ the $maxCF_h(T=0)=1.2$ and for $H_t=100m$ the $maxCF_h(T=0)=1.3$. In addition, at the center of the valley the $CF_h(T=0)$ drops below 1.0 for both heights H_t. Note that in all the previous cases, the $CF_h(T=0)$ is equal or greater than 1.0 at the center of the valley. As for the $CF_v(T=0)$, the values are mostly below 1.0 and they are lower for $H_t=100m$. Finally, It should be underlined that these values are significantly lower than for a=0.5 in **Figure 4.47**.

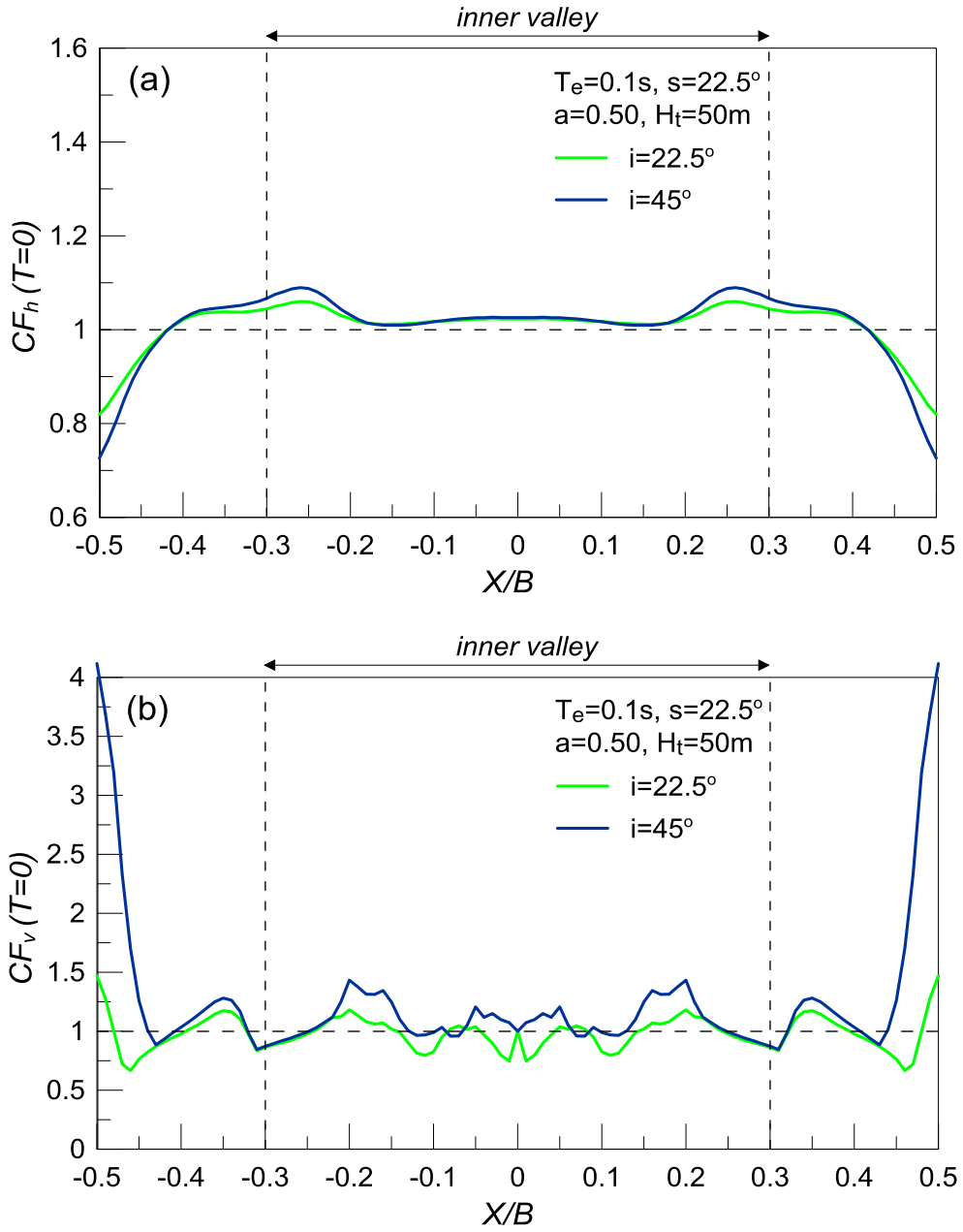

Figure 4.51: Effect of inclination angle i of outcropping bedrock on the spatial variability of correction factors CF_h and CF_v for T=0s with normalized distance X/B from the center of the mild (s=22.5°) valley with high impedance ratio a=0.5; Results for high frequency excitation with T_e = 0.1s and H_t = 50m.

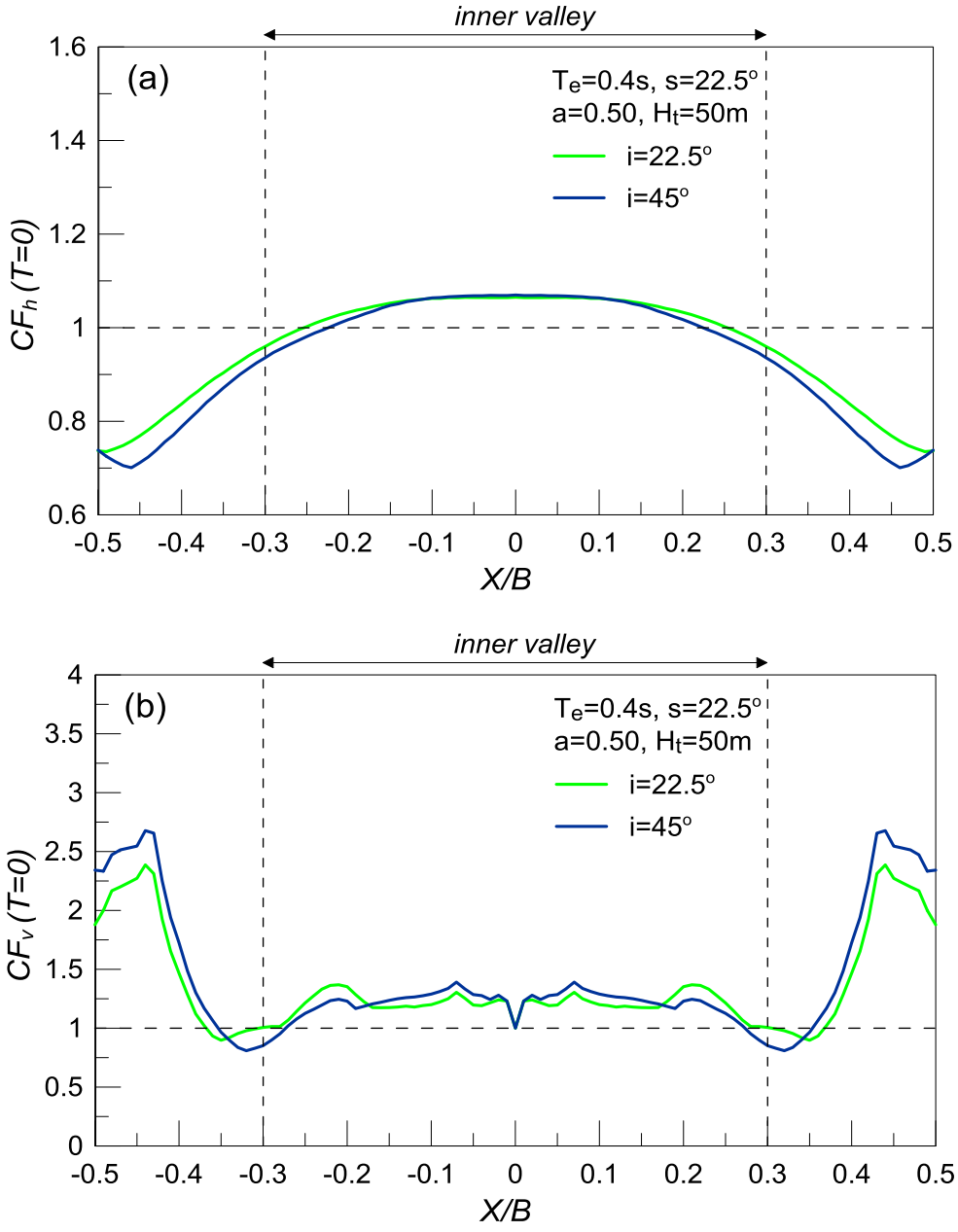

Figure 4.52: Effect of inclination angle i of outcropping bedrock on the spatial variability of correction factors CF_h and CF_v for T=0s with normalized distance X/B from the center of the mild (s=22.5°) valley with high impedance ratio a=0.5; Results for low frequency excitation with T_e = 0.4s and H_t = 50m.

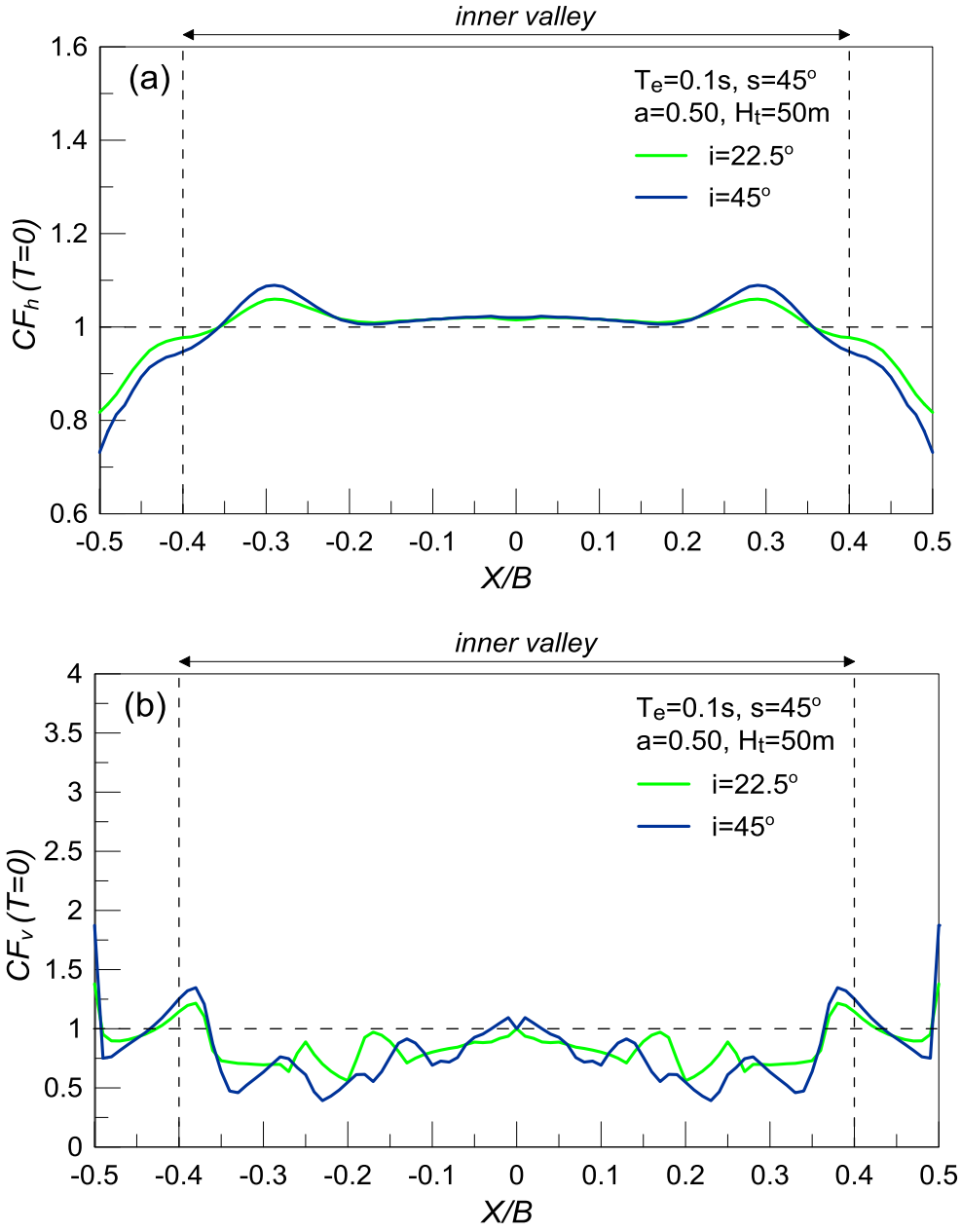

Figure 4.53: Effect of inclination angle i of outcropping bedrock on the spatial variability of correction factors CF_h and CF_v for T=0s with normalized distance X/B from the center of the steep (s=45°) valley with high impedance ratio a=0.5; Results for high frequency excitation with T_e = 0.1s and H_t = 50m.

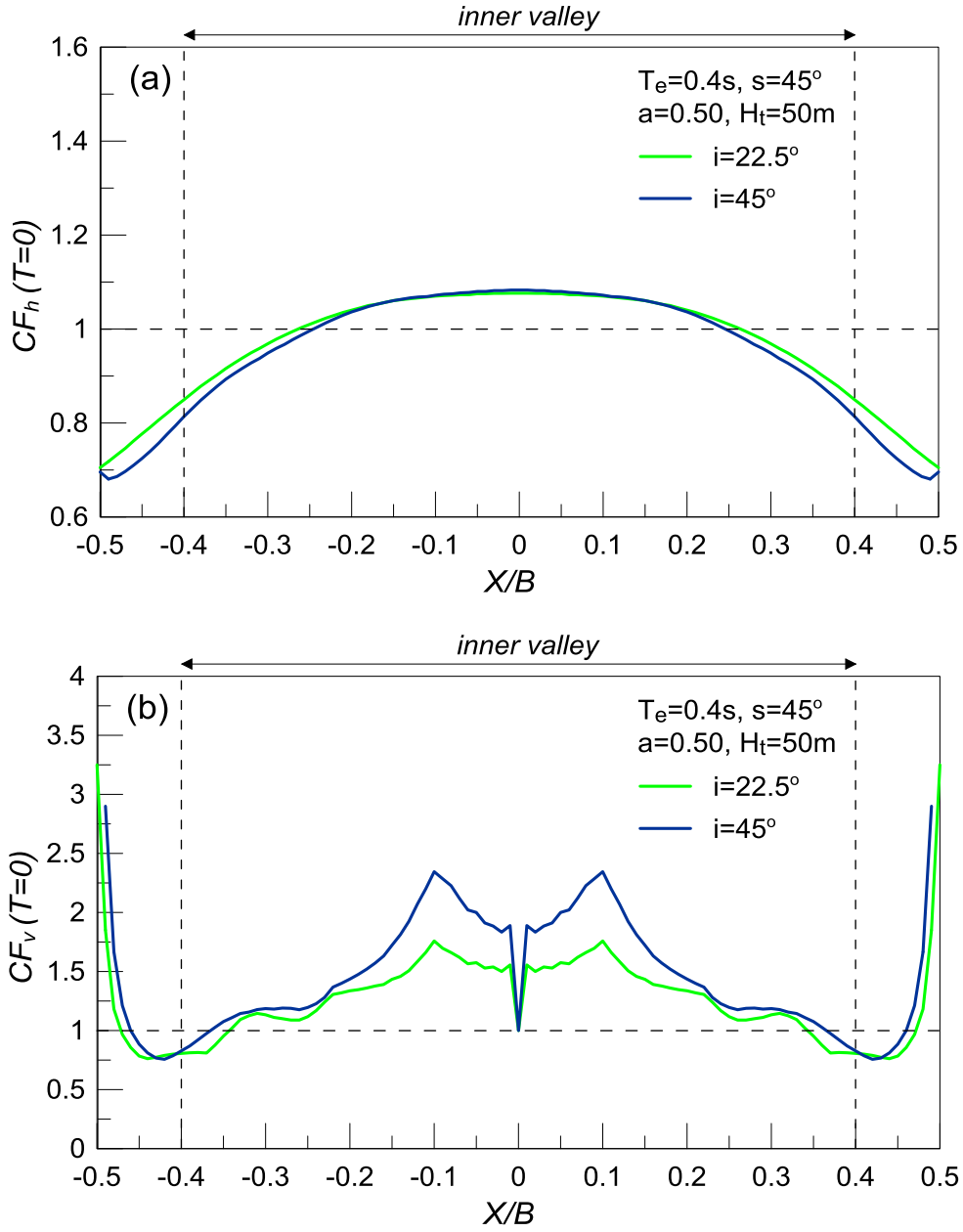

Figure 4.54: Effect of inclination angle i of outcropping bedrock on the spatial variability of correction factors CF_h and CF_v for T=0s with normalized distance X/B from the center of the steep (s=45°) valley with high impedance ratio a=0.5; Results for low frequency excitation with T_e = 0.4s and H_t = 50m.

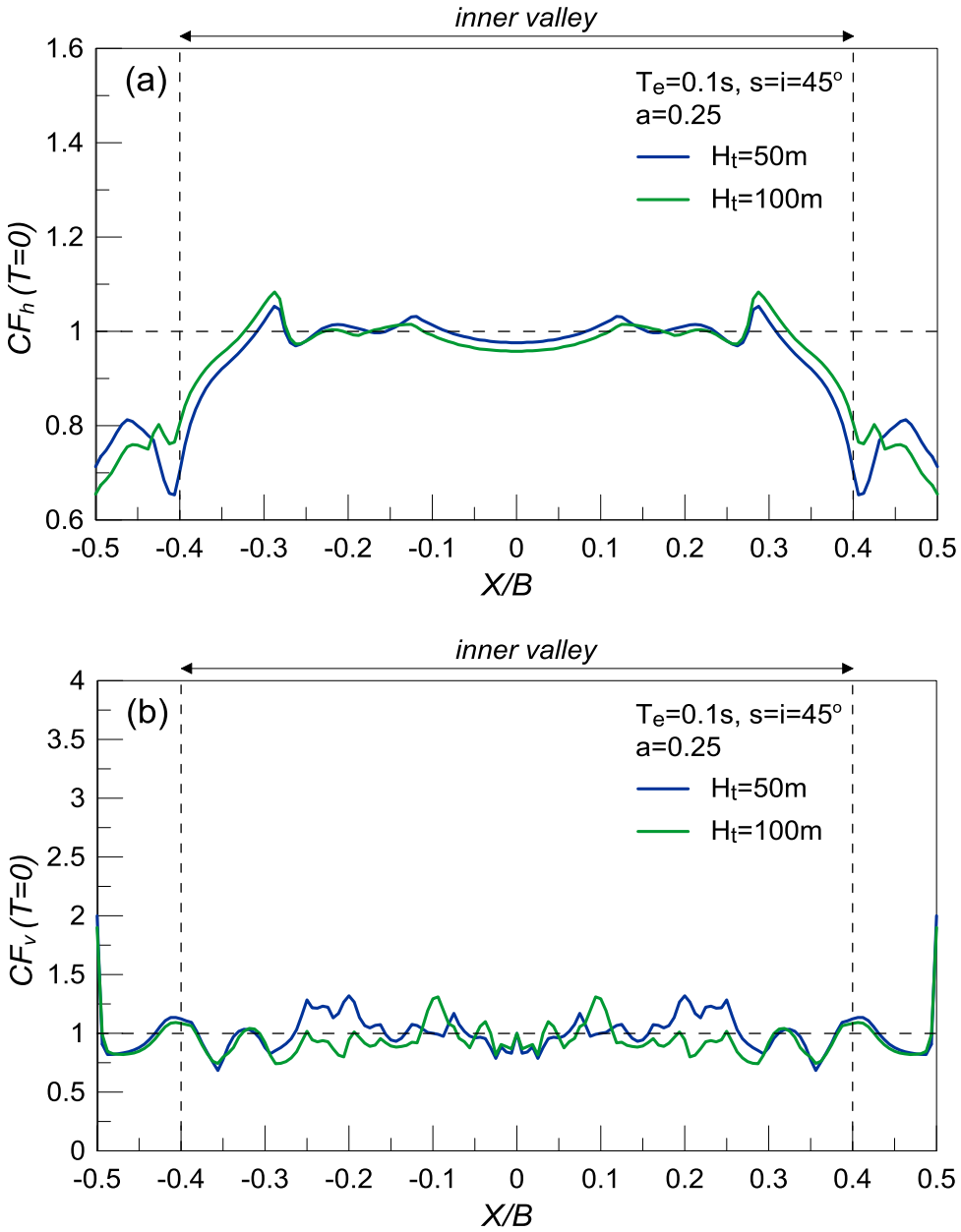

Figure 4.55: Effect of height H_t of steep (i=45°) outcropping bedrock on the spatial variability of correction factors CF_h and CF_v for T=0s with normalized distance X/B from the center of the steep valley (s=45°) with low impedance ratio a = 0.25; Results for high frequency excitation with T_e = 0.1s.

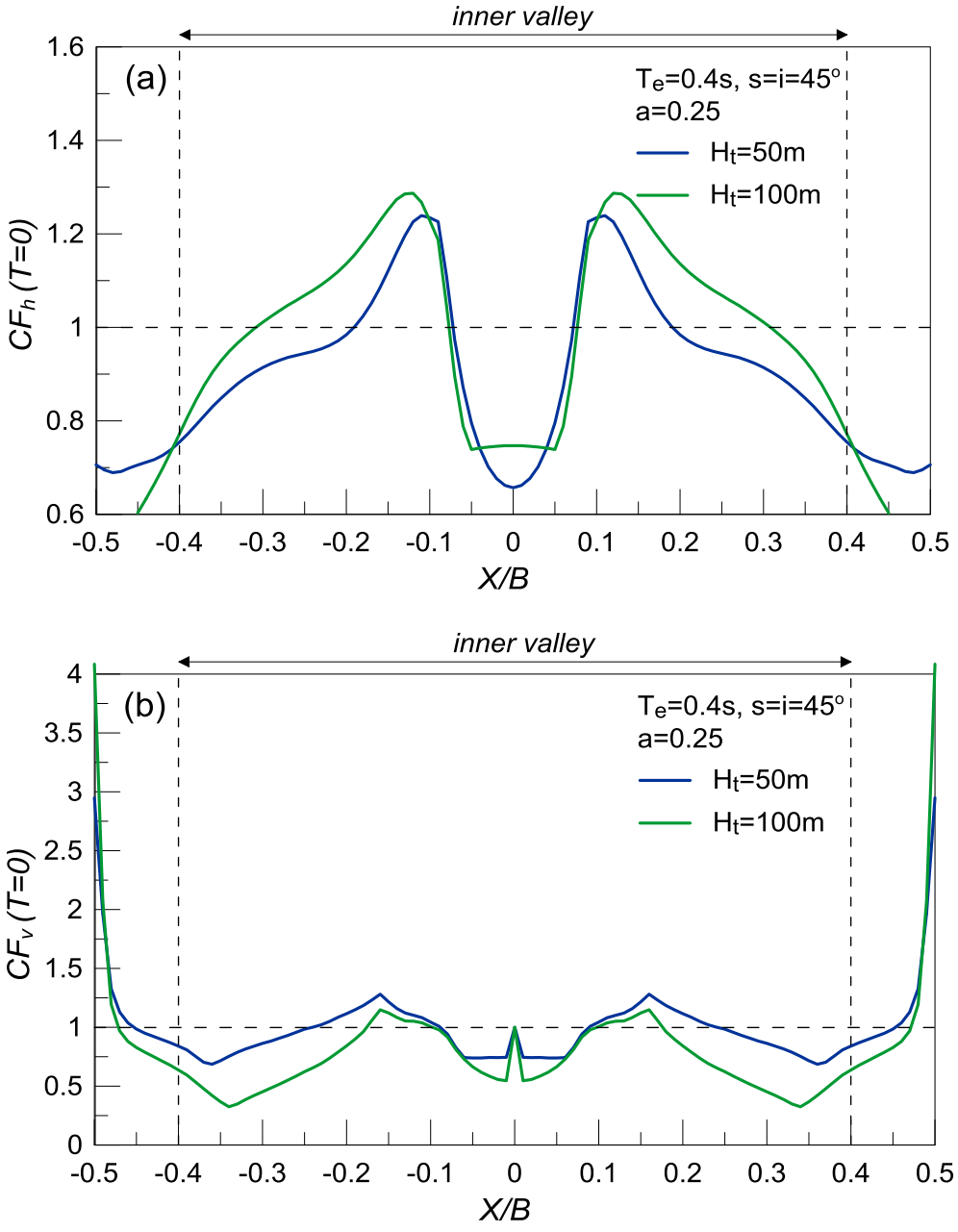

Figure 4.56: Effect of height H_t of steep (i=45°) outcropping bedrock on the spatial variability of correction factors CF_h and CF_v for T=0s with normalized distance X/B from the center of the steep valley (s=45°) with low impedance ratio a = 0.25; Results for low frequency excitation with T_e = 0.4s.

Based on the previous results, the effects of various parameters on the spatial variability of $CF_h(T=0)$ and $CF_v(T=0)$ is not independent from one another, while there is no one parameter that governs the response. Hence, in the following, the effect of each parameter on the correction factors $CF_h(T=0)$ and $CF_v(T=0)$ is investigated. To do so, the results of the performed analyses are grouped per parameter of interest, in other words, in terms of the characteristics of the outcropping bedrock (**Figure 4.57 and 4.58**), the characteristics of the valley (**Figures 4.59 and 4.60**) and of the seismic excitation (**Figure 4.61**). The results of each analysis one of the analyses in each of the groups is not depicted. What is of interest is the typical range and the average curve of all analyses within each group, as an additional attempt to quantify their effects.

Figure 4.57 depicts the effects of bedrock outcrop height H_t on the correction factors $CF_h(T=0)$ and $CF_v(T=0)$, showing the ranges and the average curves for H_t=50 and 100m. For $CF_h(T=0)$ the range and the average curve are slightly larger for H_t=100m. The same holds for $CF_v(T=0)$, but the increase with H_t is more intense. Note that for low-frequency excitation (T_e=0.4s) with high impedance ratio (a=0.5) there is an increase on both correction factors with H_t, especially on $CF_v(T=0)$, as depicted in **Figure 4.47**. However, for low impedance ratio (a=0.25) the increasing effect of H_t is observed only for the horizontal direction, since $CF_v(T=0)$ is clearly decreasing with H_t (**Figure 4.56**). For high and intermediate frequency excitations the effect of H_t is insignificant (**Figures 4.46 and 4.48**). Hence, the average curves are generally compatible with the previous results, at least for the high impedance ratio cases. In general, what **Figure 4.57** shows is that within the central part of the valley, the $CF_h(T=0)$ reaches 1.05 and 1.10 on average for H_t = 50m and 100m, respectively, and decreases below 1.0 near the valley edges. In addition, it also shows that the $CF_v(T=0)$ reaches 1.25 and 1.50 on average for H_t = 50m and 100m, respectively, and decreases to 1.0 near the valley edges. The local increase of $CF_v(T=0)$ exactly at the valley edges is not considered noteworthy, due to the problems in the definition of the geomorphic aggravation factors AS_{ah} and AS_{av} above the inclined segments of the valley near its edges.

The effect of the inclination angle i of the bedrock outcrops on correction factors is demonstrated in **Figure 4.58**. Note that the ranges for mild inclination angles ($i=22.5^o$) are limited, compared to those for steep angles ($i=45^o$). In particular, for $i=22.5^o$ $1 < CF_h(T=0) < 1.05$ and $0.75 < CF_v(T=0) < 1.5$ within the center of the valley, while for $i=45^o$ $0.7 < CF_h(T=0) < 1.3$ and $0.5 < CF_v(T=0) < 3.5$. The average values of $CF_h(T=0)$ are slightly increased for steep outcrops close to the center of the valley, but not in the center and the edges of the valley. The previous results in this paragraph showed a slight or a negligible increase of $CF_h(T=0)$ for steep outcrops. At the same time, the average $CF_v(T=0)$ values are higher for steep outcrops, which is compatible with the previous results, except those in **Figures 4.49 and 4.53**. In general, what **Figure 4.58** shows is that within the central part of the valley, the $CF_h(T=0)$ reaches 1.04 and 1.08 on average for i = 22.5^o and 45^o, respectively, and decreases below 1.0 near the valley edges. In addition, it also shows that the $CF_v(T=0)$ reaches 1.20 and 1.40 on average for i = 22.5^o and 45^o, respectively, and decreases to 1.0 near the valley edges. In other words, **Figures 4.57 and 4.58** as a whole summarize the increasing effects of the outcropping bedrock characteristics (height H_t , inclination angle i) on the correction factors $CF_h(T=0)$ and $CF_v(T=0)$ within the valley, with the effects being more intense, on average, along the central region of the valley.

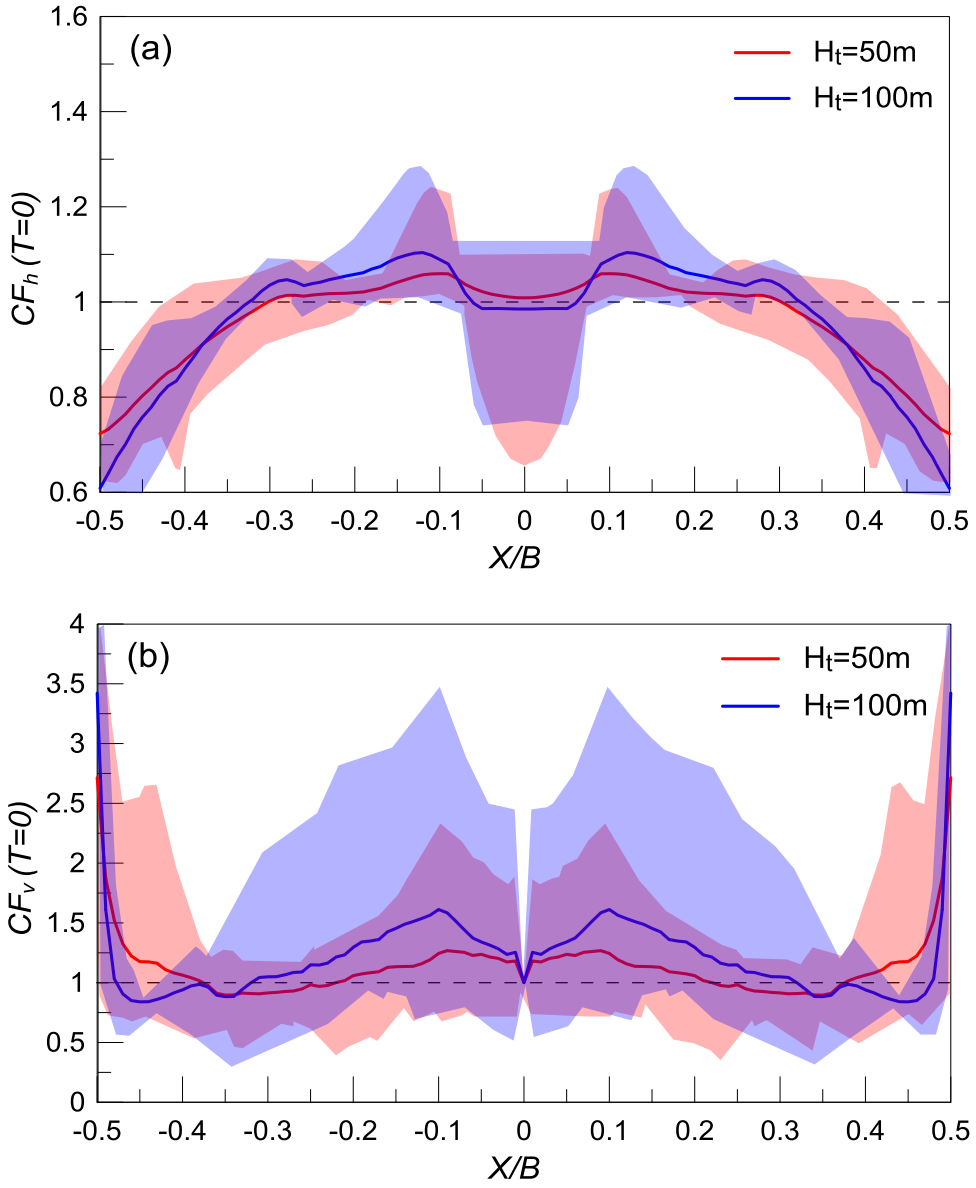

Figure 4.57: Average effect of outcropping bedrock height H_t on the spatial variability of correction factors CF_h and CF_v for T=0s within a valley with B/H = 10, on the basis of all the examined cases.

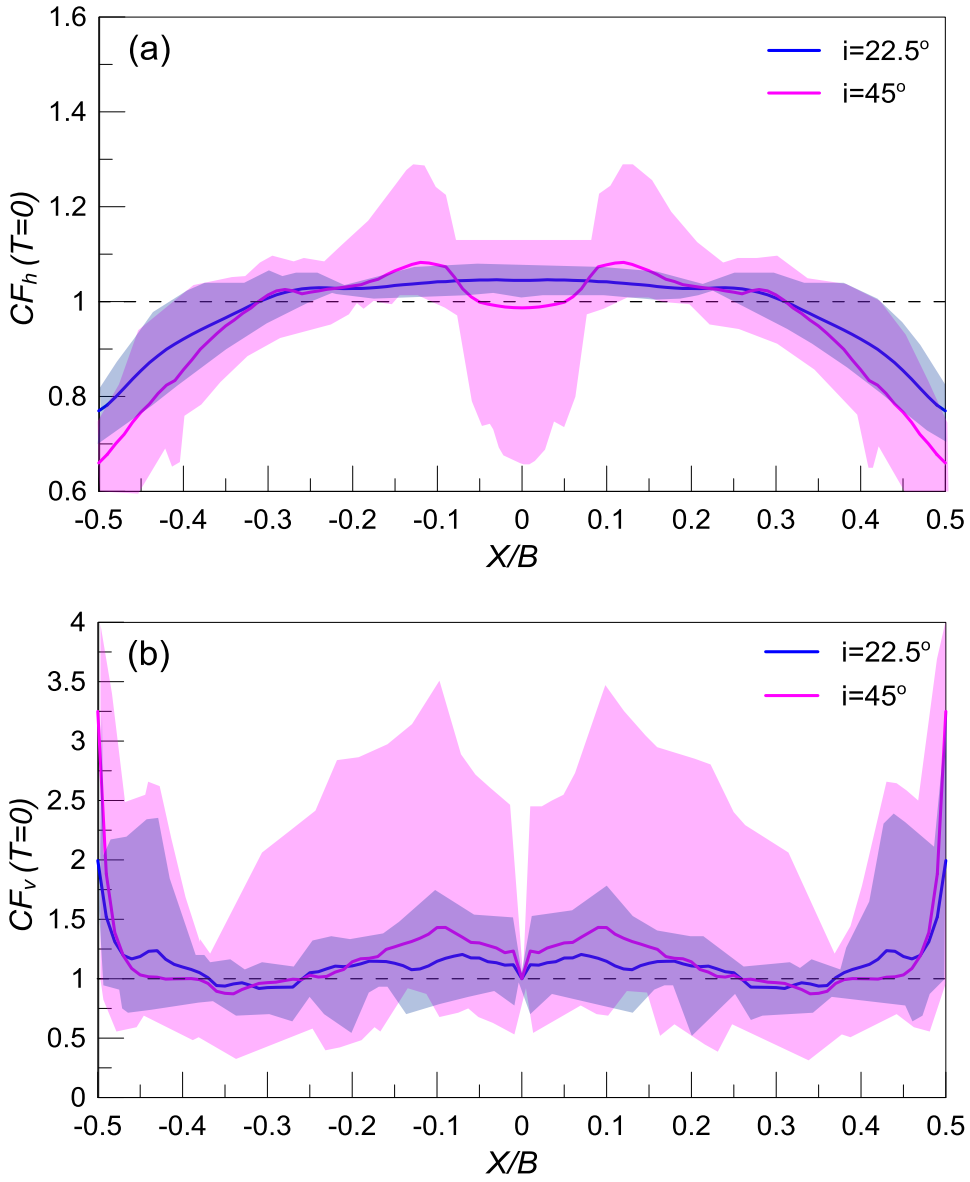

Figure 4.58: Average effect of inclination angle i of outcropping bedrock on the spatial variability of correction factors CF_h and CF_v for T=0s within a valley with B/H = 10, on the basis of all the examined cases.

In the sequel, **Figure 4.59** illustrates the ranges and average curves of correction factors $CF_h(T=0)$ and $CF_v(T=0)$ along the valley for high and low impedance ratio a. For low impedance ratio a=0.25, the range is clearly larger for $CF_h(T=0)$, but significantly lower for $CF_v(T=0)$. As expected from the previous results in this paragraph, there is a decrease of $CF_h(T=0)$ and an increase of $CF_v(T=0)$ with increasing a. This is accurate for a low-frequency excitation with T_e=0.4s, as the comparison between **Figure 4.47** (a=0.5) and **Figure 4.56** (a=0.25) leads to the same conclusion, and less so for a high frequency excitation with T_e = 0.1s where the differences are not as clear. More specifically, what **Figure 4.59** shows is that within the central part of the valley, the $CF_h(T=0)$ is characterized by a slight decreasing effect of impedance ratio a (maximum values of 1.10 and 1.05 for a = 0.25 and 0.50, respectively), which is however location-specific and therefore ambiguous for design purposes. On the contrary, the $CF_v(T=0)$ shows a clear increasing effect of impedance ratio a, with the maximum values being 1.1 and 1.4 for a = 0.25 and 0.50, respectively. It has to be underlined here that the ambiguity with respect to the curves for a = 0.25 may be partly attributed to the small number of pertinent analyses.

Similarly, **Figure 4.60** shows the effect of the inclination angle of the valley s on the correction factors $CF_h(T=0)$ and $CF_v(T=0)$ along the valley. As already observed in **Figure 4.58**, the ranges are wider for steep valleys ($s=45^o$) and the average curves here show a slight increase of correction factors with increasing angle s. The results for a low-frequency excitation with T_e=0.4s (**Figures 4.50, 4.52 and 4.54**) are compatible with the abovementioned conclusion. On the contrary, the results for a high-frequency excitation with T_e=0.1s (**Figures 4.49, 4.51 and 4.53**) are not in agreement with the average results, especially in the vertical direction. As a result, the differences of $CF_h(T=0)$ and $CF_v(T=0)$ due to the value of s are not as pronounced, on average. It has to be underlined here that again, the ranges for $s = 22.5^o$ are based on a relatively small number of analyses, something that partly explains the relative ambiguity in the respective effect of angle s.

More generally, **Figures 4.59 and 4.60** as a whole summarize the somewhat unclear effects of valley characteristics (impedance ratio a, inclination angle s) on the correction factors $CF_h(T=0)$ and $CF_v(T=0)$ within the valley. The only clear effect is the increase of $CF_v(T=0)$ along the valley due to an increase of impedance ratio a.

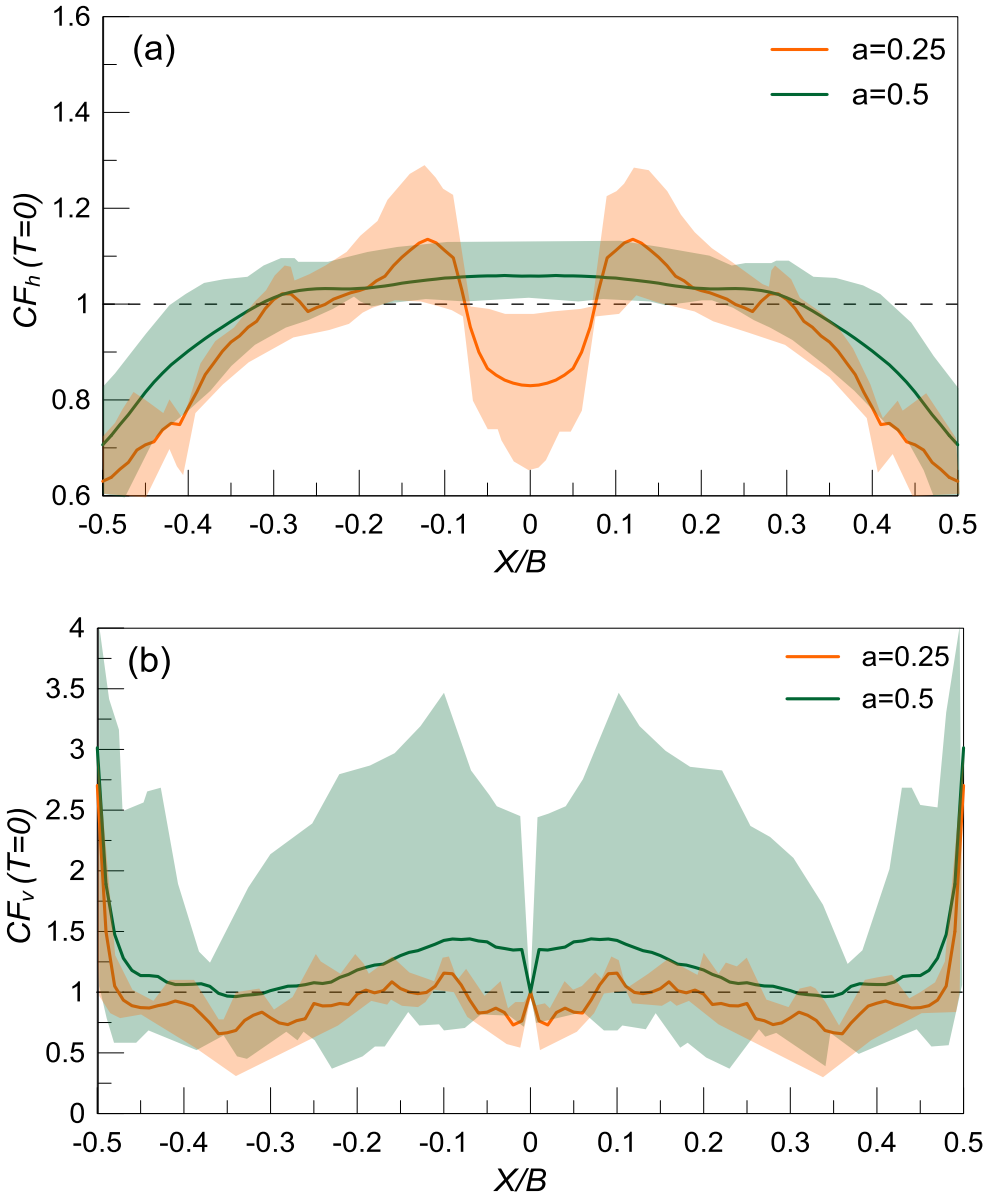

Figure 4.59: Average effect of valley impedance ratio a on the spatial variability of correction factors CF_h and CF_v for T=0s within a valley with B/H = 10, on the basis of all the examined cases.

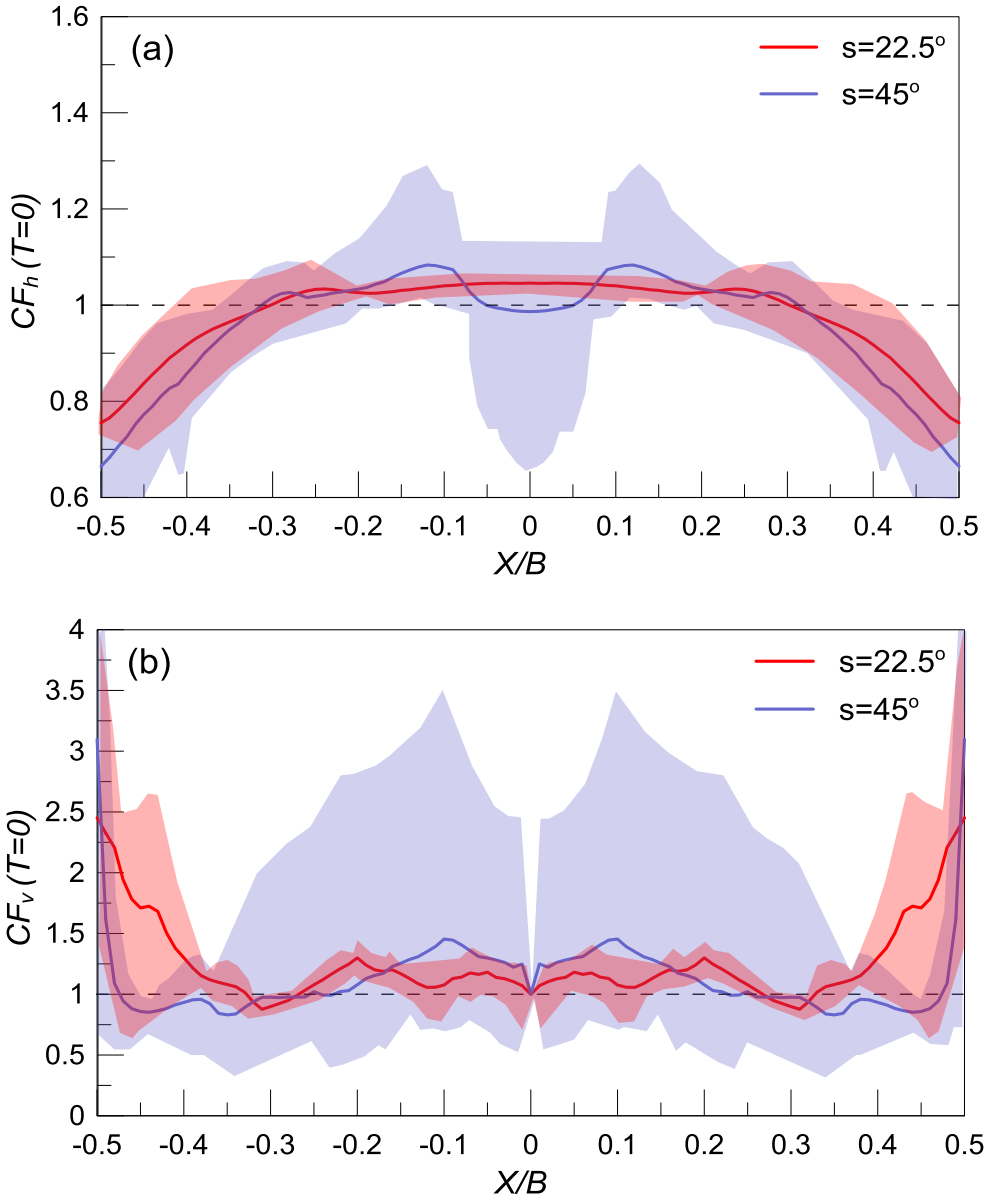

Figure 4.60: Average effect of valley inclination angle s (at its edges) on the spatial variability of correction factors CF_h and CF_v for T=0s within a valley with B/H = 10, on the basis of all the examined cases.

Finally, **Figure 4.61** investigates the effect of excitation period T_e on the correction factors CF_h-(T=0) and CF_v(T=0) along the valley. The range of the results seems limited for the high (T_e=0.1s) and the intermediate-frequency excitation (T_e=0.25s), but significant for the low-frequency excitation (T_e=0.4s). From the average curves of each subset of analyses in the horizontal direction it can be observed a shift of the location of the maxima of CF_h(T=0) for different T_e, but not a huge effect in their values. Namely, as T_e increases, the locations of maxima become slightly larger, while shifting from the boundaries to the center of the valley. At the same time, in the vertical direction there is an increase of CF_v(T=0) with increasing T_e. These conclusions are also verified in **Figures 4.46 to 4.48**. Overall, for high frequency excitations (T_e = 0.1s), the existence of outcropping bedrock creating a topographic relief does not seem important, since CF_h(T=0) < 1.1 and CF_v(T=0) < 1.2, on average. However, for intermediate frequency (T_e=0.25s) and low frequency (T_e=0.4s) excitations, the topography seems important, since the maximum values of the average CF_h(T=0) and CF_v(T=0) curves take values higher than 1.1 and 1.6, respectively.

Having determined the correction factors CF_h(T=0) and CF_v(T=0) for all the examined cases, **Figure 4.62** summarizes their range and the average curve that stems from them. Observe that for CF_h(T=0) there is a relatively small in the values, with the overall range being from 0.6 to 1.3. On average, the CF_h(T=0) varies between 1 and 1.06 in the central 60% of the valley width (|X/B|<0.3), but reduces below 1.0 gradually towards the edges and reaches a minimum of 0.7. This reduction towards the edges is systematic, but its minimum value per se is considered affected by the poor definition of AS_{ah} over the inclined segments of the valley. On the other hand, the scatter is quite large for CF_v(T=0), since the overall range is from 0.4 to 3.5. On average, the CF_v(T=0) is higher than 0.9 throughout the valley, and consistently between 1.0 and 1.4 in the central 50% of the valley width (|X/B|<0.25). Towards the edges (0.25<|X/B|<0.45), the CF_v(T=0) ranges between 0.9 and 1.1, while at the very edges it increases significantly, an increase whose maximum value (2.9) is considered partially an artifact of the poor definition of ASa_v over the inclined segments of the valleys and especially at its edges where the soil thickness is significantly smaller than H.

To sum up, the correction factors CF_h(T=0) and CF_v(T=0) are affected mostly by the outcropping bedrock geometry (height H_t, inclination angle i) and the applied excitation (predominant period T_e) and less so by the characteristics of the valley (inclination s, impedance ratio a) itself. In general, the correction factors become important for higher (H_t=100m) and steeper outcrops (i=45^o), especially if the valleys are also steep (s=45^o). A high impedance ratio (a=0.5, low contrast) causes a de-amplification of CF_h(T=0), but an amplification of CF_v(T=0) in comparison to a low impedance ratio (a=0.25, high contrast). As the frequency of the excitation decreases, the CF_v(T=0) increases, while the CF_h(T=0) is only slightly enhanced, with the local maxima shifting from the boundaries to the center of the valley. From all the examined cases, it can be concluded that the correction factors CF_h(T=0) and CF_v(T=0) become significant for low-frequency excitations (e.g. T_e=0.4s) and generally reduce for high frequency motions (e.g. T_e=0.1s). Qualitatively, these results are considered to hold true for all symmetric trapezoidal valleys. However, quantitatively, the results are considered affected by the fact that our valley retained a constant value of B/H = 10.

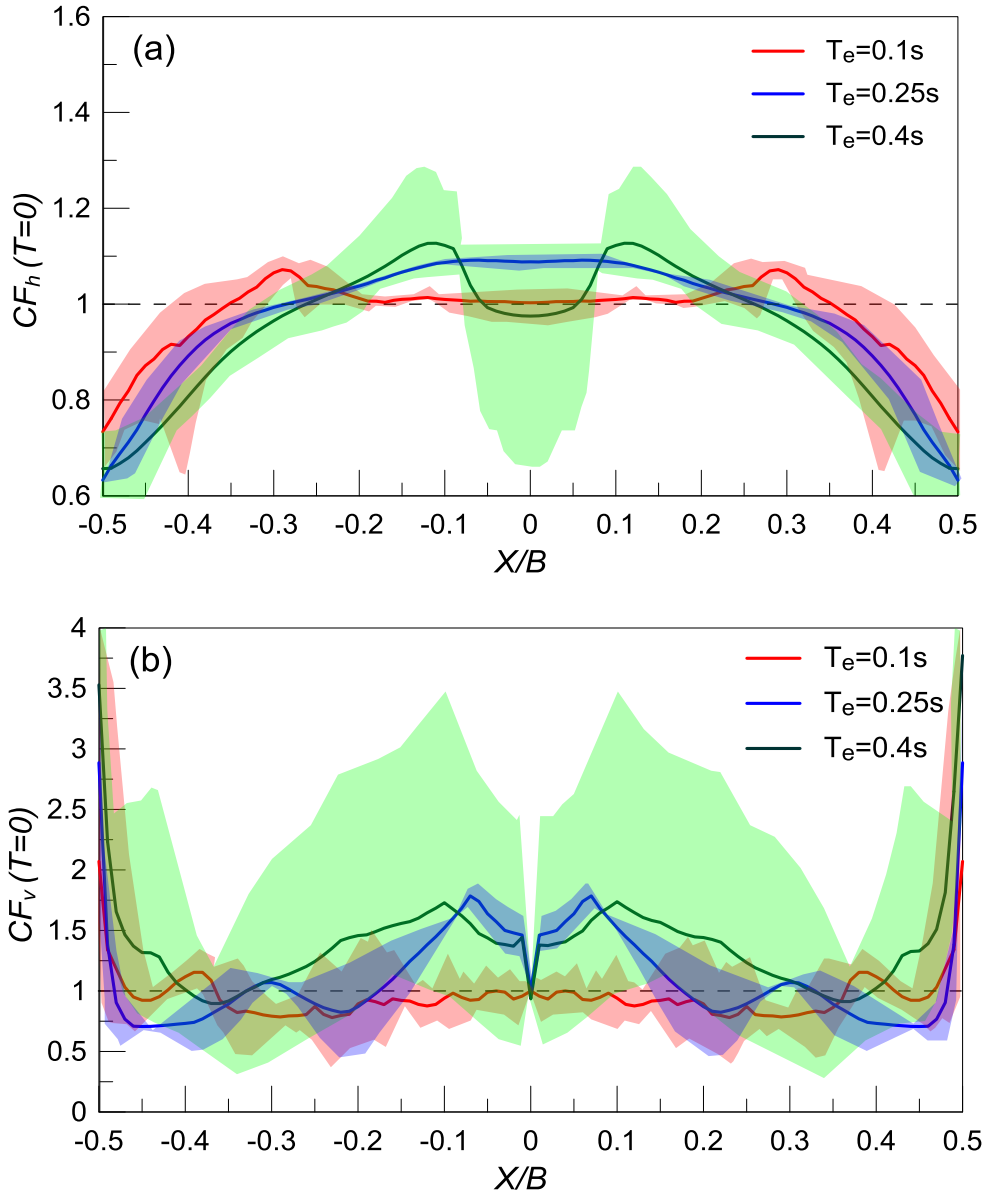

Figure 4.61: Average effect of predominant excitation period T_e on the spatial variability of correction factors CF_h and CF_v for T=0s within a valley with B/H = 10, on the basis of all the examined cases.

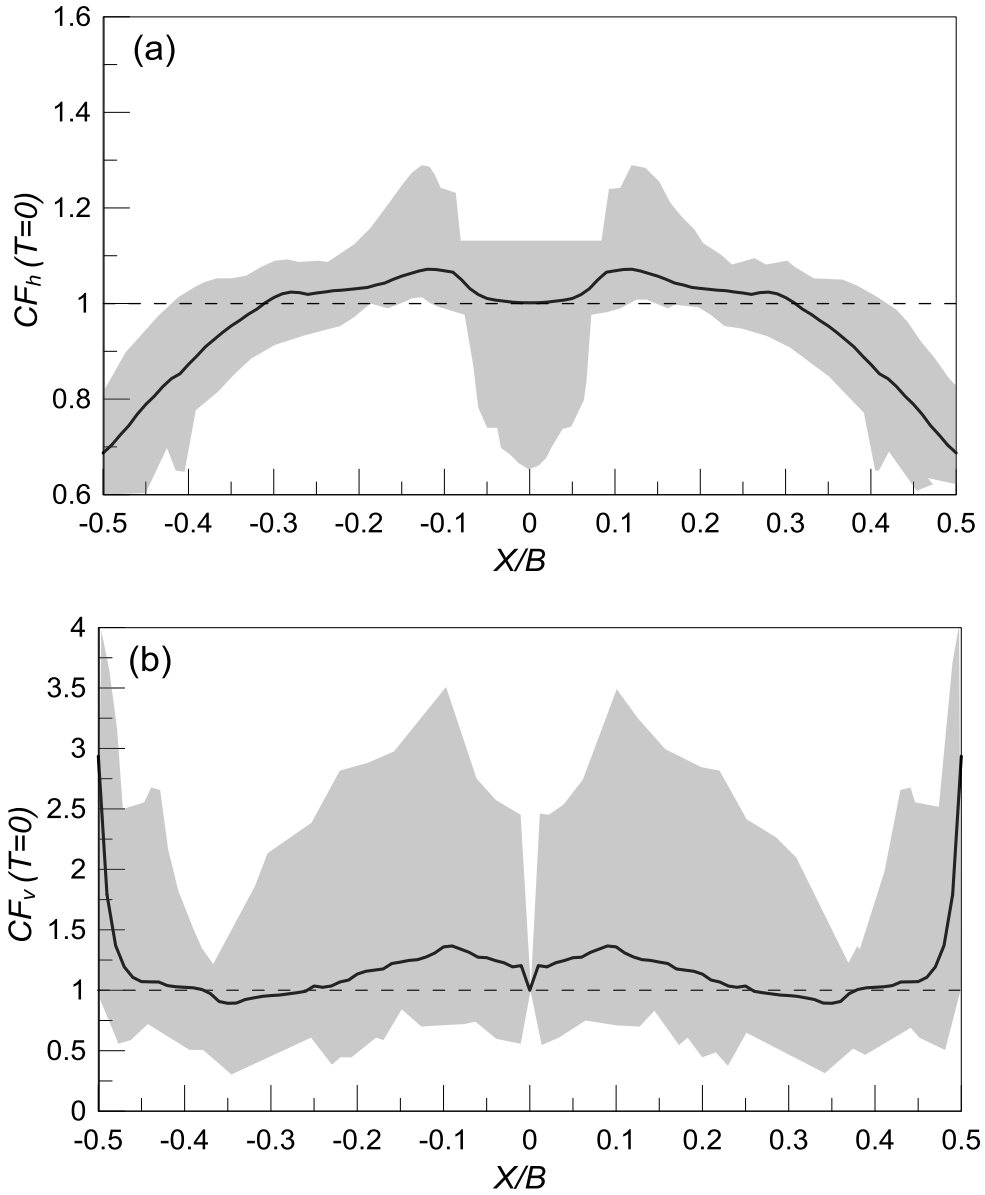

Figure 4.62: Range of variability and average spatial variability of correction factors CF_h and CF_v for T=0s within a valley with B/H = 10, on the basis of all the examined cases.

CHAPTER 5

EFFECTS OF VALLEY ON THE SEISMIC RESPONSE OF OUTCROPPING BEDROCK

5.1 Introduction

Chapter 4 investigates how the seismic response of the valley is affected by different outcropping bedrock topographies. Thus, the analyses presented there focused primarily on what happens inside the valley and secondarily on what happens at the outcropping bedrock. Of interest here is the opposite question, namely if the seismic response of a topographic relief is affected by whether there is a soft alluvial basin at its base. Hence, for each examined case in this Chapter a comparison is made between two canyons with the same topographic shape; one with a soft alluvial valley at the base of the topographic relief and one where no such valley appears. For each examined case, the seismic response of the canyon with a soft alluvial valley at its base has already been examined in Chapter 4. Here, an additional seismic response analysis is performed, in which the area of the soft alluvial soil is assigned bedrock properties. In other words, the additional analysis corresponds to an impedance ratio of 1.0, or to an analysis for a homogeneous rock canyon with V_b = 1000m/s. Finally, since the purpose of this Chapter is mainly to study the seismic response of the outcropping bedrock, the focus of the investigation is for locations outside of the valley (with a normalized horizontal distance from the center of the valley |X/B| > 0.5) and on whether the response there is affected by the existence of the valley. However, for reasons of completeness, results will also be presented for the area within the valley (with a normalized horizontal distance |X/B| < 0.5) where the results are expected to be different due to the existence of soil in 1 of the 2 analyses. In closing, 8 cases are examined here, which investigate the effects of the predominant period of the excitation T_e, the inclination angles of the valley s and the outcropping bedrock i and the outcropping bedrock height H_t.

In the following, the results are presented in 3 different types of figures. The first one shows the spatial variability of geomorphic aggravation factors AS_{ah} and AS_{av} for T=0s with distance X/B. The second one presents the geomorphic aggravation spectra AS_{ah} and AS_{av} at the locations of peak aggravation for T=0s along the valley, wherever these appear for the horizontal and the parasitic vertical acceleration. Finally, the third type of figure depicts the spatial variability of geomorphic aggravation factors AS_{ah} and AS_{av} for specific structural periods T with distance X/B. These periods T = 0, 0.2, 0.4 and 1.0 sec, correspond to the ground response and the response of usual low-rise (T =

0.2s), medium rise (T = 0.4s) and high-rise buildings (T = 1.0s). It becomes obvious that the format of these figures is identical to the format of the respective figures in Chapter 4.

5.2 Effects for steep valleys s = 45^o with steep outcrops i = 45^o

In this paragraph, the valleys have buried and outcropping bedrock inclination angles (s and i, respectively) equal to 45^o, i.e. they correspond to steep valleys with steep outcrops, and in the figures their results are denoted by "valley". The corresponding homogeneous canyons have the same height H_t and the same outcropping bedrock inclination angle i, and in the figures their results are denoted by "no valley". What varies in the analyses in this paragraph are: a) the value of H_t = 50 and 100m; b) the predominant excitation period T_e = 0.1s (high-frequency), 0.25s (intermediate-frequency) and 0.4s (low-frequency).

The effects of the existence of the valley on the seismic response under a high-frequency excitation T_e = 0.1s and for outcropping bedrock height H_t=50m are demonstrated in **Figures 5.1 to 5.3**. Specifically, **Figure 5.1** compares the spatial variability of geomorphic aggravation factors AS_{ah} and AS_{av} for T=0s with normalized distance from the center of the valley X/B. For the horizontal component, there is a small effect of the valley on the outcropping bedrock response, namely a slightly smaller amplification of the motion for distances up to |X/B|=0.7, i.e. in the close vicinity of the valley, but the value of the peak amplification which appears behind the crest of the outcropping bedrock remains unaffected. For the vertical component, a similarly small effect is detected, with the valley imposing a slightly higher amplification only at large distances from the valley |X/B| > 0.8, while retaining practically identical response in the vicinity of the valley and where the peak amplification is observed. On the contrary, within the valley boundaries (-0.5 ≤ X/B ≤ 0.5) the aggravation in both directions is significantly larger for the valley case, as expected. In detail, for the valley case $maxAS_{ah}$=1.35 and $maxAS_{av}$=0.55, while for the no valley case $maxAS_{ah}$=1.05 and $maxAS_{av}$=0.1. Focusing on the locations where the $maxAS_{ah}$(T=0) and $maxAS_{av}$(T=0) are observed at the outcropping bedrock, **Figure 5.2** compares their aggravation spectra for the valley and no valley case. It is verified that whatever happens for T=0s, appears for all T values. Namely, the existence of the valley has a small effect on the aggravation spectra at these locations, with the spectral aggravation values being slightly lower and higher for the valley case in the AS_{ah} and AS_{av}, respectively, especially for periods between 0.2 and 1s. **Figure 5.3** presents the spatial variability of aggravation factors for the no valley model for different structural periods (including the T=0s of **Figure 5.1**). Observe that the aggravation behind the crest is generally larger than in front of the toe of the canyon, and that this aggravation is larger for periods smaller or equal to 0.1s and decreases thereafter, both results that are typical for homogeneous canyon topographies. However, if we compare these results, with the pertinent results for the case when the valley exists (see **Figure 4.4**)), it becomes obvious that the aggravation within the valley boundaries is significantly smaller here than when a valley exists.

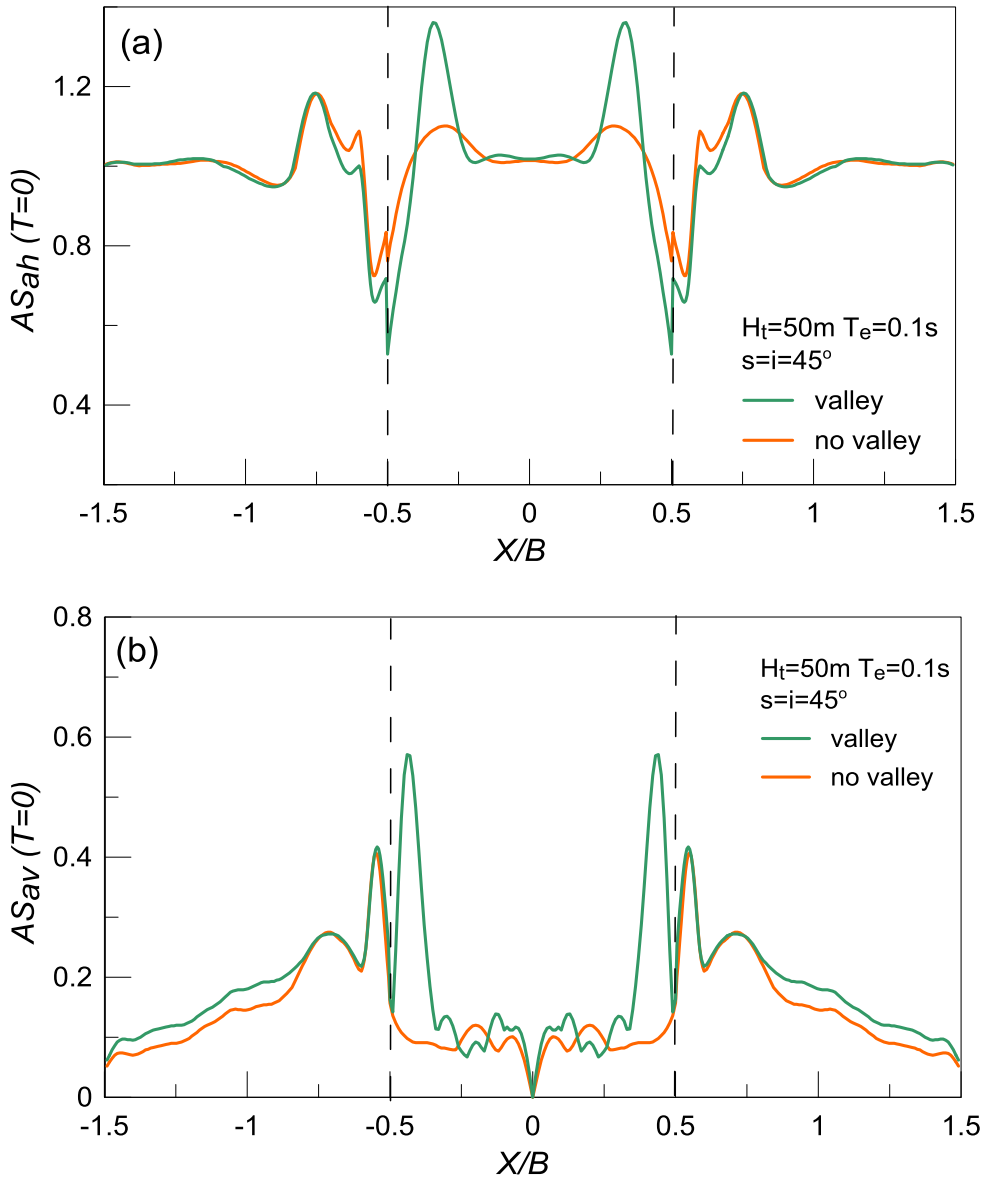

Figure 5.1: Effect of valley's existence on the spatial variability of geomorphic aggravation factors AS_{ah} and AS_{av} for T=0s with normalized distance from the center of the valley X/B; Results for H_t = 50m, s = i = 45° and a high-frequency excitation with T_e = 0.1s.

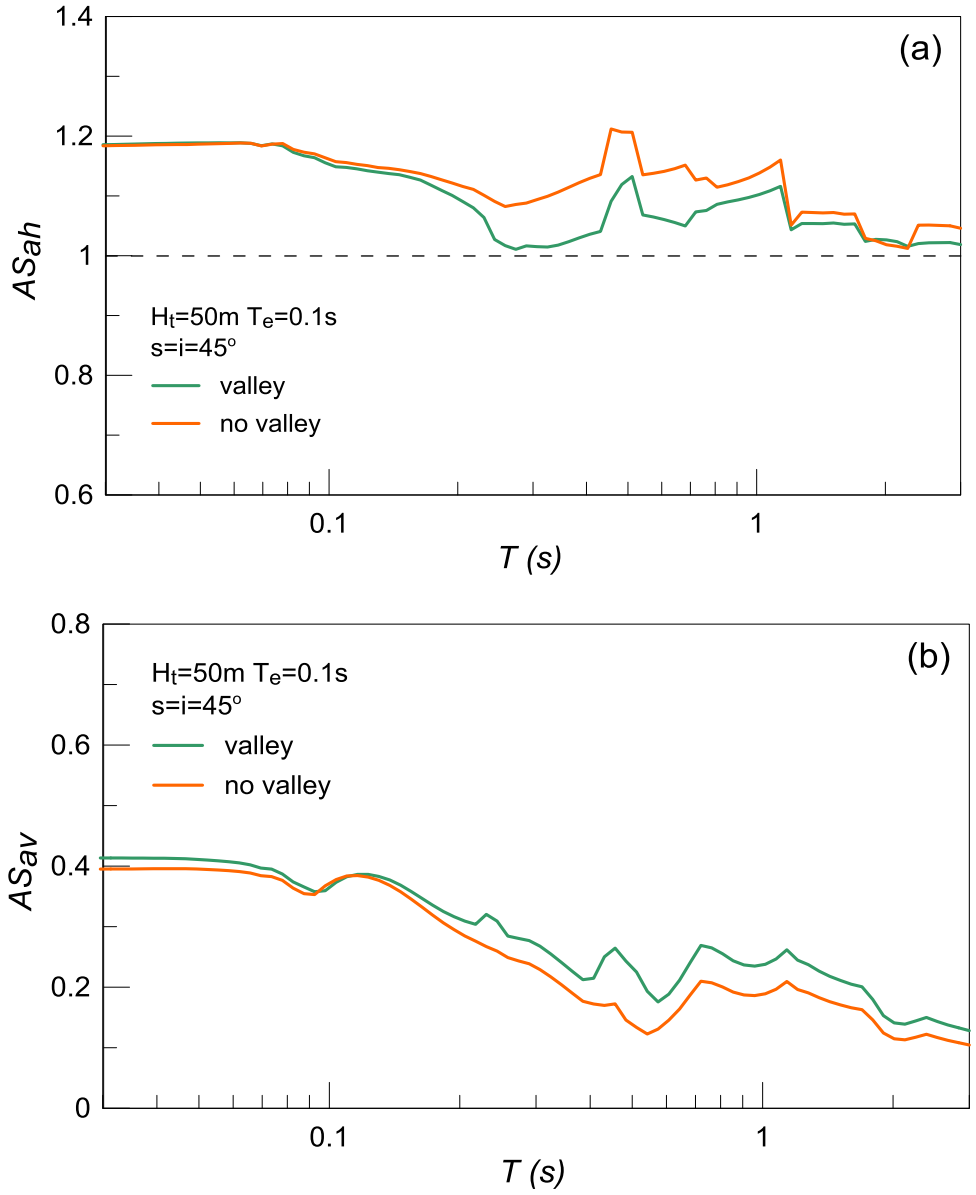

Figure 5.2: Effect of valley's existence on geomorphic aggravation spectra AS_{ah} and AS_{av} at the location of peak aggravation for T=0s along the outcropping bedrock; Results for H_t = 50m, s = i = 45^o and a high-frequency excitation with T_e = 0.1s.

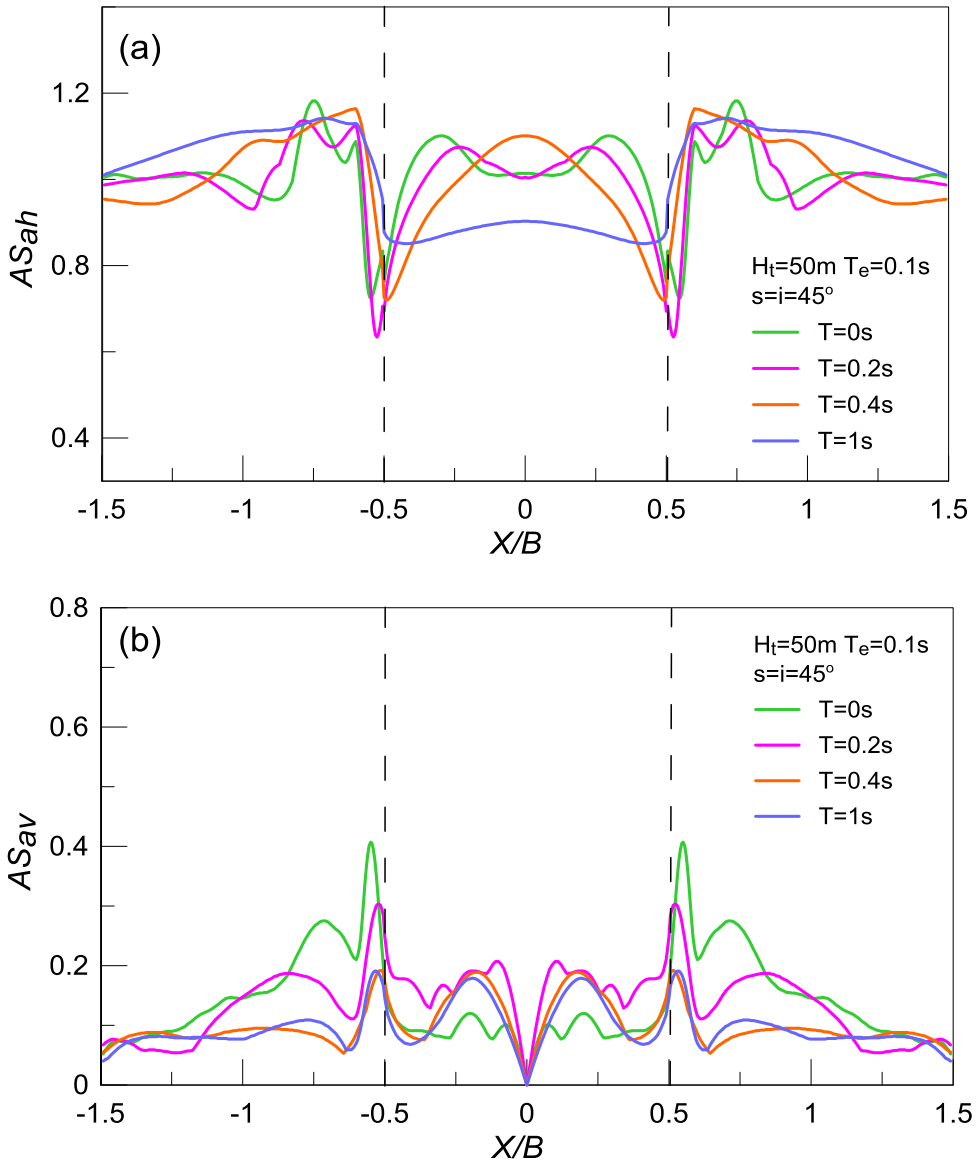

Figure 5.3: Spatial variability of aggravation factors AS_{ah} and AS_{av} for specific structural periods T with normalized distance from the center of the valley X/B; Results for outcropping bedrock height H_t = 50m, i = 45°, impedance ratio a = 1.0 (no valley) and a high-frequency excitation with T_e = 0.1s.

In the sequel, **Figures 5.4 to 5.6** present the results for the same high-frequency excitation with T_e = 0.1s, but for a higher outcropping bedrock height H_t=100m. The results are presented in the same format as **Figures 5.1 to 5.3**, respectively, and are directly comparable to them. Specifically, based on **Figure 5.4**, the valley has again no effect on the peak aggravation values for T=0s at the outcropping bedrock. Furthermore, the $AS_{ah}(T=0)$ is similarly relatively smaller for the valley case for distances up to $|X/B| < 0.7$, while the differences in $AS_{av}(T=0)$ start appearing at large values of $|X/B|$. However, there are also differences, i.e. the values of peak aggravation at the outcropping bedrock become larger in comparison to results in **Figure 5.1** due to the increased H_t value. Additionally, the differentiation due to the valley's existence in $AS_{av}(T=0)$ at large values of $|X/B|$ is not as systematic as it appeared for H_t = 50m. **Figure 5.5** compares the aggravation spectra for the valley and no valley cases at the locations where the $maxAS_{ah}(T=0)$ and $maxAS_{av}(T=0)$ are observed at the outcropping bedrock of height H_t = 100m. Again, it is concluded that whatever happens for T=0s, appears for all T values. In other words, the existence of the valley has a small effect on the aggravation spectra at these locations, with the spectral aggravation values being slightly lower for AS_{ah} and non-systematic for AS_{av}. However, in general, the aggravation is more significant for low periods. Finally, **Figure 5.6** presents the spatial variability of aggravation factors for the no valley model for different structural periods (including the T=0s of **Figure 5.4**). As expected from **Figure 5.5**, the maximum aggravation values occur for T=0s, and that the aggravation behind the crest is generally much larger than in front of the toe of the canyon, typical for homogeneous canyon topographies. However, if one compares these results, with the pertinent results for the case when the valley exists (see **Figure 4.5**)), it becomes obvious that the aggravation within the valley boundaries is significantly smaller here than when a valley exists for all periods T.

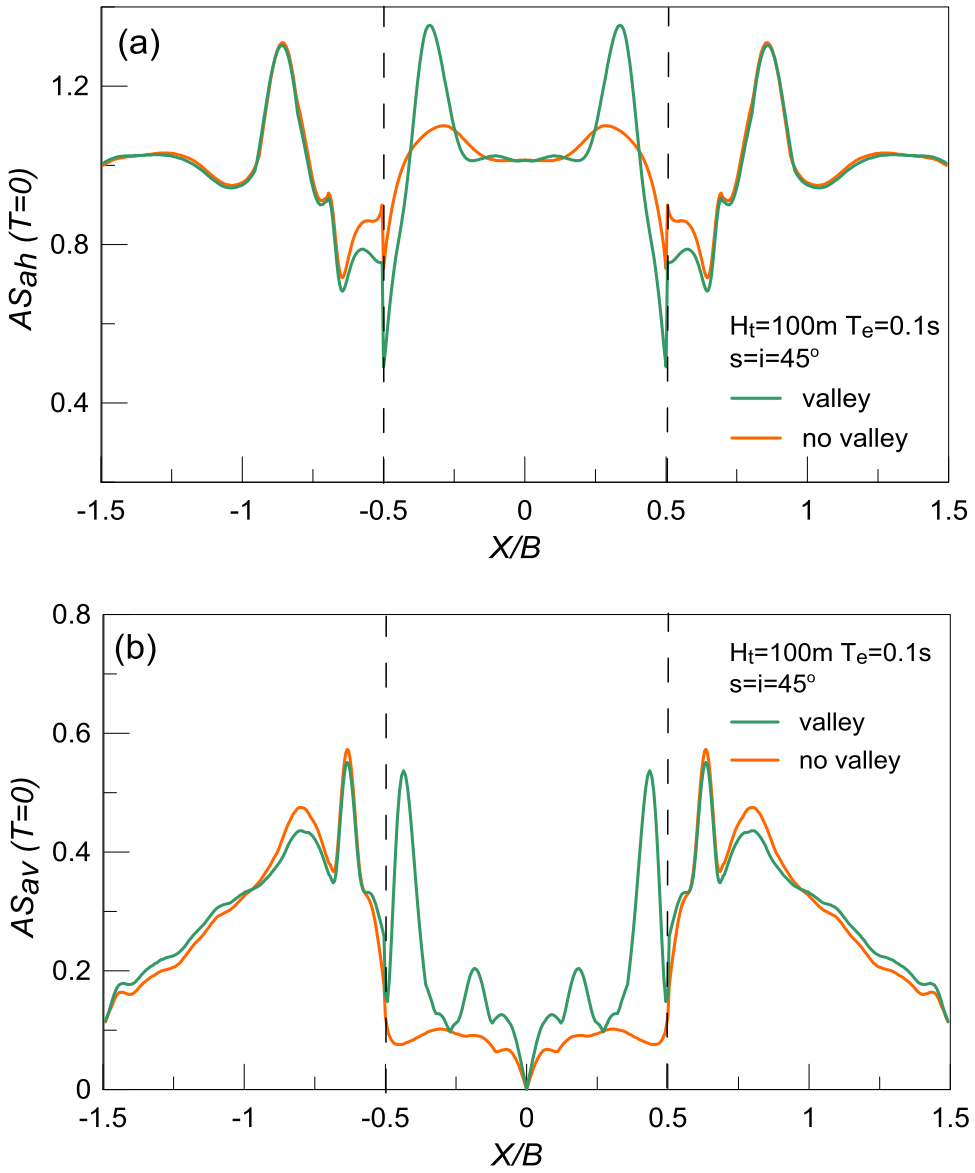

Figure 5.4: Effect of valley's existence on the spatial variability of geomorphic aggravation factors AS_{ah} and AS_{av} for T=0s with normalized distance from the center of the valley X/B; Results for H_t = 100m, s = i = 45° and a high-frequency excitation with T_e = 0.1s.

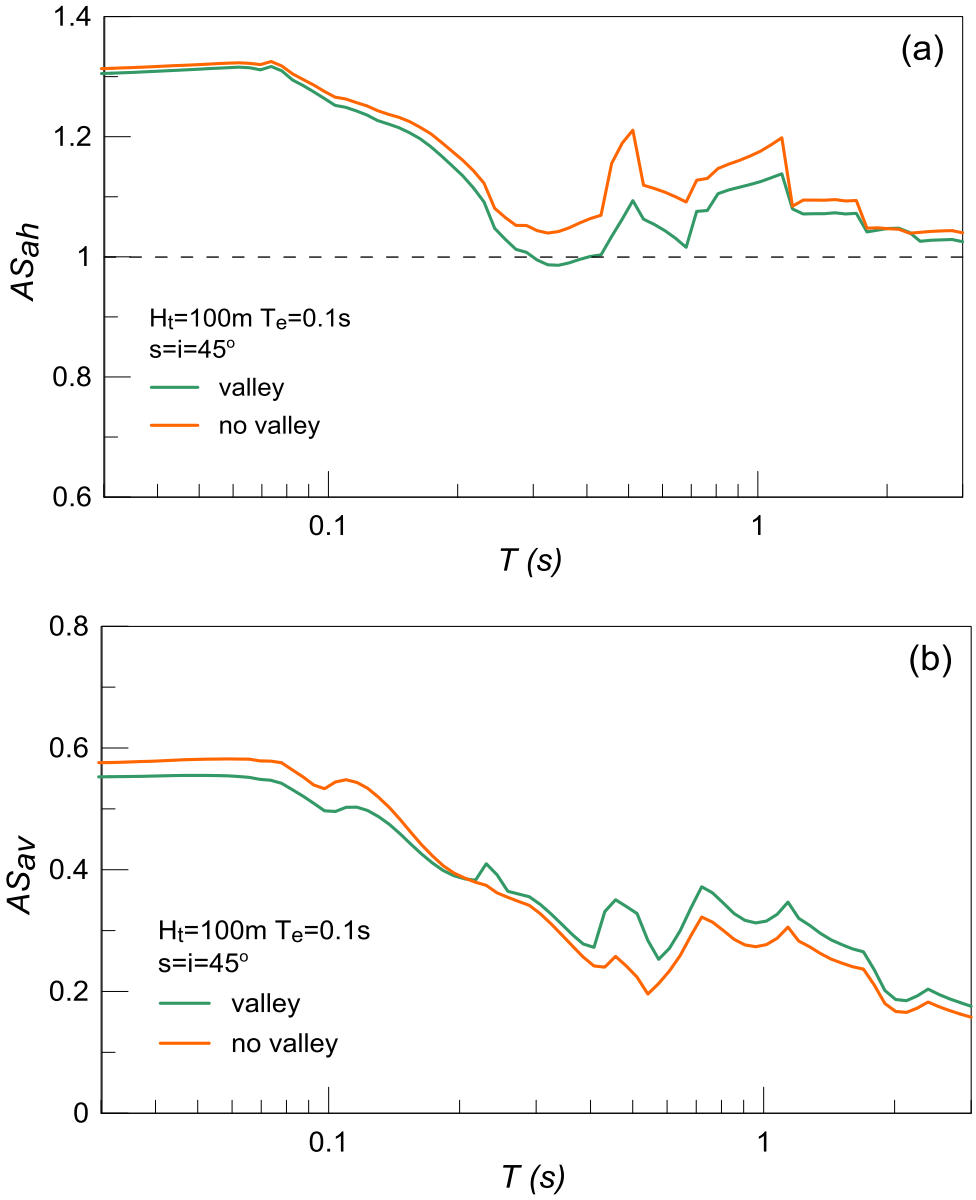

Figure 5.5: Effect of valley's existence on geomorphic aggravation spectra AS_{ah} and AS_{av} at the location of peak aggravation for T=0s along the outcropping bedrock; Results for H_t = 100m, s = i = 45° and a high-frequency excitation with T_e = 0.1s.

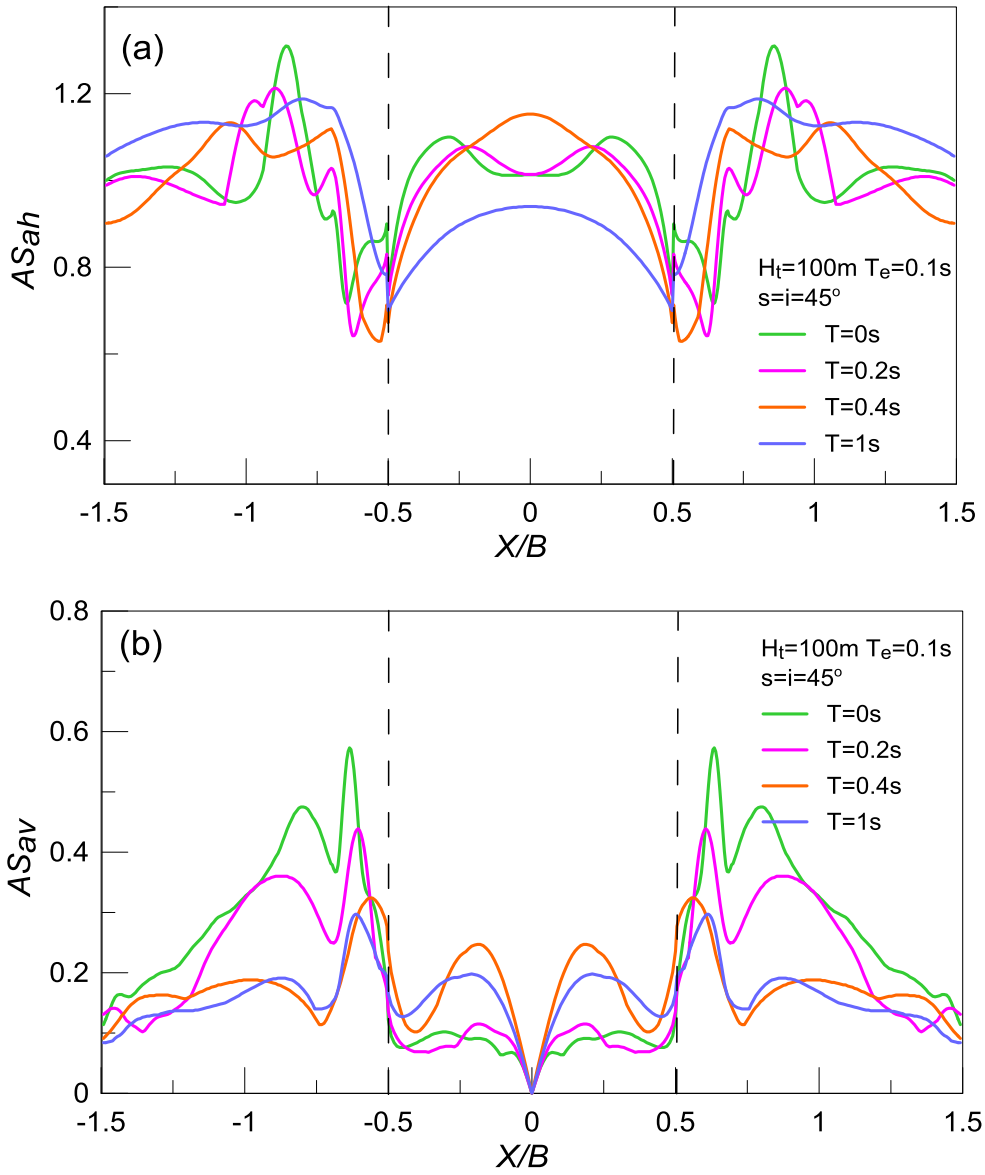

Figure 5.6: Spatial variability of aggravation factors AS_{ah} and AS_{av} for specific structural periods T with normalized distance from the center of the valley X/B; Results for outcropping bedrock height H_t = 100m, i = 45°, impedance ratio a = 1.0 (no valley) and a high-frequency excitation with T_e = 0.1s.

The effect of valley's existence on the seismic behavior of the outcropping bedrock with height H_t=50m, but for an intermediate-frequency motion with T_e=0.25s is presented in **Figures 5.7 to 5.9**. The results are presented in the same format as **Figures 5.1 to 5.3**, respectively, and are directly comparable to them. As shown in **Figure 5.7**, for $AS_{ah}(T=0)$ the valley imposes a smaller amplification at the outcropping bedrock, affecting slightly the amplitude and mostly the location of the peak. In detail, the peak aggravation for the valley model is $maxAS_{ah}(T=0)$=1.1, located at |X/B|=1, while for the no valley model $maxAS_{ah}(T=0)$=1.15, located at |X/B|=0.55. However, the differences due to the valley seem to be considerable only in the vicinity of the valley and disappear at large distances from it, qualitatively similarly to the case for T_e=0.1s (**Figure 5.1**). On the other hand, for $AS_{av}(T=0)$ the valley imposes a slightly larger amplification ($maxAS_{av}(T=0)$=0.3 versus $maxAS_{av}(T=0)$=0.25), but no shift to its location (in close vicinity to the valley). More generally, the effect of valley's existence on the aggravation at the outcropping bedrock is larger for T_e=0.25 than for T_e=0.1s (**Figure 5.1**). Within the valley, the aggravation in both directions is larger for the valley case, but the differences seem quantitatively smaller than for T_e = 0.1s. However, there is a qualitative difference, that for the no valley model the $AS_{ah}(T=0)$ is maximized at the center of the valley here, and not closer to the edges as for the T_e = 0.1s excitation. Focusing on the locations where the $maxAS_{ah}(T=0)$ and $maxAS_{av}(T=0)$ are observed at the outcropping bedrock, **Figure 5.8** compares their aggravation spectra for the valley and no valley model. As is the standard from the previous comparisons, whatever happens for T=0s, appears for all T values, i.e. a smaller and larger amplification for the no valley case for AS_{ah} and AS_{av}, respectively. Finally, **Figure 5.9** presents the spatial variability of aggravation factors for the no valley model for different structural periods (including the T=0s of **Figure 5.7**). As implied by **Figure 5.8**, the horizontal aggravation at the outcrops is similar for T=0, 0.2 and 0.4s and smaller for T=1s. In comparison to **Figure 5.3**, one may observe than in front of the toe, |X/B| < 0.5, for T_e=0.25s the AS_{ah} all periods T seem to maximize at the valley center, while for T_e=0.1s this held true only for large periods. More importantly, if one compares these results, with the pertinent results for the case when the valley exists (see **Figure 4.14**), it is concluded, once more, that the aggravation within the valley boundaries is significantly smaller (for all periods T) in the case of no valley.

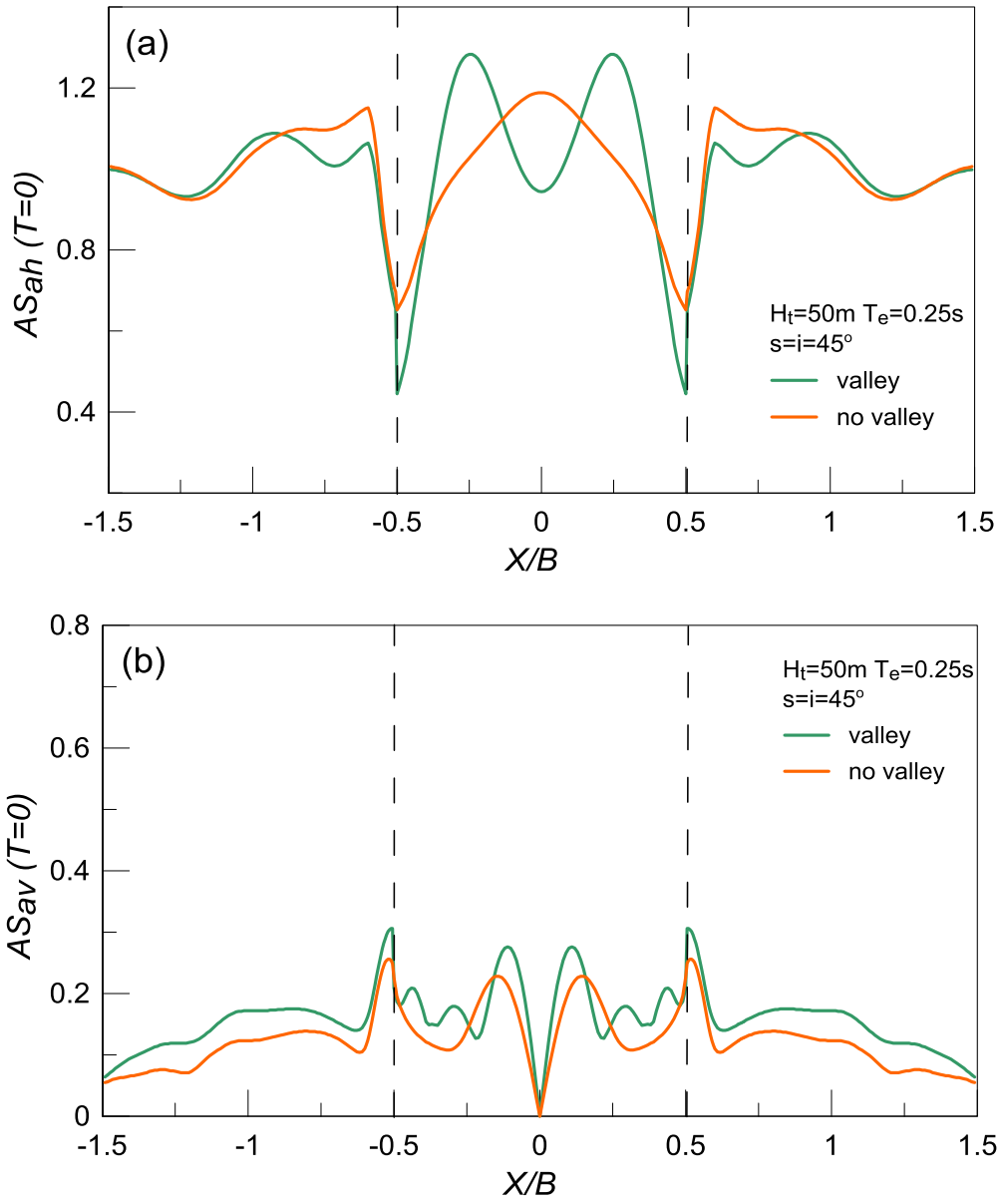

Figure 5.7: Effect of valley's existence on the spatial variability of geomorphic aggravation factors AS_{ah} and AS_{av} for T=0s with normalized distance from the center of the valley X/B; Results for H_t = 50m, s = i = 45° and T_e = 0.25s.

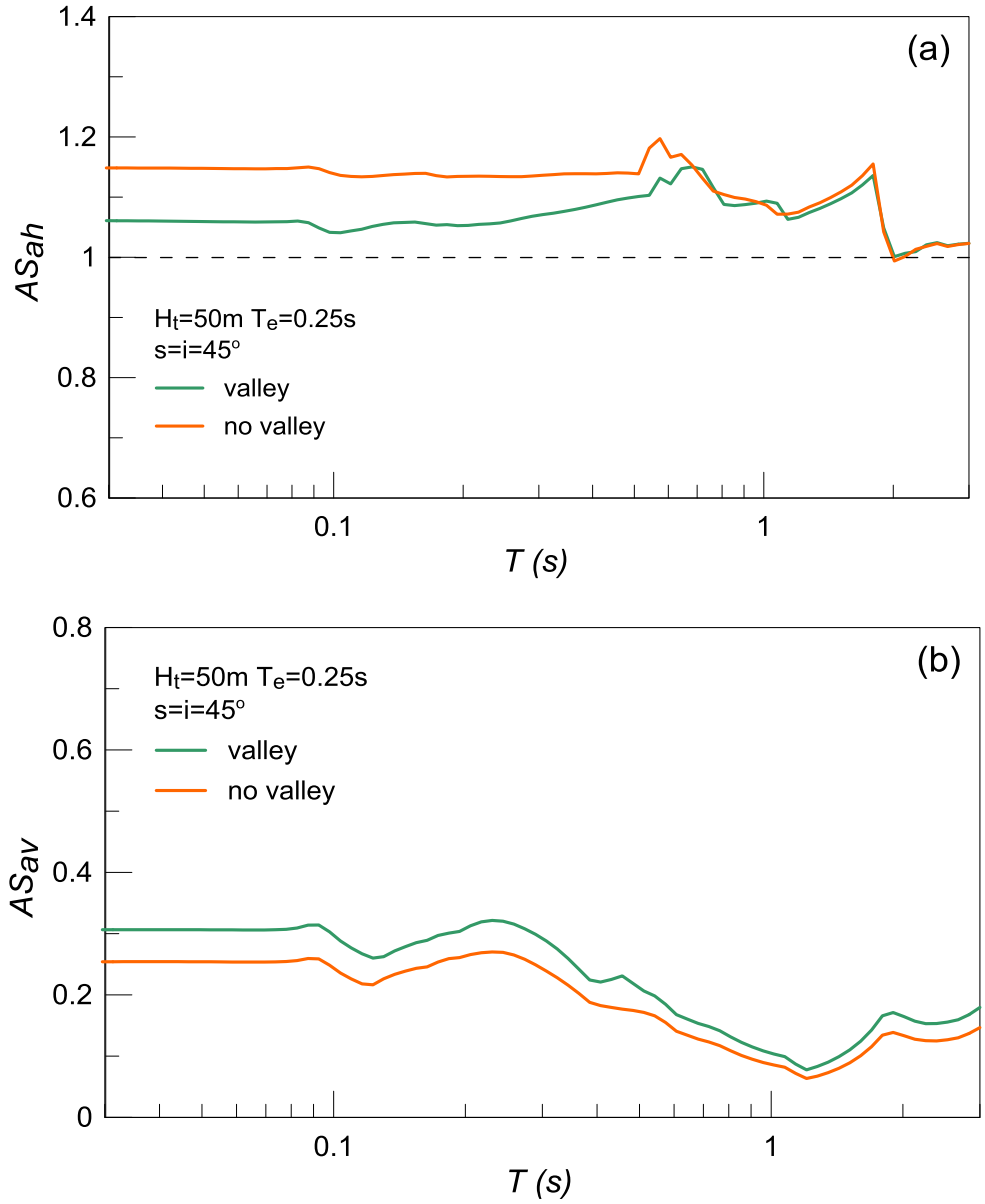

Figure 5.8: Effect of valley's existence on geomorphic aggravation spectra AS_{ah} and AS_{av} at the location of peak aggravation for T=0s along the outcropping bedrock; Results for H_t = 50m, s = i = 45^o and T_e = 0.25s.

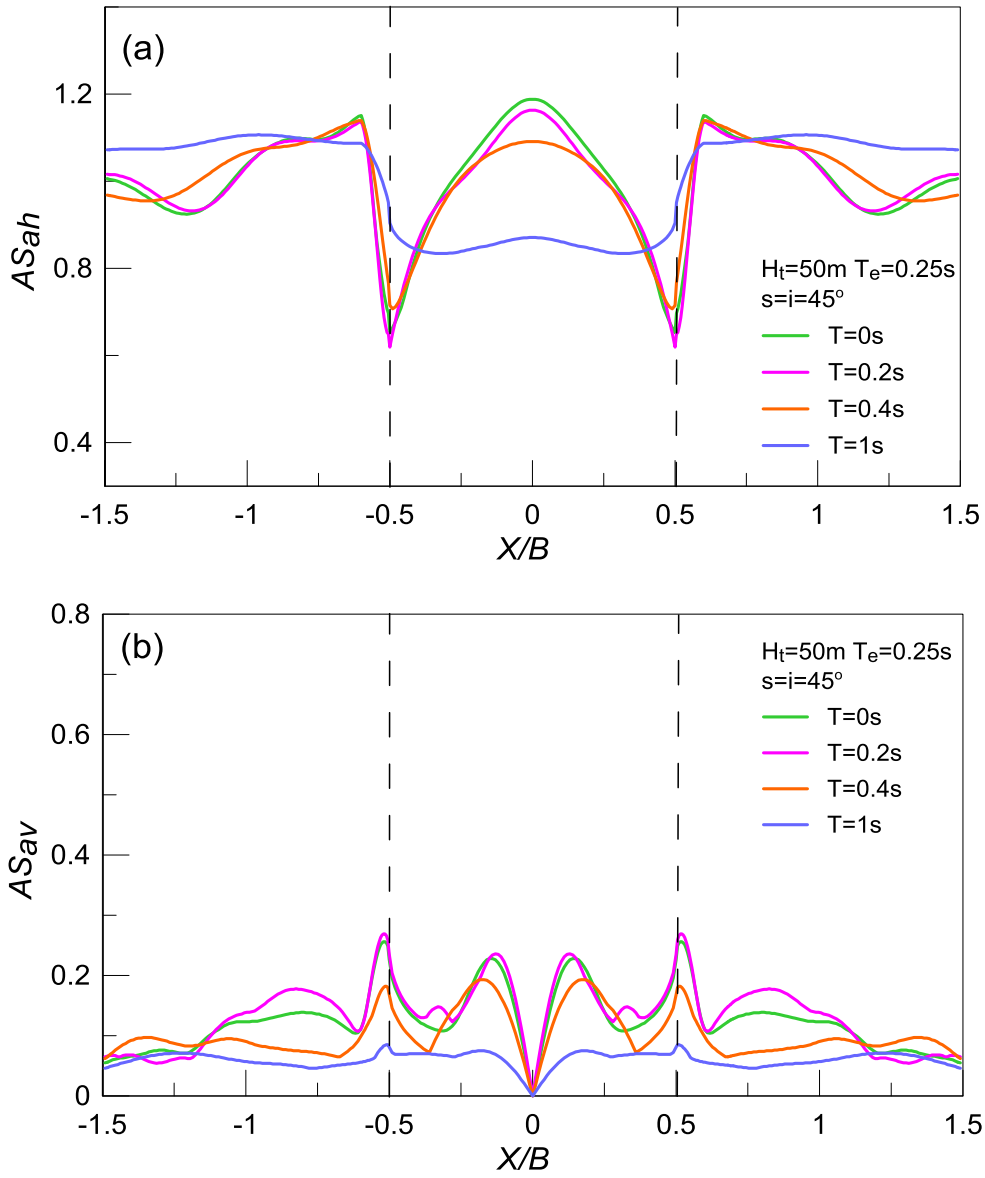

Figure 5.9: Spatial variability of gc aggravation factors AS_{ah} and AS_{av} for specific structural periods T with normalized distance from the center of the valley X/B; Results for outcropping bedrock height H_t = 50m, i = 45°, impedance ratio a = 1.0 (no valley) and T_e = 0.25s.

In the following, **Figures 5.10 to 5.12** present the aggravation results for the same intermediate-frequency excitation with T_e=0.25s, but for higher outcropping bedrock height H_t=100m. The results are presented in the same format as **Figures 5.7 to 5.9**, respectively, and are directly comparable to them. As implied by **Figure 5.10**, the differentiation between the valley and no valley case is not as systematic as that in **Figure 5.7**, which corresponds to a height H_t=50m. Specifically, the valley imposes a slight de-amplification of $AS_{ah}(T=0)$ at $|X/B|=0.75$ and a slight amplification of $AS_{av}(T=0)$ for $|X/B|>0.75$. Unlike **Figure 5.7**, the peak aggravation values in both directions remain practically unaffected by the valley's existence. Within the valley boundaries, the differences in the horizontal aggravation for the 2 cases are identical with **Figure 5.7**. In other words, the $AS_{ah}(T=0)$ within the valley boundaries is independent from the outcropping bedrock height H_t. On the contrary, the results for the vertical aggravation are strongly affected by the height H_t. Namely, for H_t=100m the $AS_{av}(T=0)$ is significantly smaller for the no valley case ($maxAS_{av}(T=0)$=0.15 for the no valley model over $maxAS_{av}(T=0)$=0.4 for the valley model). However, for H_t=50m, the $maxAS_{av}(T=0)$=0.2 and 0.25 for the no valley and the valley cases. **Figure 5.11** compares the aggravation spectra for the valley and no valley cases at the locations where the $maxAS_{ah}(T=0)$ and $maxAS_{av}(T=0)$ are observed at the outcropping bedrock. The aggravation spectra are almost identical for the two cases. Yet, observe that the de-amplification caused by the valley in the horizontal direction is more intense for periods T = 0.6 to 1s. Furthermore, it is important to mention that the corresponding results for H_t=50m in **Figure 5.8** showed that the differences between the two cases are noticeable for small periods. Finally, **Figure 5.12** presents the spatial variability of aggravation factors for the no valley case for different structural periods (including the T=0s of **Figure 5.10**). For the horizontal component, the results at the outcropping bedrock are similar for T=0, 0.2 and 0.4s, but significant values appear for T=1s. For the vertical component the aggravation decreases for larger periods. As expected, if one compares these results, with the pertinent results for the case where the valley exists (see **Figure 4.15**), it is concluded, once more, that the aggravation within the valley boundaries is significantly smaller (for all periods T) in the case of no valley.

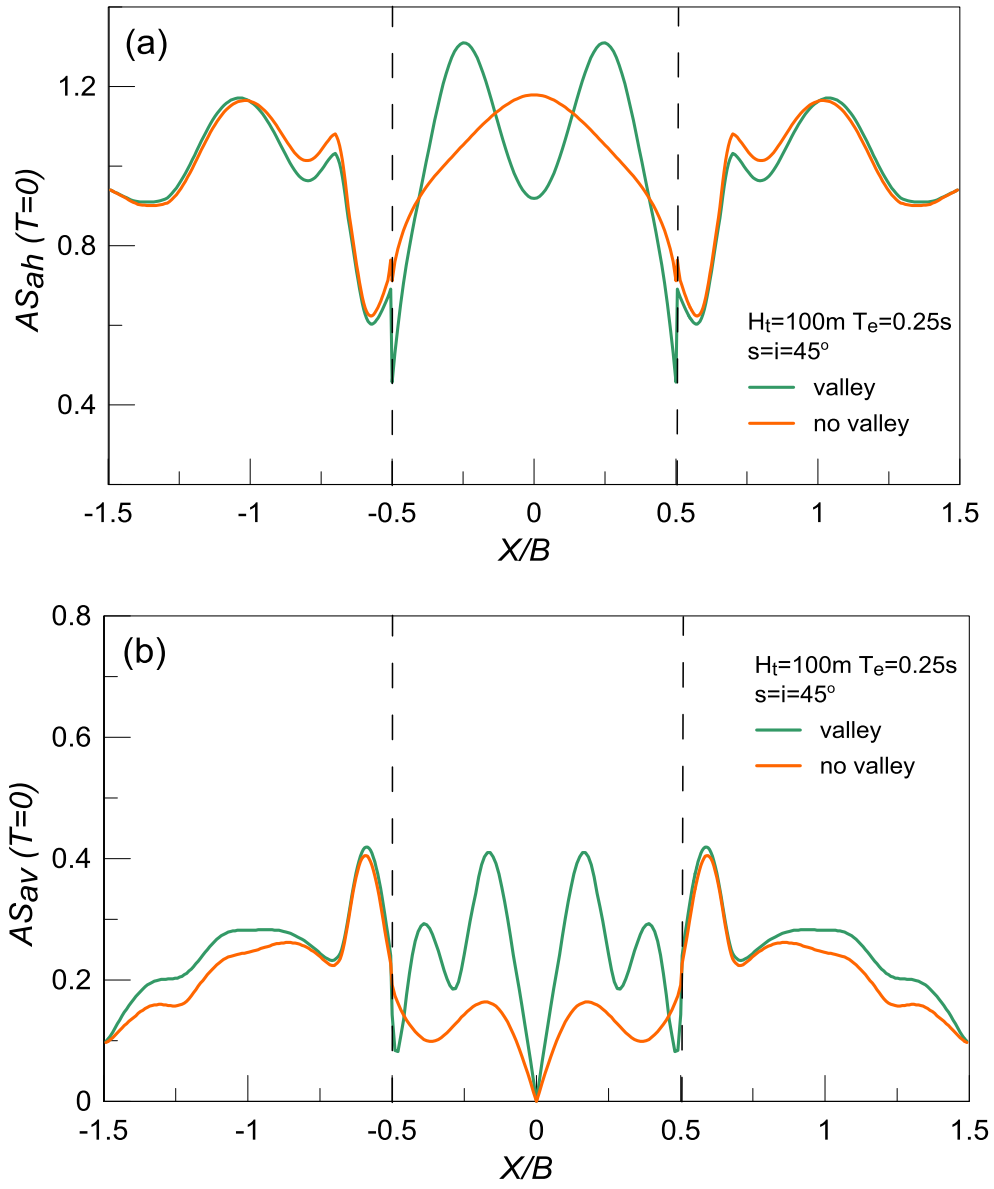

Figure 5.10: Effect of valley's existence on the spatial variability of geomorphic aggravation factors AS_{ah} and AS_{av} for T=0s with normalized distance from the center of the valley X/B; Results for H_t = 100m, s = i = 45° and T_e = 0.25s.

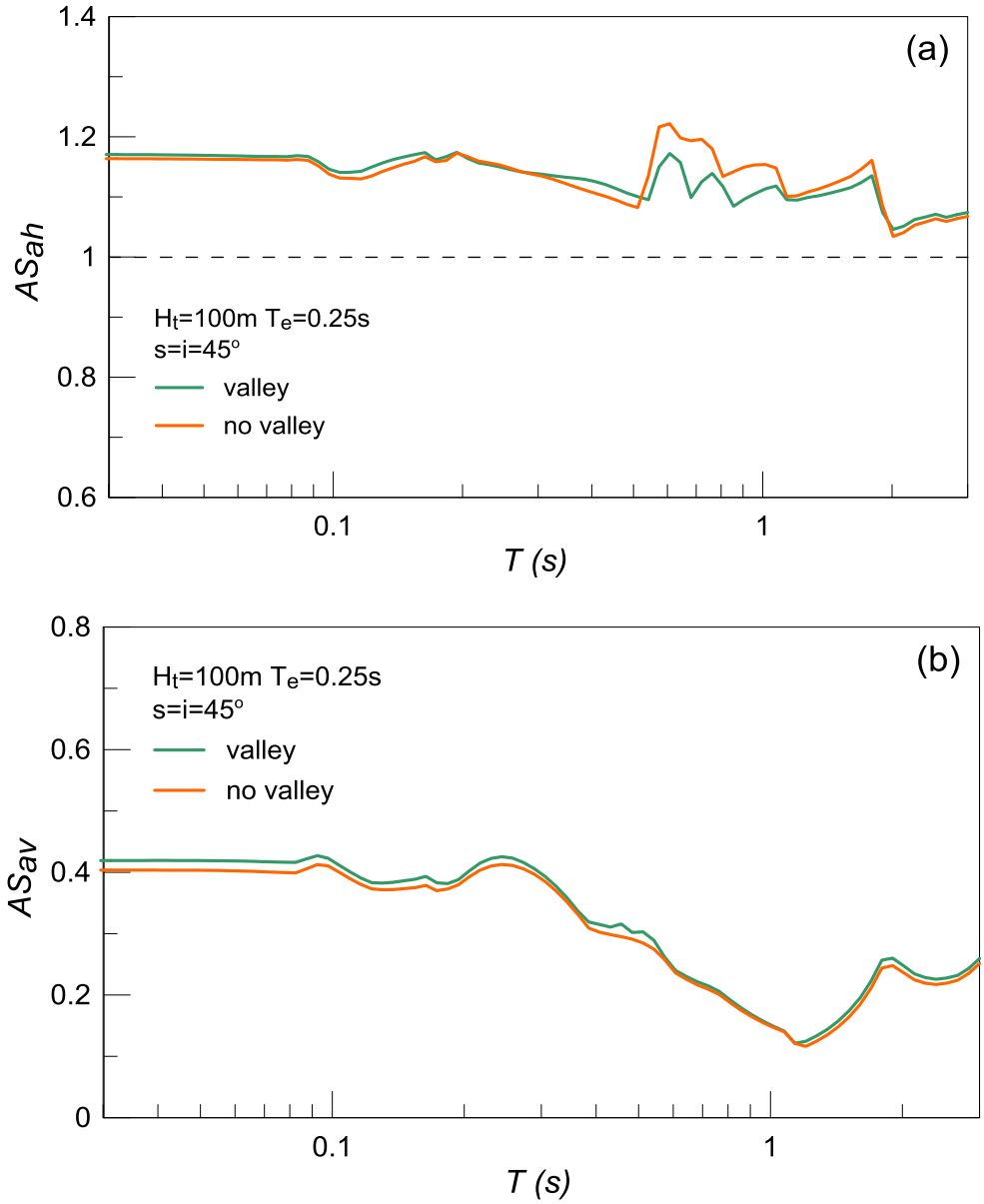

Figure 5.11: Effect of valley's existence on geomorphic aggravation spectra AS_{ah} and AS_{av} at the location of peak aggravation for T=0s along the outcropping bedrock; Results for H_t = 100m, s = i = 45° and T_e = 0.25s.

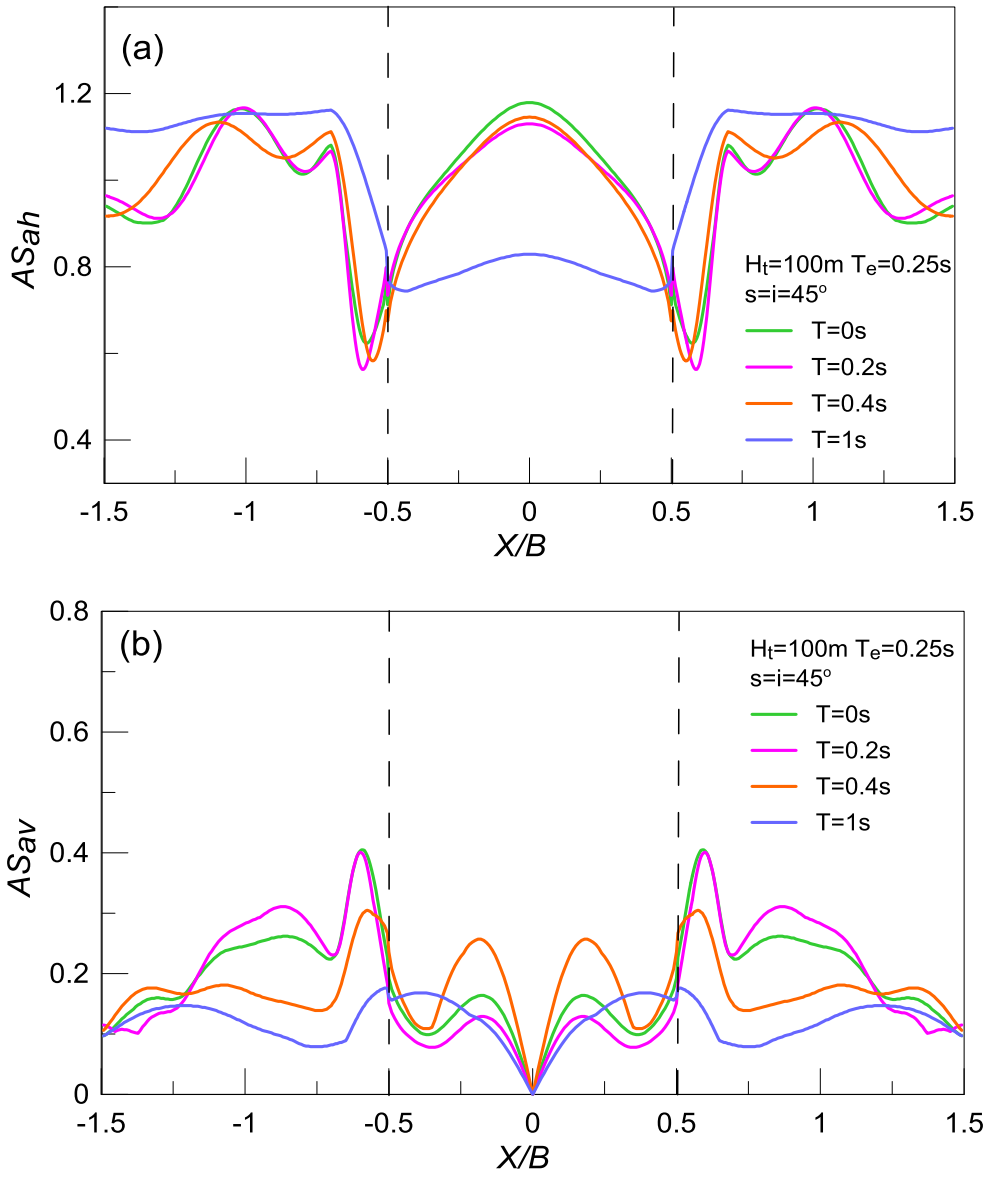

Figure 5.12: Spatial variability of aggravation factors AS_{ah} and AS_{av} for specific structural periods T with normalized distance from the center of the valley X/B; Results for outcropping bedrock height H_t = 100m, i = 45°, impedance ratio a = 1.0 (no valley) and T_e = 0.25s.

The effects of valley's existence under a low-frequency excitation T_e = 0.4s and for outcropping bedrock height H_t=50m are demonstrated in **Figures 5.13 to 5.15**. Once again, the existence of the valley decreases the $AS_{ah}(T=0)$ at the outcrops and increases the $AS_{av}(T=0)$ at large distances from the valley, similarly to what appeared for the high and the intermediate frequency excitations (**Figures 5.1 and 5.7**, respectively). Nevertheless, the valley effect is more significant for the low-frequency motion, especially for the horizontal direction, as illustrated in **Figure 5.13**. In detail, for the valley case, $maxAS_{ah}(T=0)$=1.1 and $maxAS_{av}(T=0)$=0.2 appear, while for the no valley case the respective values are 1.2 and 0.15, respectively. In both directions, only the amplitude of the peak values is affected by the valley. In all cases, the maximum aggravation values appear at the vicinity of the valley boundaries. At the same time, the differences in $AS_{ah}(T=0)$ between the two models within the valley boundaries are reduced, compared to the previous results. An unexpected result is a slight amplification of $AS_{av}(T=0)$ within the valley boundaries for the no valley model, since in all other cases the aggravation is larger for the valley model. Focusing on the locations where the $maxAS_{ah}(T=0)$ and $maxAS_{av}(T=0)$ are observed at the outcropping bedrock, **Figure 5.14** compares their aggravation spectra for the valley and no valley cases. Observe that whatever happens for T=0s, appears for all T values, but definitely the effect of the valley's existence does not diminish for large T values. **Figure 5.15** presents the spatial variability of aggravation factors for the no valley case and different structural periods (including the T=0s of **Figure 5.13**). Similarly to what occurs for T_e = 0.25s in **Figure 5.9**, this figure shows that the AS_{ah} at the outcrops is almost the same for T=0, 0.2 and 0.4s, but lower for T=1s. At the same time, the peak value of AS_{av} at the outcrops appears for T=0.4s, while in **Figure 5.9** the $maxAS_{av}$ appeared for T=0.2s. If one compares these results, with the pertinent results for the valley case (see **Figure 4.9**), it is concluded that the horizontal aggravation within the valley boundaries is smaller (for all periods T) in the case of no valley. However, this is not the case in the vertical direction, where the aggravation is slightly larger for the no valley case.

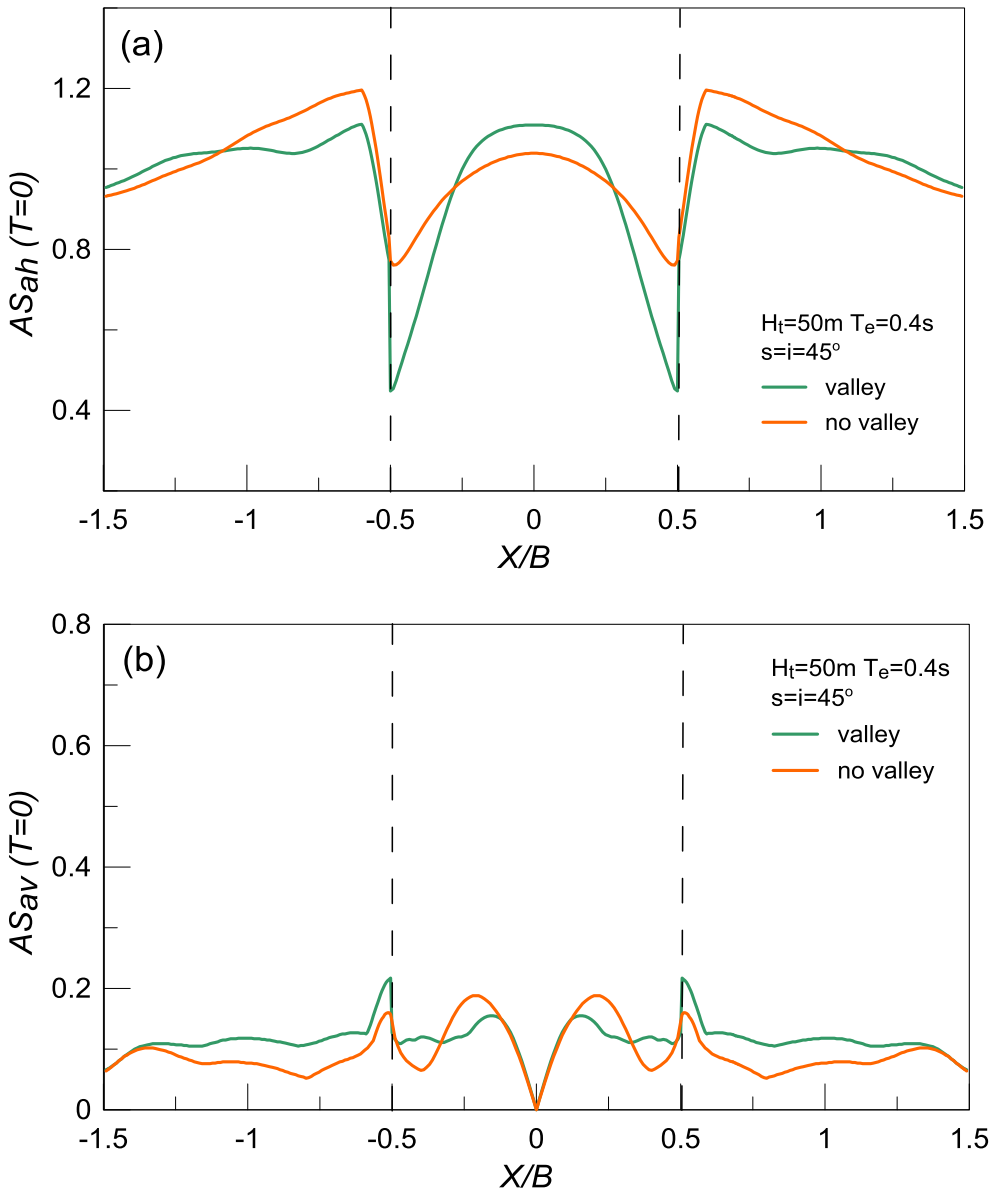

Figure 5.13: Effect of valley's existence on the spatial variability of geomorphic aggravation factors AS_{ah} and AS_{av} for T=0s with normalized distance from the center of the valley X/B; Results for H_t = 50m, s = i = 45° and a low-frequency excitation with T_e = 0.4s.

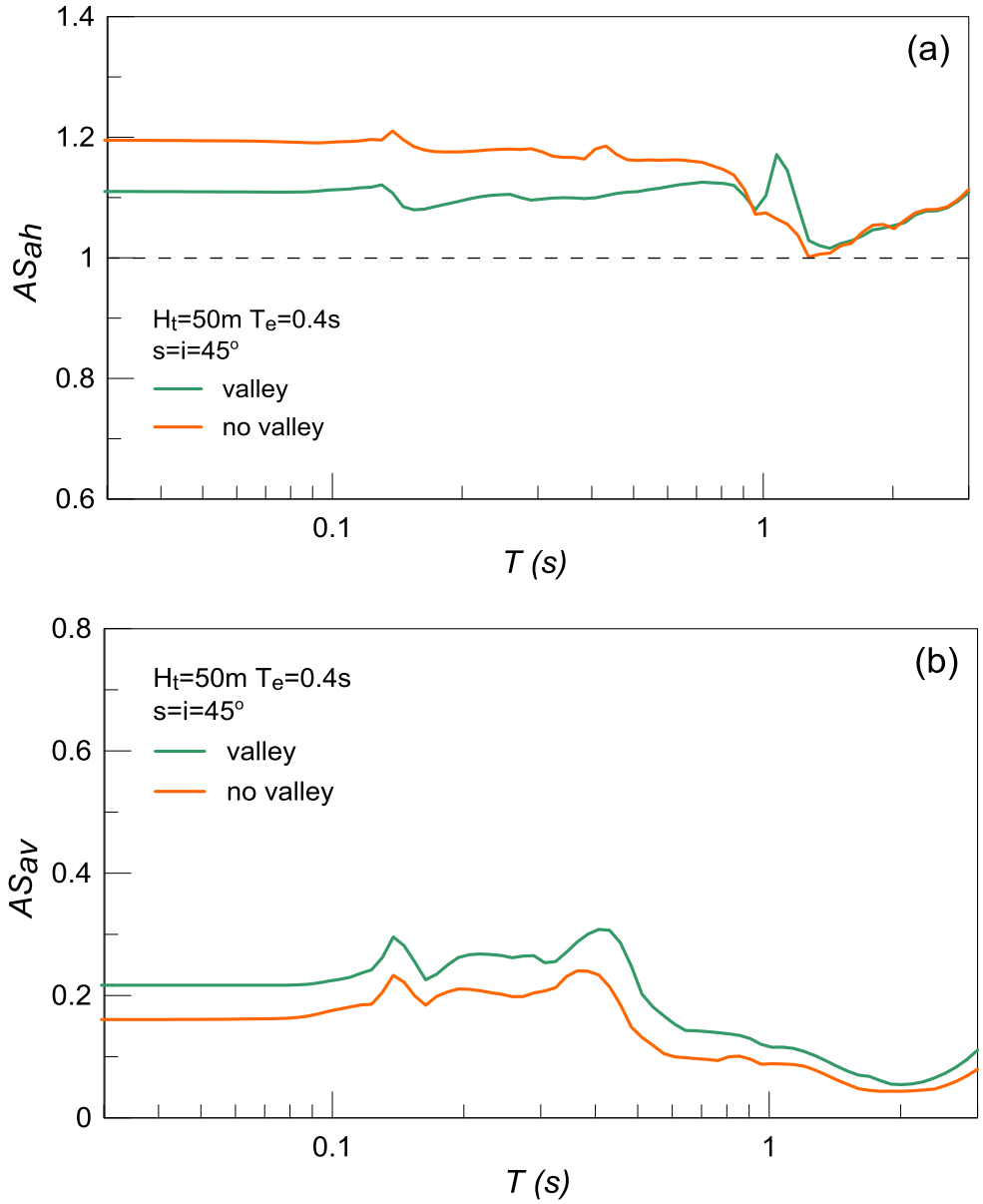

Figure 5.14: Effect of valley's existence on geomorphic aggravation spectra AS_{ah} and AS_{av} at the location of peak aggravation for T=0s along the outcropping bedrock; Results for H_t = 50m, s = i = 45° and a low-frequency excitation with T_e = 0.4s.

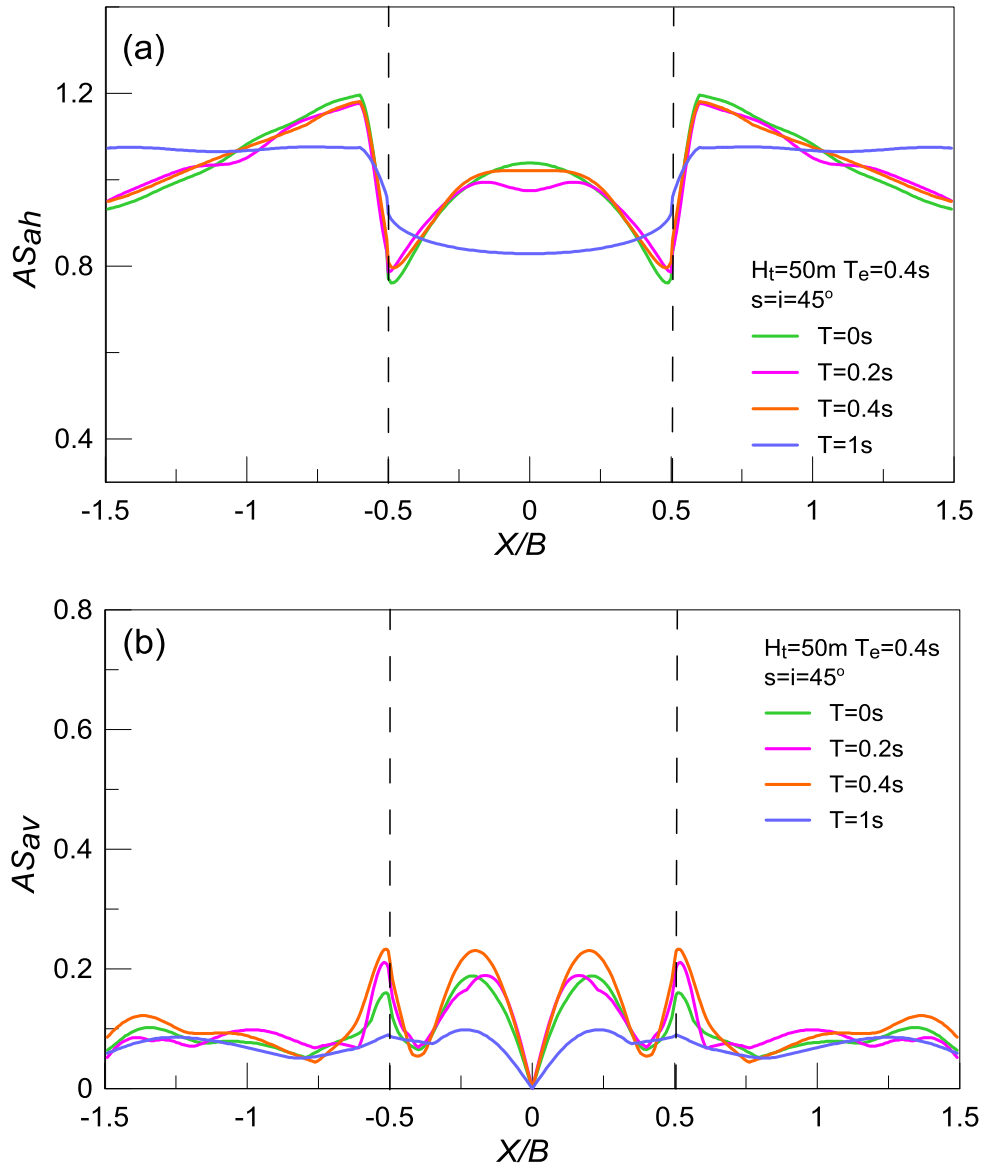

Figure 5.15: Spatial variability of aggravation factors AS_{ah} and AS_{av} for specific structural periods T with normalized distance from the center of the valley X/B; Results for outcropping bedrock height H_t = 50m, i = 45°, impedance ratio a = 1.0 (no valley) and a low-frequency excitation with T_e = 0.4s.

In the same line of thought, the results for the same excitation but for higher outcropping bedrock height H_t=100m are presented in **Figures 5.16 to 5.18**. The results are presented in the same format as **Figures 5.13 to 5.15**, respectively, and are directly comparable to them. As shown in **Figure 5.16**, the valley imposes a de-amplification of $AS_{ah}(T=0)$ and an amplification of $AS_{av}(T=0)$ at the outcropping bedrock, as observed for the case with H_t=50m in **Figure 5.13** as well. Comparing these results with the previous cases with the same height H_t but different excitation periods, it is concluded that the valley has a stronger effect on the outcropping bedrock response for a low-frequency excitation. Moreover, note that within the valley boundaries the results are almost identical for the valley and no valley cases. Both horizontal and vertical aggravation are slightly lower for the no valley case. Remember that the pertinent results for H_t=50m in **Figure 5.13** showed a slight increase of $AS_{av}(T=0)$ within the valley boundaries for the no valley case. Focusing on the locations where the $maxAS_{ah}(T=0)$ and $maxAS_{av}(T=0)$ are observed at the outcropping bedrock, **Figure 5.17** compares their aggravation spectra for the valley and no valley cases. Once again, whatever happens for T=0s appears for all T values, as was also shown in **Figure 5.14** for H_t=50m. In addition, the shape of the aggravation spectrum is not affected by the existence of the valley, while the important differences are observed for periods smaller than 1s. **Figure 5.18** presents the spatial variability of aggravation factors for the no valley case for different structural periods (including the T=0s of **Figure 5.16**). The horizontal aggravation at the outcrops is similar for all the examined periods, while the peak vertical aggravation appears for T=0.4s, within and outside of the valley boundaries. If one compares these results, with the pertinent results for the case where the valley exists (see **Figure 4.10**), it is concluded that the horizontal aggravation within the valley boundaries is smaller (for all periods T) in the no valley case, but the differences are insignificant compared to **Figures 5.6 and 5.12** for T_e=0.1 and 0.25s, respectively. Especially for the vertical aggravation, the differences within the valley boundaries are negligible.

To sum up, the analyses for steep valleys (s=45^o) with steep outcrops (i=45^o) showed that the valley effects on the seismic response of the outcropping bedrock become more intense with increasing excitation period T_e. In other words, the differences between the valley and the no valley cases are more significant for a low-frequency excitation with T_e=0.4s. The comparison between analyses with the same T_e and different H_t verify this statement. From all the above-mentioned analyses, it can be conducted that the valley imposes a de-amplification of $AS_{ah}(T=0)$ and an amplification of $AS_{av}(T=0)$ at the outcropping bedrock, for all excitation periods T_e and outcropping bedrock heights H_t. These effects appear for all T values, but seem to diminish for periods T > 1s. As expected, the aggravation within the valley boundaries is significantly higher in the case of valley, with this increased aggravation diminishing with the predominant period T_e of the excitation. As a result, as the predominant period T_e increases, the effects become more significant at the outcrops than within the valley boundaries.

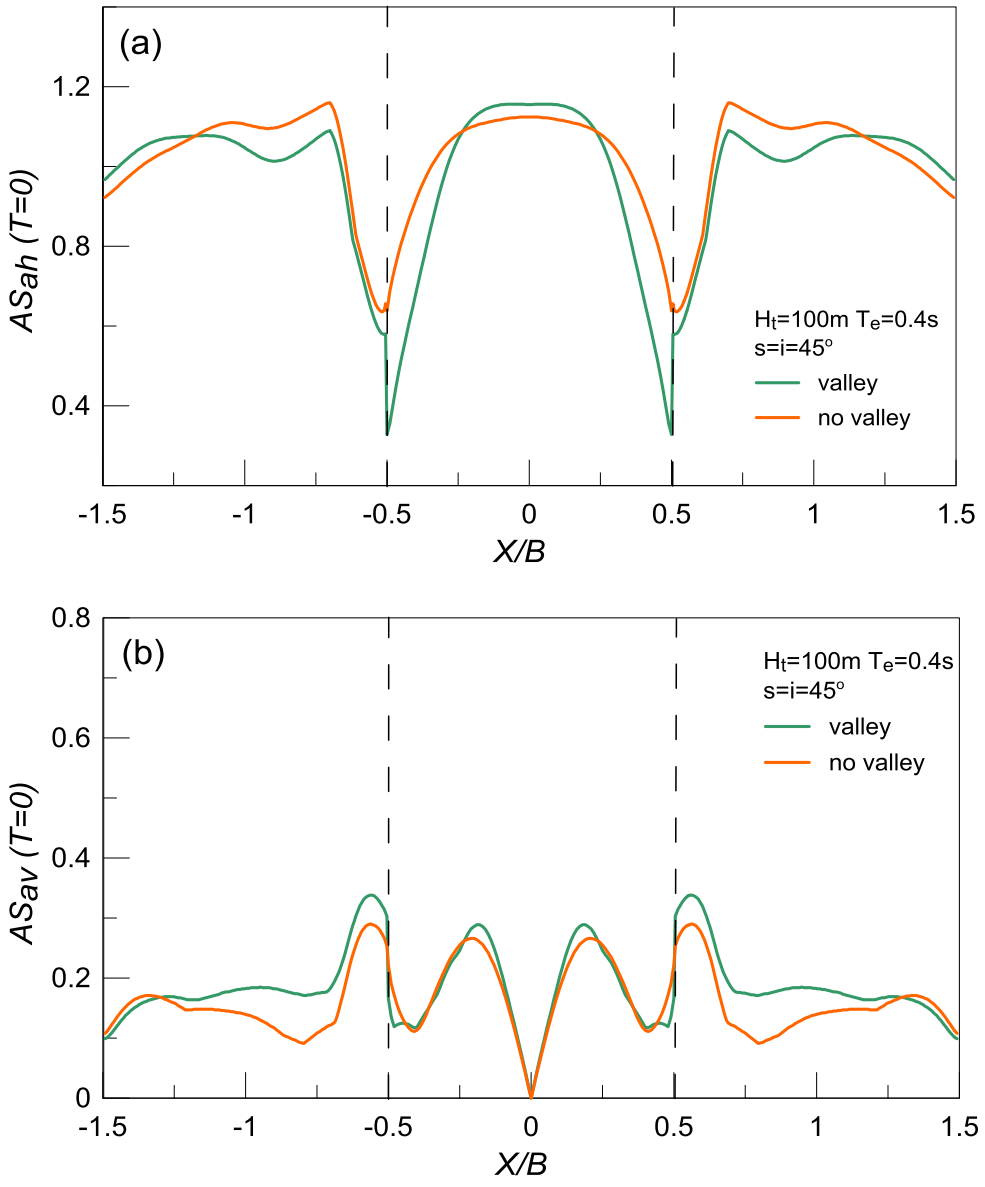

Figure 5.16: Effect of valley's existence on the spatial variability of geomorphic aggravation factors AS_{ah} and AS_{av} for T=0s with normalized distance from the center of the valley X/B; Results for H_t = 100m, s = i = 45° and a low-frequency excitation with T_e = 0.4s.

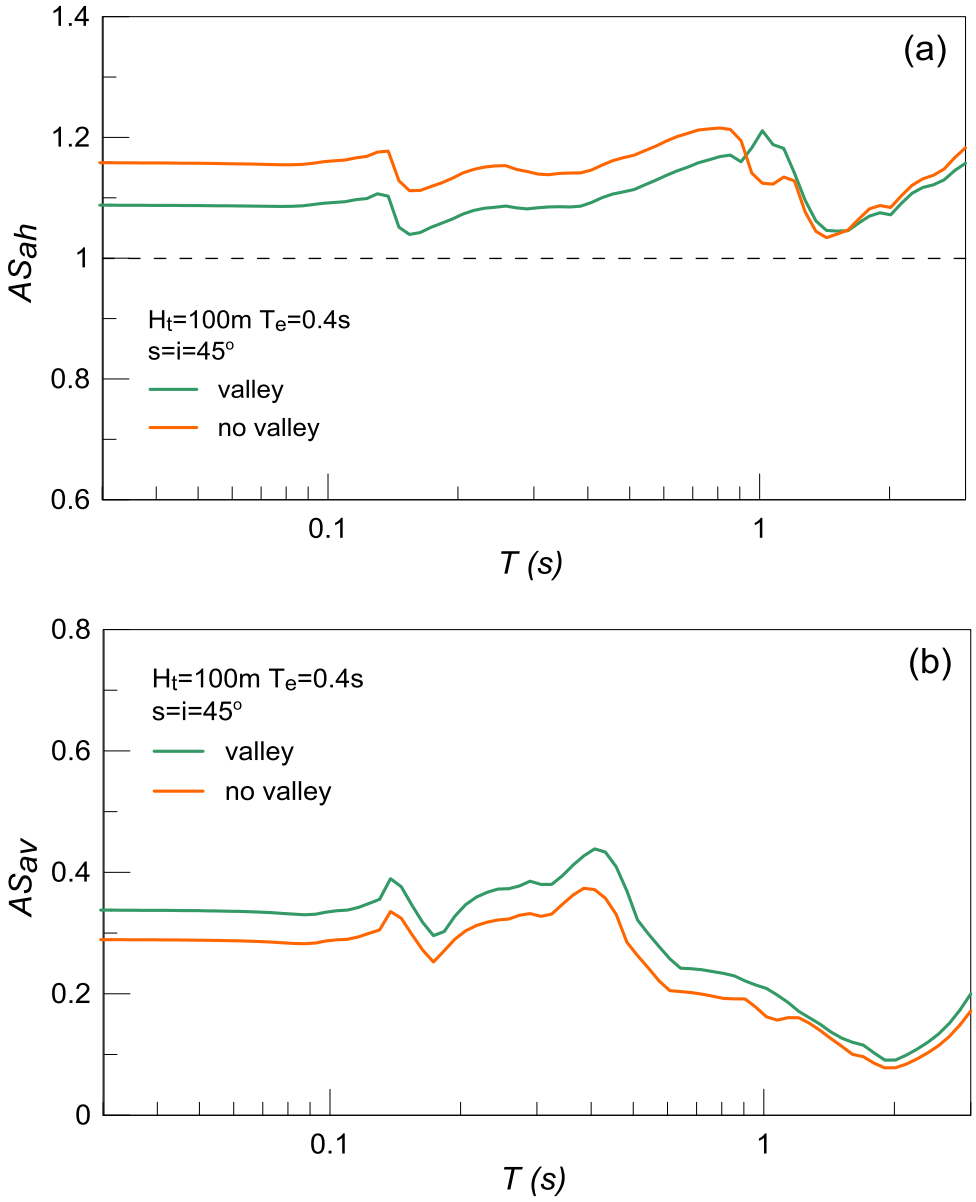

Figure 5.17: Effect of valley's existence on geomorphic aggravation spectra AS_{ah} and AS_{av} at the location of peak aggravation for T=0s along the outcropping bedrock; Results for H_t = 100m, s = i = 45° and a low-frequency excitation with T_e = 0.4s.

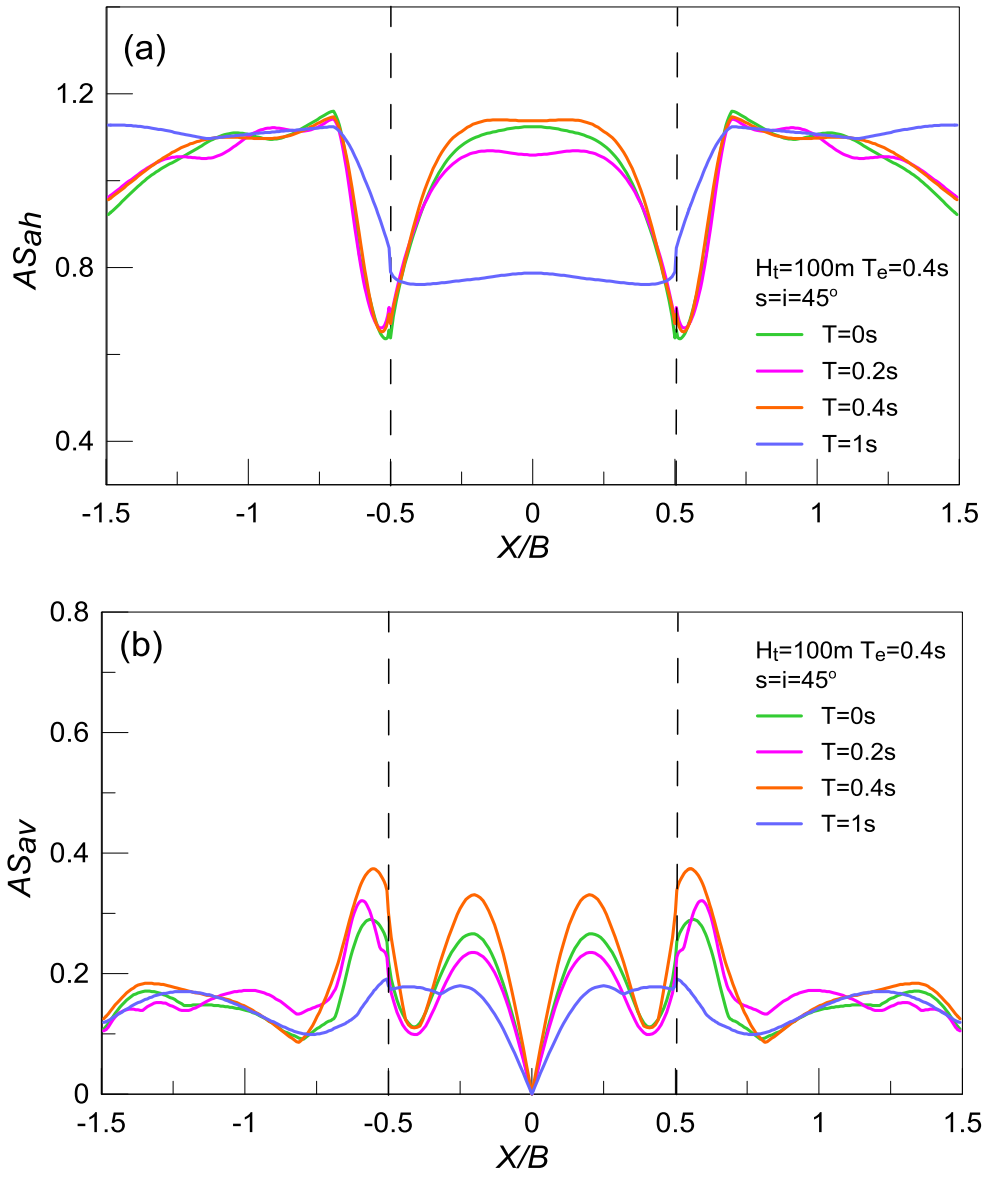

Figure 5.18: Spatial variability of aggravation factors AS_{ah} and AS_{av} for specific structural periods T with normalized distance from the center of the valley X/B; Results for outcropping bedrock height H_t = 100m, i = 45°, impedance ratio a = 1.0 (no valley) and a low-frequency excitation with T_e = 0.4s.

5.3 Effects for mild valleys s = 22.5^o with mild outcrops i = 22.5^o

In this paragraph, when alluvial valleys exist, they have the same mild inclination angle s = 22.5^o as the inclination angle i = 22.5^o of the outcropping bedrock. In the pertinent figures, their curves appear denoted by "valley". The outcropping bedrock height is set equal to H_t=50m in all the examined cases of this paragraph. The corresponding homogeneous canyons have the same height H_t and the same outcropping bedrock inclination angle i, and in the figures their results are denoted by "no valley". What varies in the analyses in this paragraph is the predominant excitation period, that takes the values T_e = 0.1s (high-frequency) and 0.4s (low-frequency).

The effects of a (mildly inclined) valley's existence under a high-frequency excitation T_e = 0.1s are presented in **Figures 5.19 to 5.21**. As shown in **Figure 5.19**, the valley imposes minor effects on the seismic response of the outcropping bedrock. Observe that the valley causes a very slight amplification of AS_{ah}(T=0) only at $|X/B|$= 0.75 at the outcropping bedrock. Remember that in paragraph 5.2, it was stressed out that for steep valleys with steep outcrops (s=i=45^o) the valley always de-amplifies the AS_{ah}(T=0). In addition, the valley amplifies the AS_{av}(T=0) for $|X/B| > 0.75$, but imposes a slight de-amplification close to the boundaries of the valley. Within the valley boundaries the aggravation remains higher for the valley case, especially in the vertical direction. If one compares these results with the pertinent results for steep valleys with steep outcrops (see **Figure 5.1**), it is obvious that the differences between the valley and the no valley case are smaller for mild valleys with mild outcrops (s=i=22.5^o). **Figure 5.20** compares the aggravation spectra for the valley and no valley case at the locations where the maxAS_{ah}(T=0) and maxAS_{av}(T=0) are observed in the outcropping bedrock area. In both directions the aggravation is larger for T=0s and decreases for higher periods. Observe that the valley amplifies the AS_{ah} for periods smaller or equal to T=0.3s and de-amplifies it thereafter. Nevertheless, the overall differences between the two cases remain minor. **Figure 5.21** presents the spatial variability of aggravation factors for the no valley model for different structural periods (including the T=0s of **Figure 5.19**). Note that the peak values at the outcropping bedrock appear for T=0s and reduce thereafter for both AS_{ah} and AS_{av}. Furthermore, if one compares these results, with the pertinent results for the case where the valley exists (see **Figure 4.19**), it becomes obvious that the aggravation within the valley boundaries is significantly smaller here than when a valley exists for all periods T, as expected.

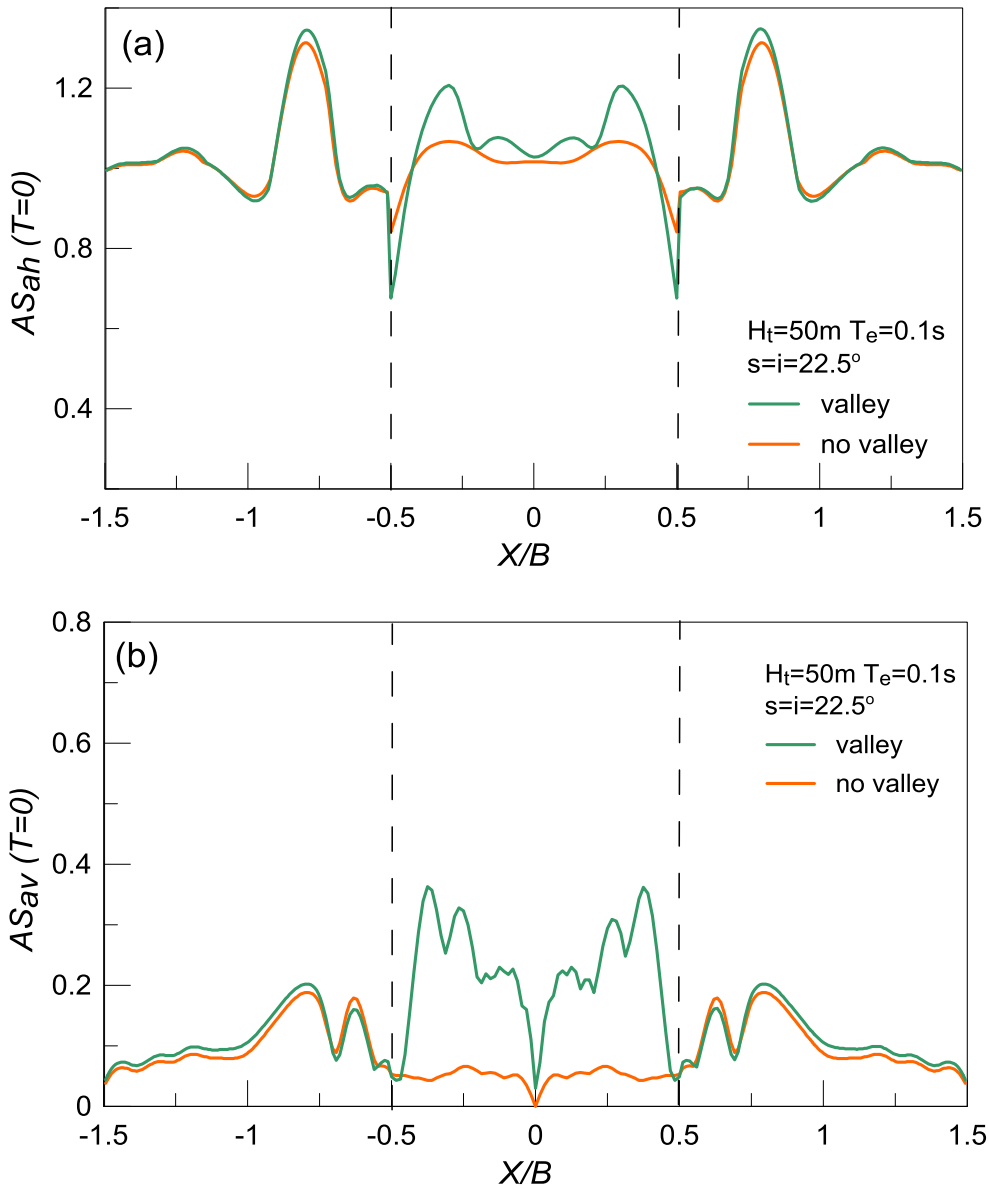

Figure 5.19: Effect of valley's existence on the spatial variability of geomorphic aggravation factors AS_{ah} and AS_{av} for T=0s with normalized distance from the center of the valley X/B; Results for H_t = 50m, s = i = 22.5° and a high-frequency excitation with T_e = 0.1s.

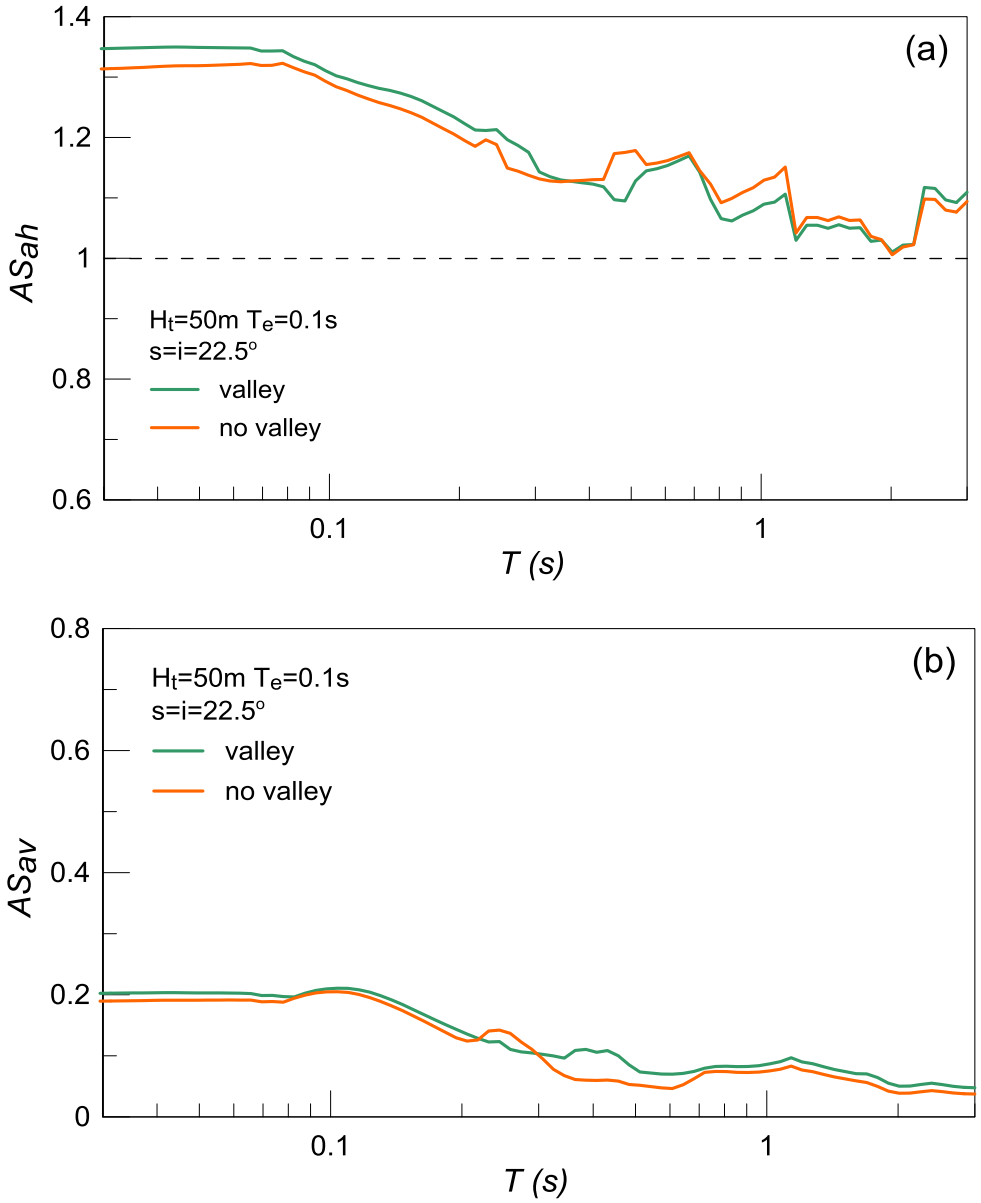

Figure 5.20: Effect of valley's existence on geomorphic aggravation spectra AS_{ah} and AS_{av} at the location of peak aggravation for T=0s along the outcropping bedrock; Results for H_t = 50m, s = i = 22.5° and a high-frequency excitation with T_e = 0.1s.

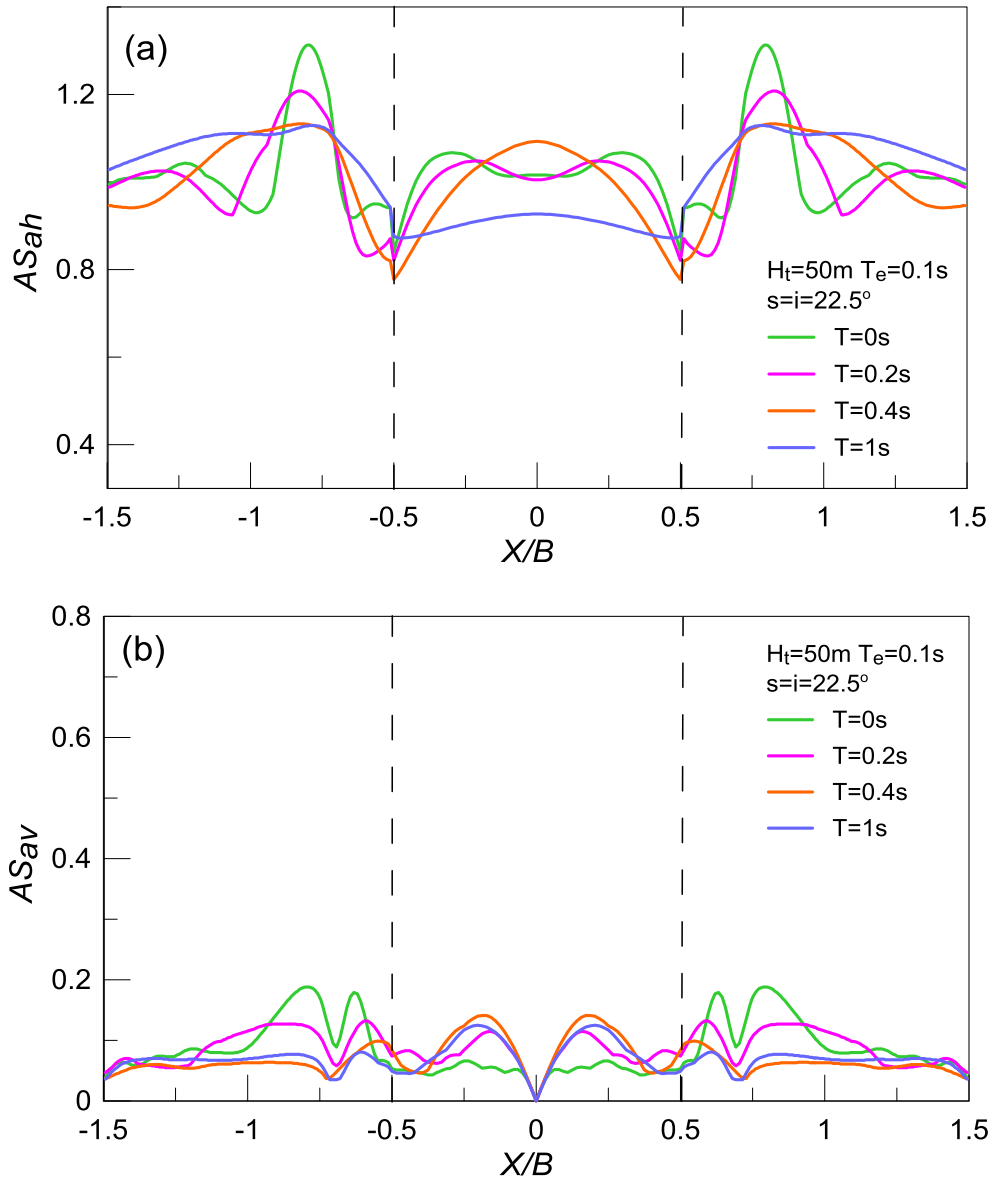

Figure 5.21: Spatial variability of aggravation factors AS_{ah} and AS_{av} for specific structural periods T with normalized distance from the center of the valley X/B; Results for outcropping bedrock height H_t = 50m, i = 22.5°, impedance ratio a = 1.0 (no valley) and a high-frequency excitation with T_e = 0.1s.

In the sequel, the effect of the (mildly inclined) valley's existence on the response of outcropping bedrock is investigated for a low-frequency excitation with T_e=0.4s, with the results demonstrated in **Figures 5.22 to 5.24**. As shown in **Figure 5.22**, the valley decreases $AS_{ah}(T=0)$ and increases $AS_{av}(T=0)$ at the outcropping bedrock crest. Similar effects were observed for the pertinent results for steep valleys with steep outcrops in **Figure 5.13**, but for s=i=22.5^o the differentiation in the response between valley and no valley cases is diminished. Moreover, for s=i=22.5^o the location of the peak horizontal aggravation is different for the 2 cases. Namely, for the valley case the $maxAS_{ah}(T=0)$ is located at $|X/B|$= 0.75, while for the no valley case the $maxAS_{ah}(T=0)$ is spotted at $|X/B|$= 1. At the same time, the valley effects remain more remarkable for the case of a low-frequency excitation (T_e=0.4s), compared to **Figure 5.19** for a high-frequency excitation (T_e=0.1s). Similarly to what is shown in **Figure 5.13**, the differences of the 2 cases within the valley boundaries are minor, especially in the vertical direction. **Figure 5.23** compares the aggravation spectra for the valley and no valley cases at the locations where the $maxAS_{ah}(T=0)$ and $maxAS_{av}(T=0)$ are observed in the outcropping bedrock area. The more remarkable differences between the two aggravation spectra are observed for periods T = 0.4 to 1s for AS_{ah} and for periods T ≤ 0.6s for AS_{av}. **Figure 5.24** presents the spatial variability of aggravation factors for the no valley case for different structural periods (including the T=0s of **Figure 5.22**). The AS_{ah} at the outcrops is similar for all the examined periods, except for T=1s, where the values are much lower. The peak AS_{av} value appears for T=0.4s, as happened in **Figure 5.15** for steep valleys with step outcrops as well. Furthermore, the comparison between the pertinent results for the case when the valley exists (see **Figure 4.23**) shows that within the valley boundaries the vertical aggravation is slightly smaller in the case of no valley. With respect to the horizontal aggravation, it seems to be similar for T=0, 0.2 and 0.4s for the no valley case. Thus, in comparison with **Figure 4.23**, it is observed that AS_{ah} is larger for the valley case, with more remarkable differences appearing for T=0.4 and 1s.

In general, the analyses showed that the valley effects on the outcropping bedrock response are less important for mild valleys with mild outcrops (s=i=22.5^o), compared to the analyses with s=i=45^o. However, the main conclusions from paragraph 5.2 are valid in this paragraph, too. In other words, the valley effects are qualitatively the same for mild and steep inclination angles s and i. Hence, from all the above-mentioned analyses in this Chapter, it can be concluded that the most important parameter for the valley effects is the excitation predominant period T_e. Namely, as the excitation period increases, the effects on the outcropping bedrock become more significant. This is the opposite of what happens within the valley boundaries, where the differences between the valley and no valley cases become more important as the excitation period decreases. Generally, the valley de-amplifies AS_{ah} and amplifies AS_{av} at the outcropping bedrock, regardless of the outcropping bedrock height H_t and the inclination angles of the valley (s) and the outcrops (i). On the contrary, within the valley boundaries, the valley amplifies the aggravation values in the majority of the cases, especially for high-frequency excitations.

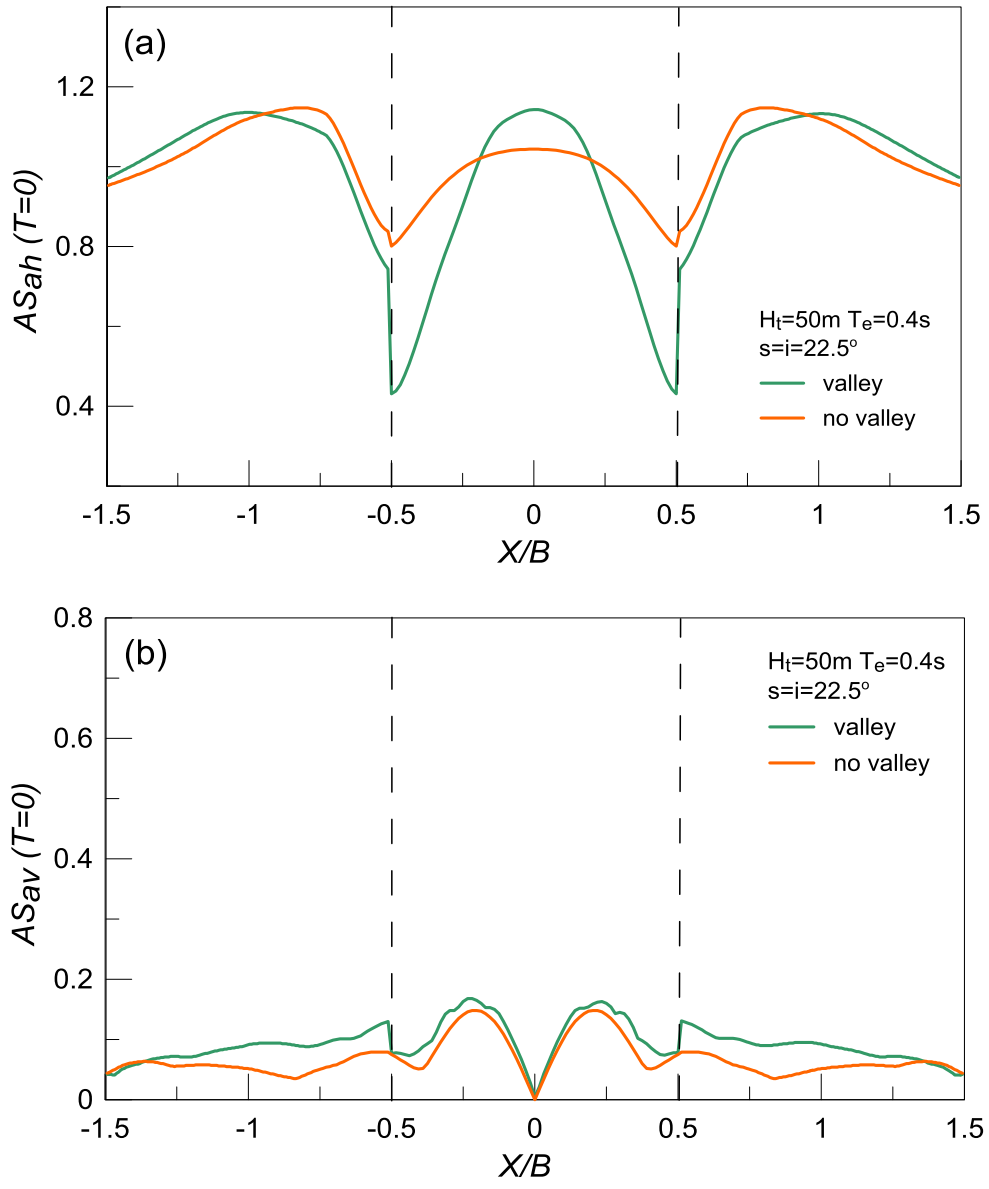

Figure 5.22: Effect of valley's existence on the spatial variability of geomorphic aggravation factors AS_{ah} and AS_{av} for T=0s with normalized distance from the center of the valley X/B; Results for H_t = 50m, s = i = 22.5° and a low-frequency excitation with T_e = 0.4s.

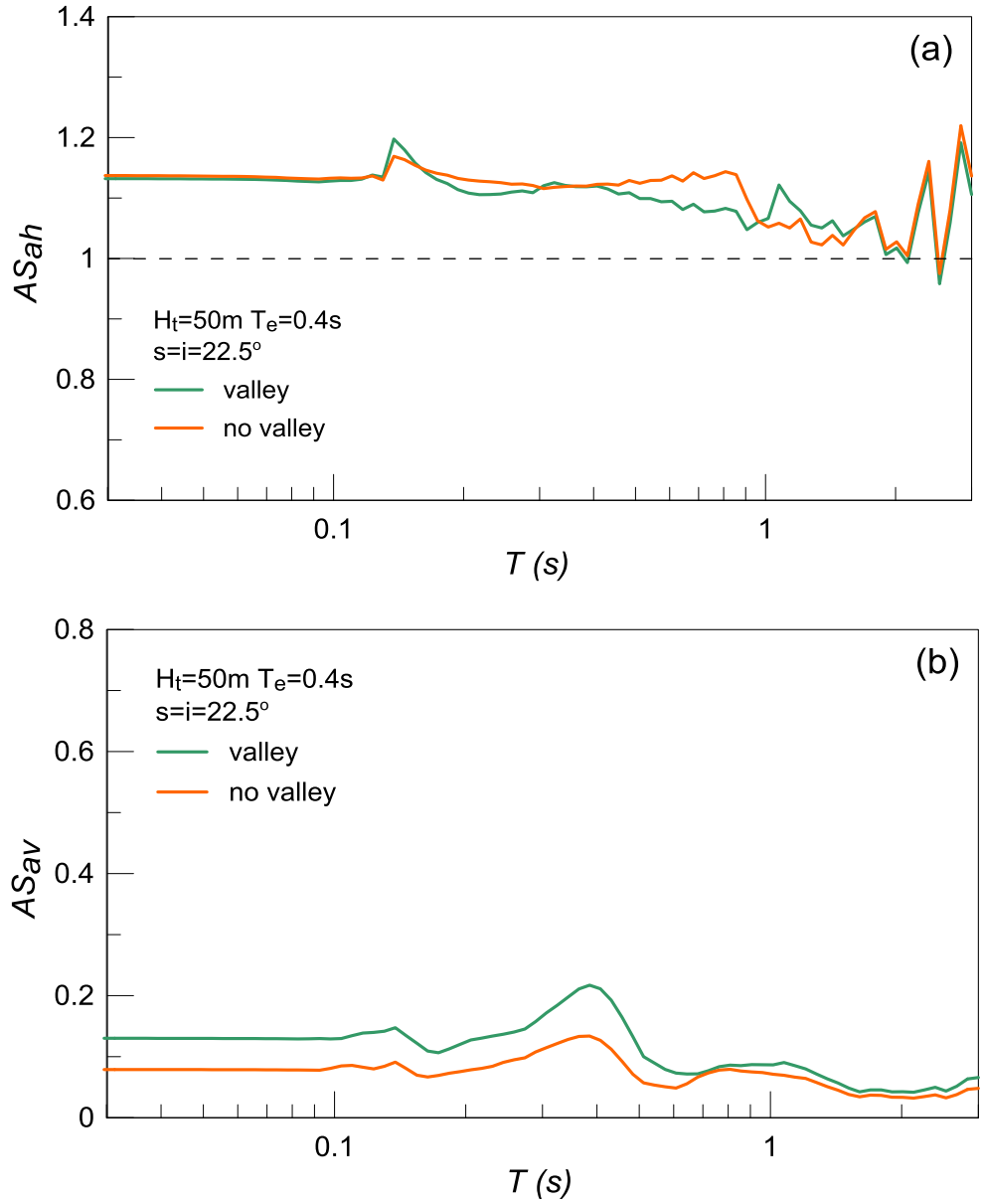

Figure 5.23: Effect of valley's existence on geomorphic aggravation spectra AS_{ah} and AS_{av} at the location of peak aggravation for T=0s along the outcropping bedrock; Results for H_t = 50m, s = i = 22.5° and a low-frequency excitation with T_e = 0.4s.

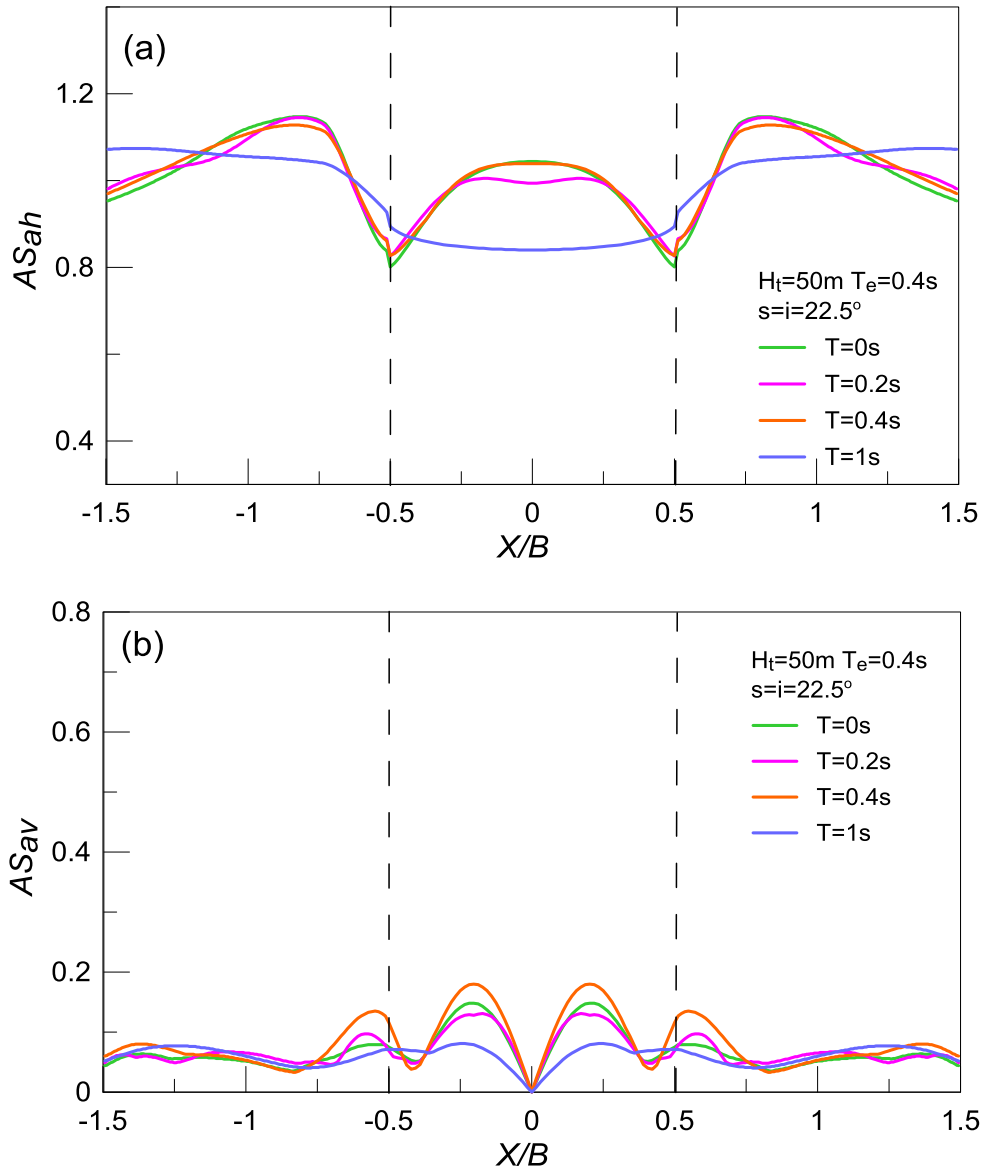

Figure 5.24: Spatial variability of aggravation factors AS_{ah} and AS_{av} for specific structural periods T with normalized distance from the center of the valley X/B; Results for outcropping bedrock height H_t = 50m, i = 22.5°, impedance ratio a = 1.0 (no valley) and a low-frequency excitation with T_e = 0.4s.

5.4 Quantification of valley effects on outcropping bedrock response

As pointed out in paragraph 2.3, topography effects on seismic ground motion have been widely investigated over the last few decades. Based on this literature, some seismic codes (e.g. EC8) suggest topographic factors (e.g. S_T = 1.2 – 1.4) applied in slopes, ridges and canyons with significant heights and inclination angles (e.g. H_t > 30m and i > 15^o). Yet, these factors have been proposed for homogeneous topographic relieves and it is uncertain whether they should be applied when a soft alluvial valley appears at their base. In such cases, the topographic factors should be multiplied by the appropriate correction factors, considering that the existence of the valley affects the outcropping bedrock response. In this paragraph, such correction factors are being determined for the peak ground acceleration, namely for T=0s, for both the horizontal component (CF_h) and the parasitic vertical component (CF_v).

Particularly, using the 8 sets of analyses presented in the previous paragraphs of this Chapter, the correction factors are determined in both directions as follows: The horizontal correction factor $CF_h(T=0)$ is defined at each location of the outcropping bedrock as the ratio of the horizontal geomorphic aggravation factor AS_{ah} for T=0s that corresponds to canyons with soft alluvial valleys at their base over the value of the horizontal geomorphic aggravation factor $AS_{ah}(T=0)$ that corresponds to homogeneous rock canyons with the same topography and under the same seismic excitation. In the same way, the vertical correction factor $CF_v(T=0)$ is defined at each location of the outcropping bedrock as the ratio of $AS_{av}(T=0)$ that corresponds to canyons with soft alluvial valleys at their base over the $AS_{av}(T=0)$ that corresponds to homogeneous rock canyons with the same topography under the same seismic excitation. Evidently, if the correction factor takes values above 1.0, the valley imposes increase of the topographic aggravation at the outcropping bedrock in comparison to its value if the canyon was homogeneous. Similarly, correction factors lower than 1.0 imply a relative decrease of the topographic aggravation in comparison to its value for the homogeneous canyon.

The scope of this paragraph is to quantify valley effects on topographic aggravation of the outcropping bedrock. Thus, the correction factors $CF_h(T=0)$ and $CF_v(T=0)$ are determined only at the outcrops and not within the valley boundaries. Since the studied canyon cases are symmetrical and the SV waves are vertically incident, the aggravation results (in terms of AS_{ah} and AS_{av}) are identical for both the left and right outcrops. This is clear in all the figures in the previous paragraphs. For this reason, the correction factors $CF_h(T=0)$ and $CF_v(T=0)$ are presented here only for one of the outcrops, namely the right outcrop. Note also that depending on the characteristics of the outcropping bedrock (height H_t, inclination angle i), the crest of the slope is not at the same location for each set of analyses. In order to compare and evaluate the correction factors for different canyon geometries, the outcropping bedrock crest must coincide in all the analyses as a reference point. For this purpose, Y is introduced as the horizontal distance from the outcropping bedrock crest, no matter its geometry. Hence, Y > 0 corresponds to flat bedrock areas behind the crest, while Y < 0 corresponds to inclined bedrock areas in front of the crest. In this way the results for different cases become directly comparable. In addition, in order to generalize the results, this distance Y is normalized over the height of the outcropping bedrock H_t.

Figures 5.25 and 5.26 present the spatial variability of correction factors $CF_h(T=0)$ and $CF_v(T=0)$ with normalized distance from the outcropping bedrock crest Y/H_t for the 8 cases investigated in this Chapter. Firstly, the results for steep outcrops ($i=45^o$) with height H_t=50m are demonstrated in **Figure 5.25**. The valley effects on topographic aggravation are determined for predominant excitation period T_e = 0.1s (high-frequency), 0.25s (intermediate-frequency) and 0.4s (low-frequency). The outcropping bedrock crest is located at $Y/H_t=0$, denoted with dashed vertical line. It is observed that $CF_h(T=0)$ becomes slightly lower than 1.0 in front of the crest, regardless of the excitation period T_e, while it becomes slightly higher than 1.0 at some distance behind the crest, this distance increasing with T_e. Overall, the value of $CF_h(T=0)$ is close to 1.0 (between 0.9 and 1.1) and hence of little practical importance. At the same time, $CF_v(T=0)$ is always greater than 1.0 in the whole bedrock area, meaning that the valley amplifies $AS_{av}(T=0)$. In general, the $CF_v(T=0)$ increases with increasing excitation period T_e, i.e. $maxCF_v(T=0)=1.3$ when T_e=0.1s, $maxCF_v(T=0)=1.7$ when T_e=0.25s and $maxCF_v(T=0)=2$ when T_e=0.4s. In the same line of thought, **Figure 5.26** presents the correction factors for steep outcrops ($i=45^o$), but with height H_t=100m. If one compares these results with the pertinent results for height H_t=50m (see **Figure 5.25**), it is observed that the results are qualitatively the same for both heights H_t. Quantitatively, the H_t does not seem to affect significantly the $CF_h(T=0)$ that remain close to 1.0, while an increase of H_t seems to decrease the values of $CF_v(T=0)$. This decrease brings the $CF_v(T=0)$ values for T_e=0.1s below 1.0.

The effects of a mildly inclined valley ($s=22.5^o$) with mild outcrops ($i=22.5^o$) and height H_t=50m on the correction factors is investigated in **Figure 5.27**. More specifically, for a high-frequency excitation with T_e=0.1s the $CF_h(T=0)$ is slightly greater than 1.0 in front and behind the crest. With respect to the vertical direction, $CF_v(T=0)$ is lower than 1.0 in front of the crest ($minCF_v(T=0)=0.8$), except from the toe of the slope, where $CF_v(T=0)=1.2$. Behind the crest $CF_v(T=0) > 1.0$ with $maxCF_v(T=0)=1.2$. These values come in contrast to what occurs for $s=i=45^o$ in **Figure 5.25**, where $CF_h(T=0) < 1.0$ and $CF_v(T=0) > 1.0$ in front of the crest. On the other hand, the results for a low-frequency excitation with T_e=0.4s are qualitatively similar for both steep and mild inclination angles s and i. However, the correction factors are increased in both directions for $s=i=22.5^o$. This effect is more pronounced in the vertical direction, since for $s=i=45^o$ $maxCF_v(T=0)=2.0$, whereas for $s=i=22.5^o$ $maxCF_v(T=0)=2.6$. Hence, valley effects on topographic aggravation seem most important in the parasitic vertical acceleration, especially for mild inclination angles s and i, under a low-frequency excitation.

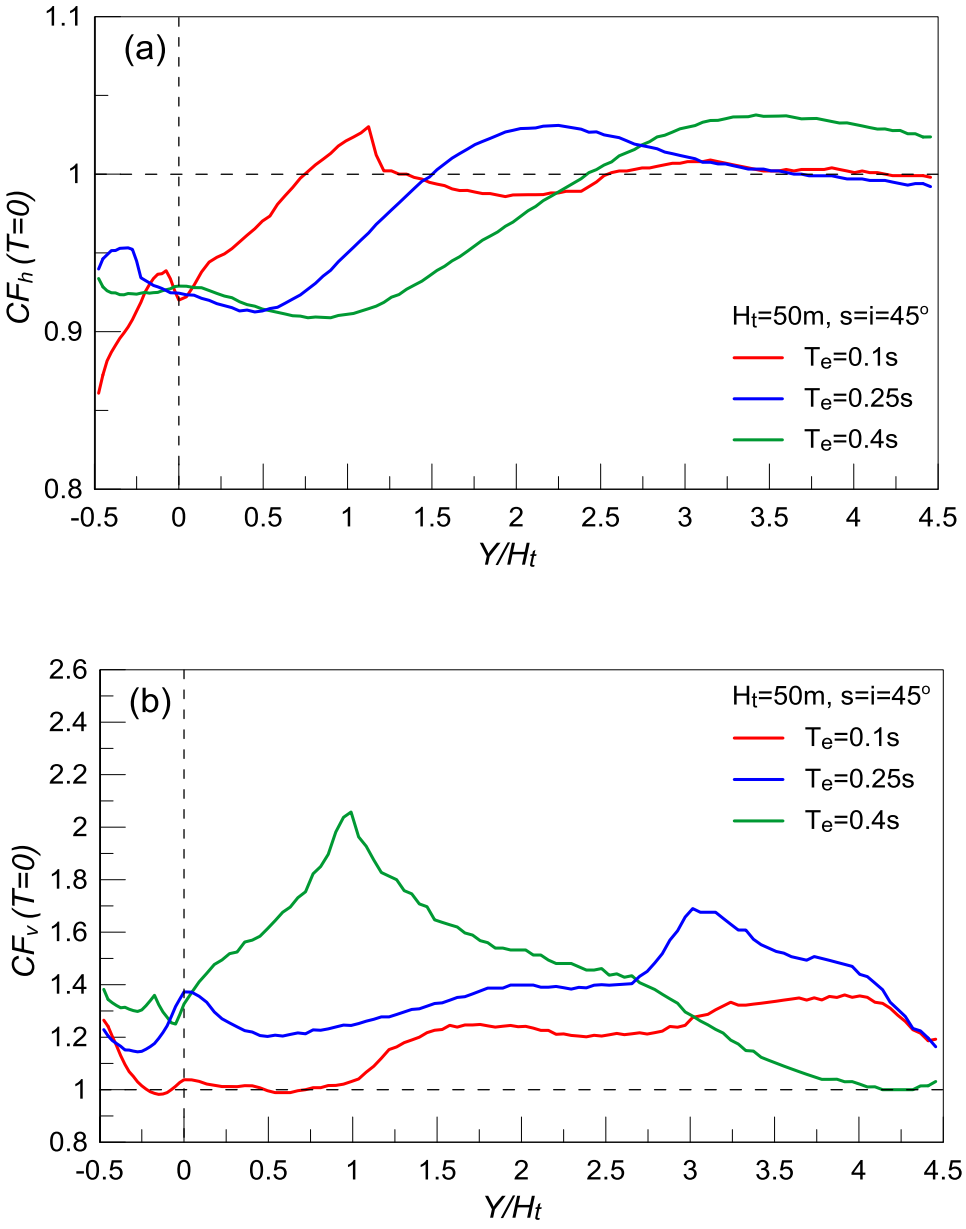

Figure 5.25: Spatial variability of Correction Factors $CF_h(T=0)$ and $CF_v(T=0)$ with normalized distance from the outcropping bedrock crest Y/H_t; Results for s=i=45°, excitation periods T_e=0.1, 0.25 and 0.4s and outcropping bedrock height H_t=50m.

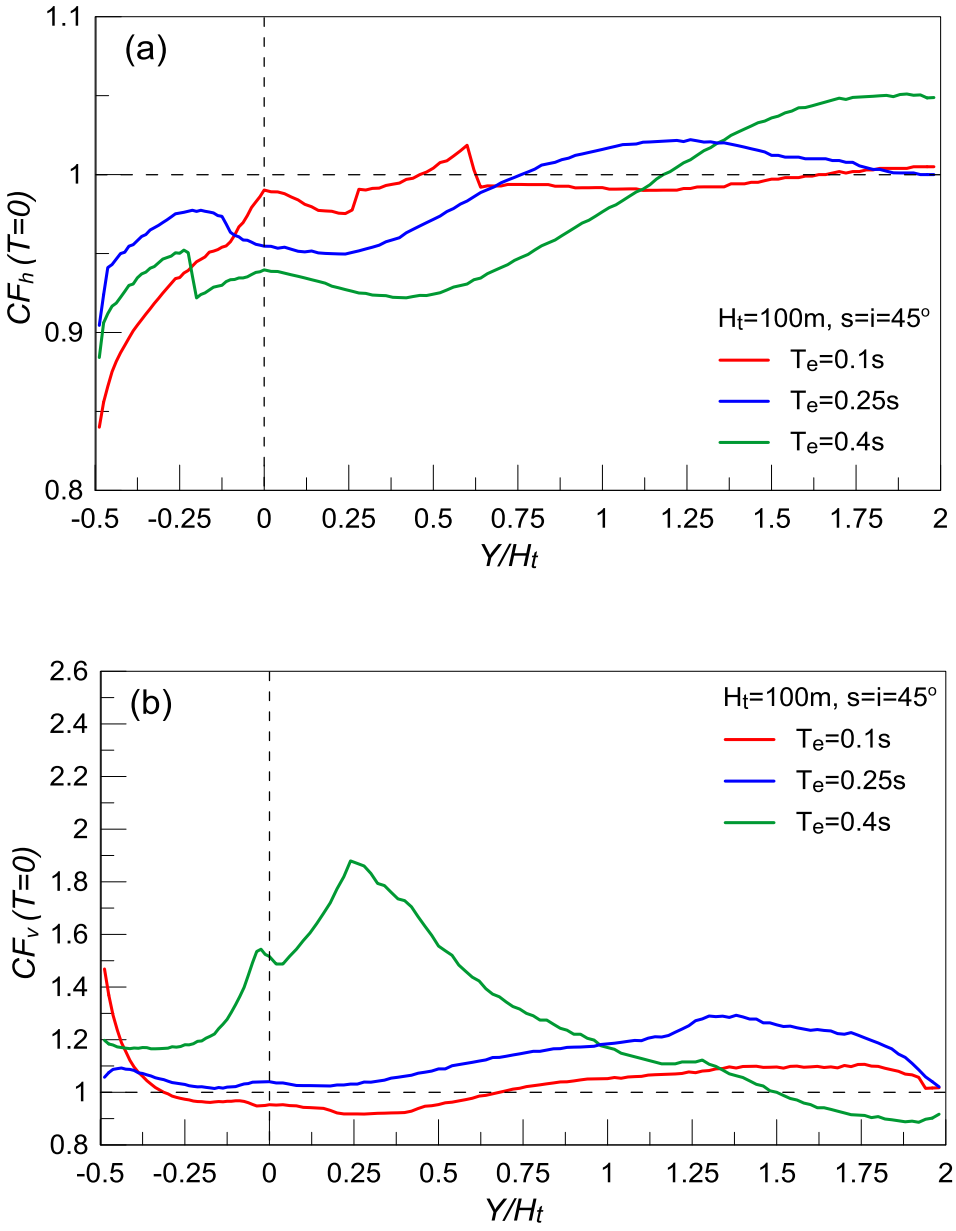

Figure 5.26: Spatial variability of Correction Factors $CF_h(T=0)$ and $CF_v(T=0)$ with normalized distance from the outcropping bedrock crest Y/H_t; Results for s=i=45°, excitation periods T_e=0.1, 0.25 and 0.4s and outcropping bedrock height H_t=100m.

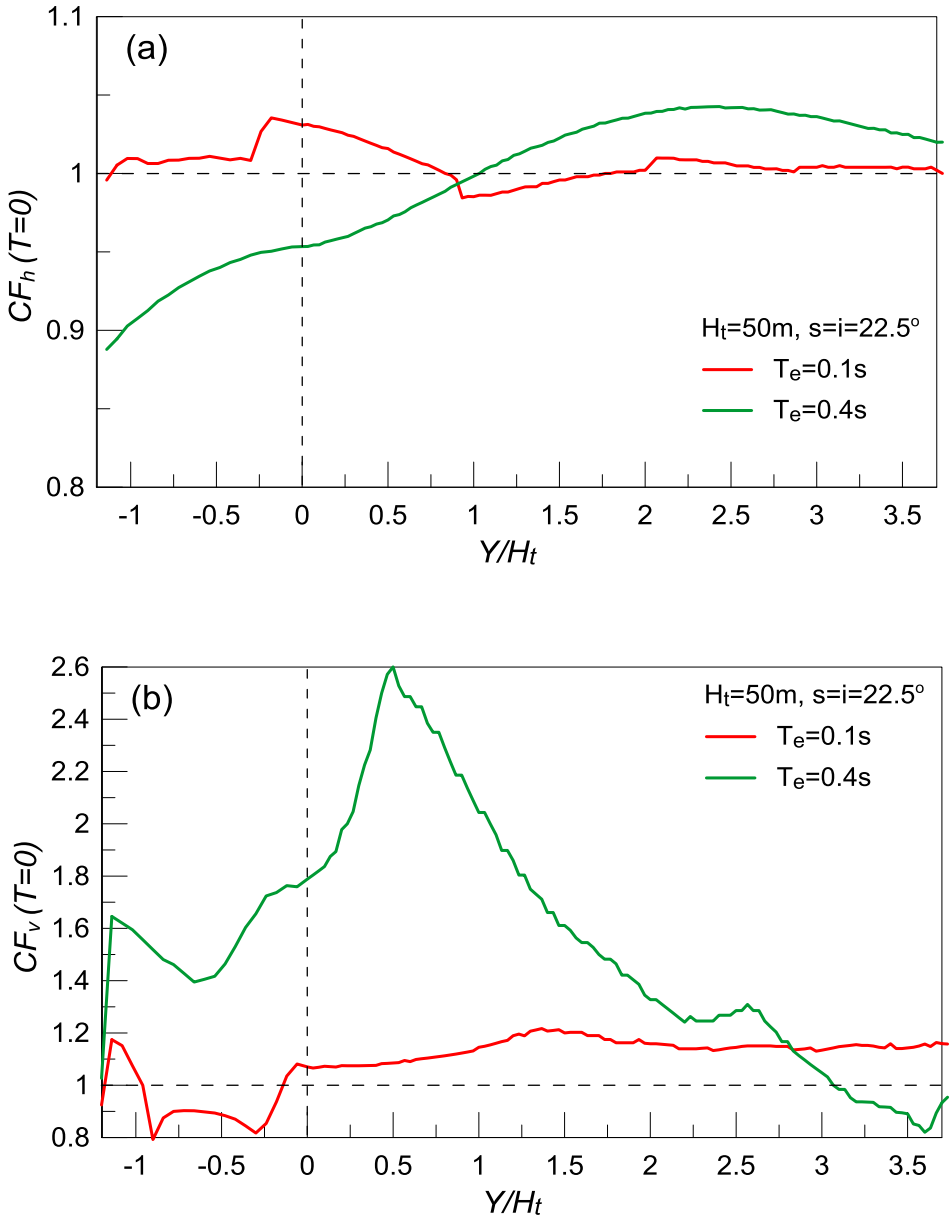

Figure 5.27: Spatial variability of Correction Factors $CF_h(T=0)$ and $CF_v(T=0)$ with normalized distance from the outcropping bedrock crest Y/H_t; Results for s=i=22.5°, excitation periods T_e=0.1 and 0.4s and outcropping bedrock height H_t=50m.

In the following, the typical ranges and the average curves from **Figures 5.25 to 5.27** are determined, as an additional attempt to quantify the effects of height H_t and inclination angles s and i on the correction factors. As shown in **Figure 5.28**, for H_t=50m and s=i=45^o the range for CF_h(T=0) is limited compared to CF_v(T=0). Namely, the average CF_h(T=0) increases from 0.92 to becoming practically equal to 1.0 for $Y/H_t > 2.0$. At the same time, the CF_v(T=0) is systematically greater than 1.0, on average, ranging from 1.2 to 1.4 throughout the outcropping bedrock area.

The pertinent results for height H_t=100m are depicted in **Figure 5.29**. In comparison with **Figure 5.28** for H_t=50m, the results in the horizontal direction are only quantitatively different for H_t=100m. Namely, the average CF_h(T=0) increases from 0.88 to becoming practically equal to 1.0 for $Y/H_t > 1.0$, i.e. closer to the crest in terms of normalized distance. Concurrently, the CF_v(T=0) is systematically greater than 1.0, on average, ranging from 1.0 to 1.25 throughout the outcropping bedrock area, i.e. at values slightly lower than for H_t = 50m. In other words, as the height H_t of a canyon increases, the valley effects on topographic aggravation are reduced, especially for the parasitic vertical acceleration.

Finally, the typical ranges and the average curves of CF_h(T=0) and CF_v(T=0) for mild valleys with mild outcrops (s=i=22.5^o) and height H_t=50m are demonstrated in **Figure 5.30**. Observe that the average CF_h(T=0) values are practically equal to 1.0 in every location of the outcrop ($0.95 \leq CF_h(T=0) \leq 1.02$). Remember that the corresponding average curve for s=i=45^o and H_t=50m (see **Figure 5.28**) varied from 0.92 to 1.0 close to the crest, these differences due to inclination angles in CF_h(T=0) seem negligible. Nevertheless, the inclination angles s and i play an important role when it comes for the correction factor of the topographic aggravation of the parasitic vertical acceleration. As shown in **Figure 5.30**, for s=i=22.5^o the CF_v(T=0) reaches 1.2, on average in front of the crest and 1.4 at the toe of the slope. Behind the crest $maxCF_v(T=0)=1.8$, while in **Figure 5.28** for s=i=45^o $maxCF_v(T=0)=1.4$. In addition, the range in the vertical direction increases for milder inclination angles. Specifically, for s=i=45^o $0.85 \leq CF_v(T=0) \leq 2.05$, while for s=i=22.5^o $0.8 \leq CF_v(T=0) \leq 2.6$. Thus, with decreasing inclination angles s and i, the range and the average values of CF_v(T=0) are increased, especially behind the crest.

Overall, the valley effects on the topographic aggravation at the outcropping bedrock are potentially remarkable for the parasitic vertical acceleration, but almost negligible for the horizontal acceleration. For the CF_v(T=0), the values range from 1.0 to 1.25 for s=i=45^o and H_t=100m, from 1.2 to 1.4 for s=i=45^o and H_t=50m and from 1.2 to 1.8, approximately for s=i=22.5^o and H_t=50m. In other words, they appear mostly significant for mild (valley and slope) inclinations and low bedrock heights H_t. It has to be underlined here that all results above refer to correction factors on topographic aggravation due to the existence of the valley, and not to topographic aggravation itself. For example, the values $CF_h(T=0) < 1$ that appear in front of the crest do not necessarily mean a deamplification of the horizontal acceleration, but a reduction of the topographic aggravation of the horizontal acceleration that would be estimated if the canyon was homogeneous.

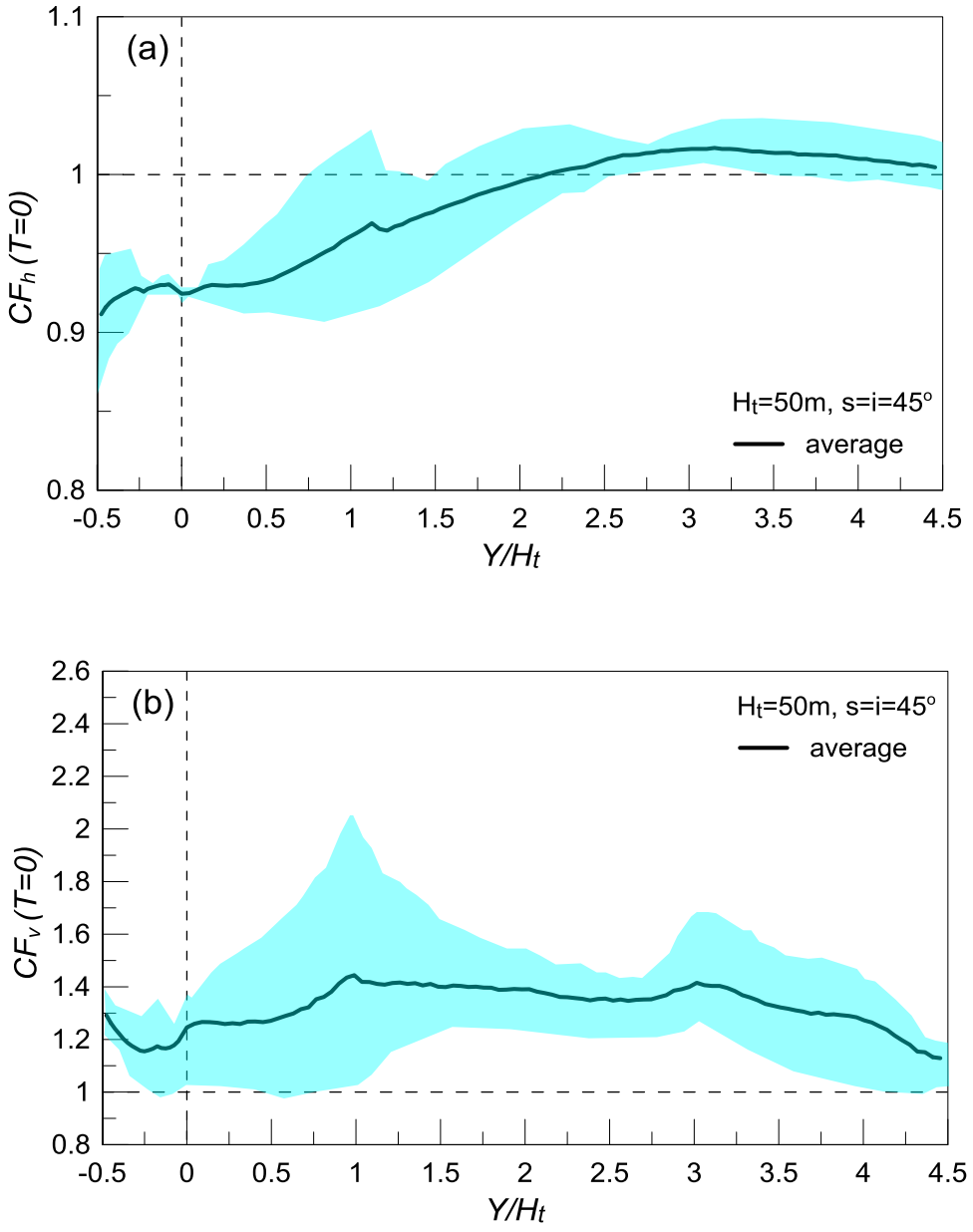

Figure 5.28: Range of variability and average spatial variability of Correction Factors $CF_h(T=0)$ and $CF_v(T=0)$ with normalized distance from the outcropping bedrock crest Y/H_t; Results for s=i=45°, excitation periods T_e=0.1, 0.25 and 0.4s and outcropping bedrock height H_t=50m.

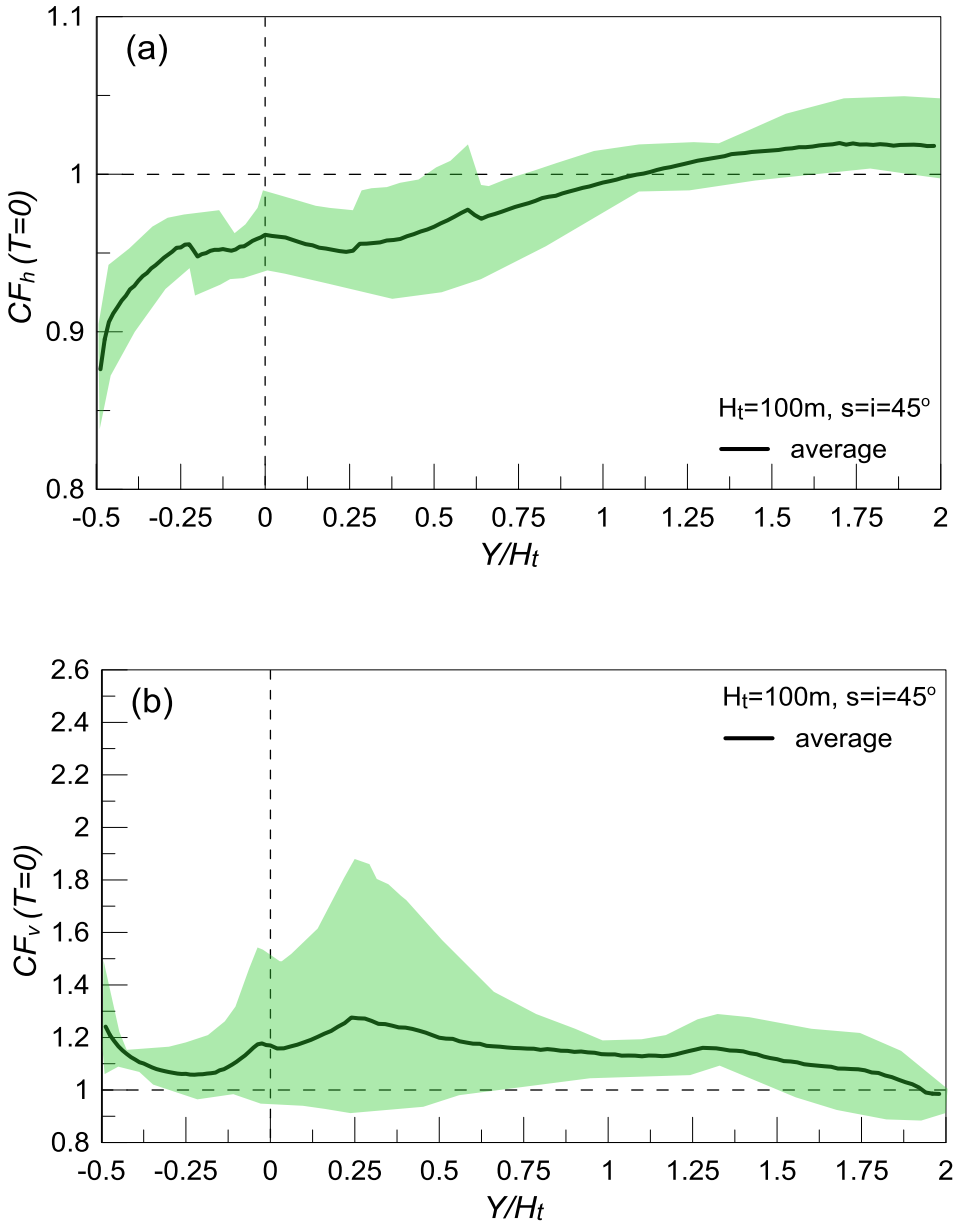

Figure 5.29: Range of variability and average spatial variability of Correction Factors CF_h(T=0) and CF_v(T=0) with normalized distance from the outcropping bedrock crest Y/H_t; Results for s=i=45°, excitation periods T_e=0.1, 0.25 and 0.4s and outcropping bedrock height H_t=100m.

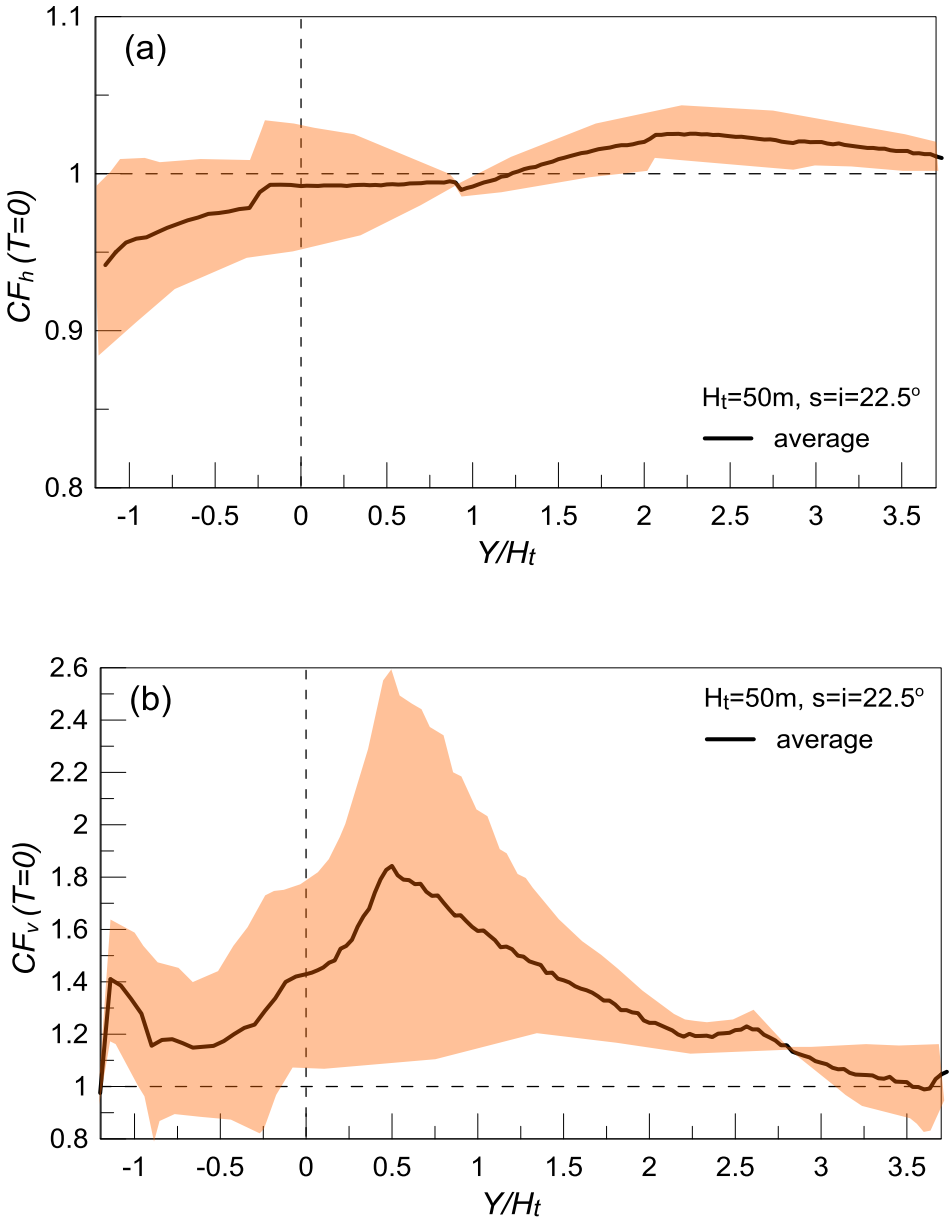

Figure 5.30: Range of variability and average spatial variability of Correction Factors CF_h(T=0) and CF_v(T=0) with normalized distance from the outcropping bedrock crest Y/H_t; Results for s=i=22.5°, excitation periods T_e=0.1 and 0.4s and outcropping bedrock height H_t=50m.

CHAPTER 6

CONCLUSIONS

6.1 Topographic effects on the seismic response of valleys

For the purpose of investigating the effects of outcropping bedrock topography on seismic valley response, numerical visco-elastic analyses were performed for a 2D symmetrical trapezoidal valley with width over thickness aspect ratio B/H=10 and buried bedrock inclination angle s. The parametric analyses compared the seismic response of the valley with flat outcropping bedrock to that of the same valley under the same excitation when the homogeneous outcropping bedrock creates a single step-like slope of height H_t and inclination angle i. The analyses were performed with the finite difference code FLAC (Itasca Inc. 2005) by imposing excitations pertaining to vertically incident SV waves. The results for the seismic response along the ground surface were presented in terms of geomorphic aggravation factors AS_{ah} and AS_{av} for the horizontal and the parasitic vertical acceleration, respectively, which properly exclude the aggravation due to 1D soil effects.

In order to quantify the effect of outcropping bedrock topography on the horizontal geomorphic aggravation, a correction factor CF_h was defined at each location as the ratio of AS_{ah} for the case of the non-flat outcrop over the corresponding AS_{ah} for the case of the flat outcrop. Similarly, a correction factor CF_v was defined at each location in terms of the AS_{av} values for the 2 cases of outcrop geometry. The values of AS_{ah} and AS_{av} varied per structural period T and so do the correction factors CF_h and CF_v. Nevertheless, the emphasis here was given on the CF_h and CF_v values for T=0s. On the basis of all performed analyses, the following main conclusions were drawn:

1. In accordance to the literature, for steeper valleys (e.g. s=45^o), the geomorphic aggravation spectra AS_{ah} and AS_{av} take larger values than for mild valleys (e.g. s=22.5^o), for high impedance ratio (e.g. a=0.50). In addition, as the impedance ratio a decreases, the geomorphic aggravation spectra values AS_{ah} and AS_{av} increase throughout the valley. However, the seismic response of the outcropping bedrock remains practically the same for high and low impedance ratio a.
2. Generally, the geomorphic aggravation factors AS_{ah} and AS_{av} become larger for structural periods T close to the predominant excitation period T_e. For T > 1s, the aggravation values in both directions are systematically reduced, similarly to what the literature finds.

3. Within the valley, the geomorphic aggravation spectra AS_{ah} and AS_{av} remain practically unaffected by the inclination angle of the outcrops i, for all tested values of the inclination angle of the valley s and the predominant period of the excitation T_e.
4. The effect of outcropping bedrock height H_t on aggravation factors AS_{ah} and AS_{av} is increasing for high impedance ratio (e.g. a=0.50), but decreasing for a low impedance ratio (e.g. a=0.25). For both high and low impedance ratio a values, the effect of height H_t is more intense for low-frequency excitations (e.g. T_e=0.4s).
5. The horizontal correction factor CF_h(T=0s) within the valley varied between 0.7 and 1.06, on average, while the average vertical correction factor CF_v(T=0s) varied between 0.9 and 1.4. The scatter is relatively small in the horizontal component ($0.6 \leq CF_h \leq 1.3$, overall) but quite larger in the parasitic vertical component ($0.4 \leq CF_v \leq 3.5$, overall).
6. Generally, the correction factors CF_h and CF_v for T=0s become more significant for higher and steeper outcrops (e.g. H_t=100m, i=45^o), especially for the parasitic vertical acceleration.

6.2 Valley effects on the seismic response of outcropping bedrock

For the purpose of investigating the valley effects on the seismic response of outcropping bedrock, numerical visco-elastic analyses were performed for parametrically comparing the seismic response of pairs of 2D symmetrical trapezoidal canyons with the same shape (width B, height H_t, inclination angle i). In each pair of canyons, one has an alluvial valley at the base of the topographic relief (valley model) and the other has no such valley (no valley model), while they both undergo the same excitation. In the valley models, the valley has a 2D symmetrical trapezoidal shape with a width over thickness aspect ratio B/H=10 and buried bedrock inclination angle s. Again, the analyses were performed with the finite difference code FLAC (Itasca Inc. 2005) by imposing excitations pertaining to vertically incident SV waves. As in section 6.1, the results for the seismic response along the ground surface were presented in terms of geomorphic aggravation factors AS_{ah} and AS_{av} for the horizontal and the parasitic vertical acceleration, respectively, which properly exclude the aggravation due to 1D soil effects.

Similarly, in order to quantify the valley effects on the horizontal geomorphic aggravation, a correction factor CF_h was defined at each location as the ratio of AS_{ah} for the valley model over the corresponding AS_{ah} for the no valley model of each pair of canyons. Similarly, a correction factor CF_v was defined at each location in terms of the AS_{av} values for the 2 cases in each pair. The values of AS_{ah} and AS_{av} varied per structural period T and so do the correction factors CF_h and CF_v. However, the emphasis here was given on their values for T=0s. Based on these analyses, the following have been concluded:

1. Generally, the valley decreases AS_{ah} and increases AS_{av} at the outcropping bedrock, regardless of the outcropping bedrock height H_t and the inclination angles of the valley s and the outcrops i.
2. The valley effects on the topographic aggravation at the outcrops are potentially significant for relatively small structural periods T. For structural periods T > 1s, the valley effects become negligible.

3. The valley effects on the response of outcropping bedrock can be neglected for the horizontal acceleration, since the horizontal correction factor CF_h varied between 0.85 and 1.05. However, the parasitic vertical correction factor CF_v is potentially remarkable ($0.8 \leq CF_v \leq 2.6$), especially for mild valleys and outcrops (e.g. $s=i=22.5^o$) under low-frequency excitations (e.g. T_e=0.4s).
4. The valley effects at the response of outcropping bedrock are slightly reduced with increasing outcropping bedrock height H_t (e.g. $maxCF_v$=2.0 for H_t=50m, but $maxCF_v$=1.9 for H_t=100m).
5. In general, the parasitic vertical correction factor CF_v is smaller in front of the outcrop crest ($1.1 \leq CF_v \leq 1.4$, on average) and larger behind it ($1.2 \leq CF_v \leq 1.8$, on average).

6.3 Proposals for future research

For the purpose of studying the coupling of valley and topography effects on seismic ground motion, in this thesis 2D (plane strain) numerical visco-elastic analyses were performed for uniform symmetrical trapezoidal valleys, using the finite difference method (FLAC, Itasca Inc 2005). The examined parameters were the predominant period of the excitation T_e, the inclination angles of the valley s and the outcropping bedrock i, the outcropping bedrock height H_t and the impedance (soil-over-bedrock) ratio a, all for a valley with width over thickness aspect ratio B/H=10. The coupling was studied in terms of aggravation factors for the whole of the elastic response spectrum, but for the correction factors the emphasis was put on T=0s, i.e. for the peak values of horizontal and parasitic vertical acceleration at the ground surface.

Hence, the first target of future research should be to study thoroughly the correction factors for the whole elastic response spectrum, based on the already performed analyses. Thereafter, there are still many cases and issues that have not been examined. Thus, future research is necessary, in order to supplement or even correct the obtained results from this study. Firstly, different values of B/H, and mainly smaller than 10 that correspond to narrow valleys where the geomorphic aggravation is expected more intense, at least for flat outcropping bedrocks. Secondarily, valley shapes different than trapezoidal may also be studied, although the shape is expected to be less important than the B/H ratio, at least for practical applications and realistic valleys for which a trapezoidal shape is generally a good approximation. What would also be useful to study are the waveform and the incidence angle of the excitation, since here only the predominant period T_e was varied. However, these issues are considered less important for practical applications than the T_e.

In closing, the basic assumptions of the present analyses (visco-elastic soil & 2D plane strain shaking) may also be waived in future research. It is expected that this coupling may be significantly affected due to soil nonlinearity and 3D geometries and shaking conditions. However, these last assumptions should be waived only after the proposals of the previous paragraph have been thoroughly examined.

References

1. Aki K. and K. Larner (1970), Surface motion of a layered medium having an irregular interface due to incident plane SH waves, J. Geophys. Res. 75, 933-954.

2. Aki K. (1988), Local site effects on strong ground motion, Proceedings, Earthquake Engineering and Soil Dynamics II - Recent Advances in Ground Motion Evaluation, ASCE, Geotechnical Special Publication No. 20, pp. 103-155.

3. Ashford S., Sitar N. (1994), Seismic Response of Steep Natural Slopes, Report No. UCB/EERC 94-05, Earthquake Engineering Re- search Center, College of Engineering, University of California at Berkeley.

4. Ashford S, Sitar N. (1997), Analysis of topographic amplification of inclined shear waves in a steep coastal bluff. Bull Seismol Soc Am; 87(3): 692–700.

5. Assimaki D. and Gazetas G. (2004), Soil and topographic amplification on canyon banks and the 1999 Athens earthquake, Journal of Earthquake Engineering, 8:1, 1-43.

6. Assimaki D., Gazetas G., and Kausel E. (2005), Effects of Local Soil Conditions on the Topographic Aggravation of Seismic Motion: Parametric Investigation and Recorded Field Evidence from the 1999 Athens Earthquake, Bulletin of the Seismological Society of America, Vol. 95, No. 3, pp. 1059–1089.

7. Athanasopoulos G.A., Zervas C.S. (1993), Effects of ridge-like surface topography on seismic site response, Transactions on the Built Environment vol 3, WIT Press.

8. Bard P.Y., Bouchon M. (1980), The seismic response of sediment-filled valleys. Part 1. The case of incident SH waves, Bulletin of the Seismological Society of America, Vol. 70, No. 4, pp. 1263-1286.

9. Bard P.Y. (1983), Site Effects: Two-Dimensional Modeling and Earthquake Engineering, Proc. USGS Conference XXII: 231-250, Santa Fe.

10. Bard P.Y., Bouchon M. (1985), The two-dimensional resonance of sediment-filled valleys, Bulletin of the Seismological Society of America, 75, n. 2, pp. 519-541.

11. Bard P.Y., Gariel J.C. (1986), The seismic response of two-dimensional sedimentary deposits with large vertical velocity gradients. Bulletin of the Seismological Society of America, 76, pp. 343-356.

12. Bard P.Y. (1995), Effects of surface geology on ground motion: recent results and remaining issues, Proc. 10th European Conference on Earthquake Engineering, Duma (ed.), Rotterdam, 305-323.

13. Bouchon M. (1973), Effect of topography on surface motion, Bulletin of the Seismological Society of America 63 (2): 615-632.

14. Boore D.M. (1972), A note on the effect of simple topography on seismic SH waves, Bulletin of the Seismological Society of America. Vol. 62, No. 1, pp. 275-284.

15. Bouckovalas G., Papadimitriou A. (2005) - Numerical evaluation of slope topography effects on seismic ground motion, Soil Dynamics and Earthquake Engineering, 25, 547-558.

16. Bouckovalas G., Papadimitriou A. (2006) - Aggravation of seismic ground motion due to slope topography, First European Conference on Earthquake Engineering and Seismology, Geneva, Switzerland, 3-8 September 2006 Paper Number: 1171.

17. Castellani A., Chesi C., Peano A., Sardella L. (1982), Seismic response of topographic irregularities. In: Cakmak A.S, Abdel-Ghaffar A.M., Brebbia C.A. Balkema/Rotterdam, editors. Proceedings of soil dynamics and earthquake engineering conference, Southampton, July, 1982, vol. 1, pp. 251±268.

18. Eurocode 8 (2001), Design of structures for earthquake resistance. Part 5: Foundations, retaining structures and geotechnical aspects.

19. Faccioli E. (1991), Seismic amplification in the presence of geological and topographic irregularities. In: Proceedings of the second international conference on recent advances in geotechnical earthquake engineering and soil dynamics. St Louis, Missouri, vol. II, p. 1779±97.

20. Faccioli E., Vanini M., Frassine L. (2002), Complex site effects in earthquake ground motion, including topography, 12th European Conference on Earthquake Engineering Paper Reference: 844

21. Field E. (2000), A Modified Ground-Motion Attenuation Relationship for Southern California that Accounts for Detailed Site Classification and a Basin-Depth Effect, Bulletin of the Seismological Society of America, S209-S221.

22. Gatmiri B., Amini - baneh D. (2014), Impact of geometrical and mechanical characteristics on the spectral response of sediment-filled valleys, Soil Dynamics and Earthquake Engineering, 67, 233-250.

23. Gatmiri B., Arson C. (2008), Seismic site effects by an optimized 2D BE/FE method II. Quantification of site effects in two-dimensional sedimentary valleys, Soil Dynamics and Earthquake Engineeing, Vol. 28, Issue 8, p. 646-661.

24. Gatmiri B., Foroutan T. (2012), New criteria on the filling ratio and impedance ratio effects in seismic response evaluation of the partial filled alluvial valleys. Soil Dynamics and Earthquake Engineering Vol. 41, pp. 89 - 101.

25. Gelagoti et al. (2010), Seismic Wave Propagation in a Very Soft Alluvial Valley: Sensitivity to Ground-Motion Details and Soil Nonlinearity, and Generation of a Parasitic Vertical Component, Bulletin of the Seismological Society of America, Vol. 100, No. 6, pp. 3035–3054.

26. Geli L., Bard P.Y. and Jullien B. (1988), The Effect of Topography on Earthquake Ground Motion: A Review and New Results", Bulletin of the Seismological Society of America, Vol. 78, No. 1, pp. 42-63.

27. Giovanna Vessia, Savino Russo, Diego Lo Presti (2011), A new proposal for the evaluation of the amplification coefficient due to valley effects in the simplified local seismic response analyses.

28. Hartzell S.A., Carver, D., Cranswick, E., and Frankel, A. (2000), Variability of site response in Seattle, Washington, Bull. Seism. Soc. Am., 90, 1237-1250.

29. Helmberger D.V., Vidale J.E. (1988), Modeling Strong Motions Produced by Earthquakes with Two-Dimensional Numerical Codes, Bulletin of the Seismological Society of America, Vol. 78, No. 1, pp. 109-121.

30. Jibson R. (1987), Summary of research on the effects of topographic amplification of earthquake shaking on slope stability, Open-File Report 87-268, U.S Geological Survey, Menlo Park, California.

31. King J.L., Tucker B.E. (1984), Observed variations of earthquake motion across a sediment-filled valley. Bulletin of the Seismological society of America, 74, n. 1, pp. 137-151.

32. Kramer S., (1996), Geotechnical Earthquake Engineering. Prentice Hall, Upper Saddle River, New Jersey.

33. Lee Y., Anderson J. (2000), Potential for Improving Ground-Motion Relations in Southern California by Incorporating Various Site Parameters, Bulletin of the Seismological Society of America S170-S186.

34. Papadimitriou A., Tetta Z., Mellios M. (2011), Numerical evaluation of basin effects on peak seismic acceleration at the ground surface, Proceedings, ERTC-12 Workshop of Evaluation of EC-8, Athens.

35. Pedersen H., Le Brun B., Hatzfeld D., Campillo M. and Bard P.-Y. (1994), Ground-Motion Amplitude Across Ridges, Bulletin of the Seismological Society of America, Vol. 84, No. 6, pp. 1786-1800, December 1994.

36. Psarropoulos P.N., Tazoh T., Gazetas G., Apostolou M. (2007), Linear and nonlinear valley amplification effects on seismic ground motion. Soils and Foundations, Japanese Geotechnical Society, Vol. 47, No. 5, 857 - 871, Oct. 2007.

37. Silva W.J. (1988), Soil response to earthquake ground motion. EPRI Report NP-5747, Electric Power Research Institute, Palo Alto, California.

38. Stewart P.J., Chiou S., J, Bray J.D., Graves R.W. ,Somerville P.G., Abrahamson N.A. (2001), Ground motion evaluation procedures for performance based design, PEER Report 2001/09.

39. Stewart, J.P., and Sholtis, S.E. (1999), Topographic effects on seismic ground motions above and below a cut slope in sand, Report to U.S. Geological Survey, University of California, Los Angeles.

40. Trifunac M.D., Hudson D.E. (1971), Analysis of the Pacoima Dam accelerogram - San Fernando, California, Earthquake of 1971, Bulletin of the Seismological Society of America. Vol. 61, No. 5, pp. 1393-1141. October, 1971.

41. Trifunac M.D. (1973), Scattering of plane SH-waves by a semi-cylindrical canyon, Intern. J. Earthquake Eng. and Stress Dynamics 1, 267-281.

42. Wong H. L. and M. D. Trifunac (1974), Scattering of plane SH-waves by a semi-elliptical canyon, lntern. J. Earthquake Eng. and Stress Dynamics 3, 157-169.

43. Yegian M.K, Ghahraman V.G. and Gazetas G. (1994), Seismological, Soil and Valley Effects in Kirovakan, 1988 Armenia Earthquake, Journal of Geotechnical Engineering, Vol. 120, Issue 2, February 1994.